FLOWBACK OF SOLIDS THROUGH DISTRIBUTION PLATES OF GAS FLUIDIZED BEDS AND ASSOCIATED PHENOMENA

A thesis submitted

by

Walid Mohamud Salih Kassim, B.Sc.(Wales),M.Sc.

for the degree of

Doctor of Philosophy

Department of Chemical Engineering

University of Aston in Birmingham

August, 1972

SUMMARY

This work is concerned with a study of certain phenomena related to the performance and design of distributors in gas fluidized beds with particular regard to flowback of solid particles. The work to be described is divided into two parts.

I. In Part one, a review of published material pertaining to distribution plates, including details from the patent specifications, has been prepared. After a chapter on the determination of the incipient fluidizing velocity, the following aspects of multi-orifice distributor plates in gas fluidized beds have been studied:

(i) The effect of the distributor on bubble formation related to the way in which even distribution of bubbles on the top surface of the fluidized bed is obtained, e.g. the desirable pressure drop ratio $\Delta p_D/\Delta p_B$ for the even distribution of gas across the bed.

Ratios of distributor pressure drop Δp_D to bed pressure drop at which stable fluidization occurs show reasonable agreement with industrial practice. There is evidence that larger diameter beds tend to be less stable than smaller diameter beds when these are operated with shallow beds.

Experiments show that in the presence of the bed the distributor pressure drop is reduced relative to the pressure drop without the bed, and this pressure drop in the former condition is regarded as the appropriate parameter for the design of the distributor.

(ii) Experimental measurements of bubble distribution at the surface has been used to indicate maldistribution within the bed. Maldistribution is more likely at low gas flow rates and with distributors having large fractional free area characteristics (i.e. with distributors having low pressure drops).

Bubble sizes obtained from this study, as well as those of others, have been successfully correlated. The correlation produced implies the existence of a bubble at the surface of an orifice and its growth by the

addition of excess gas from the fluidized bed.

(iii) For a given solid system, the amount of defluidized particles stagnating on the distributor plate is influenced by the orifice spacing, bed diameter and gas flow rate, but independent of the initial bed height and the way the orifices are arranged on the distributor plate.

II. In Part two, solids flowback through single and multi-orifice distributors in two-dimensional and cylindrical beds of solids fluidized with air has been investigated. Distributors equipped with long cylindrical nozzles have also been included in the study.

An equation for the prediction of free flowback of solids through multi-orifice distributors has been derived. Under fluidized conditions two regimes of flowback have been differentiated, namely dumping and weeping. Data in the weeping regime have been successfully correlated. The limiting gas velocity through the distributor orifices at which flowback is completely excluded is found to be independent of bed height, but a function of distributor design and physical properties of gas and solid used. A criterion for the prediction of this velocity has been established.

The decisive advantage of increasing the distributor thickness or using nozzles to minimize solids flowback in fluidized beds has been observed and the opportunity taken to explore this poorly studied subject area. It has been noted, probably for the first time, that with long nozzles, there exists a critical nozzle length above which uncontrollable downflow of solids occurs. A theoretical model for predicting the critical length of a bundle of nozzles in terms of gas velocity through the nozzles has been set up. Theoretical calculations compared favourably with experiments.

TABLE OF CONTENTS

INTRODUCTION

A bed of solid particles in an upwards stream of gas is said to be in a fluidized state when the particles are no longer resting upon each other but are fully supported by the gas. The fluidized medium is characterised by liquid-like behaviour: its surface remains horizontal, it flows like a liquid and the static pressure difference across the bed is equal to the weight of solids per unit cross-sectional area of the bed.

The type of fluidization generally observed in gas fluidized beds is called aggregative fluidization and is characterised by bubble-like pockets of gas rising through the bed. Another cause of heterogeneity in gas fluidized beds is channelling: the bed is said to be channelling when the gas follows preferred tracks across the bed, the remainder of the bed being partially defluidized. Channelling reduces the contact between the gas and the solids and is therefore highly undesirable.

For given solids and a given superficial velocity, the physical properties of a fluidized bed are determined by the distributing device (distributor plate and wind box). For example, a change in design of a distributor can suppress channelling, modify the size of the bubbles and change the density and height of the bed. In a fluidized bed reactor most of the chemical reaction occurs in the close vicinity of the distributor. The conversion rates are highly dependent upon the gas-solids contacting and consequently upon the distributor geometry.

An industrial distributor often consists of a simple metal plate with an arrangement of orifices between 0.15 - 2.5 cm. in diameter. Other types of distributor with various nozzles and bubble-caps are also used to improve the regularity of gas distribution or prevent solids flowback. However, for mainly economical reasons multi-orifice distributors are most commonly used.

Only in recent years some progress has been made in evolving methods for the design of distribution plates (27, 70, 64). The same, unfortunately, cannot be said of our real knowledge of certain phenomena occurring at the distributor, e.g. the regularity of gas distribution, the formation of defluidized zones and flowback of solid particles. An understanding of distributor phenomena is vitally important for the rational scale-up and design of large fluidized beds. In these units, little reaction occurs in the bed once the bubble is fully grown. Most of the reaction takes place at the distributor where the gas is jetted into the solids and where the bubbles are still small.

Solids flowback (or leakage) is a phenomenon which occurs at the distributor of gas fluidized beds and can easily be observed with multi-orifice distributor plates. Excessive flowback of solids quite often results in the destruction of the distributor plate. For example, particle reentrainment at high velocity into the fluidized bed causes erosion of the distributor orifices. Secondly if an exothermic reaction is carried out in the bed, the reaction will start inside the wind box due to the presence of catalyst particles under the distributor and submit the distributor to temperatures for which it has not been designed.

Unfortunately, very few data have been reported on flowback despite its importance. A review of published material pertaining to distribution plates, including details from the patent specifications, indicates the particular emphasis which has been placed on the prevention of flowback, the problem of defluidized zones, regularity in distribution. For these reasons, the present work has been undertaken.

CHAPTER ONE

1. SURVEY OF AVAILABLE DESIGN INFORMATION FOR DISTRIBUTION PLATES AND DEVICES

1.1 Introduction

The distributor design of an industrial fluidized bed has pronounced effects on the performance of gas-fluidized systems and different types of distributors have been used. This subject is still surrounded with considerable obscurity and has received little attention from the academic side. Recent review articles by Harrison(1) and Gregory (2) comment on the lack of information concerning the effect of gas distribution devices on the behaviour of fluidized beds. Such information as is available derives partly from the patent literature and partly from industrial publications dealing with specific process applications.

When the application of distribution plates in various industries is studied in more detail one of the important facts which emerges is the vastly different way in which industry has tended to deal with its problems. Reflection shows that these particular differences in development may be related to the type of dense-phase bed required or used in the particular industries. Once this aspect has been appreciated it becomes possible to make use of the experiences of these various industries in more general manner.

1.2 The Emergence of Practical Design

1.2.1. Historical Development - Winkler Process

Although it is possible to point out occasional examples of fluidization practice with dense-phase beds before the introduction of the Winkler system of gas generating, such as the early patents of Robinson(3) and Card and Dance(4), the development of this item of gasification equipment effectively made fluidization a matter of more than

local interest. Further, the application of the Winkler generator on the large scale inevitably led to the preparation of working designs based upon practical experience. Thus it can be fairly said that the Winkler generator showed the first important examples of practical distribution plate design.

The earliest examples of the Winkler generator (Germany 1921) used horizontal bars. This was a natural development, since in the generator the grate supported the fuel. The development of the Winkler grate has been recorded in some detail(5). The record shows that some of the early generators had a travelling chain grate. Later these were replaced by fixed beams with water-cooling. These beams in turn were replaced by fire-brick elements.

As an alternative to some form of grid for supporting the bed and distributing the incoming gas a cone-type base has been proposed and from 1941 onwards had been the subject of experiments. Obviously a cone served only for gas distribution and had little function in the support of a bed above the wind box. In comments upon the performance of the grids and the cone base the report states that the grids gave good gas distribution and that "the distribution ..... cannot be so good with the grateless type.

With a grid plate typical performance details show a pressure drop of 20 cm. W.G. over the grate and 50 cm. W.G. over the bed. In spite of the relatively shallow bed used the normal gasification system makes great use of reaction in the dilute-phase above the bed and the process is only suitable for highly reactive fuels.

1.2.2. Historical Development - U.S.Bureau of Mines

The earliest interest of the U.S. Bureau of Mines in fluidization with gases appears to be involved in the work of T. Frazer and H.F. Yancey in 1925 in connection with the separation of shale from coal(6). They used a cast-iron cell in which sand was supported on a

porous plate and reported successful tests with multi-orifice metal plates, Filtros plates, and porous concrete slabs. For a large scale design they proposed the use of a sloping distributor with the porosity adjusted to provide satisfactory air flow at all points.

Another employee of the U.S.Bureau of Mines, Odell(7), applied some years later for a patent on a general method of carrying out gas-solid operations and reactions. This specification begins the generalization of fluidization, probably using the term for the first time. Odell referred to the use of "grate, perforated plate, porous plate or equivalent" but gave no information on pressure drop or velocity through the perforations.

Precisely how much practical work was undertaken by Odell is unclear, but his claims are so broad that it is unlikely that he investigated all the processes mentioned on a large scale. For this reason there is little evidence of the development of practical differences of distributor plate designs to suit particular processes.

1.2.3 Historical Development - W.K.Lewis & E.R.Gilliland Patent(8).

This patent was applied in 1940 in which Lewis and Gilliland, well-known members of the staff of Massachusetts Institute of Technology and consultants to ESSO, give a basis for the design of perforated plates for distribution in dense-phase beds. Their patent claims in particular shaped inlet ports in the plate, cylindrical at the entry on the under-side and expanding upwards in the shape of an inverted pyramidal section, preferably a 7^{o} taper. In addition there would be many of these upon a plate in spaced relationship, their upper ends in substantial continuity and uniformly distributed. The total minimum cross section would be not greater than 1/5 to 1/10 of the total area of cross section of the plate, while the diameter of each opening should be substantially greater than the maximum diameter of the solid particles, understood to be of uniform size.

An explanation is given for the design. Under conditions of fluidization individual particles of solid will penetrate downwards into an opening. An upward gas or vapour velocity must be produced sufficient to stop this. If the constriction (the first noted use of this word in connection with distribution plates) is only to be 1/4 of the area of the plate it may require a long portion some 20 to 70 diameters of the constriction in length to reach a point where no solids will penetrate. If, on the other hand, the constriction is only some 1/15 to 1/20 of the treating area, the penetration of solids is reduced to as low as 1 to 4 diameter of such tubes, thereby greatly reducing the thickness of the plate required. This statement makes very clear that the "velocity upwards of the gases or vapours through the openings in the gas distribution plate be sufficient to prevent solids from falling through these openings".

1.2.4 Practical Development of Fluidized Catalytic Cracker Distribution

Apart from the patent literature there are several surveys available which throw light on the development of and practice with distributors in 'cat-cracker'. An early outline is by Sittig(9) and by Braca and Fried(10). More recent articles are by Stemerding and colleagues(11), and Turner(12).

In many of the early designs solid particles were required to flow upwards through the grid plate of the regenerator. In any case plants tend to be large and construction has to be cheap and robust, relying upon metal. The earliest multi-orifice plates were flat and perforations consisting of cylindrical orifices which were regularly arranged in the plates. Typical features may be obtained from a patent specification which records orifices $\frac{1}{2}$ in to 1 in or more in diameter(13).

In the line of development of multi-orifice distributor plates dished structures were then introduced, the concavity facing downwards.

In such a design the bed was deeper at the edge of the vessel than towards the axis. With evenly-spaced orifices less gas tended to pass near the walls. Because of this lack of balance solids fall through the outer orifices and are blown up through the centre orifices. In this situation there is severe erosion of the centre orifices, but no wearing of the outer ones. The resulting enlargement of the centre orifices..... allows even more gas to pass up.

To improve this a first move was to space orifices preferentially near the walls. Some opinions held that it was better to have the dished plate with its concavity upwards. With regularly spaced perforations there was flow at the edge of the plate, this being considered advantageous in some cases. But, even with this, "it is possible to have solids circulating under the gas distributor if the pressure drop across the grid is too low compared with the difference in static head of the bed at the low and high points of the grid."

Stemerding comments on the greater 'turn-down' range of the upward concavity plate. In earlier practice Colmonoy (a hard surfacing material of nickel base and chromium boride) inserts had been added to the orifices, but Carbofrax had superseded as the material.

Much of the development in practice with plates using circular orifices is associated with the Esso organization and with various plant contractors. The exploration of the use of parallel beams, comparable to the grate bars used by Winkler, seems particularly to be associated with the Shell organization. Indeed there was a possibility that this may have some cross-connection with the "Turbogrid" design of distillation plate which was introduced in 1950.

There is little process design information on parallel beam plates. The paper by Turner(12) suggests that this type of plate gives a better performance than the variations in the multi-orifice plate suggested.

More recently has come the development of the pipe grid systems. These appear to provide low pressure drops without the use of pre-distribution devices. These clearly resemble the sparge devias used in the aeration of various types of microbiological cultures on the large scale. Stemerding's paper gives more detail on such systems. The application of such pipe grids is only possible when solid particles are fed by a dense-phase riser and no longer in dilute-phase through the grid. The use of these two methods together have still further improved the performance of the regenerator in catalytic cracking. The design of the pipe grid also avoids the possibility of flowback of solids during any shut-down.

Typical orifice size for a pipe grid is $\frac{1}{2}$ in. with the orifices located at the lower side of the pipe to avoid entry of solids on shut-down.

Reported practice in the Esso Mark IV Cracker, the pressure drop recommended across the grid was given as 2.0 p.s.i. In the case of the Shell design of pipe grid the pressure stated was 1.0 p.s.i. This appears to be for a bed pressure drop of the order of 5 p.s.i. The purpose of the pressure drop was stated to be that it should be large relative to any local fluctuations downstream, thereby avoiding the possibility of local irregularity in gas flow.

Closer attention to the requirement for good gas distribution seem particularly to be associated with more detailed investigation of the behaviour of the fluidized catalytic cracker regenerator. This showed itself in at least two different ways. First came the emphasis upon an adequate pressure drop across the grid, as stipulated by Esso for the good working of their Mark IV design. The alternative approach, which aimed at the achievement of good gas distribution without greatly increased pressure drop, relied upon the introduction of suitable pre-distribution devices for the upflowing gas before it reached the distribution plate proper.

Such devices which included the pipe system known as the "porcupine" occupied a considerable space under the distribution plate, inside the main structure of the containing vessel. No process disadvantages ensued for catalytic cracking but, with the advent of other fluidized processes such as hydroforming, which operated at high temperatures with hydrocarbon gases, it became important to cut down the volume beneath the distribution plate. One method of achieving this result led to the "double-cone" design in which the gas enters the space between the base of the vessel and a cone fitted with orifices of varying sizes to give the desired flow.

With increase in size of reactors it becomes appreciated that the introduction of gas into a conical base and its direct distribution, without intermediate device, by the distribution plate, led to some inequality of distribution. This led to the suggestion of various schemes for the preliminary distribution of the gas, similar to the well-known wind box used, for example, on blast-furnaces.

1.3 Pressure Drop across Distributor and its Relationships

The pressure drop across the distributor ΔP_D must be of a certain magnitude if it is to distribute the fluidizing gas evenly. This pressure drop is often related to the bed pressure drop ΔP_B. An analysis of the recommendations, implied or direct, and observations available, indicates the existence of high and low "schools of thought", i.e. where $\Delta P_D/\Delta P_B \geq 0.4$ or alternatively $\Delta P_D \leq 0.2$.

As already noted, the Winkler generator practice(5) was to operate with pressure drop 40% that of the bed (20 cm. W.G. relative to 50 cm. W.G.). Daniels(14) in 1946, indicated distributor pressure drop of 0.72 p.s.i. for a bed drop of 2.82 p.s.i. in cat-cracking. Reported practice in the Esso Mark IV cracker was 40% (noted as 2 p.s.i. on the regenerator).

Zenz and Othmer(15) recommended that, to obtain 'good' gas distribution, the velocity through the distributor orifices of a multi-orifice place should be sufficient to produce a plate pressure drop at least 40% of that across the bed. At these velocities, solids flowback is presumed negligible although data was not given by the authors cited.

These pressure drop recommendations have also been indicated by Cooper and Colleagues(16). Stemerding et al(11) provide comparable recommendations. Pyzel(17) claims in his recent patent, for successful operation of the fluidized bed reactor, the pressure drop ratio should be 0.25 or more.

In contrast to the 40% figure, which receives strong support from the practice of many cat-cracker installations, there are two significant alternative or 'extreme' recommendations. The first of these is the 'high' ratio. This has come from porous plate manufacturers. It is also to be found in process patent specifications, with such a wording as: "perforations consist of a multiplicity of ports across which, with the necessary rate of flow ..... there is appreciable pressure drop of the same order as the pressure drop across the bed." Federov(18) gives a similar recommendation in respect of shallow beds, in which the grid resistance should be the same or larger than the resistance of the bed.

White(19) suggested 50 - 100% of the bed drop. In a recent paper, Avery and Tracey(20) state that "bed stability required a pressure drop through the supporting plate of the same order as the bed pressure drop." That was in relation to beds of very low aspect ratio of bed depth to bed diameter. Later Pictor and Robinson(21) gave similar recommendation in respect of drying of coal in shallow beds, in which the distributor pressure drop about the same as the pressure drop through the fluidized bed itself. For the design of an industrial fluidized bed driers and coolers, Wormald and Burwell(22) recommend 50 - 100% of the bed pressure drop in respect of shallow beds.

The high ratio received experimental support from Gvozdev and colleagues(23) who found that the plate pressure drop should be less than 125% of the bed drop. This, in fact, covers all known recommendations.

The 'low' ratio to be found in the literature comes from Agarwal et al(24). This suggests a plate drop of 10% of the bed. However, there is the restriction that, in no case, should the plate drop be less than 35 cm. W.G. This recommendation comes from experience with deep beds of high density material (iron ore). For shallow beds of low density, they recommended a minimum drop of 35 - 30 cm.W.G.

Gregory(25) found 10% plate drop to be a workable figure for shallow beds of relatively dense material in a plant which had been designed specifically to keep down energy costs. Also indicated was the possibility of working very shallow beds with a specific variety of multi-orifice plates.

Hiby(26) and Whitehead et al.(27,28) provide support for the 'low' ratio opinion. According to Hiby the maximum ratio is needed at the commencement of fluidization. Once the bed is freely moving the ratio can be smaller. Whitehead et al. consider the choice of the ratio $\Delta P_D/\Delta P_B$ in relation to three critical operating velocities, viz: (i) U_1 - the velocity to initiate fluidization throughout the bed, in particular at the gas inlet points, (ii) U_m - the minimum operating velocity, i.e. that which just maintains operation at each gas inlet point at all times and (iii) the velocity to ensure acceptable distribution of gas at the distributor level.

Zuiderweg(29) has also considered the subject and suggested that the value of this ratio can be as low as 10%. Wright(30) found that a plate drop of 10 - 15% of that across the bed was adequate for smooth operation of the fluidized bed. An average of 10 - 20% also to be found in the reviews by Vanecek et al.(31) and Gregory(2).

1.3.1. Pressure Drop Ratio ($\Delta P_D/\Delta P_B$) and its Relationship to Bed Aspect Ratio (H/D)

Several of the studies in the literature, notably Kelsey(32), have shown that the ratio of bed height H to bed diameter D is important in affecting distributor design. Beds with small H/D clearly require a proportionally greater pressure drop in their distributors.

Harrison(1) in his review article, also refers to the effect of bed diameter on the pressure drop ratio. Various investigators have shown that irregular fluidization is more likely in a vessel which has a high depth/diameter ratio. Factors such as particle size, density, size distribution, gas velocity and gas density interact with the H/D ratio to make smooth fluidization possible with a high H/D ratio in one case, but not in another. Actually, in catalytic reactors with given gas velocity and catalyst size, the reaction rate and bubble size will determine the bed height while the gas treatment rate fixes the bed area, smaller catalyst particles will lower the gas velocity and require a shallower bed, whereas larger particles will require a bed of larger H/D ratio.

In industrial work the H/D ratio seldom exceeds 3, and is usually nearer 1. Irregular fluidization may occur in large vessels because of the formation of bubble "tracks". Squires(33) has discussed this problem at length. He suggests the existence of tracks of large diameter bubbles (but not as large as the bed) wherein most of the gas passes through the bed in high velocity tunnel, tube or track in the solids. The gases in these tracks do not contact the solid at all well, and they also produce bad fluidization.

A summary of reported design data for pressure drop ratio as a function of bed aspect ratio is given in table (1.1) (page 11) and it can be seen that the experimental results reported by Kelsey(32), for a two-dimensional bed system, agree roughly with ratios recommended for some industrial processes.

TABLE 1.1 Summary of some reported design data for pressure drop across distributors in gas fluidized beds

Source	Process	Distributor	$\frac{\Delta P_D}{\Delta P_B}$	$\frac{H}{D}$
Losh et al(36)	Calcination of Zirconium Flouride wastes.	Bubble-cap	20%	1.0
Horsler and Thompson(35)	Hydrogeneration of crude oil and coal gasification.	Multi-orifice plate	2.5-5%	1.0-2.0
Avery and Tracey(20)	Fluidized bed absorber for the recovery of solvents from gases. (Viscose plant)	Multi-orifice plate	100%	0.05 approx.
Pyzel(17)	Fluidized solids reactor (patent)	Nozzle	25%	0.2
Wright(30)	Fluidized bed boiler (combustion of solid fuel).	Bubble-cap	10-15%	0.82
Gregory(25)	Frodingham gas desulphurising unit.	Baffled slot plate + initial distribution	10%	0.17-0.23
Deshpande et al(34)	Experimental air fluidized beds of small diameters*	Sandwiched packed bed	5-20% 15-60%	6.0 3.0
Kelsey(32)	Experimental two dimensional air fluidized beds (data taken from his Figure 5)	Multi-orifice plate	2-17.5%	1.55-0.2

* Near transition to slugging.

This wide range in recommended pressure drop follows from the use of various distributing devices, variations in the desired initial gas distribution, and the differing behaviour of the solid required to be fluidized. It is apparent that no single ratio can be advocated or can be applied to all situations. As already mentioned, the distributor pressure drop is important in influencing fluidized behaviour and the lack of agreement among various authors shows the need for further study. In the present work, therefore, ratios of distributor pressure drop to bed pressure drop at which stability occurred were studied in cylindrical beds of various height and diameter (see Chapter 3). It was concluded that the aspect ratio affected the pressure drop criteria required, beds of high aspect ratios requiring low pressure drop ratio for stable operation and beds of low aspect ratios requiring high pressure drop ratio. The results agreed only qualitatively with those of Kelsey(32), but showed reasonable agreement with industrial practice.

1.3.2 When are Lower Pressure Drop Ratios Required?

The relatively low pressure drop distributors may be used under the following circumstances (Whitehead(72) has already discussed this in some detail).

(a) When fluidizing in beds with small cross-sectional area.

(b) In conditions where maximum use of the distributor is not essential, e.g. in drying some inert materials.

(c) When full operation of the distributor is essential but can be achieved by one or more of the following methods: (i) using an alternate supply of high pressure air to start the system, (ii) by installing a pre-distribution device in the wind box below the distributor, (iii) by installing a post-distribution device (e.g. baffles) in the bed just above the distributor. These devices may improve fluidization without appreciably increasing the pressure drop.

(d) When operating with shallow beds.

(e) When high distributor pressure drop incurs extra expenses for energy consumed in overcoming the distributor pressure drop.

(f) When solids flowback can be tolerated or is actually required in the process, e.g. in multi-stage systems.

(g) When high gas inlet velocities are not required to bring about gas-solid contact or solids movement near the distributor.

1.3.3. Why and When are Higher Pressure Drop Ratios needed?

We just noted that some large plants operate with low ratios. However, many important plants, particularly cat-crackers, operate at ratios of the order 0.4. The use of this ratio probably caused unjustifiable increase in consumption of electrical power.

The explanation is not likely to be in terms of process improvement. Several authors have concluded that good solids mixing and high heat transfer rates are favoured by lower pressure ratios. The simplest explanation, mentioned earlier for cat-crackers, is the need to prevent solids flowback through the perforation which, otherwise, would lead to erosion of the perforations.

1.4. Problems of Large-diameter Shallow Beds

By large is understood magnitudes of the order 1 to 10 meters diameter. By shallow is understood 5 to 50 cm., but in practice, the aspect ratio may be more significant, e.g. H/D = 0.05 - 0.10. Beds of this type generally require:

(a) No flowback of solid particles.

(b) Defluidized zones or semi-fluidized zones in the vicinity of the distributor surface may have to be eliminated.

(c) Some means of good contact of gas with solid in the immediate vicinity of the distributor surface.

(d) Relatively fine immediate division of the gas in view of the small depths available for the process.

(e) Good distribution over a wide area.

(f) Possibly a low pressure drop during distribution: this will hold particularly for multi-stage systems.

The older methods of distribution used in Catalytic Cracker were not at all satisfactory for such work. As more recent work has shown the large orifices or slots give rise to relatively coarse bubbles. Further, patterns of wear inside reactors have shown that there is a relatively narrow expansion of gas from the perforation. This suggests a large area of relatively dead space for solid between the perforation, unless very many small orifices are drilled. Blanding(37) claimed a grid with openings small enough to prevent downward pass of particles.

To overcome most of the difficulties led to the suggestion of two alternative kinds of procedure. The first implied the use of some form of porous plate, either monolittic, or made of tiles, or built up by the use of a bed of loose immobile particles.

In a series of patents deriving from I.C.I., particularly those applied for after 1945, there is reference to the injection of gas through a "series of jets arranged in the bottom, or the bottom of the vessel may contain or consist of a suitably perforated or porous plate or plates through which the gas can pass. Alternatively, the bottom of the vessel may be perforated sheet or other suitable support for a layer or layers of granular material of regular or irregular shape, the weight of the granules being such that they remain substantially undisplaced by the stream of gas. When layers of granules are used it is preferable for the granules in the upper layers to be smaller than those in the lower layers."

Examples of this may be seen in the patent published by Arnold and Young and I.C.I.(38) which deals with the processing of hot carbonaceous

material; again it appears in the patent of Franklin and I.C.I.(39) which concerns the dehydration of gypsum. A later modification from I.C.I. comes in a patent specification which deals with the manufacture of phthalic anhydride by a dense-phase process(40). This specification states that "it is very desirable to ensure uniform distribution of the gas through the bed of particles, and this has usually achieved by supporting the bed of particles on a grid or plate of metal or of other material through which there are suitable orifices or perforations through which gas can pass. It has also been proposed to introduce the gases into processes of this nature through a porous plate. "In the claim is outlined the use of porous ceramic plate made by bonding refractory particles of uniform size with the minimum amount of clay; the plates are set in a metal frame. A number of these are set in the distribution plate.

Porous metal plates or ceramic plates are commonly used with bench-scale equipment, but they are not normally used in larger units because of their high cost and poor resistance to the high mechanical and thermal stresses in large units.

To avoid such kinds of difficulty it has become practice either to use the technique, already mentioned, of employing loose but immobile material, or to give better control, some form of bubble-cap or equivalent system.

1.4.1. Proposals for Nozzles, Bubble-Caps and Special Devices

Early thinking about fluidized catalytic cracking led to the attention to distribution. In a patent specification of 1940 Lewis and Gilliland(8) claimed shaped inlet ports for the distribution plate. These were to be cylindrical at the entry on the underside, expanding upwards, preferably with a 7° taper, with their upper ends in continuity, regularly spaced. Each opening would be substantially greater than the size of the normal particle.

To prevent penetration of particles on upward velocity is needed which is sufficient to prevent downward motion. The constriction will need a channel of some length to provide "braking" of incoming particles. The length of this channel appears to be dependent on the plate free area.

Pyzel(17) claims the opposite in a patent specification published recently. The grid is of arch form in cross section and it is formed with a multiplicity of closely spaced air passages which decrease in diameter upward, preferably with a taper of 1/4" to 1/2" per foot (about 6^{o}). This arrangement is claimed to be particularly suitable for materials which tend to agglomerate. The growth of agglomerate is obviated by the action of nigh velocity of gas streams entering the bed through the tapered passages in the grid. It is also claimed that the taper of the orifices prevents clogging of the orifices during periods of interrupted fluidization and facilitates bed discharge after shut down.

People investigating metal-smelting processes claimed vertical jets (41), inclined jets(42) and control of nozzle velocity by moveable grids (43). Also they claimed(44) "a multiplicity of substantially uniformly distributed, pressure reducing apertures" capped by what "may be conveniently termed a bubble-cap....."

Bubble-caps had already been claimed from within the oil industry (45) and there is a list(46) of such recommendations particularly for use with multi-bed fluidized systems.

A recent summary on bubble-caps in fluidization has been given by Vaněcek and Drbohlav(31). The bubble cap approach is related(i) to the need to overcome 'sifting' or flowback after shut down; and (ii) to multi-bed systems where solids blown form below should not block the distributor.

As already noted within the British chemical industry devices were proposed such as a "series if jets arranged in the bottom, or the bottom

of the vessel may contain or consist of a suitably perforated or porous plate or plates through which the gas can pass.

Much of the interest lay in the development of nozzles. This was particularly associated with the Dorr organization. Most of their processes concerned reactions of inorganic materials at relatively elevated temperature and, for this reason, they built their distribution plates of refrectory. The perforations were lined with alloy tubes to give reasonable strength. To avoid build-up of solid in the tube, a sharp-orifice was introduced(47).

1.4.2. Perforations, Nozzles and Equivalents which Diminish Solids Flowback

As already noted some important chemical plants in particular cat-crackers operate with high pressure ratios. The reason is the need to prevent flowback of solid particles through the perforations, which, otherwise, would lead to erosion of the perforations.

Zenz and Othmer(15) recommend that, to stop solids flowback, the velocity through the distributor orifices of a multi-orifice plate should be sufficient to produce a plate pressure drop of at least 40% of that across the bed. At those velocities, gas distribution is generally good. However, flowback may not be prevented when a fluid bed is run temporarily at a lower gas flow rate than the nominal one, or when a bed of heavy particles is operated at a relatively small grid pressure drop to minimize the cost of gas compression. For example, with iron ore fines, a grid pressure drop of only 10% of the bed drop has been used in industrial fluidized beds(24).

Sintered and porous plates have been used in bed driers but are prone to blinding of the pores through the presence of atmospheric dust, and even filtering the air will not prevent blinding. Also porous plates are expensive to operate. Porous ceramic plates have been used but

suffer from the additional disadvantages of poor resistance to mechanical and thermal shocks. Porous plastic plates can be used but not at high temperatures. Fabric or fine mesh is sometimes fitted over the top of an air distributor plate. This permits the use of larger orifices, therefore thicker and stronger sheets prevents the product from falling back during a shut down.

Pegging of the perforations sometimes occurs when product particle size and orifice diameter are similar. It can be prevented by making the orifices smaller than the particles, but with many products this would mean perforations too small for the plate to be made economically in material thick enough to give the necessary mechanical strength. Supporting grid bars will allow the use of thinner plate but it is still preferable to avoid very small perforations and in practice the distributor plate often has orifices appreciably larger than the particles.

1.4.3. Practical Development

Bubble-caps have just been noted. In multi-bed systems to operate at elevated temperature unsealed perforations in refractory materials are provided by inserting alloy tubes into vertical orifices.

An early suggestion to prevent flowback was the use of a ball-seal at the top of each tube. In the patent specification(42) is stated: "the diameter and number of cylindrical apertures is so chosen that under conditions of operation the pressure drop through the apertures will be 50 - 100% of the pressure drop of the bed above. This is done to cause the upflowing gas to distribute itself uniformly across the reaction vessel. The ball-seal itself did not work well in practice(48).

The next development(49) was a flat cap on the alloy tube below which radial holes were drilled. The holes were dimensioned to include an angle less than the angle of repose of the non-fluidized particles thereby preventing their flow out through the gas inlets.

Experience of this period showed that a number of people had developed or exploited versions of bubble-caps. One simple idea was to bore a standard hexagon-head bolt up the shaft and terminate the bore inside the head. Radial holes were then drilled from each flat to join the main shaft bore. The bolt would then be inserted head upwards in a hole in a suitable plate and fastened in position by a standard nut.

Another design of the same period made use of staggered perforated plates. A staggered plate consists of two successive sheets of perforated metal superimposed in such a way that perforations did not correspond and were displaced in such a way that non-fluidized solid would not flow. This required some maximum separation of the two plates. This type is convenient for industrial operation because it retains the advantages of the single plate - ease of design and construction coupled with good gas distribution(50). An alternative procedure was to use orifices which would not permit the passage of particles because of the exploitation of other principles. Porous plates and fine screens rely upon absolute 'bridging' of the orifices by individual particles. At least one early patent(37) claimed the use of a grid with openings small enough to prevent the downward passage of particles. Some recent recommendations have repeated such limits(51,52).

In 1952 it was becoming clear that vertical perforations might exceed in diameter the particle diameter by a factor not greater than five and prevent flowback by the formation of a multi-particle bridge(53). This principle was exploited in the patent of Gregory and Trees(54). It uses narrow horizontal slots formed by the overlapping of suitable metal strips held together with suitable spacers in such a way as to yield horizontally when undergoing thermal expansion or contraction. The dimensions of the slots are set, in the first place, to form bridges or arches so that solid will not flow back. Normally the gas velocity is

arranged to exceed the horizontal conveying of particles, and the extra feature of a substantial horizontal flow of gas to provide coverage of the total cross section.

Similar design appeared two years later in the specification(55) which also utilised strip construction, perforated baffles are placed below the grid; these baffles prevent the solids from flowing. The distance between the baffle and grid, the size of the holes in the baffle and grid, and the displacement of the hole centres between the grid and baffle are chosen so that the following condition should be fulfilled (Figure 1.1).

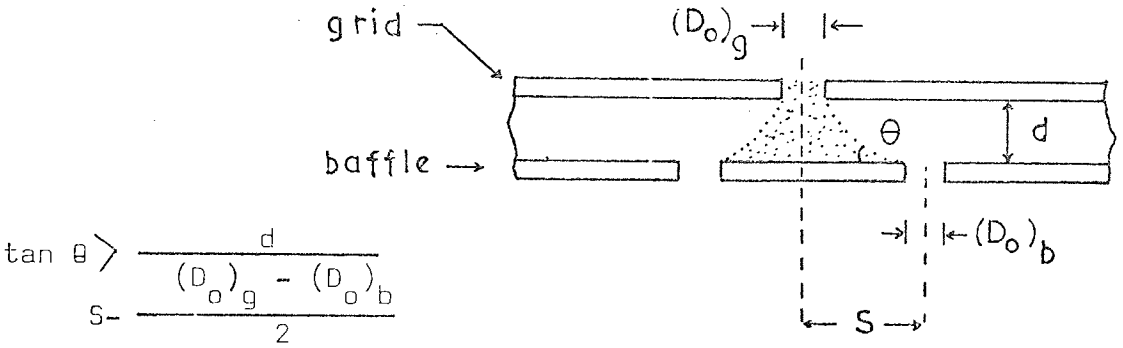

$$\tan\theta > \frac{d}{S - \frac{(D_o)_g - (D_o)_b}{2}}$$

Figure 1.1 Section of grid and baffle

Where θ is the angle of repose of the solids,

d is the distance between the grid and baffle,

S is the displacement of orifice centres,

$(Do)_g$ is the diameter of orifice in the grid,

$(Do)_b$ is the diameter of orifice in the baffle.

Similar ideas of design have recently appeared in a paper by Petrie and Black(56). The primary elements of their design are shown in Figure (1.2). The angle θ_1 is made greater than the angle of repose of the solid particles in the fluidized bed. In this way the occurrence

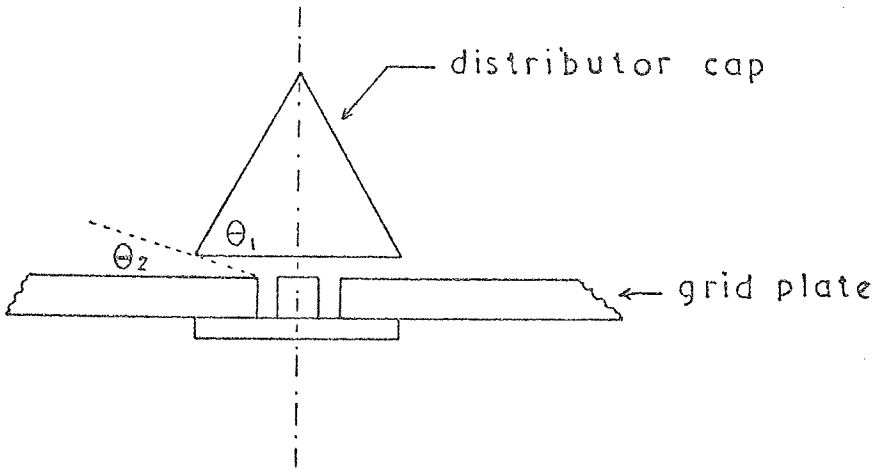

θ_1 > angle of repose of solids - for elimination of defluidized zones on cap.

θ_2 < angle of repose of solids - for complete elimination of solids flowback.

Figure 1.2 - A distributor design of Petrie and Black(56)

defluidized zones above the top of distribution cap as reported by Whitehead and Dent(27) and Kunii and Leverspiel(50) is avoided. The angle θ_2 is made smaller than the angle of repose so that under static conditions there is no sifting of material through the distributor. The spacing is chosen to give an injection velocity such that there is no possibility of particles being swept into the wind box, while the injection velocity is not high enough to cause serious particle attrition.

Two ideas should be noted for preventing build-up of solid in vertical perforations. White(19) added a thin orifice to the gas passage, as in the alloy insert previously mentioned. This apparently changed the particle flow-line, with suitable speeds, prevented build-up. Practical work(57) in the steel industry showed that countersinking from below to give a relatively sharp orifice at the top gave perforations less likely to block by bridging.

1.5. Effect of Distributor on Fluidized Behaviour - Studies in Small-Scale Equipment

As already pointed out, little systematic work has been reported on the influence of the bed support on fluidized behaviour, although many data have been collected by industry on the design of distributors for specific purposes, as noted already from the patent literature. This has not received much attention from the academic side and on the whole the books published on fluidization have not given much assistance in the development of the subject.

In recent years some progress has been made in evolving methods for the design of distribution plates. The same cannot be said about our real knowledge of some aspects of distributor behaviour, e.g. flowback behaviour of the distributor which received little attention in the past.

1.5.1. Survey of Previous Investigations

Most of these investigations have been carried out on bench-scale equipment using a variety of distributors and different conclusions have been drawn.

A summary of some of these investigations has been outlined recently by Geldart and Kelsey(58) who classify them into two types: (i) those related to hydrodynamic effects, e.g. effect of distributor on fluidization uniformity, density transients, bubble frequency and size, mixing and (ii) those aimed at establishing desirable operating conditions for a particular process, e.g. effect of distributor on conversion, heat transfer rates.

No attempt can be made here to go into the details of these investigations. We may only indicate some overall conclusion at which the authors have arrived.

1.5.2. Investigations Related to Hydrodynamic Effects

The period 1947 - 1951 saw the publication of many papers dealing with investigation of small-scale beds. Little precise information was published on the effect of different types of distribution device on bed behaviour. The best available was probably that of Agarwal and Storrow(59). Although it was on very small equipment, this paper by its simple and direct presentation of data shows pressure drops across the disc for support of the bed to vary over a very wide range relative to the bed pressure drop. It was shown that there was no difference in fluidization behaviour whether filter paper was used which had a high pressure drop relative to the bed drop or a coarse-pore sintered disc was used which had a low pressure drop relative to the bed.

Morse and Ballou(60) showed that the use of a fine-cloth distributor improved "smoothness" of fluidization over no distributor for as much as 16 in. above the distributor but that at higher levels the improvement was negligible. It was concluded that the effects of initially good distribution were lost in deep beds.

Some years later, Grosh(61) and Dotson(62) who studied density transients in fluidized beds confirmed the findings of Morse and Ballou(60). They also concluded that provided the bed height was not very small, it had no measurable effect on the behaviour of the bed near the distributor. However, it must be emphasised that their experiments were carried out in a small-scale fluidized bed. In contrast to those findings, Rowe and Stapleton(63) using a 12 in. diameter bed fitted in turn with a bubble-cap distributor, a conical distributor, and a porous plate concluded that the effect of distributor design on quality of fluidization extended over the total bed height, and that generally the benefit of a good gas distributor was not lost in a deep bed.

In a recent study, Fakhimi and Harrison(64) showed that the propor-

tion of total bed height affected by the distributor plate was dependent on the specific design of the plate (and in particular the spacing between the gas outlets in the distributor plate).

Geldart and Kelsey(58) commented on the use of porous distributors in fluidized beds and claimed that defluidized zones and tracks could exist even with porous plates and that they were not necessarily superior to other distributor designs. For any distributor of a given geometry, they found a definite pressure drop ratio ($\Delta P_D/\Delta P_B$) for successful operation of the bed and operation below this ratio would lead to instability in the bed.

However, the recent study by Hovmand et al.(65) has indicated that porous distributors would give better gas-solid mixing and hence better gas distribution.

1.5.3. Investigations Aimed at Establishing Successful Operating Conditions for a Particular Process

Grekel et al.(66) studied contacting efficiencies in a 7.8 in. diameter hydrocarbon synthesis pilot plant reactor. Five gas distributing devices were employed without bed internals, and one set of internals was tested. The first distributor was a 1 in. I.D. Pipe at the bottom of a 1.2 ft. long cone. The second was a multi-orifice plate with four orifices of 1/4 in. diameter and 4% free area. The third distributor was a multi-orifice plate with twelve orifices having the same free area as the four orifices. The last two were (a) a fine porous plate and (b) a glass cloth over wool packing.

In the following table the relative contacting efficiencies at 86% conversion of CO reacted for the five distributors used by Grekel et al.(66) are compared:

Catalyst mesh size	Distributor	Contacting efficiency,%
-100	Cone	70
-40	Cone	100
-90	4-orifice plate	109
-40	12-orifice plate	143
-40	12-orifice plate plus horizontal tube internals	225
-40	Porous plate	106
-40	Glass Cloth	115

The results show that the contacting efficiency is progressively increased by changing from a single cone entry to a multi-orifice plate and then increasing the number of the orifices. The trend of improvement in the direction of more orifices per unit area in the plate would indicate that the ultimate might be a porous plate for gas distribution. However, it would appear that the contacting efficiency of the porous plate or the glass cloth, as can be seen from the table, is not significantly higher than the cone entry under similar experimental conditions. Grekel et al.(66) gave no explanation, but indicated that the addition of bed internals with a 12-orifice plate resulted in the same conversion as with less than half the catalyst required with the 4-orifice plate and no internals. These findings are in rather strong contrast to those indicated by Volk et al.(67) that baffles were not a feasible method of increasing contacting efficiency. However, it must be emphasised that Volk et al.(67) in discussing reactor internals did not discuss the effect of distributor design.

Similar work has been carried out by Gomezplata and Schuster(68) who studied the effect of the distributor on the catalytic decomposition of cumene using two types of distribution plates, a porous plate and

screen mesh. Their conclusion was that the porous plate gave 30% more conversion than screen distributor, which has been observed to give coarser bubbles than the porous plate. The latter resulted in smoother fluidization and smaller bubbles, particularly at the distributor level.

Furthermore, Hovmand et al.(65), in a recent study of chemical reaction (the rate of conversion of ozone to oxygen in a bed of catalyst particles fluidized by the reacting gas) in a slugging bed 46.0 cm. diameter and 400 cm. high, have studied, with other factors, the influence of distributor design on conversion rate. The distributors employed were sintered plate and two multi-orifice plates of the same free area but different orifice diameter and spacing.

They concluded that with multi-orifice distributors, mal-distribution would have an important effect on conversion, particularly at low gas velocities. A sintered distributor plate, however, would give a better conversion than a multi-orifice distributor. It should be noted that the slugging conditions make comparison with other situations difficult.

If rate of decomposition of reacting gas on a solid catalyst depends on the extent of gas-solid mixing, then it would appear from their results that the porous plate had enhanced gas-solid mixing and gave better distribution. This is, obviously, in disagreement with Geldart and Kelsey (58).

If on the other hand the two multi-orifice plates are compared, we would find the one in which the given free area was divided into a large number of orifices closely spaced had resulted in a higher conversion rate than the one with small number of orifices widely spaced.

These results would seem to confirm the findings of Grek(69) who studied the effect of the geometrical characteristics of distributors on the uniformity of gas-solids mixing, using a number of multi-orifice plates of the same area but having different orifice diameter and spacing.

For a given flow rate, his experiments showed it is best to divide the free area into small orifices closely spaced for a more uniform mixing of gas-solid.

1.6. Factors Affecting Distributor Design - Development of Design Equations

1.6.1. Whitehead and Dent's Correlation

Whitehead and Dent(27) carried out elaborate studies on the performance of distribution plates in gas fluidized beds. In relatively large-scale column ranging from 1-64 $ft.^2$ in cross section sand was fluidized up to 4 ft. depth. Two gas-injection nozzles with horizontal discharge were employed: a lower gas efflux velocity and a high gas efflux velocity respectively. The pressure over these nozzles could be adjusted at will. By measurement and observation at the individual nozzles, the minimum gas velocity U_m, at which all the nozzles were operational could be determined.

The authors indicate that the criterion used does not imply homogeneous fluidization. For instance, gas flows per nozzle were not the same; also the bed pressure drop was not entirely equal to the bed weight, probably caused by local jetting and by-passing of the gas.

Whitehead and Dent were able to correlate their data for the minimum gas velocity by equating the distributor pressure drop change per operative nozzle with the bed pressure drop change per operative nozzle. The latter effect is caused by the defluidization of the bed above an inoperative nozzle and the consequence shrinkage of the total bed weight.

$$\frac{U_m}{U_{mf}} = 0.7 + \left[0.49 + \frac{10^{-7}(3.23\, N^{0.22}\, K_D \rho_s\, H_{mf})}{U_{mf}^2}\right]^{0.5} \qquad (1.1)$$

where $K_D = 60\, U\, \Delta P_D$, the gas flow factor and Δp_D is the distributor pressure drop.

Equation (1.1) shows that the minimum gas flow U_m required to achieve full operation of all nozzles is dependent upon the distributor pressure drop, number of nozzles, bed height and the density and the incipient fluidizing velocity of the solid phase.

Zuiderweg(29) used (1.1) to calculate the pressure drop ratio $\Delta P_D/\Delta P_B$ for the larger vessel, which turned out to be dependent on the fluidization velocity to be applied, and he showed

$$\frac{\Delta P_D}{\Delta P_B} = 0.012 \Big/ 1 - 1.4 \left(\frac{U_{mf}}{U_m}\right) , \qquad (1.2)$$

where U_m is the minimum velocity required to render all nozzles operative. Using this relationship, Zuiderweg was able to show that at $U_m/U_{mf} = 2.0$, the value of the ratio $\Delta P_D/\Delta P_B$ was only 4%, and at $U_m/U_{mf} = 8$ the ratio was even less, $\Delta P_D/\Delta P_B = 1.5\%$.

Some years ago Hiby(26) studied the distribution plate problem by artificially imposing a gas mal-distribution, in a small scale fluidized bed at conditions near to incipient fluidizing velocity, by having an independent air feed to a central section of the distribution and hence, by measuring the differential pressure between the two parts of the bed, to determine the relationship of the product of the fractional change of depth and the reciprocal fraction change of fluidizing velocity to the ratio of the critical pressure across the plate and the drop across the bed. Consequently, a criterion for designing a fluidized bed so that mal-distribution does not occur was deduced, i.e.

$$\left(\frac{\Delta P_D}{K\Delta P_B}\right) = \frac{UdH}{HdU} , \qquad (1.3)$$

where K is a factor dependent on the initial bed height and the fluidizing velocity.

Hiby considered the fluidized bed to remain stable when the decrease in local bed pressure drop as a result of change in local velocity was

overcompensated by an increased pressure drop across the plate. Thus the stability criteria, as have been derived by Zuiderweg(28), of Whitehead and Dent(27) and that of Hiby(26) can be compared as follows:

$$\left[\frac{\delta(\Delta P_B)}{\delta U}\right]_{\substack{\text{constant}\\ \text{gas flow}}} = -\frac{\delta(\Delta P_D)}{\delta N} \qquad \text{Whitehead and Dent} \qquad (1.4)$$

$$\left[\frac{\delta(\Delta P_B)}{\delta U}\right]_{\substack{\text{constant}\\ \text{number of orifices}\\ \text{on distributor}}} = -\frac{\delta(\Delta P_D)}{\delta U} \qquad \text{Hiby} \qquad (1.5)$$

The data obtained by Hiby indicated that for a multi-orifice or nozzle distributor the required pressure drop changes with fluidizing velocity are as follows:

$$\frac{\Delta P_D}{\Delta P_B} = 0.15 \quad \text{for} \quad \frac{U_m}{U_{mf}} \sim 1 - 2 \qquad (1.6)$$

and

$$\frac{\Delta P_D}{\Delta P_B} = 0.015 \quad \text{for} \quad \frac{U_m}{U_{mf}} \gg 1 \qquad (1.7)$$

This finding is in good agreement with that of Whitehead and Dent. In fact the two authors provide evidence that a high pressure ratio is needed only at the commencement of fluidization. Once the bed is freely moving the ratio can be smaller. Their argument clearly demonstrates that multi-orifice plates should be cheaper to operate in terms of power consumed. Gregory(2) emphasised that, with single-stage reactors, it is possible to start up with a shallow bed and build up the bed as the lower material is put into motion.

The work of Hiby(26) and Whitehead et al.(27) clearly recommends a low pressure drop ratio for design purposes. However, Guozedev and Colleagues(23) came to the opposite conclusions. But it is important to recognise the limitations attached to their work. In particular, it

refers to bubble caps in a vessel 20.5 cm. diameter, and the criterion of adequacy of performance was the index of mixing of sand and salt in a given time. On this basis they recommended that the pressure drop ratio $\Delta P_D/\Delta P_B$ should be no less than 1.25.

Rather moderate values have been reported by Deshpande et al.(34) The onset of slugging has been used as the main criterion of the performance of the system. One also must recognize the serious limitations of this work, as it was carried out in small diameter bed, and slugging rarely occurs in practice.

1.6.2. Jet Formation and Distributor Design - Zenz's Correlation

Zenz(70) made a study of single vertical jets issuing in a two-dimensional bed of cracking catalyst. As a first approximation, to provide a basis for calculating the orifice spacing in a commercial distributor, he measured the penetration p_j by visual observation and found the empirical equation,

$$\log_{10} (U_o \sqrt{\rho_g}) = 0.0144 \frac{P_j}{D_o} + 1.3 \qquad (1.8)$$

He also found by experiments that the resulting bubble had a diameter about half the length of the jet p_j. In order to avoid merging of bubbles simultaneously leaving the distributor, as it is important for the stable operation of the bed, he suggested a minimum orifice spacing:

$$S_{min} = \frac{3}{4} P_j \qquad (1.9)$$

By considering a 30% pressure drop criterion, he was able to relate the bed pressure drop ΔP_B to the ratio of orifice spacing to orifice diameter S/D_o, i.e.

$$\log_{10} (3.52 \sqrt{\Delta P_B}) = 1.3 + 0.0256 (S/D_o) \qquad (1.10)$$

For given values of ΔP_B, equation (1.10) gives the distributor orifice spacing to diameter ratios. These ratios are to be considered representative for multi-orifice distributor plates where jets issue vertically through the fluidized bed and when the bed contains no internal baffles which would restrict the natural growth of bubbles. Here, Zenz recommended the 30% pressure drop criterion for design purposes. The use of this figure is probably derived from his own experience, but a 10% criterion has been found to be a workable figure for multi-orifice distributors. In any case the experiments of Chapter 3 have indicated that the pressure drop criteria are determined by the bed aspect ratio (height/diameter), a fact which appears to be disregarded by Zenz(70).

1.6.2. Distributor Design from Theory - Fakhimi and Harrison's Model

Fakhimi and Harrison(64) recently studied the design problem of distributors in gas fluidized beds. They derived a theory for predicting the performance of a multi-orifice distributor, supported by experiments on a two-dimensional bed. The theory was based on the observation that at gas velocities above U_{mf} a spout is formed above certain orifices and that bubbles are generated from the top of each spout. Spouting orifices were termed as operative orifices and the remainder were termed as non-operative orifices. They equated (i) the pressure drop through an operative orifice plus the spouted bed above with (ii) the pressure drop through a non-operative orifice plus the static bed above. This represented a balance of pressure given by the expression

$$\Delta P_S + \Delta P_{d1} = \Delta P_{d2} + \Delta P_{mf} \quad , \qquad (1.11)$$

where ΔP_s = pressure drop over a spouted bed of height Z,
the height of entrance region immediately above
the plate.

ΔP_{mf} = pressure drop across a fixed bed of height Z at incipient fluidization.

ΔP_{d1} = pressure drop through an orifice at gas flow rate above incipient fluidization.

ΔP_{d2} = pressure drop through an orifice at incipient fluidization.

(A similar approach was pursued by Zabrodsky(73) when he considered the distribution plate problem, but probably, by mistake, the term Δp_s has been omitted from his equation (1.46).

In this way, Fakhimi and Harrison obtained the number of operative orifices n as a fraction of ghe total number of orifices N in the distributor:

$$\frac{n}{N} = \frac{(U - U_{mf})}{(u_{mf}^2 + (2\phi^2/\rho_f)\cdot(\Delta P_{mf} - \Delta P_s))^{\frac{1}{2}} - U_{mf}} \qquad (1.12)$$

Where ϕ is the fractional free area and ρ_f is the fluid density. The height of the entrance region immediately above the distributor is defined as Z, it is the height of each spout and the static bed above each inoperative orifice. Z is related to S, the orifice spacing. Fakhimi and Harrison(64) found $\frac{Z}{S} = 3.8$ for two dimensional beds with U just above U_{mf}.

The pressure drop over a spouted bed of height Z is given by

$$\Delta P_s = 2\rho_s\cdot(1 - e_{mf})g\cdot Z/\pi \qquad (1.13)$$

and the pressure drop over a fixed bed of height Z and voidage e_{mf}, at U_{mf} is

$$\Delta P_{mf} = \rho_s\cdot(1 - e_{mf})\cdot Z\cdot g \qquad (1.14)$$

where ρ_s is the density of solid particles.

Using (1.13) and (1.14) in (1.12) gives

$$\frac{n}{N} = \frac{(U - U_{mf})}{\left[U_{mf}^2 + 0.727(1 - e_{mf}).g.(\frac{\rho_s}{\rho_f}).\phi^2.Z\right]^{\frac{1}{2}} - U_{mf}} \qquad (1.15)$$

This is another form of equation (1.12) suggested by Fakhimi(74).

For a given system, with known gas and particles properties and known plate characteristics, equations(1.12) and (1.15) have the form

$$\frac{n}{N} = K(\frac{U}{U_{mf}} - 1) \qquad (1.16)$$

where K is constant for a given gas-solid/distributor system. Thus $\frac{n}{N}$ is a linear function of $\frac{U}{U_{mf}}$.

The above theory shows that for larger values of U_{mf} a smaller U/U_{mf} is required to render all orifice operative. Similarly, the theory predicts that for larger values of ϕ larger values of U/U_{mf} are required for full operation. It also predicts that for a given operating conditions and equipment $\frac{n}{N}$ is a function of $1/\sqrt{S}$, since Z is a function of S. Therefore, according to theory for a given free area better gas distribution is achieved by using a large number of small orifices closely spaced than a few large orifices widely spaced. The theory finds support from the work and conclusions of Grek(69), Yufa(71) and Hovmand et al.(65).

Some Comments on Theory

Fakhimi and Harrison(64) in deriving their model treated Z as a constant (always $Z/S = 3.8$) for a given solid distributor system. Probably Z would not remain constant once U exceeds U_{mf} and in particular with solids having very low U_{mf}. Hovmand et al.(65) referred to the use of lower values of $\frac{Z}{S}$ at higher gas rates and a value of $\frac{Z}{S} = 2$ was recommended for a three-dimensional bed system. In the present work experiments were carried out (See Chapter 5) in order to examine the

applicability of the theory to other solids, as the work of Fakhimi and Harrison was confined to sand particles only. The experimental results are presented in Chapter 5 which shows a non-linear dependence of $\frac{n}{N}$ on $\frac{U}{U_{mf}}$, thus deviating from equation (1.15). The deviation appears to be most pronounced with cracking catalyst (having low U_{mf}). When Z was treated as a variable (i.e. Z = f(S,U) in (1.12) or (1.15) closer agreement with theory was obtained. This may be attributed to the fact that cracking catalyst is difficult to defluidize. Qualitative observations with 106 μ catalyst showed that

(i) Some orifices were not spouting but forming bubbles immediately above the surface of the distributor.

(ii) Defluidized zones which were observed with other solids appeared to be semi-fluidized with catalyst. These diminished very rapidly with gas flow rate.

(iii) Some orifices remained inoperative and persisted to a higher gas flow rate.

(iv) The experiments failed entirely when these were repeated with unsieved catalyst (having wide size range, 20 - 150 μ). Experiments showed a considerable deviation from theory. It was found that in order to render at least 50% of the distributor orifices operative, it required a gas rate about an order of magnitude higher than what (1.15) predicts. Full operation was found rather difficult to achieve because of the excessive amount of gas required and the considerable carry over of fine particles.

In conclusion some doubt may be felt over this theory with respect to its application to solids with low U_{mf}, but the matter still remains to be clarified.

1.7. Advantages and problems of Multi-Orifice Distributors

Multi-orifice distributors have been used industrially because of their economic and technical advantages over other types of contacting devices: simplicity of design, relatively low pressure drop, and the possibility of high flow rates. Their use in multi-stage systems where they act both as gas distributors and stage separators has proved to be cheap and effective (20,75), thus reducing the overall height of the equipment by eliminating overflow pipes and downcomers provided that solids control can be adequately achieved without these extra devices.

From the viewpoint of fluidization uniformity, multi-orifice distributors may be better than cap-distributors, since they give more uniform and stable gas streams and have all the consequent advantages. Gas streams passing through the orifices are directed vertically into the solid phase to be fluidized, and not in a partly lateral direction as with the bubble-cap type. Multi-orifice plates are cheap, easy to clean and provide self-emptying beds, advantages which gas distributor plates with capped nozzles lack. For gaseous applications it is perhaps the best form of distributor particularly for drying, absorption and desorption processes (22).

The multi-orifice plates can be made to suit each specific process requirement. The orifices usually are in the size ranging from 0.15 up to 2.5 cm. and the free area is from 1% to 3%. The plates are generally available in two basic varieties, depending on the orifice diameter: (i) plates with a large number of small orifices, and (ii) plates with a small number of large orifices. In the first of these, however, the orifices are frequently blocked by particles (especially after a temporary interruption or reduction in the gas flow). This design, as already noted, has the advantages of giving better gas distribution and good gas-solid mixing.

Clogging of the orifices can be overcome by making the orifices large enough in comparison with the solid. It has been reported(51) that the diameter of the orifices should be at least ten times larger than particle diameter, and with a polydisperse mixture, at the most twice the diameter of the largest particles(52).

The second design has two undesirable characteristics: (i) the problem of defluidized zones and (ii) the problem of solids flowback.

1.7.1 The Problem of Defluidized Zones

One of the serious drawbacks of this type of distributor is the formation of defluidized zones in the space between the orifices. The solid phase in these regions remains completely immobile. For materials that tend to agglomerate on these zones, even when small, may grow after prolonged operation resulting in distributor blockage and thereby hindering fluidization. This subject received little attention in the past. In the present work, defluidized zones have been studied experimentally (see Chapter 5). Previous work on defluidized zones is also discussed in Chapter 5.

1.7.2 The Problem of Solids Flowback

With this type of distributor particles are apt to flow back through the orifices when the gas flow is temporarily reduced or after shutdown. This is particularly serious with single-bed systems since the presence of solids below the distributor can cause severe erosion and lowers fluidization efficiency. When the gas velocity is too low there will be a tendency for the solid particles to fall through the orifices in the plate. There is also a tendency for some particles to fall through the plate even if the velocity of the gas is high enough to blow particles out of the bed. This phenomenon, has been observed even at average orifice velocities one hundred times greater than the particle free-fall velocity(15). The reason for this is not well understood, but it is

thought to result from some sort of eddy current effect produced just above the distributor plate or from local pressure surges.

As we noted earlier, various kinds of nozzles and bubble-caps are used industrially to prevent solids flowback. The above devices may also improve the regularity of gas distribution, but because of intense erosion at the plate level and high energy cost, multi-orifice plates are still widely used.

Flow back in gas fluidized beds is a subject which has received little attention in the past. It has been neglected to the same degree as defluidized zones on the distributors have been neglected. In the literature there is little reported work on solids flowback. Gregory(2) studied the problem and as he shows in his paper, flowback as a function of gas flow rate passes through a maximum. Probably a low leakage rate at low gas velocity is due to bridging of the solids, an effect which causes the behaviour of fluidized bed distributor plate to be quite different from that of distillation plates with which Gregory compares it.

Recent work by Serviant et al.(76) on solids flowback through single-orifice plates revealed two types of orifice flowback, namely weeping and dumping. These terms are associated with gas liquid systems where they describe the leakage of liquid from sieve plates counter-current to the flow of gas. In distillation, dumping is generally referred to as heavy weeping. In fluidized beds weeping and dumping are not yet understood clearly. However, since the incipiently fluidized bed behaves so much like a liquid, it seems reasonable to suppose that the rate of solids flowback through the orifices of the distributor should occur in the same way as for liquid on sieve plates. Despite the uncertainty about liquid leakage from sieve plates, it is possible to gain some partial insight into the likely behaviour by using this analogy.

The present author(77), who previously carried out some preliminary

studies on flowback, discussed the analogy between gas-liquid and gas-solid systems. Gregory(2) also discussed this at length and listed possible weaknesses in the analogy, these are

(i) The solid particles do not flow as freely as liquid over the whole range of aeration.

(ii) In the fluidized bed there is no surface tension between gas and solid, and gas can interchange freely between the bubble phase and the emulsion phase, thus permitting bubble growth.

(iii) Fluid particles differ from solid particles in that they may change their shape as they fall and this modifies their behaviour.

1.7.3. Flowback in Gas-Liquid Systems

Numerous papers have been published for liquid flowback (or weeping) in gas-liquid systems. The summary of some of these can be found in the book by Van Winkle(78), but the most satisfactory theoretical study of the problem has been that of Jameson and Kupferberg(79,80) and McCann and Prince(86).

Jameson and Kupferberg(79) attribute liquid flowback to a pressure gradient in the wake of a bubble leaving the orifice. It was suggested that this pressure whose approximate magnitude can be calculated from the potential theory, is responsible for the phenomenon of liquid leakage or weeping on sieve trays. Thus when a bubble forms and rises from an orifice in a distributor in a gas fluidized bed, it may lead to pressure gradients which force particles downward through the orifice in the same way as liquid weeps. By a similar method, McCann and Prince(86) have successfully predicted, for a single orifice plate, the pressure fluctuations underneath the orifice, the size and frequency of the bubbles, flowback rate and weep point, assuming that the bubbles remain spherical during formation and weeping.

In a recent paper, Kupferberg and Jameson(80) have extended their

analysis to a multi-orifice system. A simplified model for the behaviour of a multi-orifice plate has been derived which enables calculation of the bubble size provided the frequency of pressure fluctuations in the wind box can be predicted. They showed that dumping (or weeping) through multi-orifice plates at low gas rates was caused by hydrostatic loss and suggested a criterion for the minimum gas velocity necessary to stop dumping. This hydrostatic loss is initiated within the bubble as it rises in the liquid and this can lead to negative residual heads, which causes liquid leakage through the orifices. They postulated that unless the dry plate pressure term $\rho_g K U_o^2$ is large, the hydrostatic loss $\rho_\ell g h$ will cause a negative pressure in the wind box for a considerable portion of the period of the bubble growth so that as soon as the bubble detaches there is a pressure gradient in the liquid which can cause flow through the orifice. In this way, Kupferberg and Jameson derived a criterion for the prevention of liquid flowback defined by a "dumping number":

$$N_d = \frac{\rho_g K}{\rho_\ell} \cdot \left[\frac{2\ U_o^2}{g.D_o}\right]^{0.8} \geq 1.11 \qquad (1.17)$$

and the minimum desirable orifice velocity to prevent liquid flowback is

$$U_o \geq \left[\frac{1.11\rho_\ell}{\rho_g K}\right]^{\frac{5}{8}} . (g.D_o/2)^{\frac{1}{2}} \qquad (1.18)$$

Where K is an empirical coefficient.

Therefore the important factors influencing the limiting orifice velocity are the properties of gas and liquid and the plate design. Thus, in fluidised beds, U_o is also expected to be influenced by the physical properties of gas and solid and plate geometry.

CHAPTER TWO

2. DETERMINATION OF INCIPIENT FLUIDIZING VELOCITY OF SOLID PARTICLES

This chapter is concerned with the determination of the incipient fluidizing velocity U_{mf} since many of the subsequent calculations depend on an accurate knowledge of this velocity.

2.1 Definition

The incipient fluidizing velocity required for a given bed of solids is that superficial mass velocity which is sufficient to buoy completely all of the solid particles within the bed so that any particle is just able to move relative to the bed.

Under these conditions the pressure drop over the particles comprising the bed is given by:

$$\Delta P_{Bt} = H_{mf} \cdot (\rho_s - \rho_f) \cdot g \cdot (1 - e_{mf}) \qquad (2.1)$$

where

g = acceleration due to gravity, cm/sec^2.

ρ_s = density of particles, gm/cm^3.

ρ_f = density of fluid, gm/cm^3.

H_{mf} = incipient bed height, cm.

ΔP_{Bt} = theoretical bed pressure drop, $dynes/cm^2$.

e_{mf} = bed voidage at incipient fluidization, -.

For gas-solid systems $\rho_s \gg \rho_f$, then (2.1) can be written with adequate accuracy as

$$\Delta P_{Bt} = H_{mf} \cdot \rho_s (1 - e_{mf}) \cdot g \qquad (2.2)$$

which is approximately equal to the weight of particles comprising the bed divided by its cross-sectional area.

As the incipient fluidizing velocity cannot be estimated with sufficient accuracy from a visual observation of the bed, it is generally determined from the experimentally found dependence of the pressure drop on the superficial velocity of the fluid. The plot of this relationship

changes direction sharply at incipient fluidization, because the pressure drop across a fluidized bed, contrary to that of a fixed bed, does not depend on the velocity of the fluid. With further increase in gas velocities beyond incipient fluidization the pressure drop remains practically unchanged as long as particle entrainment is prevented.

Incipient fluidizing velocities of diverse materials have been determined by many authors, and from these results a number of empirical relations for the estimation of the incipient fluidization U_{mf} have been established.

A widely used semi-empirical correlation for the prediction of gas velocity at incipient fluidization is that due to Leva(81):

$$U_{mf} = (0.0007\ R_{e_{mf}}^{-0.063})\ \frac{g.\ D_p^2.\ (\rho_s - \rho_f)}{\mu_f} \qquad (2.3)$$

where

U_{mf} = incipient fluidizing velocity, cm/sec.

g = acceleration due to gravity, cm/sec^2.

D_p = mean particle diameter, cm.

ρ_s = density of particles, gm/cm^3.

ρ_f = density of fluid, gm/cm^3.

μ_f = viscosity of fluid, gm/cm.sec.

and

Re_{mf} = particle Reynolds number at U_{mf}, i.e.

$$Re_{mf} = \frac{U_{mf}.\ D_p.\ \rho_f}{\mu_f}$$

Davidson and Harrison(82) derived from theory the following expression for incipient fluidizing velocity:

$$U_{mf} = 0.00114\ \frac{g.D_p^2\ (\rho_s - \rho_f)}{\mu_f} \qquad (2.4)$$

The derivation of this expression was based on Carman's equation, by using the voidage at the point of incipient fluidization ϵ_{mf} and assuming the pressure drop to be equal to the weight per unit area of particles. Davidson and Harrison assumed that the particles at incipient fluidization set themselves in the loosest possible mode of packing at which individual particles remain in contact with each other. For spherical particles this would be the cubic mode of packing and the voidage at incipient fluidization is given by

$$e_{mf} = \frac{1}{6}(6 - \pi) = 0.476 \qquad (2.5)$$

Rowe(83) derived an expression similar to that given by Leva(81) based on the results of experiments in which the drag forces on a single sphere in isolation and in an array of the same spheres were measured. His results showed that the force on the single sphere in the array was approximately 68.5 times the force on an isolated sphere at the same superficial velocity of fluid. Rowe then applied this result to fluidized beds and obtained the expression

$$U_{mf} = 0.00081 \frac{D_p^2 . (\rho_s - \rho_f).g}{\mu_f} \qquad (2.6)$$

As Re_{mf} ranges from 10^{-2} to 10^{2} for most fluidized systems, $Re_{mf}^{-0.063}$ in Leva's correlation is of order unity and therefore (2.3) is very close to (2.6).

In the present work, the experimental results have been correlated by a semi-theoretical equation analogous to Rowe's expression.

2.2 Experimental Equipment

The equipment used in the experimental work is shown schematically in Figure (2.1). The fluidization column is a 45 cm. length of 9 cm. inside diameter glass tube with a wall thickness of 0.3 cm. The fluidizing gas was air taken from 80 p.s.i.g. main and reduced to 20 p.s.i.g. by a pressure reducing valve. This was fed into an inlet manifold which supplied a bank of variable area flow meters. The outlet manifold was connected via a valve to the fluidized bed wind box. Figure (2.3) is a photograph showing the general arrangement of the equipment.

The flow meters were a range of metric type rotameters two of which were suitable for small gas flows. With this arrangement, it was possible to meter flows between 10 $cm.^3/sec.$ and 1.50×10^3 $cm.^3/sec.$

The flow to each meter was finely controlled by its own needle valve which also served to isolate any meter not in use. The needle valve at the inlet to the fluidized bed enabled the meters to be operated under pressure if it was found necessary to increase their range and to reduce float oscillation.

2.3 The Distributor Section

The bed distributor section is shown in Figure (2.2). This consisted of a section packed with 10 mm glass beads and 0.476 cm. (3/16") thick Vyon disc (a porous plastic material obtained from Porous Plastic Ltd.). Pressure tappings consisted of three holes at 120 deg. to each other were drilled on the porous plate. Short lengths of 3/32" I.D. copper tubing were glued into each of these tappings and then covered with a patch of 350 mesh stainless steel gauze (flush with the surface) to prevent solid particles entering the pressure tappings. The tappings were connected to a wall-type manometer filled with coloured water via a manifold using p.v.c. tubing. This was intended to obtain a reliable measure of the bed pressure drop. These tappings created a dead patch approximately 0.13%

of the total distributor area. The effect of this dead patch was only visually apparent for initial bed heights 4 cm or less.

A recess was turned in the duralumin bases and the distributor was assembled as shown in Figure (2.2). Earlier designs had an additional flange to assist in changing distributors, but this was unnecsssary once the type of distributor had been chosen. In order to ensure that the experimental results were not influenced by the bed diameter and type of distributor, some of the particles were fluidized in the 14 am diameter column described in Chapter three using multi-orifice distributors. However, no differences were detected (see Figure (2.6)).

2.4 Particles

A variety of materials was investigated. In Table (2.3) these materials are listed and characterised by the particle density, the void fraction of the settled bed, the shape factor and roundness factor of the individual particles and by the mean particle diameter D_p, calculated by:

$$D_p = \frac{1}{\sum \frac{x_i}{d_{pi}}} \qquad (2.7)$$

where x_i is the weight fraction of particles with diameter d_{pi}. The physical properties of the solid particles were determined by methods described in Appendix A2.

2.5 Experimental Procedure

Known weights of particles were loaded into the column to give static beds of various depths. Before readings were taken the beds were vigorously fluidized, and then defluidized very slowly. The settled bed height was recorded as the incipient bed height H_{mf}. Then the velocity was increased gradually from zero and readings of bed pressure drop were taken at intervals. The pressure drop across the bed was measured directly from the three pressure tappings located on the distributor plate.

2.6 Experimental Results

The results for pressure drop have been plotted logarithmically as in Figures (2.4) - (2.6). In Figure 2.4, for example, it will be noted that the pressure drop does not equal the weight per unit area of bed until a gas velocity of 0.7 cm/sec. is reached even though the bed appeared to be well fluidized at lower velocities. This shows that fluidized and fixed bed regions are present simultaneously in the bed over a range of gas velocities. Following Godard and Richardson(84), the point of intersection of the straight lines drawn respectively through the fixed bed and fluidized zones has been taken to give the incipient fluidizing velocity U_{mf}, and consistent values have been obtained for different bed heights.

2.7 Correlation of Experimental Results

Following the approach of Davies and Richardson(85), the incipient fluidizing velocity U_{mf} can be predicted approximately by assuming that at the point of incipient fluidization the drag force on the particle is equal to its weight, and that it is a constant (C_D) times the drag force on an isolated particle at the same superficial velocity. When Reynolds number is low, Stocke's law applies, and therefore

$$C_D \cdot 3\pi \cdot \mu_f \cdot D_p \cdot U_{mf} = \frac{\pi}{6} \cdot D_p^3 \cdot (\rho_s - \rho_f) \cdot g \qquad (2.8)$$

assuming particles are spherical. Thus

$$C_D = \frac{D_p^2 \cdot (\rho_s - \rho_f) \cdot g}{18 \mu_f \cdot U_{mf}} \quad , \qquad (2.9)$$

where C_D is a coefficient analogous to that obtained by Rowe(83) and may be defined as the ratio of the drag force on a single particle in an array to the drag force on a single particle in an infinite medium at the same superficial velocity.

Values of C_D obtained from the present experimental results are given in Table (2.2). These values may be compared with the value of 68.5 ob-

tained by Rowe(83) for the drag force of a single sphere in an array. Taking an average value of 72.12 for C_D, the incipient fluidizing velocity is given by

$$U_{mf} = 0.00077 \frac{D_p^2 . (\rho_s - \rho_f) . g}{\mu_f} \qquad (2.10)$$

which is reasonably close to (2.3) and (2.6). Davies and Richardson(85) also give similar expression for small particles.

2.8 Comparison of Experimental Results and Theory

In the following table (Table 2.1) we present a comparison of the experimental results and the theoretically predicted values for all solids tested.

Where ΔP_{Bt} = theoretical fluidized bed pressure drop predicted using (2.2),

$\Delta P_{Bt/Eq}$ = fluidized bed pressure drop calculated from bed weight,

ΔP_{BM} = fluidized bed pressure drop measured,

$U_{mf/M}$ = incipient fluidizing velocity measured,

$U_{mf/K}$ = incipient fluidizing velocity predicted using(2.10),

$U_{mf/DH}$ = incipient fluidizing velocity predicted using(2.4),

$(U_{mf/DH})_{corrected}$ = incipient fluidizing velocity predicted using(2.12).

The experimental results indicates that expression (2.10) is more satisfactory for the prediction of the incipient fluidizing velocity U_{mf} than the theoretical expression presented by Davidson and Harrison(82). We note that the equation of Davidson and Harrison is reasonably accurate for small particles, but that the difference between the predicted and the measured values is greater than the difference between the present correlation and the measured values for large particles. These observations reinforce the conclusion of Davidson and Harrison(82) that the only way to obtain U_{mf} accurately is to measure it.

TABLE (2.1)

Comparison of Experiment and Theory

Particles	D_p,μ	e_{mf}	H_{mf} cm.	Bed.wt $W_B \cdot g_m$	ΔP_{Bt} cm.H_2O	$\Delta P_{Bt/eq.}$ cm.H_2O	ΔP_{BM} cm.H_2O	$U_{mf/DH}$ $^{-1}$ cm.sec	$U_{mf/K}$ $^{-1}$ cm.sec	$U_{mf/M}$ $^{-1}$ cm.sec	$(U_{mf/DH})$ corrected
Coal	128	0.63	30.3	944	15.1	14.8	14.2	1.36	0.92	0.944	0.72
Catalyst C_1	74	0.43	32.7	1042	17.1	16.4	15.95	0.310	0.210	0.284	0.164
Catalyst C_2	106	0.41	32.1	1008	17.6	15.86	15.30	0.638	0.432	0.455	0.336
Diakon	281	0.40	35.1	1543	24.6	24.20	23.50	5.72	3.86	3.25	3.02
Glass G_1	84	0.422	26.8	2656	41.8	41.7	40.6	1.18	0.80	0.95	0.623
Glass G_2	120	0.383	26.9	3018	46.8	47.3	46.0	2.52	1.70	1.426	1.34
Glass G_3	237	0.419	28.0	7049	47.5	44.9	44.8	10.30	6.97	7.00*	5.45
Sand S_1	177	0.424	25.9	2345	37.9	36.9	36.1	5.14	3.48	3.60	2.71
Sand S_2	277	0.40	25.0	2400	39.6	37.8	37.1	12.56	8.50	8.10	6.62
Sand S_3	138	0.455	29.6	2676	42.6	41.9	40.8	3.10	2.095	1.95	1.63
Sand S_4	224	0.422	27.8	6580	42.5	42.9	41.8	8.22	5.56	5.70*	4.39

* Multi-orifice distributor - 14 cm.diam. bed.

It should be noted that the deviation noted by Davidson and Harrison which led them to suggest that the only satisfactory way of arriving at values of U_{mf} was by measurement may in fact arise from the use of an unsatisfactory model.

In deriving(2.4), Davidson and Harrison assumed the cubic mode of packing for predicting the bed voidage at the point of incipient fluidization. However, Gregory(57) postulates that the closest regular packing at which it is possible for individual particles to move relative to others that are in the bulk is when particles take the orthorhombic mode of packing, i.e.

$$e_{mf} = \frac{1}{3\sqrt{3}} \left(3\sqrt{3} - \pi \right) = 0.3954 \qquad (2.11)$$

Applying (2.11) instead of (2.5) in the analysis pursued originally by Davidson and Harrison, a new expression for the incipient fluidizing velocity is obtained, i.e.

$$U_{mf} = 0.00060 \frac{D_p^2 . (\rho_s - \rho_f) . g}{\mu_f} \qquad (2.12)$$

which appears to be reasonably close to the present correlation although on the lower side. In the last column of Table (2.1) values of U_{mf} have been recalculated using (2.12) which indicates possibly better agreement with experiments. With large particles, the deviation between experiments and theory is largely reduced.

The $(U_{mf/DH})_{corrected}$ which is based on the orthorhombic mode of packing is likely to provide the lowest possible value and to hold best for perfect spheres. A check of the data in Table(2.1) shows that the rounded particles approach the $(U_{mf/DH})_{corrected}$ value more closely.

TABLE (2.2)

Particles	Particle diam. D_p, cm.	Particle density ρ_s, gm.cm^{-3}	U_{mf} measured cm.sec^{-1}.	C_D calculated
Coal	0.0128	1.35	0.944	71.0
Catalyst C_1	0.0074	0.915	0.284	53.50
Catalyst C_2	0.0106	0.915	0.455	70.65
Diakon	0.0281	1.167	3.450	85.70
Glass G_1	0.0084	2.70	0.950	60.80
Glass G_2	0.0120	2.82	1.426	86.30
Glass G_3	0.0237	2.925	7.00	71.20
Sand S_1	0.0177	2.64	3.65	70.0
Sand S_2	0.0277	2.64	8.10	76.0
Sand S_3	0.0138	2.63	1.95	77.8
Sand S_4	0.0224	2.64	5.70	70.4

Mean Value of C_D = 72.12

TABLE 2.3

Characteristics of Solid Particles

Material *	Mean particle diam. D_P, μ	Particle density ρ_s, gm.cm^{-3}	Bulk density ρ_B, gm.cm^{-3}	Voiad fraction e_{mf} -	Shape factor λ_s, -	Roundness factor λ_r, -	Geometric Description
Coal	128	1.35	0.49	0.63	0.70	0.20	Angular
Cracking Catalyst C_1	74	0.915	0.532	0.43	0.866	0.51	Rough nearly round
Cracking Catalyst C_2	106	0.915	0.54	0.41	0.852	0.468	Rough nearly round
Diakon	281	1.167	0.696	0.40	1.0	1.0	Smooth, spherical
Glass beads G_1	84	2.70	1.560	0.422	1.0	1.0	Smooth, spherical
Glass beads G_2	120	2.82	1.74	0.383	1.0	1.0	Smooth, spherical
Glass beads G_3	237	2.925	1.70	0.419	1.0	1.0	Smooth, spherical
Glass beads G_4	270	3.00	1.79	0.40	1.0	1.0	Smooth, spherical
Silver sand S_1	177	2.64	1.52	0.424	0.725	0.20	Angular
Silver sand S_2	277	2.64	1.58	0.40	0.73	0.22	Angular
Rounded sand S_3	138	2.63	1.44	0.455	0.83	0.51	Round
Ungraded silver sand S_4	224	2.64	1.55	0.422	0.74	0.226	Angular

* Except where otherwise indicated, the above materials are closely graded.

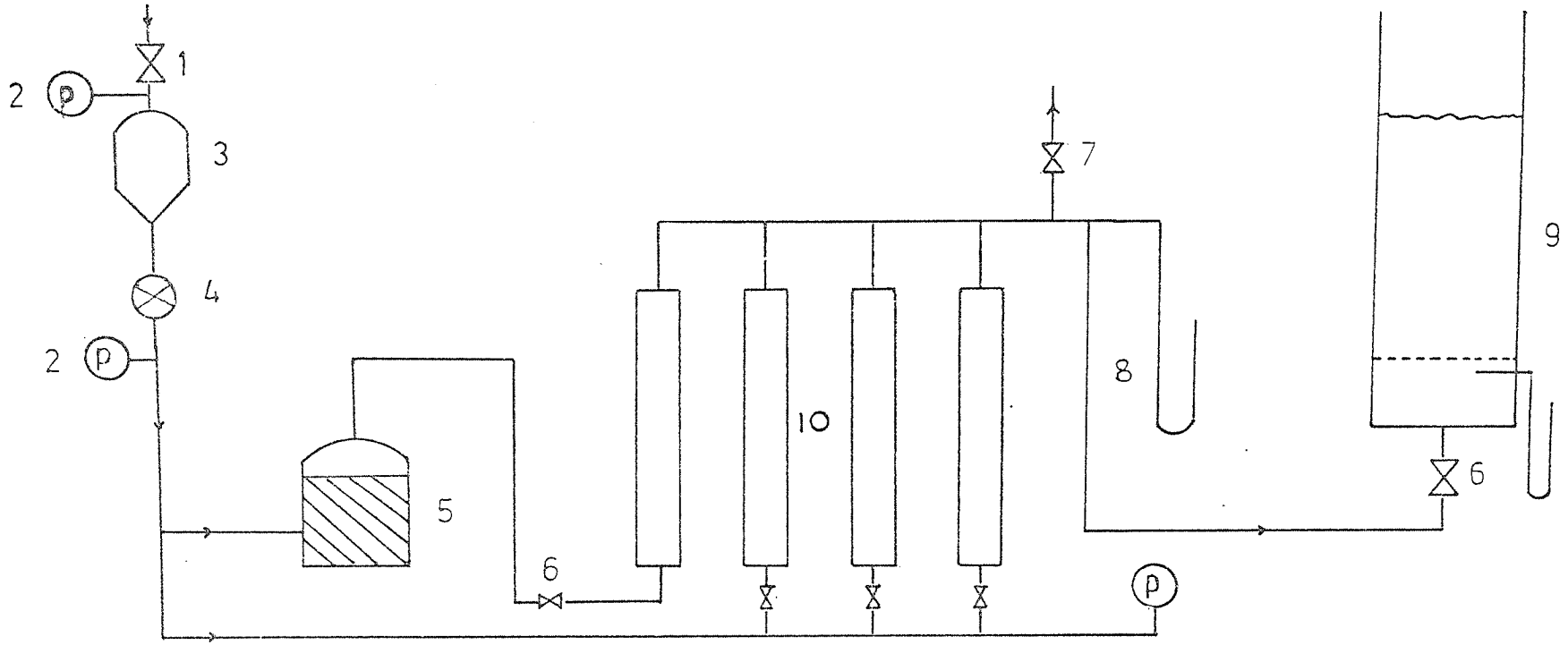

1 MAIN AIR VALVE
2 PRESSURE GAUGE
3 150 PSIG NORGN. AIR FILTER
4 PRESSURE REDUCING VALVE
5 HUMIDIFIER (OPTIONAL)
6 NEEDLE VALVES
7 FINE CONTROL
8 MANOMETERS
9 FLUIDIZATION COLUMN
10 FLOW METERS

FIG. (2.1) SCHEMATIC DIAGRAM OF EQUIPMENT

Fig. 2·2 Details of distributor section

(All dimensions in centimetres. Scale: $\frac{1}{2}$ full size)

List of Materials

A Duralumin
B Glass
C 10 cm. diam. copper tube
D 0·95 cm. diam. copper tube
E 0·65 cm. diam. copper tube
F Wire gauze
G 0·16 cm. thick rubber gasket
H Vyon disc *
I Araldite
J 6 x 0·8 cm. diam. bolts

* Pressure tappings are not shown.

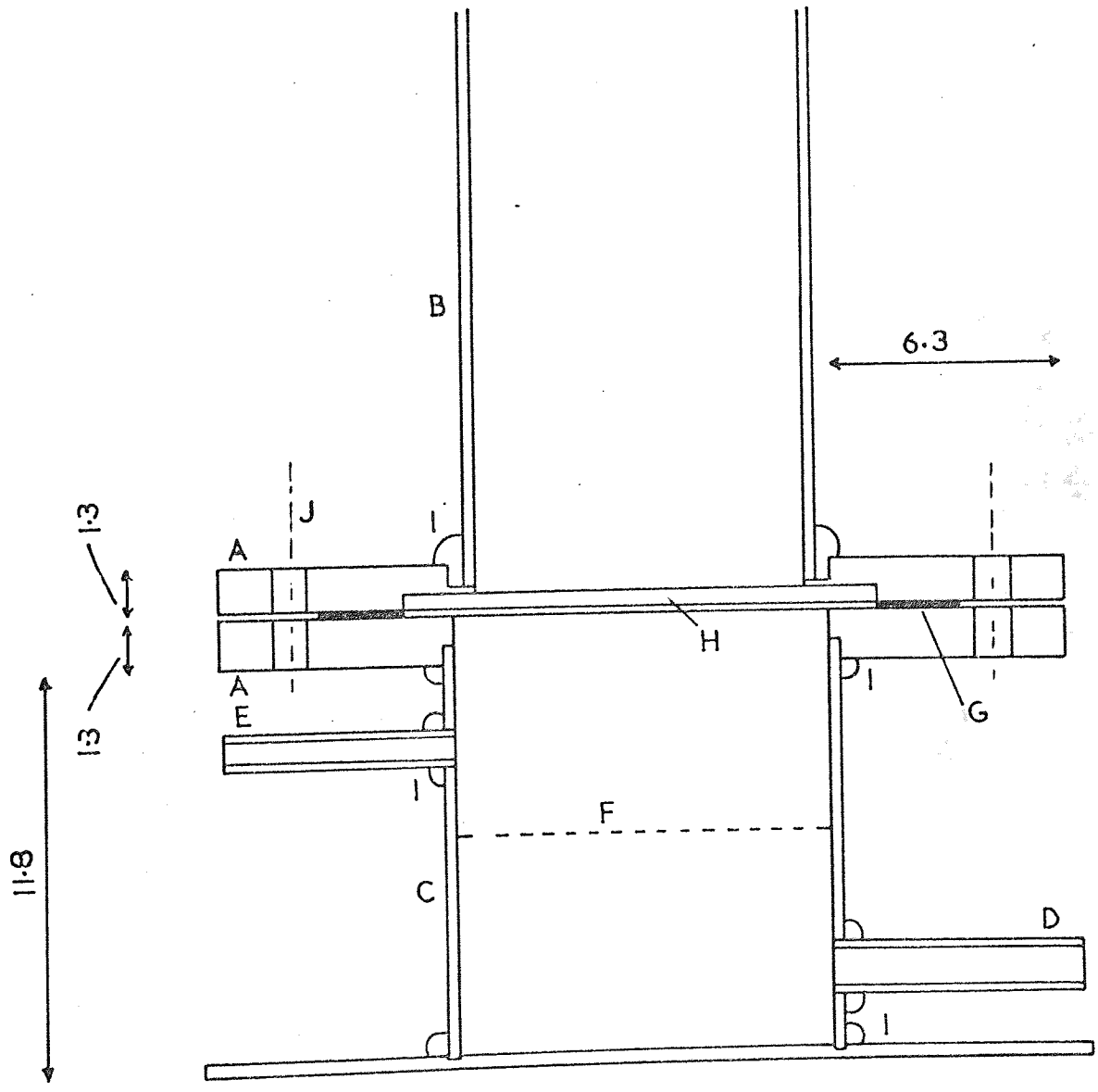

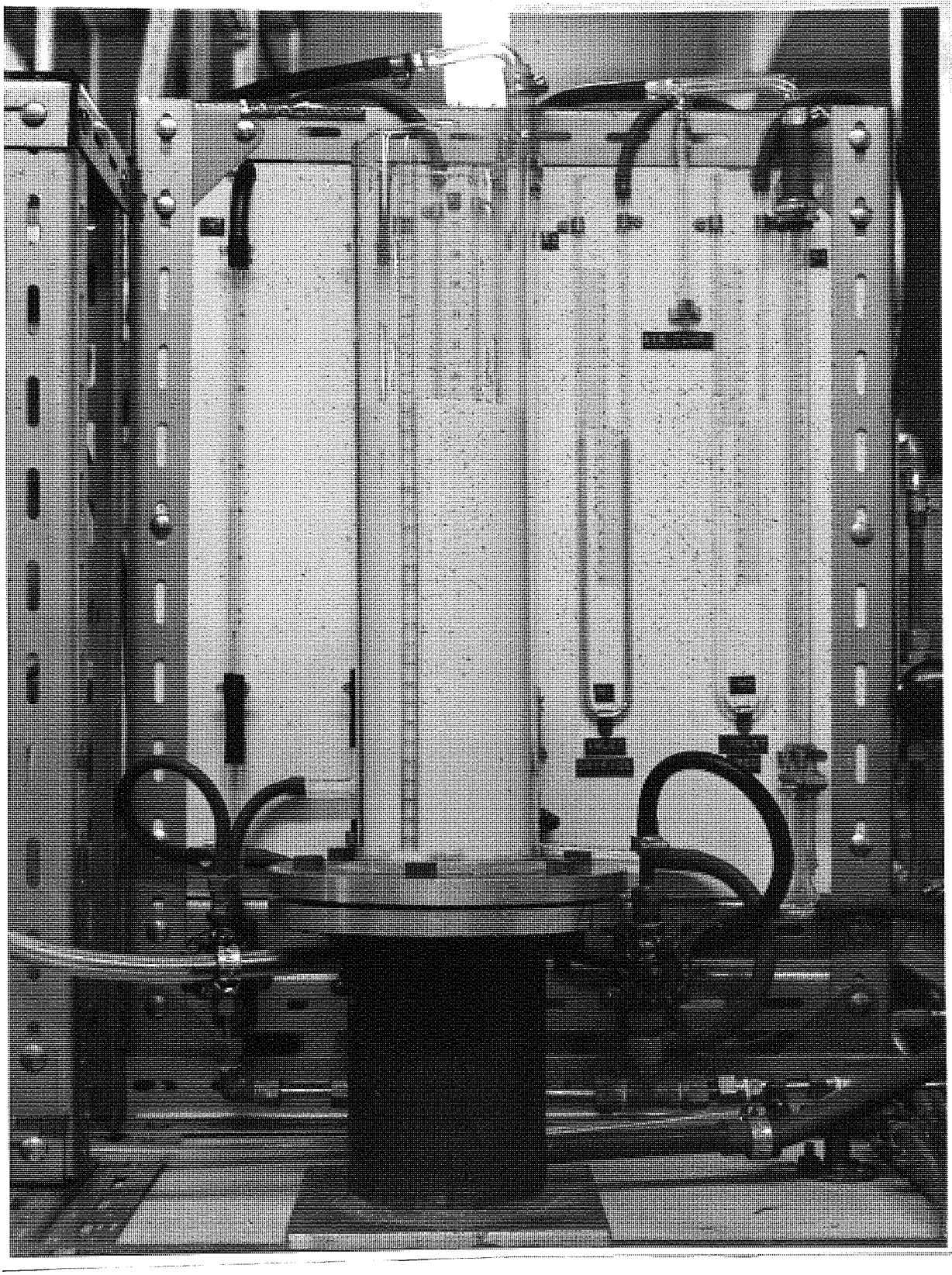

FIG. 2.3 9 cm diameter glass column.

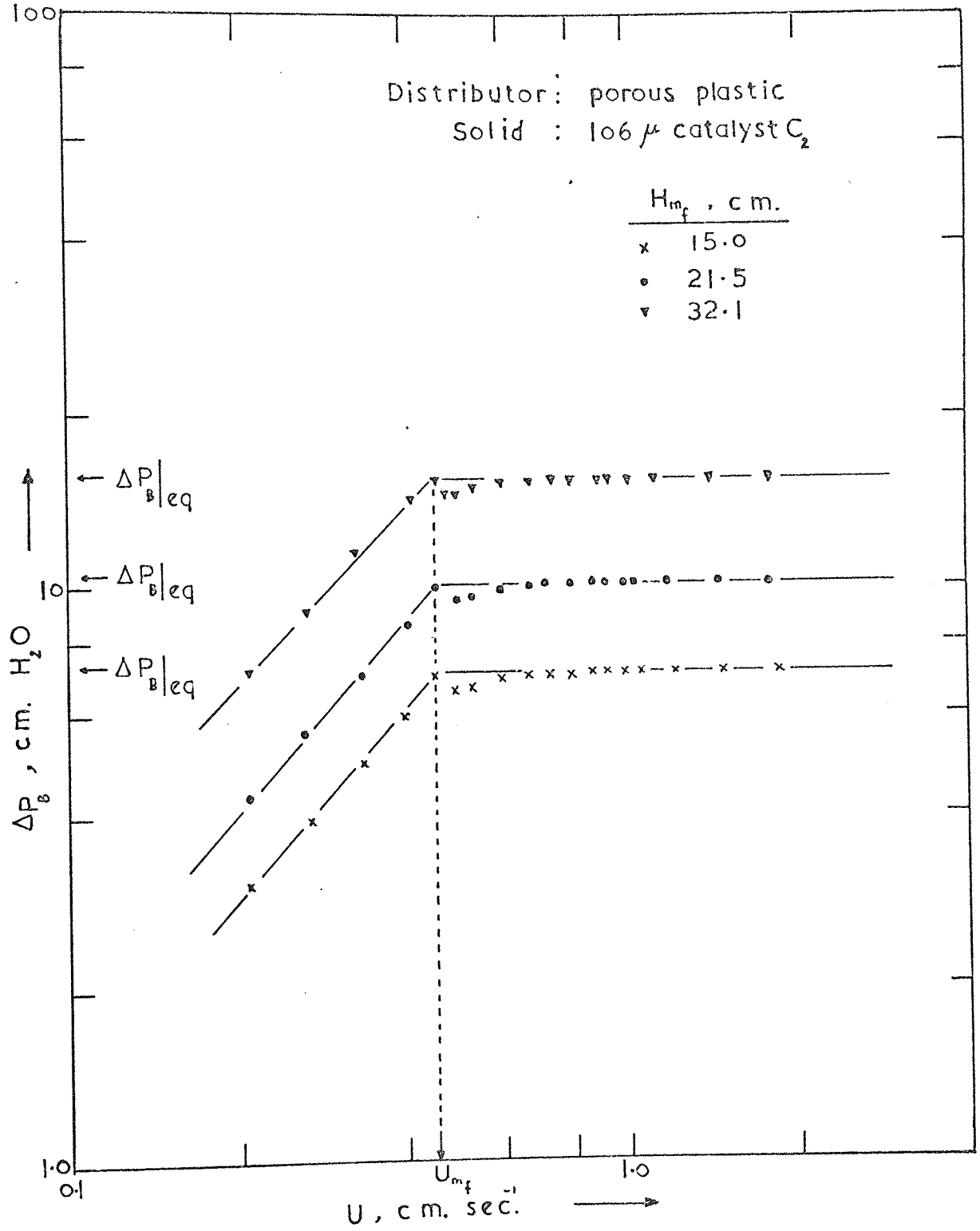

FIG. 2·4 PRESSURE DROP—VELOCITY RELATIONSHIP

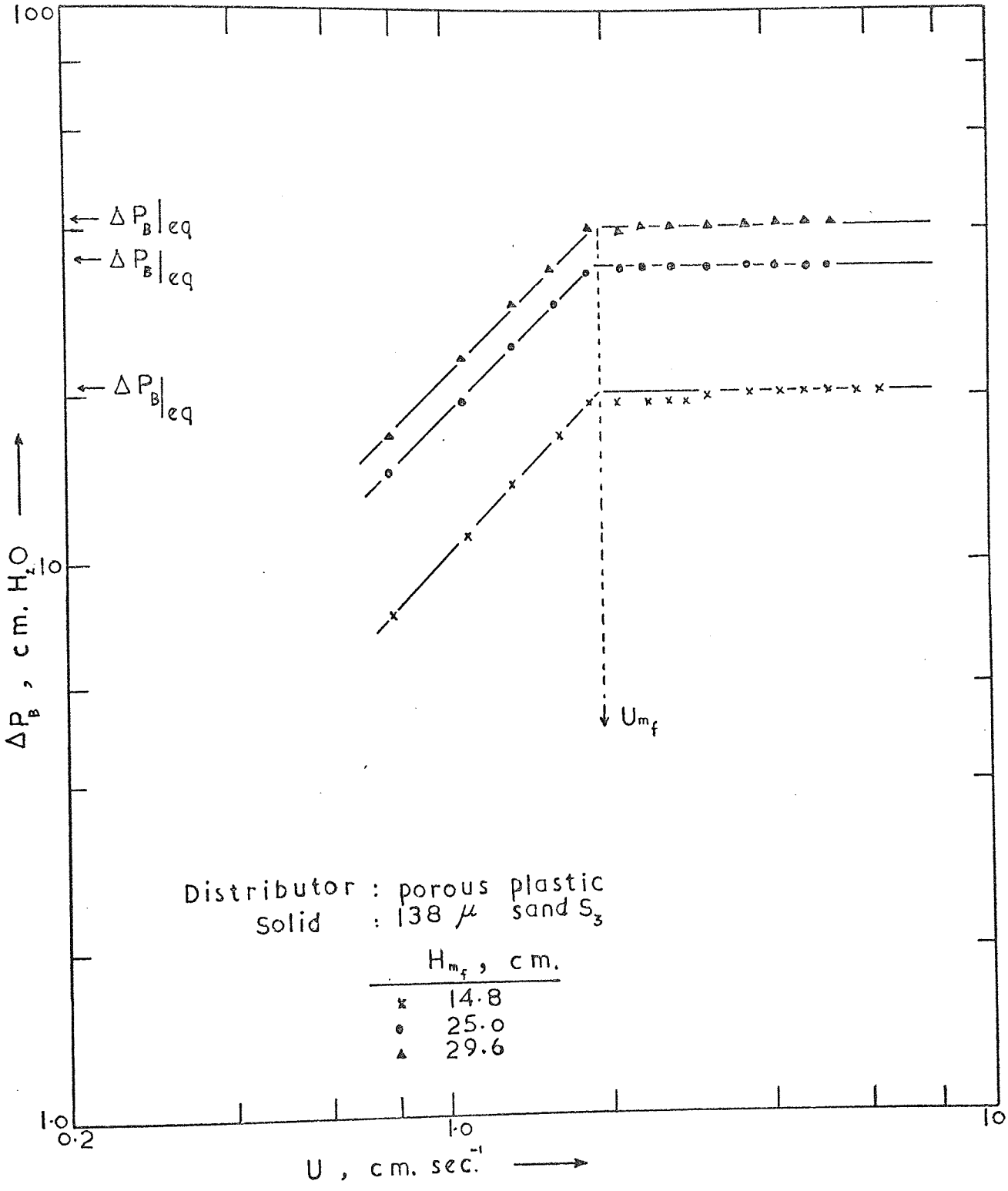

FIG. 2·5 PRESSURE DROP—VELOCITY RELATIONSHIP

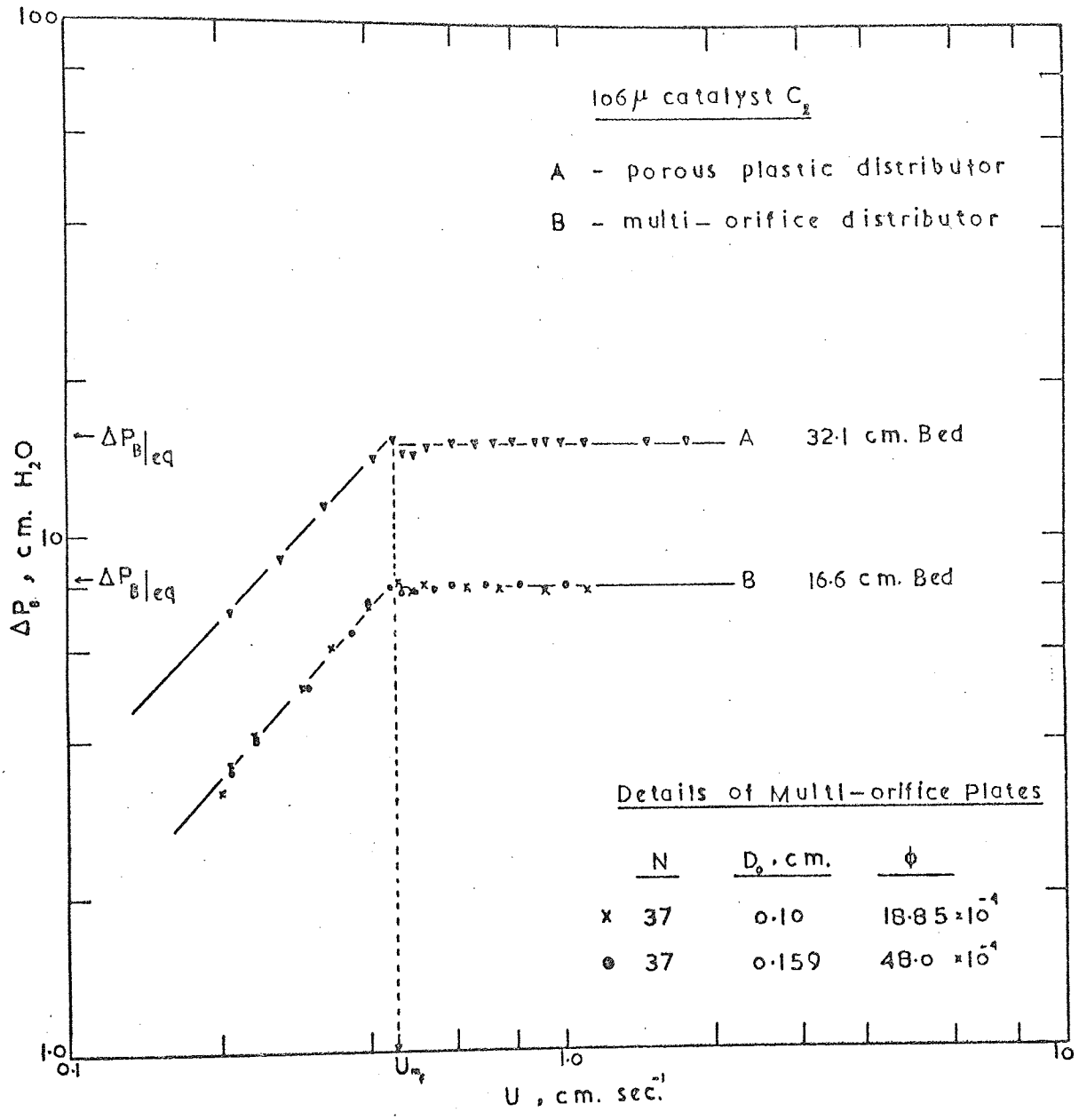

FIG. 2·6 EFFECT OF DISTRIBUTOR

CHAPTER THREE

3. PRESSURE DROP ACROSS THE DISTRIBUTOR PLATE AND ITS RELATIONSHIPS

This chapter is concerned with a study of certain aspects of pressure drop through distributor plates and their relationship to fluidized behaviour.

3.1 Pressure Drop - Flow Relationships for multi-orifice Distributors

3.1.1 Types of Orifice Flow

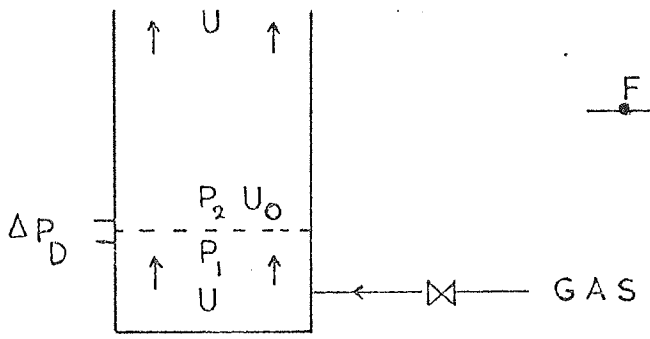

FIG. 3·1

When a fluid is flowing through a tube or across an orifice the pattern of flow will vary with velocity, the physical properties of the fluid and the geometry of the orifice. Flow can be of three types:

1. Laminar or streamline;
2. Transitional regime between streamline and turbulent;
3. Turbulent.

1. Laminar Flow

This type of flow is characterised in the steady state conditions by the absence of bulk motion of fluid at right angles to the main stream direction and the velocity of flow at any point remains constant and shows no variation with time. Such conditions are satisfied at low Reynolds numbers where the inertia forces are small compared with viscous forces. Under these conditions and for the situation shown in Figure (3.1), the pressure drop-flow relationship for incompressible flow is represented by the Hagen-Poseuille equation:

$$U_o = \frac{D_o^2 . (P_1 - P_2)}{32 . \mu_f . \ell} \qquad (3.1)$$

Also we have,

$$U = \phi . U_o \qquad (3.2)$$

and on substitution into (3.1) gives,

$$U = \frac{a_o . \phi}{8\pi . \mu_f . \ell} . \Delta P_D \qquad (3.3)$$

where

U = superficial velocity of fluid, cm/sec.

ΔP_D = differential pressure, dynes/cm^2.

μ_f = viscosity of fluid, gm/cm.sec.

a_o = surface area of orifice, cm^2.

ℓ = orifice length, cm.

ϕ = fractional free area of distributor, -.

Therefore, for a given distributor, the pressure drop across a distributor in the laminar regime is a linear function of gas flow rate, i.e.

$$\Delta P_D \alpha U \qquad (3.4)$$

This type of flow rarely occurs with distributors in gas fluidized beds unless these are operated at very low gas rates. Distributors having linear characteristics are usually found with narrow-pore plates.

3. Turbulent Flow

This is characterised by the rapid movement of fluid as eddies in random directions across the tube. The velocity at a point varies with time and a certain bulk transfer of fluid takes place at right angles to the main direction of flow. Momentum transfer within the fluid therefore occurs at a very much greater rate and the consequent shear stresses are greater and velocity gradients are smaller, except close to boundaries.

Turbulent flow occurs at high Reynolds numbers where inertia forces predominate with the result that the relationship between pressure drop and flow is no longer linear (i.e. the law of Hagen-Poseuille no longer applies).

Applying the incompressible flow form of Bernoulli's equation for the fluid flowing as shown in Figure (3.1), we have

$$\frac{P_1}{\rho_f} + \frac{1}{2} U^2 = \frac{P_2}{\rho_f} + \frac{1}{2} U_o^2 \qquad (3.5)$$

or

$$\frac{1}{\rho_f} \cdot (P_1 - P_2) = \frac{1}{2} \cdot (U_o^2 - U^2) \qquad (3.6)$$

Combining (3.2) and (3.6), we have

$$U = \frac{\phi}{(1 - \phi^2)^{\frac{1}{2}}} \cdot \left(\frac{2}{\rho_f}\right)^{\frac{1}{2}} \cdot \Delta P_D^{\frac{1}{2}} \qquad (3.7)$$

where

U = superficial velocity of fluid, cm/sec.

ΔP_D = differential pressure, dynes/cm^2.

ρ_f = density of fluid, gm/cm^3.

ϕ = fractional free area, -.

With single-stage systems ϕ hardly exceeds 5% and with multi-stage systems ϕ can be as high as 16%. For both systems $\phi^2 << 1$, then (3.7) simplifies to

$$U = \left(\frac{2}{\rho_f}\right)^{\frac{1}{2}} \cdot \phi \cdot \Delta P_D^{\frac{1}{2}} \qquad (3.8)$$

It should be noted that for free areas up to 30%, the error introduced by dropping ϕ^2 from the denominator of (3.7) is less than 0.5%.

As can be seen from (3.8), the pressure drop is a quadratic function of gas flow for a given ϕ, i.e.

$$\Delta P_D \alpha U^2 \qquad \text{for } \phi = \text{constant} \qquad (3.9)$$

and $$\Delta P_D \alpha \frac{1}{\phi^2} \quad \text{for } U = \text{constant} \tag{3.10}$$

or $$\Delta P_D \propto U_o^2 , \tag{3.11}$$

where U_o is the orifice fluid velocity.

The Orifice Constant

From (3.8) the volumetric rate of flow through a single orifice of diameter D_o, caused by the pressure differential ΔP_D is given by:

$$Q_o = (\frac{\pi}{4}) \cdot (\frac{2g}{\rho_f})^{\frac{1}{2}} \cdot D_o^2 \cdot \Delta P_D^{\frac{1}{2}} \quad (cm.^3/sec.) , \tag{3.12}$$

or $$Q_o = k_o \Delta P_D^{\frac{1}{2}} \tag{3.13}$$

Where $$k_o = (\frac{\pi}{4}) \cdot (\frac{2g}{\rho_f})^{\frac{1}{2}} \cdot D_o^2 , \tag{3.14}$$

= a constant for a given orifice.

3.1.2 Equipment and Experimental Procedure

The experiments were carried out in two vertical cylindrical columns. One was Perspex 14 cm. in diameter and 100 cm. high and the other was standard Q.V.F. glass 7.9 cm. in diameter and 80 cm. high. Air from 80 p.s.i.g. main was reduced to a pressure of 20 p.s.i.g. and metered through calibrated rotameters. Needle valves were used to regulate the flow through the rotameters. Table (3.1) gives the details of the multi-orifice distributors used. These were 1/8" thick aluminium plates with orifices drilled on a triangular-pitch arrangement. The orifice diameter and the spacing between the orifices were variables. Pressure tappings consisted of three holes at 120 deg. to each other which were drilled in the wall of the wind box below the distributor and connected by p.v.c. tubing to a 100 cm. wall-type water manometer with one limb open to the atmosphere. For the measurement of small pressure differences, an adjustable inclined manometer filled with dyed paraffin (S.G. = 0.787) was used. With this arrangement the pressure drops across the multi-orifice distributors were measured for the range of superficial gas velocities from 1.2 cm./sec. to 30 cm./sec. (depending on the available free area of the distributor).

3.1.3 Experimental Results and Discussion

The experimental results are given in Tables (3.2) - (3.6) and as plots in Figures (3.2) - (3.3).

In Figure (3.2) are plotted the total measured pressure drop across the multi-orifice distributor as a function of the average flow rate through the orifice, with orifice diameter as a parameter. Air flow rates shown were calculated by dividing the total volumetric flow of air ($cm^3./sec.$) by the total number of orifices on a given plate. In the computation of orifice constant, k_o, an average air density of 1.2×10^{-3} $gm./cm^3.$ was used, corresponding to the generally prevailing

temperature and pressure of the laboratory.

For any given orifice diameter and for triangular spacing, the data are seen to fall on straight lines with a slope appproximately equal to 2.0 when plotted with logarithmic scales. This shows that the orifice flow is turbulent, i.e. pressure drop across the distributor is directly proportional to the square of superficial gas velocity, and inversely proportional to the square of the distributor free area (or plate characteristics) ϕ.

From Figures (3.2) amd (3.3) it can also be seen that, for turbulent orifice flow, pressure drop across the distributor plate, as would be expected is found to be independent of the orifice spacing. Therefore, it is expected that for turbulent orifice flow the layout of the orifices on the plate will have no effect on the plate pressure drop. In contrast to that of turbulent flow, the orifice spacing and, possibly, the arrangement of the orifices would influence the pressure drop in the laminar regime.

In Figure (3.4) a plot of k_o values vs. D_o^2 shows their comparison with the theoretical line predicted from (3.14) for the orifices used. As may be seen, the experimental line falls below the theoretical line, but the agreement between them is close. It seems probable that this discrepancy arose from the fact that equation (3.14) was derived for a single orifice and not an array of parallel paths. Presumably interference between adjacent jets, and velocity gradient irregularities within the orifices have caused the deviation.

From these simple experiments we may conclude that multi-orifice distributors possess a quadratic characteristics, i.e. the pressure drop - flow relationship falls within the turbulent flow regime. However, it is not known whether this relationship also holds when the distributor is supporting a bed of solid particles. It is believed that the normal

pattern of gas flow through an orifice might be disturbed by the presence of solid particles in the column. The effect of bed presence on the distributor pressure drop will be considered in the following section.

None of the distributors studied exhibited a linear relationship between pressure drop and gas flow. A narrow-pore plate could, probably, make distributors with linear characteristics.

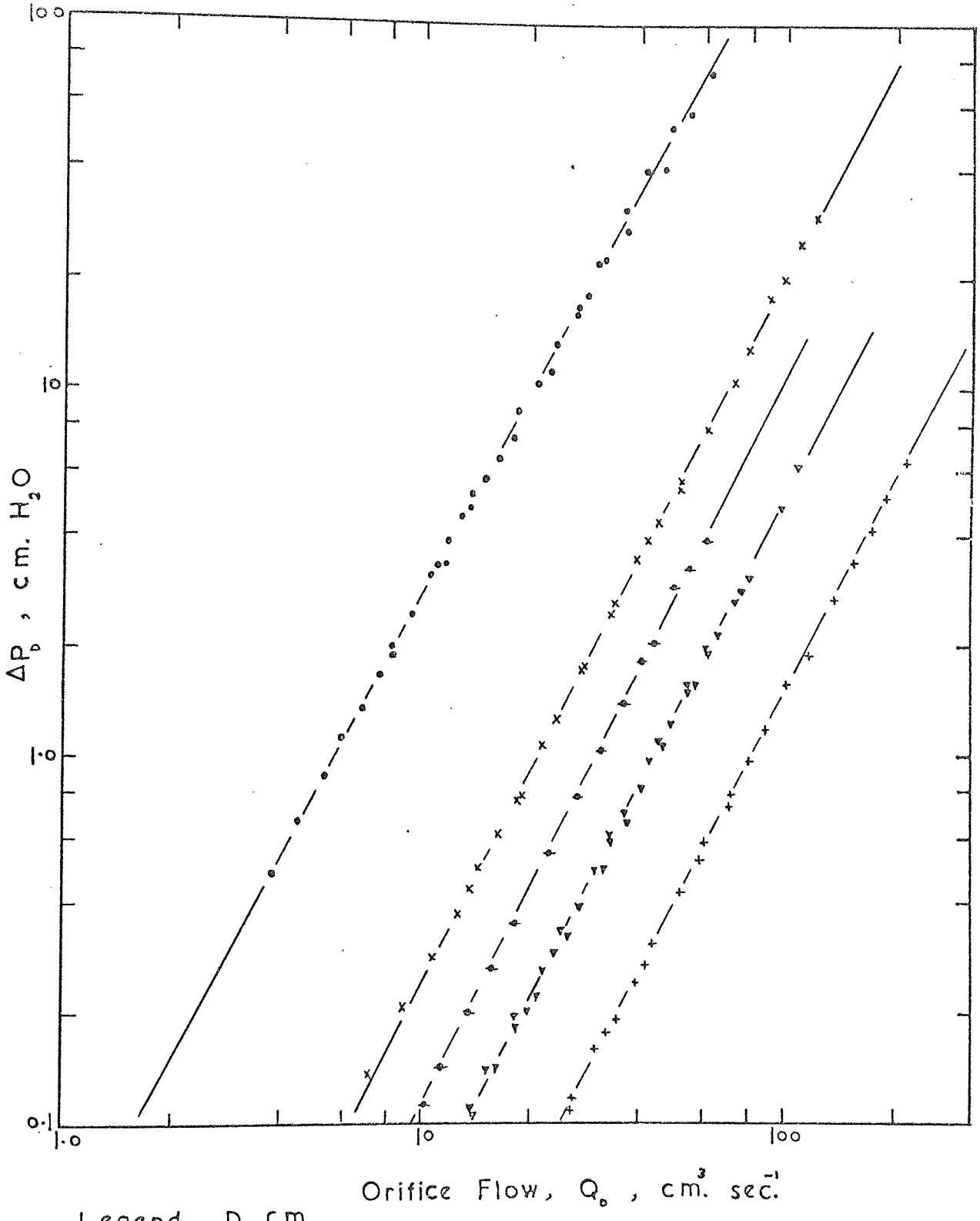

Legend	D_o, cm.
●	0·1
x	0·159
◆	0·2
▼	0·238
+	0·318

FIG. 3·2

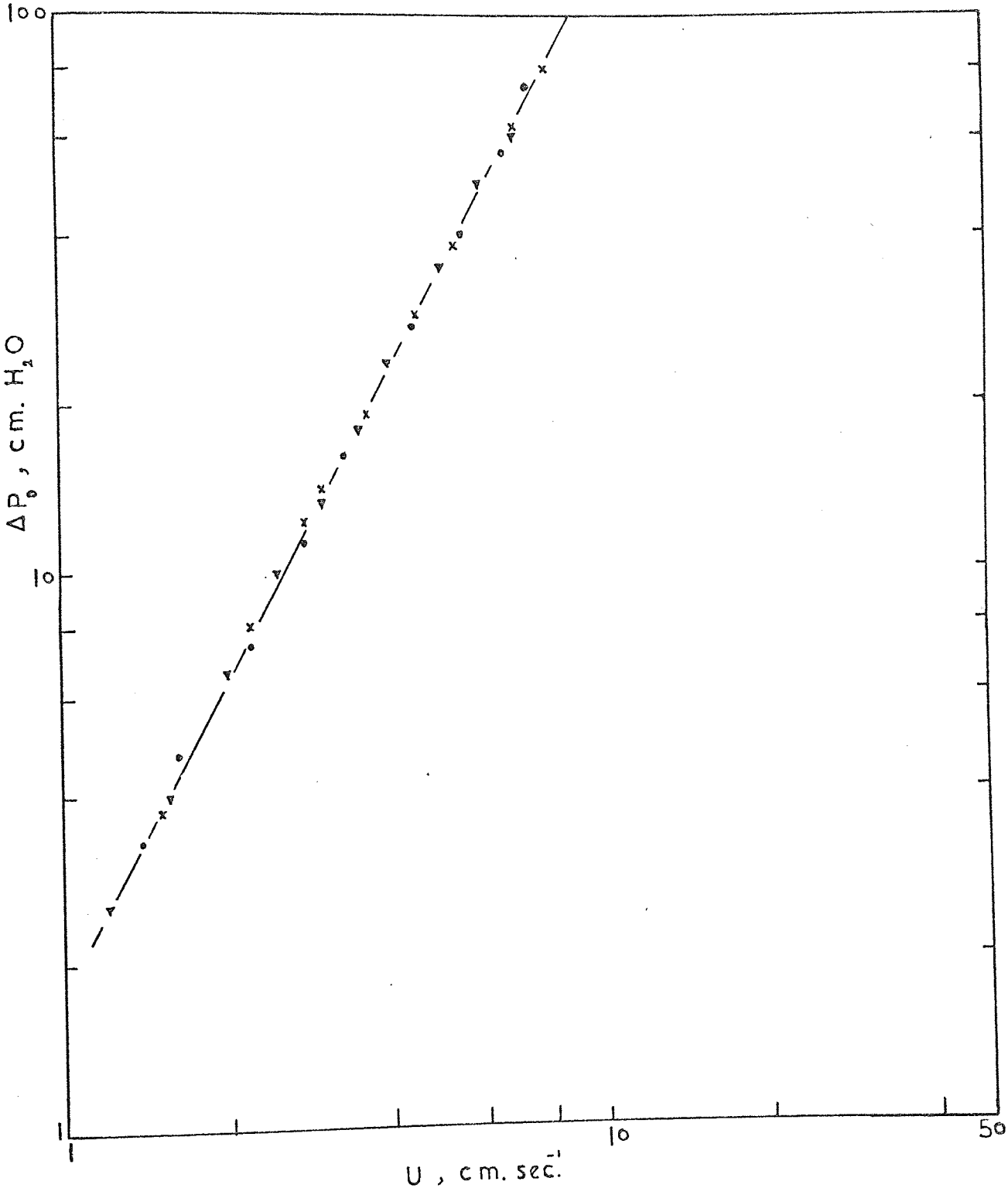

Legend	S, cm.
x	1·27
▼	1·9
●	3·0

FIG. 3·3

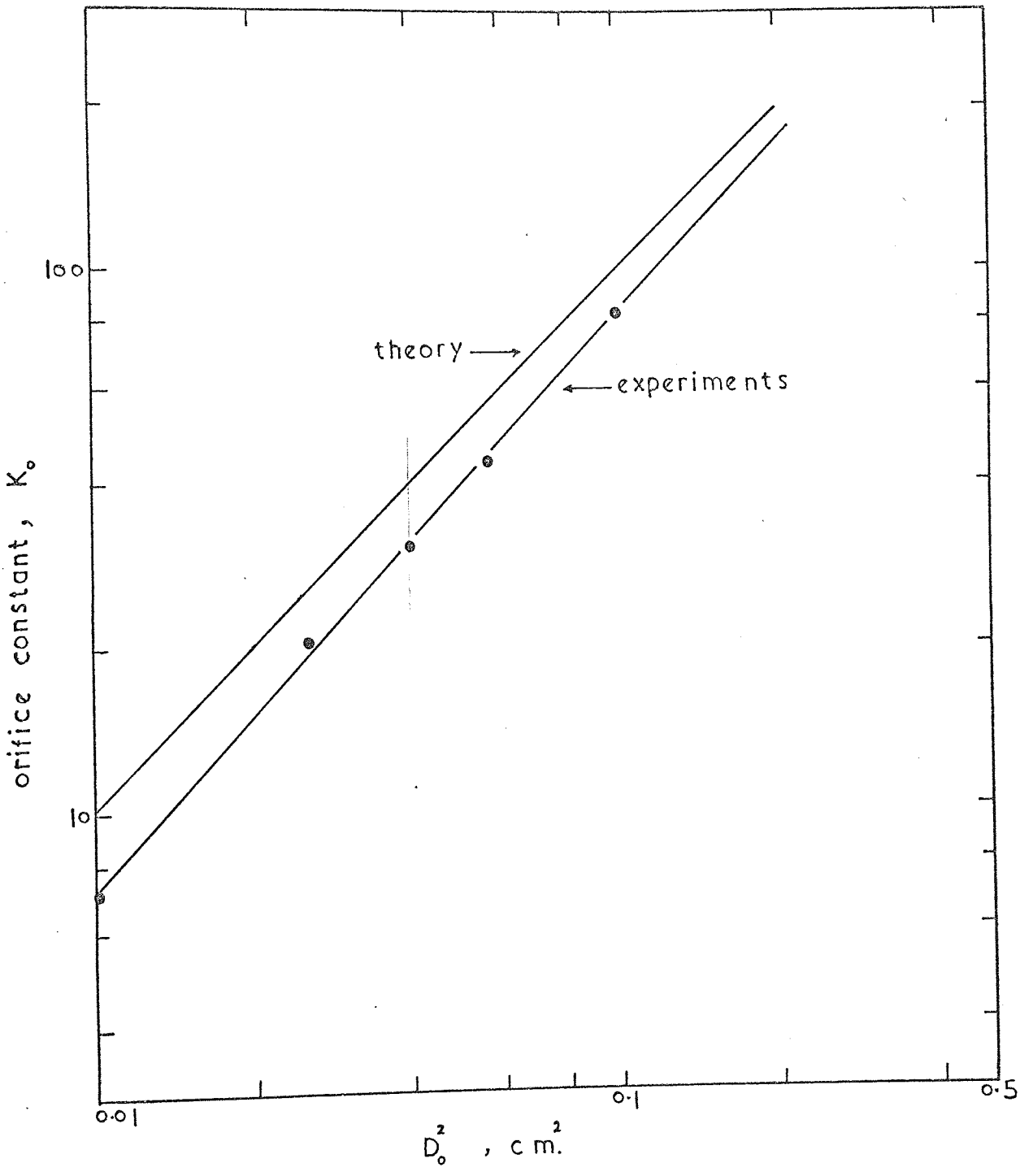
100
10
theory
experiments
orifice constant, K_o
0·01
0·1
0·5
D_o^2 , c m.^{2}

FIG. 3·4

3.2 Distributor Pressure Drop in the Presence of a Bed of Solid Particles

In the literature review, we noted that most work carried out concerning the regularity of gas distribution in fluidized beds has finished with the conclusion that the type of distributor plate, and the pressure drop across it, ΔP_D, have an important effect on the stability of the fluidized bed. This pressure drop is often related to the bed pressure drop ΔP_B and thus ΔP_B is also a measure of fluidized behaviour. For example, a rise in pressure drop with increasing gas flow over the fluidized region is taken as indicative of slugging, whilst a decrease in pressure drop suggests channelling. Therefore, accurate knowledge of bed pressure drop is necessary for the rational design of a distributor. It should also be acknowledged that the pressure drop across the distributor plate which is relevant to design is that measured in the presence of the particles bed.

3.2.1 Measurements of Bed Pressure Drop

Measurements of the pressure drop through a fluidized bed are generally obtained by one of the following methods:

1. Measuring the bed pressure drop directly from a pair of pressure tappings, the downstream one being located above the bed and the upstream one being located just above the distributor plate.

2. Measuring the overall pressure drop of the bed plus the distributor by locating the upstream pressure tapping in the wind box immediately below the distributor plate. The pressure drop across the bed is then determined by subtracting from the overall pressure drop, the pressure drop across the distributor as measured in the absence of the bed at the same mass flow rate of gas.

Sutherland(87) and Trivedi and Rice(88) have listed these methods when they considered methods of measuring pressure drop across a fluid-

ized bed. Here, we may include a third method which is found to be quite accurate for estimating the bed pressure drop, i.e.

3. Measuring the static pressure up the bed from a vertical set of pressure tappings stationed along the column wall. Since the pressure varies linearly with height, then the overall bed pressure drop is determined by extrapolation to the distributor level.

Sutherland(87) studied the problem and showed theoretically, supported by experiments, that for a given mass flow rate (assuming isothermal flow) the pressure drop through a porous distributor is lower if the bed of solids is present than it is absent. Therefore, according to Sutherland, when one subtracts the pressure drop through the distributor for the empty column from the pressure drop across the bed and the distributor, one is subtracting an incorrect quantity and the resulting bed pressure drop is correspondingly in error. For this reason, Sutherland criticised method (2) of measuring bed pressure drop and cast doubts on some of the investigations reported in the literature in which this technique has been used and the effect of bed presence on the distributor pressure drop has been ignored.

His argument is based on applying the Carman-Kozeny equation to isothermal flow of gas through a porous medium (assuming laminar flow) i.e.

$$G = \rho_g . U = \frac{B_o . \rho_g}{\mu_g . \ell} (P_1 - P_2). \qquad (3.15)$$

where

B_o = permeability coefficient,

ℓ_g = gas density,

μ_g = gas viscosity,

ℓ = thickness of porous plate in direction of flow,

U = gas superficial velocity,

P_1 = upstream pressure on plate,

P_2 = downstream pressure on plate,

G = mass flow rate.

From this, Sutherland showed that

$$(P_1 + \delta P_1)^2 - (P_2 + \Delta P_B)^2 = P_1^2 - P_2^2 = \text{constant} \quad , \tag{3.16}$$

where P_1 = upstream pressure on distributor for the empty column,

P_2 = downstream pressure on distributor for the empty column,

δP_1 = increase in upstream pressure due to bed presence,

ΔP_B = increase in downstream pressure due to bed presence (i.e. bed pressure drop).

An inspection of (3.16) shows that $\delta P_1 < \Delta P_B$, therefore the new distributor drop $\Delta P_2 = (P_1 + \delta P_1) - (P_2 + \Delta P_B)$ is smaller than $\Delta P_1 = P_1 - P_2$, the distributor pressure drop measured in the bed absence, i.e.

$$\Delta P_1 - \Delta P_2 = \Delta P_B - \delta P_1 \quad , \tag{3.17}$$

$$\text{i.e.} \quad \Delta P_2 < \Delta P_1 \tag{3.18}$$

Trivedi and Rice(88) studied, among other factors, the effect of measuring pressure drop on pressure drop across beds of glass spheres fluidized with air. They determined the pressure drop by both method (1) and method (2) and found that the bed pressure drop is smaller when measured directly rather than when measured by subtraction of the distributor pressure drop from the overall pressure drop for a given mass flow rate of gas. Grosh(61) and Shannon(89) obtained similar results which Trivedi and Rice(88) quoted in order to justify their conclusions. Their observations contradicted Sutherland's theory and for this reason Trivedi and Rice felt some doubts over the theory. Therefore, according to Trivedi and Rice

$$\Delta P_2 > \Delta P_1 \tag{3.19}$$

A number of experiments have been carried out by the present author(77) in the past in order to show the effect of bed presence on the distributor pressure drop when using multi-orifice plates (note: Sutherland dealt with porous plates).

Beds of irregularly shaped silver sand particles were fluidized with air in a Perspex column 14 cm. inside diameter. The distributors were multi-orifice plates made of Perspex the thickness of which was varied between 0.32 cm. and 5.1 cm. Both method (1) and method (2) were used for measuring the bed pressure drop and the results showed that (i) the plate pressure drop was much higher in the presence of solids in the column than when the column was empty, (ii) this pressure drop was higher with the thick plate than with the thin one and (iii) the bed pressure drop was smaller when measured directly (method 1) rather than when measured by subtraction (method 2). These findings came in line with those of Trivedi and Rice, but unfortunately the results were deemed unsatisfactory because visual observations during experiments revealed that:

(i) Some of the orifices were blocked up with sand particles during operation. More and more orifices became blocked as the fluidizing rate was decreased.

(ii) With deep plates particles tended to bridge inside the orifice rather than above it. Similar observations have recently been confirmed by Fakhimi and Harrison(64).

These factors, obviously, lead to a higher observed distributor pressure drops for a given mass flow rate of gas compared to the situation when all the orifices are unobstructed and fully operational. On this basis doubts were cast on the results.

Later(90) some experiments were also carried out with silver sand. This time, a multi-orifice metal distributor was employed. Both

method (2) and method (3) were used and by comparing the two, it was found that (3.18) agreed with the results rather than (3.19). However, the agreement was rather poor due to the scattering of the data. Nevertheless, the results were encouraging because they reinforced the conclusions drawn by the present author(77) regarding his earlier experiments and provided some support to Sutherland's theory. On these grounds it was decided to investigate the problem further.

In a recent study on distribution plates with fine orifices, Fakhimi(74) analysed the problem and noted a decrease in the distributor pressure drop caused by the bed presence. This confirmed Sutherland's theory.

His analysis is, probably, the most satisfactory one because, it concerns multi-orifice distributors which, of course, are of greater practical interest than porous plates. As he indicates, these distributors can be operated so that the total available free area is the same in the absence and the presence of fluidized solids in the bed. Such operative conditions can be achieved by using high enough gas flow to make all orifices active. For a given solid-distributor system, Fakhimi used (3.12) to predict the minimum gas flow rate necessary for full operation of the distributor orifices. Blockage of the distributor orifices with particles is less likely under these conditions and, therefore, a correct measure of the effect of bed presence on the distributor pressure drop is obtained. In other words, problems such as those experienced by the present author (77) can be eliminated by the use of higher gas rates.

His analysis was based on Sutherland's theory, by assuming the air as an ideal gas and the flow through the distributor orifices as an isothermal and turbulent. For the two situations shown respectively in Figures (3.5) and (3.6), we have

$$U_1 = \frac{U_a \cdot P_a}{P_a + \Delta P_1} \qquad \text{(without bed)}, \tag{3.20}$$

and
$$U_2 = \frac{U_a \cdot P_a}{P_a + \Delta P_2 + \Delta P_B} \quad \text{(with bed)} \tag{3.21}$$

or
$$\frac{U_1}{U_2} = \frac{P_a + P_1}{P_a + \Delta P_2 + \Delta P_B} = \frac{\rho_{g1}}{\rho_{g2}} \tag{3.22}$$

where P_a is the atmospheric pressure and U_a is the superficial air velocity at pressure P_a.

For constant mass flow rate and for a turbulent flow, it can easily be shown that

$$\frac{\rho_{g1}}{\rho_{g2}} = \frac{\Delta P_2}{\Delta P_1} \tag{3.23}$$

Therefore, from (3.22) and (3.23), we have

$$\frac{P_a + \Delta P_1}{P_a + \Delta P_2 + \Delta P_B} = \frac{\Delta P_2}{\Delta P_1} \tag{3.24}$$

or
$$m^2 + (a + b)m - (1 - b) = 0 \tag{3.25}$$

where $m = \frac{\Delta P_2}{\Delta P_1}$, $a = \frac{\Delta P_B}{\Delta P_1}$ and $b = \frac{\Delta P_a}{\Delta P_1}$

This is the equation derived by Fakhimi(74) for a multi-orifice distributor which relates m to constants a and b, and on solving the positive root gives

$$m = 0.5 \left(\sqrt{(a + b)^2 + 4(1 + b)} - (a + b) \right) \tag{3.26}$$

which shows a quadratic relationship between $\frac{\Delta P_2}{\Delta P_1}$ and $\frac{\Delta P_B}{\Delta P_1}$ for a given value of $\frac{P_a}{\Delta P_1}$.

Fakhimi showed that $m \leq 1$ and postulated that for a given mass flow rate of gas G, the presence of solid particles in the fluidizing column will cause an additional compression of the incoming gas within the wind

box, and hence causing a reduction in the distributor pressure drop. This is probably the case from the physical point of view, but it is doubtful if the reduced plate pressure drop observed by Fakhimi and indicated by the present work was due to compression of gas in the wind box because it is negligible. It is possible that some other factors have contributed to the effect. These will be referred to later. However, the trend of his results indicates a quadratic form, i.e. in accord with (3.26). Results obtained from the present work showed good agreement with Fakhimi and the data were expressed by a second order polynomial.

The work described in this chapter follows from the previous study made by the present author(77) on the effect of bed presence on the distributor pressure drop. Its objectives are:

(i) To examine the validity of Sutherland's theory(87) with regard to multi-orifice distributors and in particular to clarify the conflicting evidence concerning the effect of bed presence on the distributor pressure drop reported by various authors.

(ii) Knowledge of the distributor pressure drop in the presence of the bed is required in other studies. For example, in the study of the pressure drop criteria ($\Delta P_D/\Delta P_B$) for stable fluidization (see section 3 of this chapter) the appropriate values of ΔP_D are those measured in the presence of the bed. Therefore, from this point of view this investigation is also essential.

3.2.2. Equipment and Experimental Procedure

In the present investigation the bed pressure drop was determined by two methods: (i) method (3), and (ii) from pressure tappings located directly on the distributor plate. The later technique was used by Fakhimi(74) and claimed that it gave a reliable measure of the bed pressure drop.

The experiments were carried out in a cylindrical column made of Perspex, 14 cm. inside diameter and 100 cm. high. The fluidizing air was taken from the laboratory main, reduced to a pressure of 20 p.s.i.g., and metered through calibrated rotameters. These rotameters were previously calibrated at 760 mm. Hg and 15^{o}C and therefore each flow was corrected to the actual experimental conditions. Needle valves were used to regulate the flow through the rotameters. Solids used in these experiments have the characteristics described in Table (2.3)(Chapter 2). These were ungraded silver sand (100 - 350 μ) and graded glass beads having mean particle diameters of 224 μ and 237 μ respectively. The multi-orifice distributors used were aluminium plates, 1/8" thick with orifices drilled on a triangular pitch arrangement. Details of these distributors are given in Table (3.7). On each plate five pressure tappings were also drilled and then covered with wire mesh to prevent solid particles from blocking the pressure tappings. Three tappings were placed at 120 deg. to each other. The other two were placed in the centre of the plate, one close to the orifice mouth and the other in the centre of the triangular lattice. Each tapping was equipped with a 4 cm. long stainless steel tubing glued onto it with Araldite. The tappings were connected to a 100 cm. wall-type manometer filled with coloured water using p.v.c. tubing. A small piece of glass thermometer capillary was inserted in the manometer lead to damp out pressure fluctuations inherent in the system. With this arrangement, it was possible to measure

the bed pressure drop directly with reasonable accuracy. This technique was used elsewhere in experiments concerning bed stability because, with the aid of the pressure tappings it was possible to find out if the bed was homogeneously fluidized or not. Studies on bed stability are presented in section 3 of this chapter.

The static pressures on the column wall were measured from the tappings placed vertically on the column wall. Twelve pressure tappings were located on the column wall at 5 cm. intervals. These were connected via a manifold to the manometer using p.v.c. tubing.

In these experiments static charges were a problem and, in order to minimize their effect, the inside wall of the Perspex column was sprayed with antistatic cleaner. It was also suggested to humidify the air; this was done by allowing a small flow rate of air to bubble through a jar filled with water and then mixing it with the main fluidizing air before introducing it into the bed. These measures helped to a certain extent in reducing static effects with glass beads but not with sand. This is probably due to the difference in surface properties between sand (angular) and glass (spherical). But the precise reason remains to be determined.

3.2.3. Experimental Procedure

The experimental procedure was started as follows:

(i) Measuring the distributor pressure drop for a given gas flow rate with the column empty.

(ii) A known weight of solids was loaded into the column and the measurement was repeated at the same gas flow rate.

(iii) The bed pressure drop was determined by the two methods mentioned earlier and the distributor pressure drop (in the presence of the bed) was determined by subtraction.

Almost no difference was detected between method (3) for measuring bed pressure drop and that obtained directly from the pressure tappings located on the distributor plate. The average of both measurements was always taken as the observed bed pressure drop. As can be seen from the tables of the experimental results, the measured bed pressure drop closely approximates the value predicted from the bed weight.

The experiments were carried out with various bed heights ranging between 10 to 70 cm. In order to achieve fully operative distributors, high enough fluidizing rates were used. The theoretical gas flow rate U required to make $\frac{\Pi}{N} = 1$ was predicted from equation (5.25) (see Chapter 5) which was solved numerically on a digital computer using an iterative method (see Table (3.8)). The values of U used in the present investigation were much higher than those predicted from (5.25). This was intended to avoid blockage of the distributor orifices with particles and would, obviously, avoid the need for the correction factors proposed by Fakhimi(74).

3.2.4 . Experimental Results and Discussion

The experimental results are given in Tables (3.9) - (3.10). These are shown as a plot of ΔP_1 (the distributor pressure drop measured without the bed) vs. ΔP_2 (the distributor pressure drop measured in the bed presence) for all beds and distributors tested in Figure (3.7), from which it can be seen that the effect of the bed presence is to reduce the pressure drop through the distributor. These observations are in line with Sutherland(87), but in disagreement with him the results seem to indicate the importance of the bed pressure drop in influencing ΔP_2. An inspection of Tables (3.9) - (3.10) shows that the difference between ΔP_1 and ΔP_2 is significantly affected by the magnitude of ΔP_B, the bed pressure drop. For a given distributor pressure drop ΔP_1, an increase in the bed pressure drop causes a decrease in ΔP_2. Conversely, for a given bed pressure drop ΔP_B, an increase in the gas flow rate (corresponding to high distributor pressure drop) results in smaller difference between ΔP_1 and ΔP_2. These observations indicate a trend similar to that reported by Fakhimi(74), and as can be seen from Figure (3.7) the trend of the results is suggesting a quadratic relationship between ΔP_1 and ΔP_2.

This may be readily seen from Figure (3.8) which shows a plot of $\frac{\Delta P_B}{\Delta P_1}$ vs. $\frac{\Delta P_2}{\Delta P_1}$ in the way suggested by (3.26) along with the quadratic line through the data. The best-fit line through the experimental data was determined by the method of "least squares" using a computer library subroutine. This subroutine fits a polynomial to a set of values of a function of one variable using the method of "least squares" via orthogonal polynomials. The quadratic approximation to the experimental data obtained from the computer resulted in the expression:

$$\frac{\Delta P_B}{\Delta P_1} = 22.27 - 56.1 \left(\frac{\Delta P_2}{\Delta P_1}\right) + 35 \left(\frac{\Delta P_2}{\Delta P_1}\right)^2. \qquad (3.27)$$

and a sum of squares of error of 179.1 was obtained.

As may be seen, the results broadly confirm a quadratic relationship between $\frac{\Delta P_B}{\Delta P_1}$ and $\frac{\Delta P_2}{\Delta P_1}$ (in accordance with (3.26)) with one exception, is the region close to $\frac{\Delta P_2}{\Delta P_1} = 1$ where the data exhibit some scatter. Better fit was found with higher degree polynomials in this region with a scatter about 10 - 13% less than that of a quadratic. It might be possible that some of the orifices remained blocked up with particles, despite the use of high enough gas flow rates. It is also likely that some of the orifices were jammed by particle bridging inside the orifice which makes them more resistive to the onset of bubbling or spouting. These factors are likely to contribute to the scattering shown in both Figure (3.7) and (3.8). As shown in Figure (3.7) the data obtained with silver sand are closer to the parity line than those obtained with glass beads. This is indicating that some of the orifices were more readily blocked with silver sand (angular) than with glass beads (spherical). This may be due to the static effects which, as indicated earlier, were more pronounced with silver sand than with glass beads. Static charges may well result in distributor blockage.

Figures (3.9) and (3.10) are typical plots showing the variation of static pressure of air with bed height. The measured pressures lie on a straight line that extrapolates to the theoretical bed pressure drop at the distributor level (method 3). These plots can be represented by the following equation:

$$\Delta P_{B|x} = \frac{W_B}{A} \cdot \left(1 - \frac{x}{H}\right) \quad , \qquad (3.28)$$

where W_B/A = the total bed pressure drop (weight of bed divided by bed cross section), at $x = 0$ in Figure (3.6),

H = the height of the expanded fluidized bed.

Equation (3.28) also enables the height, the density of the dense-phase region and the superficial gas velocity at level x to be determined. This method is quite satisfactory for the measurement of the bed pressure drop, but rather laborious because the bed drop is determined graphically rather than directly. However, the direct method was also used and the results from the two measurements were averaged. But it should be noted that the graphical method would give closer estimates of the bed drop than the direct method.

The important inference to be drawn from the present investigation is that the experimental results add reinforcement to Sutherland's theory and cast doubts on the findings of Trivedi and Rice. The theory predicts a reduction in the distributor pressure drop in the presence of solids in the column from that without solids and this new pressure drop is the relevant parameter for design. The higher distributor pressure drop observed by Trivedi and Rice and other workers probably means that their distributors were not functioning properly. This has already been discussed at length by Fakhimi(74). Results of the present work show good agreement with Fakhimi who also observed a lowering in the distributor pressure drop. But it should be emphasised that his analysis is of a greater practical interest than Sutherland's analysis because, it concerns multi-orifice distributors and, possibly, can be extended to other similar devices.

As indicated earlier, Fakhimi postulates that the presence of solid particles in the bed will cause additional compression of the gas within the wind box and hence reducing the plate pressure drop. It is believed

that the amount of compression of the gas is negligible and unlikely to cause the lowering observed in the distributor pressure drop. The most likely physical explanation is that the normal pattern of gas flow through an orifice is disturbed, e.g. the vena contracta may be distorted or there is a pressure recovery effect after the orifice. The phenomenon calls for further investigation.

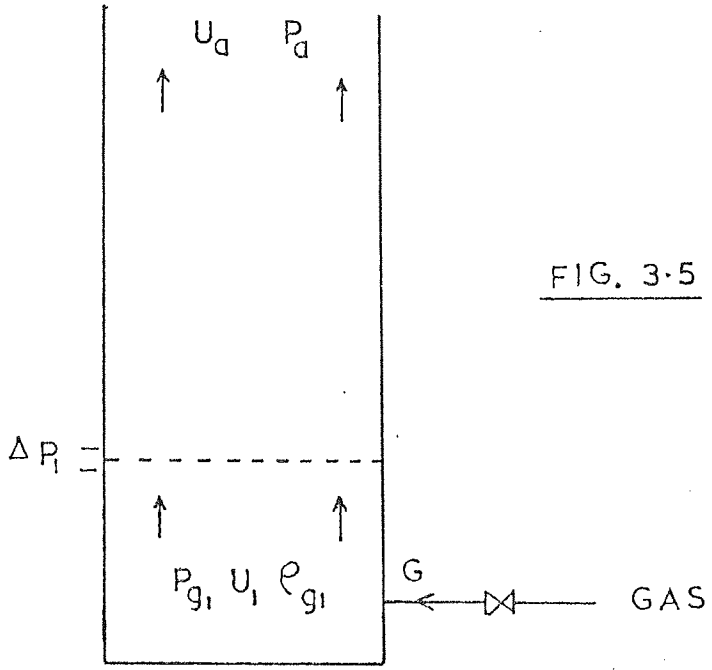

FIG. 3·5

$$P_{g1} = \Delta P_1 + P_a$$

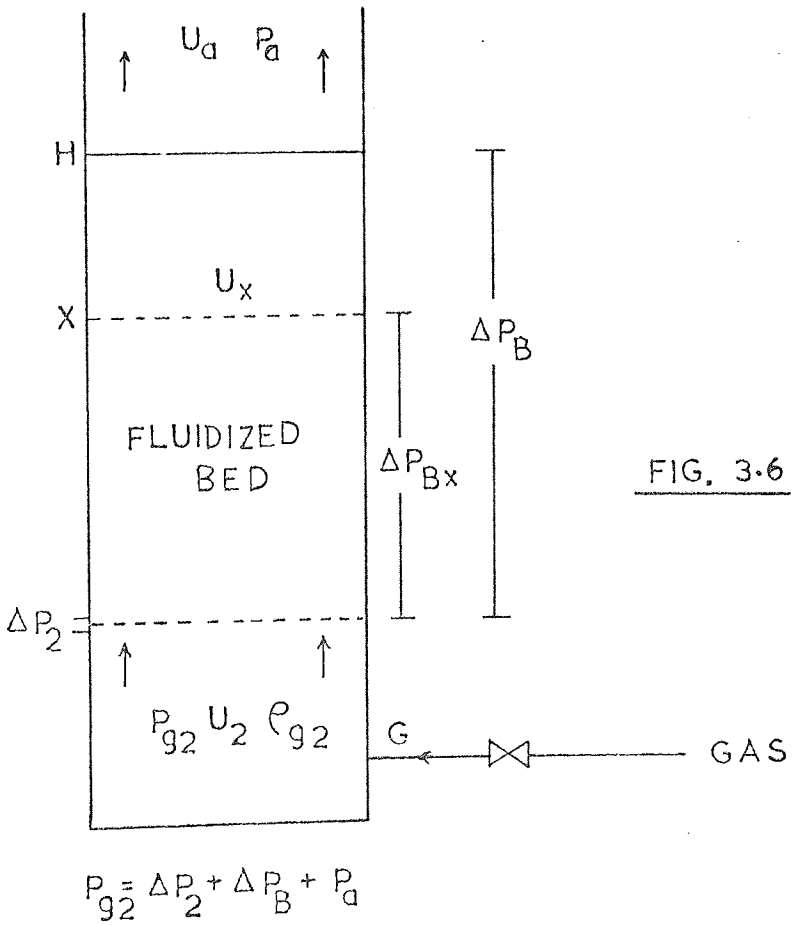

FIG. 3·6

$$P_{g2} = \Delta P_2 + \Delta P_B + P_a$$

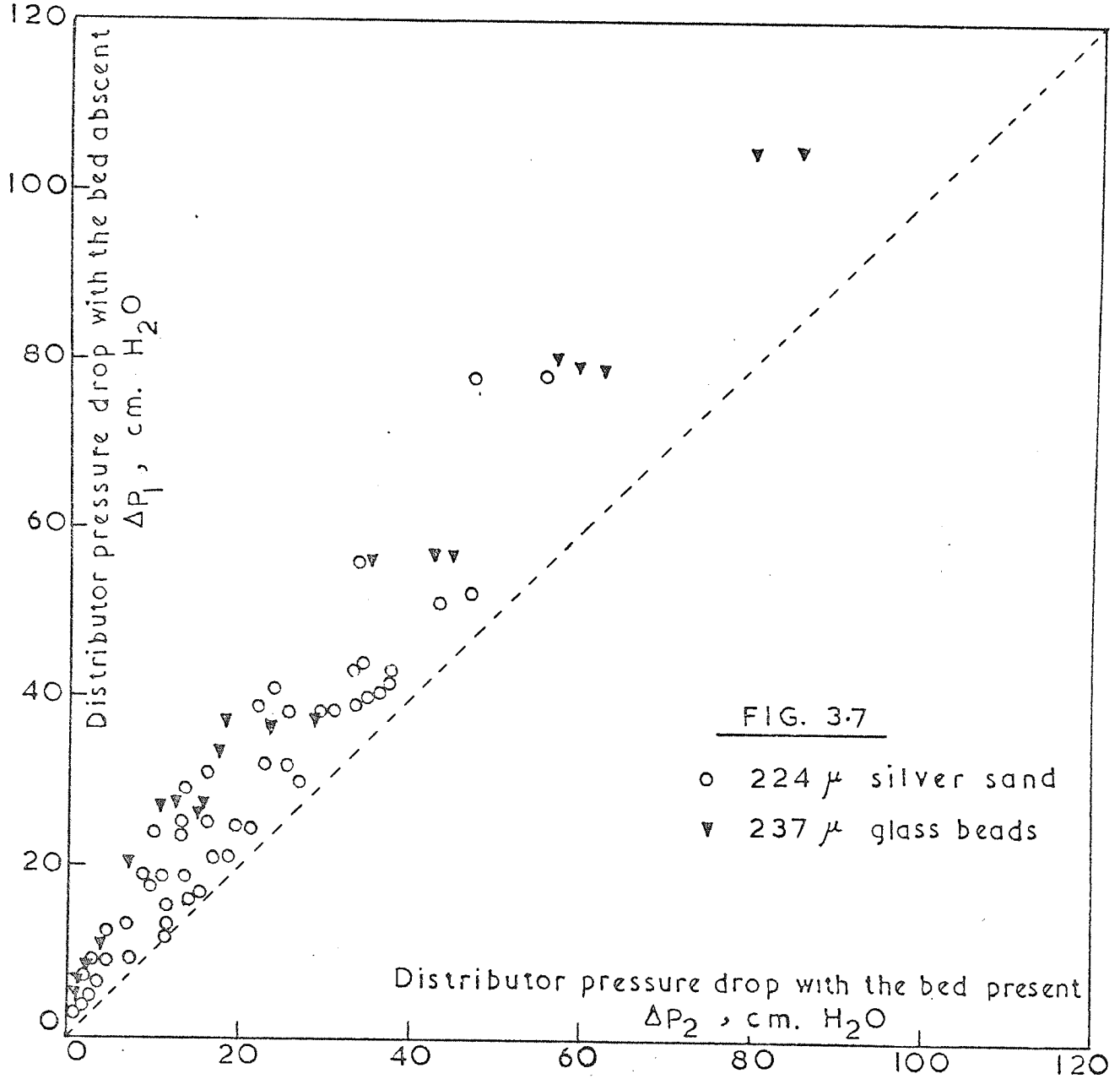
120
100
80
60
40
20
0
0
20
40
60
80
100
120
Distributor pressure drop with the bed absent
ΔP_1 , cm. H_2O
Distributor pressure drop with the bed present
ΔP_2 , cm. H_2O
FIG. 3·7
o 224 μ silver sand
▼ 237 μ glass beads

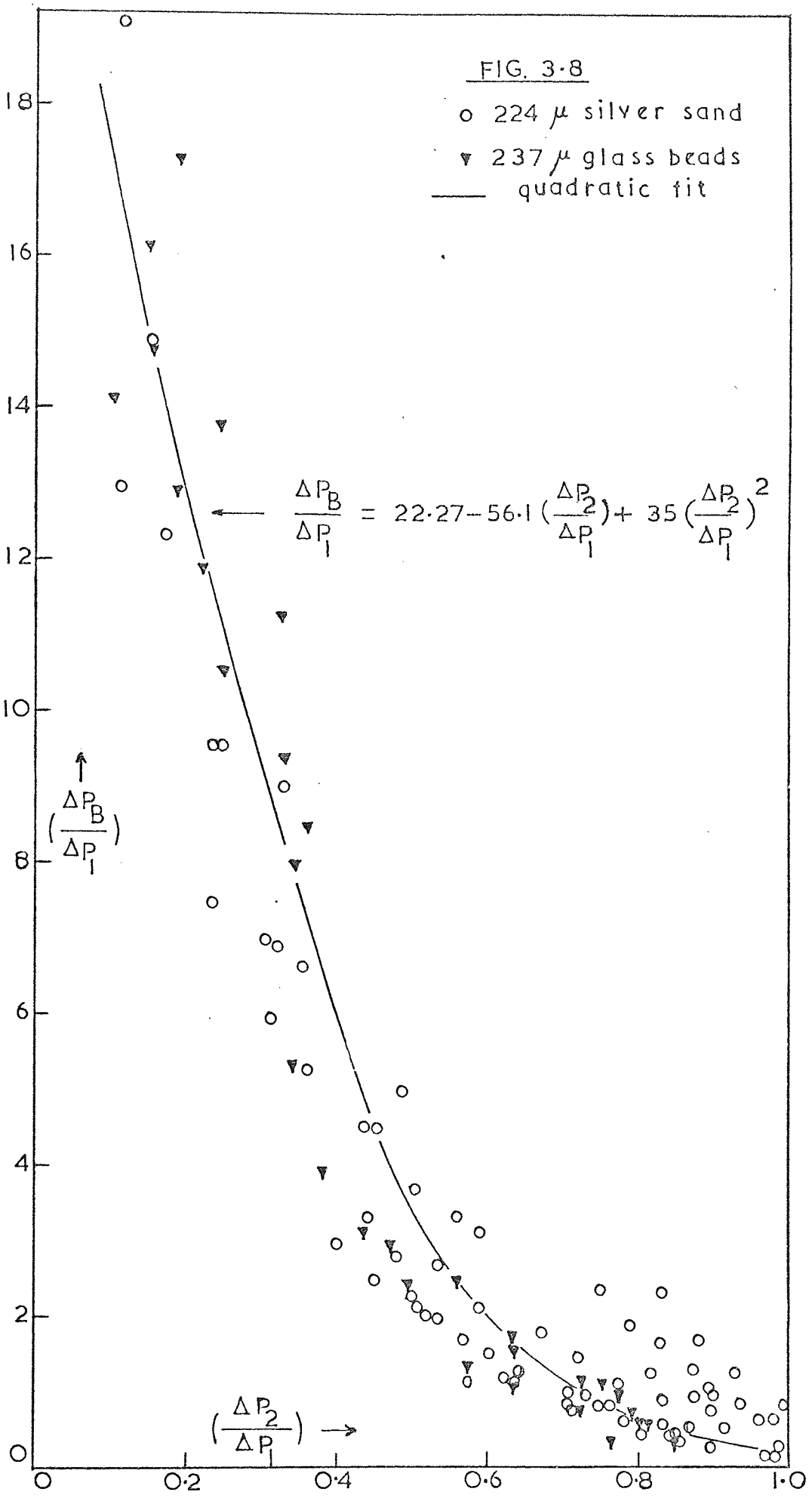
FIG. 3·8
o 224 μ silver sand
▼ 237 μ glass beads
quadratic fit
$\frac{\Delta P_B}{\Delta P_1} = 22{\cdot}27 - 56{\cdot}1\left(\frac{\Delta P_2}{\Delta P_1}\right) + 35\left(\frac{\Delta P_2}{\Delta P_1}\right)^2$
$\left(\frac{\Delta P_B}{\Delta P_1}\right)$
$\left(\frac{\Delta P_2}{\Delta P_1}\right)$
0
2
4
6
8
10
12
14
16
18
0·2
0·4
0·6
0·8
1·0

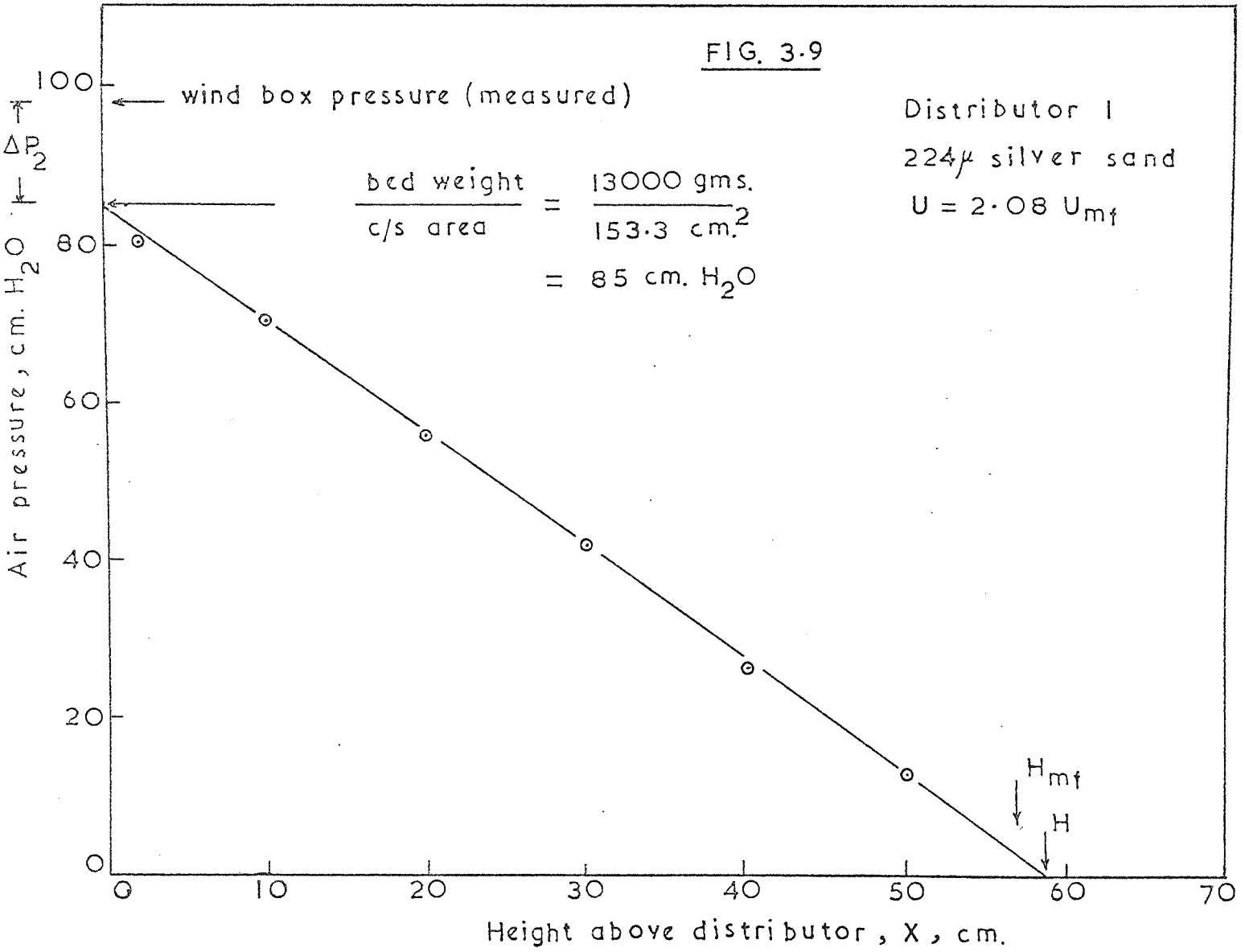
FIG. 3·9
wind box pressure (measured)
Distributor 1
224μ silver sand
U = 2·08 Umf
bed weight / c/s area = 13000 gms. / 153.3 cm.2
= 85 cm. H2O
ΔP2
Air pressure, cm. H2O
100
80
60
40
20
0
0
10
20
30
40
50
60
70
Hmf
H
Height above distributor, X, cm.

FIG. 3·10

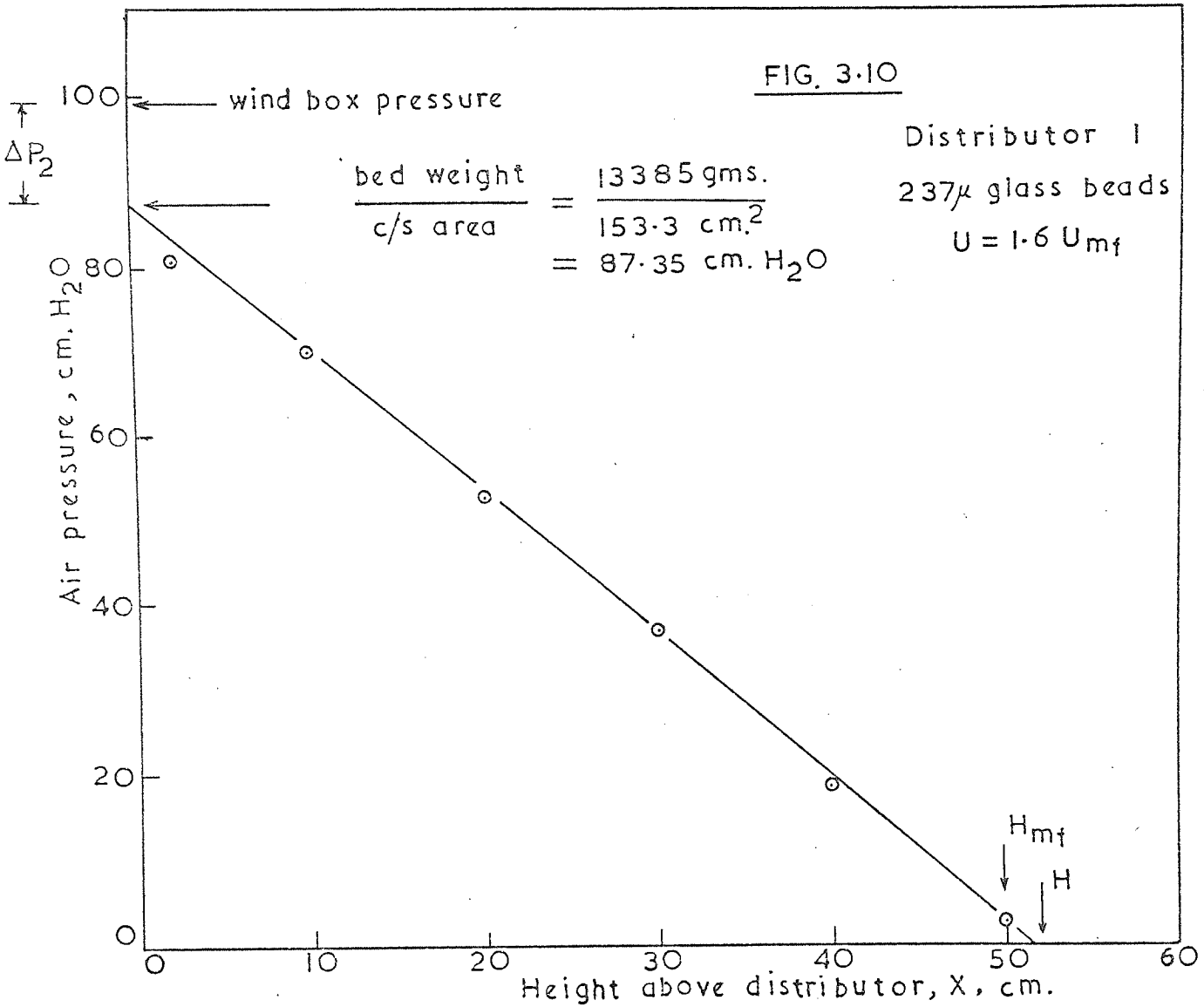
wind box pressure
ΔP_2
bed weight / c/s area = 13385 gms. / 153·3 cm.^{2}
= 87·35 cm. H_2O
Distributor 1
237μ glass beads
U = 1·6 U_{mf}
Air pressure, cm. H_2O
100
80
60
40
20
0
H_{mf}
H
0
10
20
30
40
50
60
Height above distributor, X, cm.

3.3 Effect of Pressure Drop Ratio ($\Delta P_D/\Delta P_B$) on Stability of Fluidization.

The pressure drop across the distributor ΔP_D must be of a certain magnitude if it is to distribute the fluidizing gas evenly. This pressure drop is often related to the bed pressure drop ΔP_B. An analysis of the data available (see Chapter 1) drew attention to the existence of high and low pressure drop "school of thought", i.e. where $\Delta P_D/\Delta P_B \geqslant 0.4$ or alternatively $\Delta P_D/\Delta P_B \leqslant 0.2$. It is believed that the wide variation in recommended pressure drop encountered was due to the various geometries of bed studied, and that no single pressure drop ratio could be advocated or could be used to all situations. To date studies offer little information which aids the practical designer, and the conflicting evidence regarding pressure drop criteria shows the need for further investigation.

In this work ratios of distributor pressure drop to bed pressure drop ($\Delta P_D/\Delta P_B$) at which stability occurred for a number of multi-orifice distributors having different pressure drops have been studied, with cylindrical beds of different diameters and depths using a variety of solid systems.

Two cylindrical columns were employed in the experiments: (i) a Perspex column, 14 cm. inside diameter and 40 cm. high, similar to that already described in section 2 of this chapter and (ii) a standard Q.V.F. glass column, 30.5 cm. inside diameter and about 60 cm. high.

As with earlier work, the multi-orifice distributors had pressure tappings drilled onto each of them to ensure a realiable measure of pressure drop across the bed and the distributor. With the larger bed, orifices were drilled on a square-pitch array giving a fractional free area $\phi = 26.4 \times 10^{-4}$ ($D_o = 0.159$ cm. and $N = 97$). It should be emphasised that the distributor pressure drop used in this study was that

measured in the presence of the bed. The work presented in the previous section showed that the presence of the bed lowers the distributor pressure drop relative to its pressure drop without the bed, and this lower pressure drop is the appropriate parameter for this investigation.

The stability of fluidization was assessed visually, but it was also rated by the presence and abscence in the bed of tracks and de-fluidized zones because, presence of a defluidized zone or serious channelling in any part of the bed caused the reading from the pressure tapping (one of those located on the distributor plate) in that part to differ from the rest. In that context it meant by "stable fluidization" even distribution of bubbles over the cross-section of the fluidized bed, and operation of a distributor below the critical ratio would lead to instability manifested as tracks or dead zones. Results of this work suggest that this ratio is a function of aspect ratio of bed height to bed diameter H/D, and thus is a parameter of scale-up.

Kelsey(32) has previously carried out a similar investigation in two-dimensional bed. However, it must be emphasised that two-dimensional fluidized beds require a lower pressure drop ratio than a three-dimensional unit since a dead zone or a zone of preferential bubbling had more freedom of movement in a three-dimensional bed unit than two-dimensional bed unit. Geldart and Kelsey(58) have observed lower rates of coalescence in a two-dimensional bed than three-dimensional bed when both were compared at the same operating conditions. This was believed to be due to the fact that coalescence would take place only in one plane in a two-dimensional bed. Therefore, one would expect a stable operation at a lower gas velocity and this obviously entails corresoondingly a lower pressure drop across the distribution plate.

The experimental results are presented in Tables (3.11) - (3.12) and in Figure (3.11) a plot of $(\Delta P_D/\Delta P_B)$ vs. (H/D) show their comparison

with ratios recommended for some industrial processes. Data reported by Kelsey(32) for a two-dimensional bed are also included in the plot. As may be seen, the critical pressure drop ratio increased rapidly as the aspect ratio decreased. The results suggest that the aspect ratio is important in affecting distributor design; beds of high aspect ratio (i.e. $H/D > 2$) requiring only low pressure drop ratios for stable operation and beds of low aspect ratio (i.e. $H/D < 0.1$) requiring high pressure drop ratios. In that context it meant by "high pressure drop ratio" one approaching 100% and by "low pressure drop ratio" one between 10 - 20%.

The experimental results are in broad agreement with those actually used in industrial practice. However, it must be recognised that the behaviour of industrial distributors is rather difficult to interpret due to the different geometries and shapes of the gas passages employed and the extra devices placed below and above the distributor. A commercial fluidized bed inevitably contains a variety of internals such as cyclone diplegs, baffles or cooling tubes. Such devices may help to break up the bubbles and bring about smoother operation. In some cases extra devices are placed below the distributor to secure a uniform distribution of the gas approaching the bed. These are often called pre-distribution devices, and include guide vanes, deflector plates to change the direction of the gas stream, and screens or diffusers. In the literature survey, we noted the use of pre-distribution devices with distributors in "cat-cracker"; such devices which include the pipe system known as the "porcupine". Gregory(25) mentions the use of a sparge pipe having low pressure drop beneath the distributor plate in the Frodingham gas desulphurising process. As can be seen from Figure (3.11), the ratios recommended by Gregory fall in the unstable region of the present work. This may be attributed to the effect of using the sparge pipe in

straightening the gas flow through the distributor without appreciably increasing the pressure drop. It is interesting to note that the trend of the experimental results is in line with Avery and Tracy(20) who referred to a pressure drop ratio of 100% being necessary in shallow large diameter beds used in the Courtaulds Limited Process for solvent recovery from gases.

The effect of increasing bed diameter on bed stability is significant particularly at low aspect ratios. This is apparent when results from the two cylindrical beds are compared at aspect ratios equal to or less than 0.5. (The use of this ratio more or less eliminates the possibility of 'slugging' for the smaller diameter bed). The larger bed appears to require a higher pressure drop ratio than the smaller diameter bed to fluidize it properly. The difference becomes gradually more pronounced as the aspect ratio decreases, confirming the prediction discussed in the literature survey, that irregular distribution is more likely to occur in large vessels because of the formation of tracks and dead zones.

As can be seen from the plot, results for two-dimensional bed are considerably lower than those for three-dimensional bed particularly at low aspect ratios, also confirming the prediction that maldistribution is associated with large vessels. It is evident, therefore, that pressure drop criteria measured in two- dimensional beds cannot be applied directly in three-dimensional situations. However, it is interesting to note that trends and effects observed in three-dimensional bed are also present in two-dimensional system.

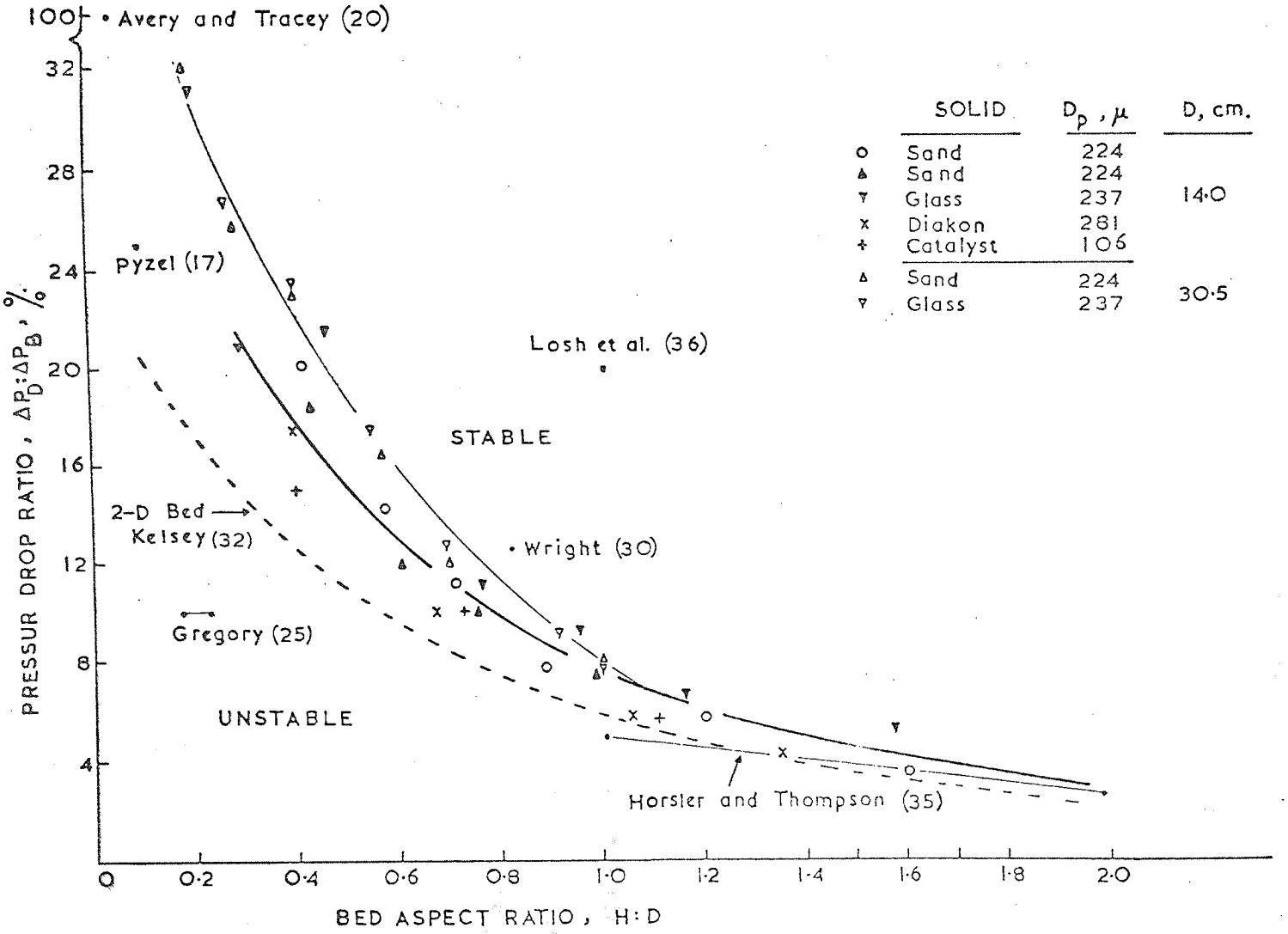

FIG. 3·11 EFFECT OF DISTRIBUTOR ON BED STABILITY

CONCLUSIONS

1. Multi-orifice distributor plates possess a quadratic characteristics, i.e. the pressure drop-flow relationship falls within the turbulent regime.

2. The presence of the bed reduces the distributor pressure drop relative to its pressure drop without the bed, and this new pressure drop is the relevant parameter for distributor design.

The experimental results confirm Sutherland's theory and show good agreement with the recently published work and, therefore, cast doubt on some of the investigations reported in the literature in which the effect of bed presence on the distributor pressure drop has been ignored. However, further work is necessary to show the precise effect of bed presence on the normal pattern of gas flow through the orifices.

3. Ratios of distributor pressure drop to bed pressure drop at which stable fluidization occurs show reasonable agreement with industrial practice. There is evidence that larger diameter beds tend to be less stable than smaller diameter beds when these are operated with shallow beds.

4. MULTI-ORIFICE DISTRIBUTOR DESIGN VARIABLES AND BUBBLE FORMATION

4.1 Introduction

According to the two-phase theory of fluidization, in gas fluidized beds the gas in excess of that required for incipient fluidization passes through the bed as bubbles. These bubbles grow as they travel up the bed, mainly because of coalescence with other bubbles. Average size, size distribution, and number of bubbles are needed in the design of fluidized beds in gas-solids contact for mass transfer, heat transfer, and chemical reactions where, for example a gaseous reaction is catalyzed by the fluidized solids(50).

4.2 Previous Work

Bubble formation has been investigated by various researchers and many experimental data have been reported. Among them the works of Yasui and Johanson(95), Toei et al.(96), Romero and Smith(97), Kobayashi et al.(98), Grosh(61), Baugarten and Pigford(99) and Lanneau(100) are noteworthy, and the literature has already been reviewed by Davidson and Harrison(82).

Following the analysis of Kobayashi et al.(98) and Kato and Wen(101), the bubble diameter D_B at a distance h above the distributor plate can be approximated by

$$D_B = 1.4\, \rho_s\, D_p \left(\frac{U}{U_{mf}}\right) h \quad , \tag{4.1}$$

where

D_B = bubble diameter, cm.

D_p = mean particle diameter, cm.

h = distance away from the distributor, cm.

U = superficial gas velocity, cm/sec.

U_{mf} = incipient fluidizing velocity, cm/sec.

ρ_s = solid density, gm/cm^3.

The above correlation is based on data obtained using porous plates as the distributor. To date studies offer little information on bubble growth either with single-orifice distributors or with multi-orifice distributors of the type likely to be used in practice. As has been indicated earlier, multi-orifice distributors, nozzles, bubble-caps and conical distributors are of greater practical interest because, of course, porous distributors are rarely used in industry.

Clearly from (4.1) it may be seen that an estimate of the bubble diameter at the distributor surface cannot be made, i.e. as $h \to 0$, $D_B \simeq 0$. For multi-orifice distributors and similar devices the size of bubbles at the distributor level are substantial and therefore must be taken into consideration.

4.3 Estimation of Bubble Size in the Vicinity of a Multi-Orifice Distributor

An estimate of the bubble size at the surface of a multi-orifice distributor having N identical orifices can be made from

$$D_{Bo} = \left[\frac{6A_o(U - U_{mf})}{\pi . N} \right]^{0.4} / g^{0.2} \quad (cm) \quad , \qquad (4.2)$$

where A is the distributor cross-sectional area, cm^2.

Although (4.2) strictly applies to a single orifice in a fluidized bed at incipient fluidization, Cookes et al.(102) and Geldart(103) showed this to be valid for multi-orifices in a freely bubbling bed. Therefore, in general, the diameter of bubbles in a fluidized bed can be expressed as

$$D_B = 1.4\ \rho_s\ D_p\ \left(\frac{U}{U_{mf}}\right)_o\ h \quad , \qquad (4.1)$$

for porous plate distributors, and

$$D_B = 1.4\ \rho_s\ D_p\ \left(\frac{U}{U_{mf}}\right)_o\ h + D_{Bo} \quad , \qquad (4.3)$$

for multi-orifice distributors, according to Cookes et al.(102).

Equation (4.3) implies the existence of a bubble at the surface of an orifice and its growth by the addition of excess gas from the bed.

4.4 Effect of Distributor Geometry on Bubble Coalescence

4.4.1 Theoretical Consideration

Coalescence of bubbles is an important feature of fluidized beds which governs the size and number of bubbles present in the bed. As mentioned earlier, these parameters are needed in the design of fluidized beds in gas-solids contact for mass transfer, heat transfer and chemical reaction.

No attempt can be made here to survey the field of coalescence. The following analysis is based on the "bubble assemblage model" for catalytic reactions proposed recently by Kato and Wen(101). This model provides a method for predicting the number of bubbles as they grow and coalesce within discrete sections of the fluidized bed using multi-orifice distributor.

Their model is based on the assumption that the fluidized bed can be approximately represented by N_c numbers of successive superimposed horizontal compartments. The height of each compartment is equal to the size of the bubble at the corresponding bed height. Each compartment is considered to consist of bubble phase and emulsion phase (see Figure (4.1)). This assumption not only makes it possible to introduce multiple sizes into the model but also makes it convenient for computer simulations. The essentials of this model are summarized below:

The change of the bubble diameter with the bed height is given by equation (4.3), i.e.

$$D_B = 1.4\, \rho_s \cdot D_p \cdot \left(\frac{U}{U_{mf}}\right) \cdot h + D_{Bo} \qquad (4.3)$$

The rising velocity of a crowd of bubbles through a fluidized bed is given(82) by

$$U_B = (U - U_{mf}) + (0.711 \sqrt{g.D_B}) \qquad (4.4)$$

The total volume of the gas bubbles within the fluidized bed may be expressed as

$$V_B = (H - H_{mf}). A \quad , \qquad (4.5)$$

where

V_B = total bubble volume in the bed, cm^3.

H = expanded height of fluidized bed, cm.

H_{mf} = incipient bed height, cm.

A = cross-sectional area of the bed, cm^2.

Taking the characteristic bubble diameter as that corresponding to the bubble at level $H_{mf}/2$, then from equations (4.3) - (4.5), the bed expansion ratio can be expressed as

$$\frac{H - H_{mf}}{H} = (U - U_{mf}) / (0.711 \sqrt{g. \bar{D}_B}) \qquad (4.6)$$

Where $\bar{D}_B$ is an average bubble diameter of the bed given by

$$\bar{D}_B = 1.4 \rho_s. D_p.(\frac{U}{U_{mf}}). \frac{H_{mf}}{2} + D_{Bo} \qquad (4.7)$$

Kato and Wen(101) examined the validity of (4.6) using experimental data available in the literature. The agreement between (4.6) and experiments appeared to be reasonably satisfactory. Data obtained experimentally from the present work also confirm (4.6). Thus equation (4.6) may be used to compute the voidage fraction within the fluidized bed as it is needed in the mathematical formulation of the model.

4.4.2 Voidage Distribution Within the Fluidized Bed

Following the studies of Bakker(104), Kato and Wen considered the bed voidage e to be approximately uniform up to a bed height corresponding to H_{mf} while above H_{mf}, e increased linearly along the bed height as shown in Figure (4.1), i.e.

$$1 - e = \frac{H_{mf}}{H_f} \cdot (1 - e_{mf}) \quad \text{for } h \leqslant H_{mf} \tag{4.8}$$

and

$$(1 - e) = \frac{H_{mf}}{H_f} \cdot (1 - e_{mf}) - \frac{H_{mf} \cdot (1 - e_{mf}) \cdot (h - H_{mf})}{2H_f \cdot (H_f - H_{mf})} \tag{4.9}$$

$$\text{for } H_{mf} \leqslant h \leqslant H_{mf} + 2(H_f - H_{mf}) = H$$

Where

e = void fraction in bed as a whole, -

e_{mf} = void fraction in bed at incipient fluidization, -

H_f = height of fluidized bed as depicted in Figure (4.1).

4.4.3 Calculation of Number of Bubbles in Each Compartment

Based on an arithmetic average of bubble sizes, the height of the initial compartment immediately above the distributor is

$$\Delta h_1 = \frac{D_{Bo} + (m \, \Delta h_1 + D_{Bo})}{2} \quad ,$$

$$\text{or} \qquad \Delta h_1 = \frac{2 \, D_{Bo}}{(2 - m)} \quad , \tag{4.10}$$

Where $m = 1.4 \, \rho_s \cdot D_p \cdot (U/U_{mf})$ = constant for a given operating condition, and that of i-th compartment becomes,

$$\Delta h_i = 2 \, D_{Bo} \cdot \frac{(2 + m)^{i-1}}{(2 - m)^i} \quad , \tag{4.11}$$

where $i = 1, 2, 3, \ldots\ldots$

If bubbles are assumed to be approximately spherical, then from (4.5) and (4.11) the number of bubbles and the volume of the bubble phase in the i-th compartment can be computed, respectively as

$$N_{Bi} = \frac{6A}{\pi (\Delta h_i)^2} \cdot \frac{e - e_{mf}}{1 - e_{mf}} \cdot , \qquad (4.12)$$

$$V_{Bi} = \frac{\pi}{6} (\Delta h_i)^3 \cdot N_{Bi} \qquad (4.13)$$

The distance from the distributor surface to the N_c-th compartment is

$$h_{Nc} = \sum_{i=1}^{N_c} \Delta h_i \quad , \qquad (4.14)$$

Where N_c = total number of compartments.

The theoretical analysis given above has been extracted from the model presented by Kato and Wen in their studies of gas-solid reactions in a fluidized bed reactor based on information of the bubble behaviour and the movement of solids.

Clearly the model does not indicate the importance of changing the orifice diameter, although a change in orifice diameter would not be expected to affect the operational effectiveness of the distributor provided that the fluidizing gas is well distributed across it. But this linked with orifice area and total free area, viz, for a given number of orifices and constant orifice spacing it is expected that the average diameter of the bubble from a coarse distributor would be larger than that from a fine distributor. Also, with a coarse distributor bubbles may pass through the bed in "tracks" rather than being uniformly distributed. The existence of tracks will undoubtedly increase the velocity of rise of bubbles. Furthermore, it may be expected that with the particle bed present not all the orifices are operative at a certain gas flow

rates, because inevitably some orifices become jammed and blocked up with particles. Kato and Wen did not consider these possibilities: to ascertain the applicability of their model they used experimental data based on porous plate distributors. Again such data have little practical relevance particularly from the view point of distributor design.

4.5 Objectives of this Investigation

The work described in this chapter has several aims:

(i) To investigate the behaviour of multi-orifice distributors with regard to bubble formation with bed height and to provide data so that the validity of the models (4.2) and (4.3) may be examined.

(ii) To evaluate the usefulness of Kato and Wen's model in predicting the number and size of bubbles as they grow and coalesce within the fluidized bed since it is relevant to the design of multi-orifice distributors.

Other aspects of distributor design related to the way in which even distribution of bubbles on the top surface of the fluidized bed was obtained (e.g. the desirable pressure drop ratio ($\Delta P_D/\Delta P_B$) for the even distribution of gas across the bed) have been investigated already (see Chapter 3).

It is hoped that this investigation will yield information which will enable bubble diameter, number of bubbles and their volume to be predicted from the distributor configuration and the pressure drop across it.

It is believed that the conclusions to be drawn from this investigation may be extended to other distributing devices (e.g. bubble-caps, nozzles or conical distributors) since these devices are basically similar to multi-orifice distributor in respect of bubble formation.

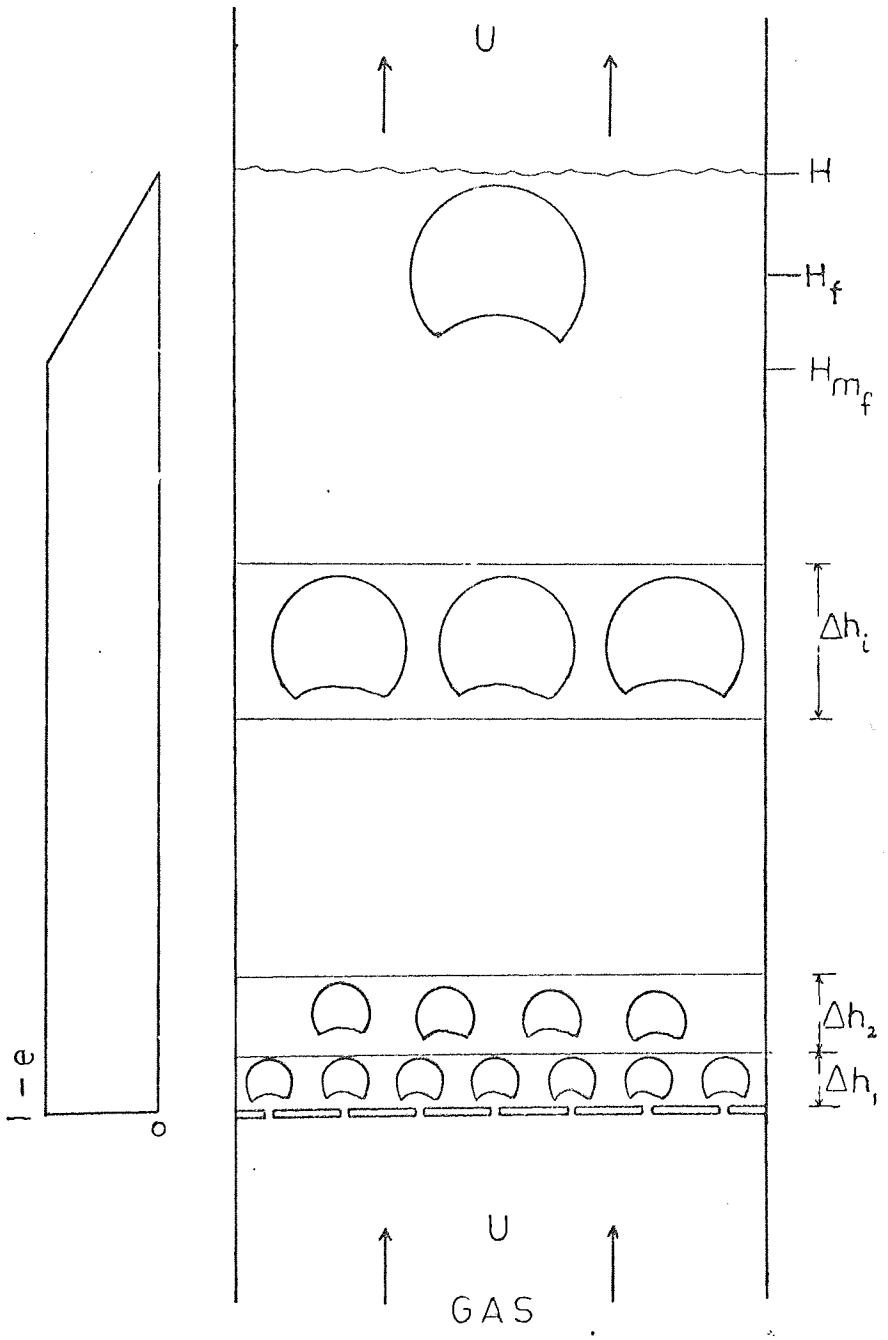

FIG. 4·1 KATO AND WEN'S MODEL

4.6 Equipment and Experiments

In the present work bubble sizes in air fluidized beds were quantitatively determined by two methods: (i) by taking ciné pictures of the bubbles breaking the top surface of the bed and by determining the size of the bubbles from the film, (ii) visually by laying a ruler across the bed surface and reading the diameter by eye.

The experiments were carried out in a cylindrical column made of Perspex, 14 cm. inside diameter and about 40 cm. high.

The fluidizing air was taken from the laboratory main, reduced to a pressure of 25 - 20 p.s.i.g., and metered through calibrated rotameters. Needle valves were used to regulate the flow through the rotameters. The inside wall of the column was sprayed with antistatic cleaner and the air was slightly humidified. These measures were taken in the attempt to reduce static build-up in the bed.

Table (4.1) gives details of the multi-orifice distributors used. These were 1/8" thick aluminium plates with orifices arranged on a triangular-pitch array. As with earlier work (Chapter 3) the distributors had pressure tappings drilled onto each of them to ensure a reliable measure of pressure drop across the bed and the distributor. The Perspex column used in this study had no wall tappings, but the bed pressure drop was obtained directly from the pressure tappings (five on each plate) located on the distributor plate.

4.6.1 Distributor Section

The bed distributor section for the 14 cm. column is shown in Figure (4.2). This consisted of a length of Perspex tube 14 cm. in diameter and 15 cm. long. It was connected at the base to a conical inlet made of standard Q.V.F. glass. The whole assembly formed a wind box 30 cm. deep and approximately 4.9×10^3 cm^3. in volume. This was intended

to provide an even velocity profile to the underside of the distributor plate.

As shown in Figure (4.2), the distributor mounting was designed to provide ease in changing plates and to give unobstructed area of gas flow.

4.6.2 Arrangement for Ciné Photography

To take photographs, it was necessary to position the camera above the bed surface. Focusing requirements originally indicated having the fluidized bed movable and the camera fixed. With the present experimental equipment, this proved to be rather undesirable. To avoid this and to meet the above requirements a mirror was placed at a 45^{o} angle to the top surface of the bed. Photographs were taken of the mirror. Thus, each photographic record showed the inside diameter of the column and bubbles as if they were viewed from the top. As shown in Figure (4.3) the camera was fixed on a tripod in front of the fluidizing column. This arrangement allowed enough freedom for the camera to be adjusted for the right distance and lens opening.

The mirror used to achieve a view of the top surface of the bed was a twin-ground glass second surface mirror. The mirror was 15 cm. x 15 cm. x 0.3 cm., placed at 45^{o} angle to the top surface of the bed and supported by a clamp arrangement in a vertical position.

To take photographs of the bubbles breaking the top surface of the bed a Beaulie Model R16, 16 mm ciné camera was used. A telephoto lens was used to minimize parallax error. Kodak Tri-X black and white was used in the camera.

The bed surface was illuminated from behind by floodlights through a diffusing screen (tracing paper) positioned about 6 cm. from the back of the bed. It was necessary to avoid placing the screen actually against the bed as this set up an electrostatic effect in the bed.

4.6.3 Positioning of the Camera and Mirror

A cathetometer with microscopic eyepiece was placed at point D (see Figure (4.3)) and by trial and error moved back and forth until it was lined up in plane $\overline{AB}$, the outside edge of the Perspex column. The camera was placed at point C and by trial and error moved up and down until the centre of the lens was exactly on the eyepiece of the cathetometer. The axis of the lens was then coincident with the plane $\overline{AB}$ and parallel to the principal light rays which formed each surface eruption image.

As previously mentioned, the mirror was supported by two clamps fixed to the metal frame work which supported the fluidized bed. The mirror was positioned at a 45^{o} angle to the plane $\overline{AB}$ by means of an armed metal protractor which is capable of measuring angles $\pm$ 30 seconds.

4.7 Particles

Two types of solids were used in the experiments. These were ungraded silver sand (100 - 350 μ) and graded glass beads having mean particle diameter 224 μ and 237 μ respectively, and these are specified in Table (2.3) (Chapter 2).

Some experiments were attempted with cracking catalyst of wide size distribution. When this was fluidized, its very fine particles formed a cloud of dust which filled the containing column above the bed surface and created poor visibility for taking cine pictures.

4.8 Experimental Procedure

In any particular run the height of the bed at rest was measured, and the bed was fluidized at a high flow rate of air. The flow was maintained at this level for a few minutes and then reduced to the desired level. Air flow rate was measured along with pressure drop across the bed directly from the pressure tappings located on the distribution plate. The floodlights were turned on, the camera was positioned for the right distance and lens opening, and the ciné pictures were taken at 32 frames/sec. for a prescribed time interval. At the same time the number of surface eruptions was counted so that a comparison with photographs can be made. However, the agreement between the two methods was quite satisfactory. Air flow rate and pressure drop were again checked and the run was completed.

The frames of the developed film were projected on coordinate paper held against the screen of a desk viewer (telescreen) and coordinates of the centre and diameter were recorded for each bubble just before bursting. For eruptions that were not round, the geometric mean of the maximum D_{max} and minimum D_{min} measured dimensions were recorded as the diameter D_i, i.e.

$$D_i = \sqrt{D_{max} \times D_{min}} \quad (cm.) \quad , \tag{4.15}$$

where D_i = diameter of surface eruptions of the i-th size.

The inside diameter of the column was used as a reference for calibrating lengths.

4.8.1 Visual Measurements

The bubble eruption diameters were also determined by laying a 10 cm. rule across the bed surface and reading the diameter by eye. At low gas flow rates, the size of surface eruptions was found to be fairly reproducible and most bubbles appeared to be round. However, at higher

gas flow rates the surface fluctuated considerably and it became very difficult to estimate the eruption diameter. In this case measurements were made by ciné pictures.

Considering the amount of labour and time that can arise from the analyses of the ciné frames it seems profitable to use this simpler method which is probably adequate for most practical purposes. On these grounds, a large number of measurements were obtained by using this technique and it produced results almost similar to those obtained by motion pictures.

Fluctuations of the bed surface did not allow the use of beds deeper than 30 cm. since above this it became difficult to measure. Moreover, particles thrown up by erupting bubbles obscured the bed surface and made photography of bubbles or estimation of bubble diameter difficult.

4.8.2 Determination of Average Eruption Diameter

For each set of observations, a simple arithmetic average eruption diameter D_c was calculated as follows:

$$D_c = \sum_{i=1}^{I} n_i D_i \Big/ \sum_{i=1}^{I} n_i \quad (cm.) \qquad (4.16)$$

Where n_i = number of surface eruptions of diameter D_i,

I = total number of different eruption sizes in a run.

4.8.3 Estimation of True Eruption Diameter

Botterill, George and Besford(105), found experimentally that the disturbance caused by a bubble bursting at the surface of the bed is larger than the bubble causing it. Their interest lay in defining bubble size from surface disturbance. They concluded that the eruption diameter is about 1.5 times the diameter of the bubble in the bed, but it is not clear whether this applies to all bubble sizes. However, their findings have been verified theoretically by Zenz(106) (see Appendix 4). The theory indicates that there exists around each rising bubble solid

particles in a concentric shell having thickness approximately $\frac{1}{4}$ the bubble diameter. Therefore, according to these findings, bubble diameters were estimated as two-thirds of the diameter of the eruptions at the top of the bed, i.e.

$$D_B = \frac{2}{3} \cdot D_c \quad , \tag{4.17}$$

where D_B = diameter of bubble causing an eruption on the top surface of the bed.

D_c = diameter of surface eruption.

FIG. 4·2 DETAILS OF DISTRIBUTOR SECTION

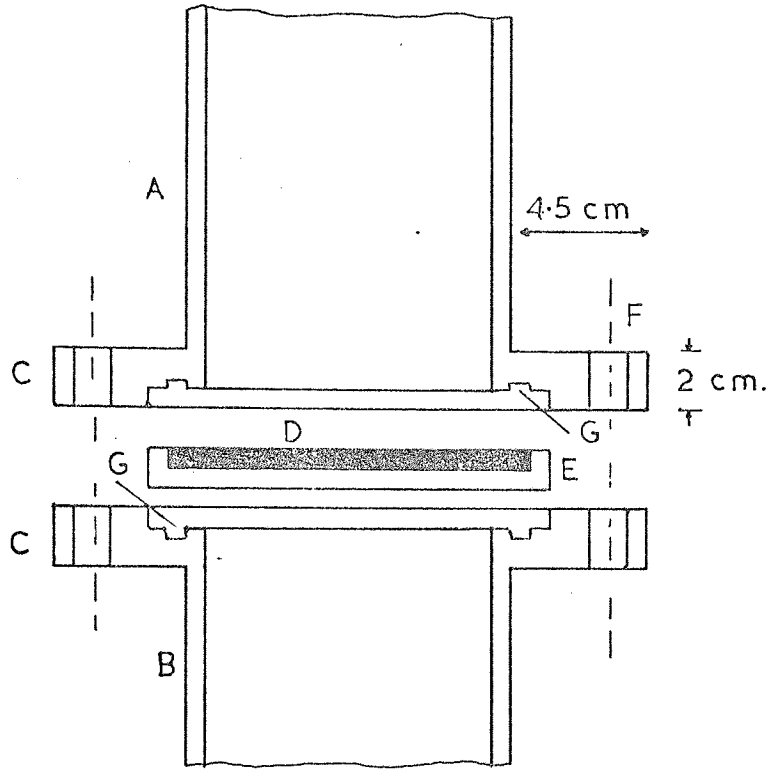

List of Materials

A 14 cm. diam. Perspex tube

B 14 cm. diam., 15 cm. long Perspex tube

D Distributor plate

C Perspex

E Perspex support ring

F 6 x 0·8 cm. diam. bolts

G o-rings

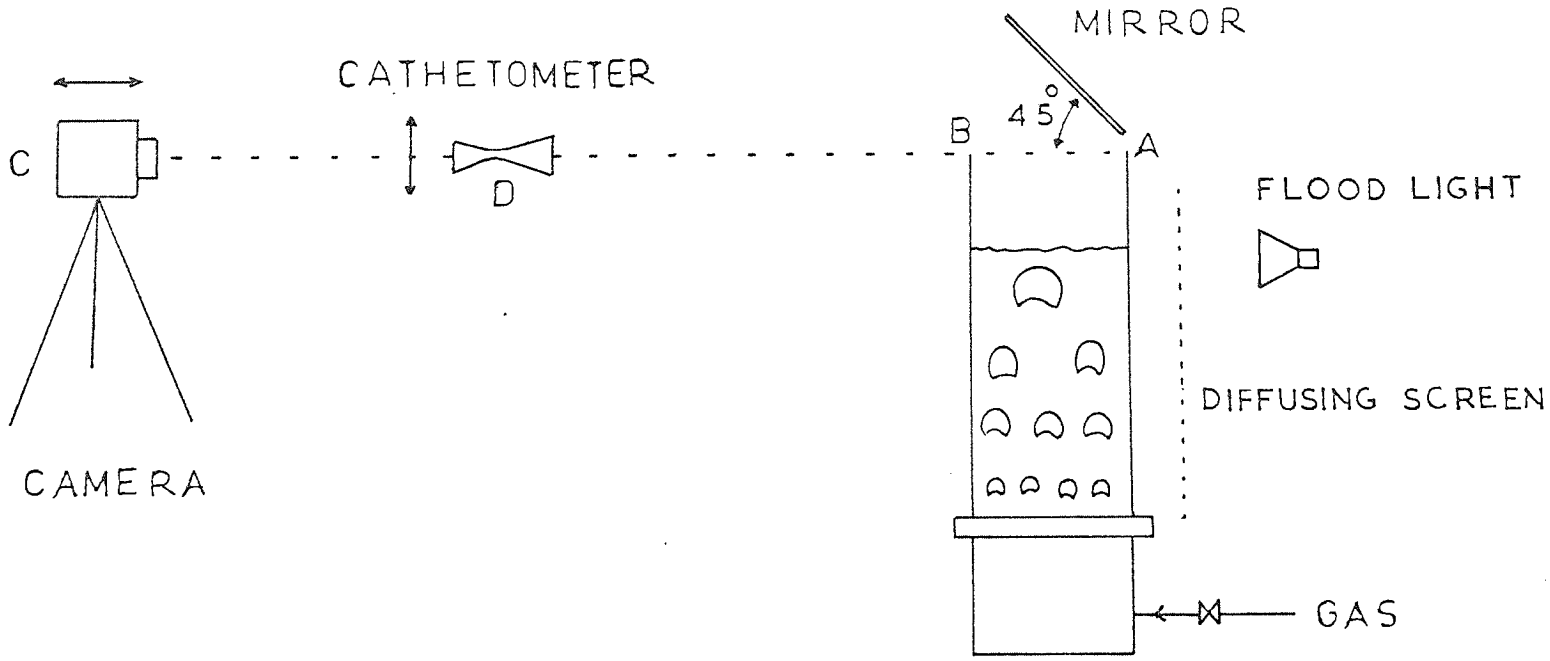

FIG. 4·3 ARRANEMENT FOR CINE PHOTOGRAPHY

4.9 Results and Discussion

Before discussing in detail the effects studied two points must be commented on:

(1) Measures were taken to avoid channelling in the bed as it would undoubtedly increase the diameter of bubbles breaking the top surface. Observations made on the gas flow cycle rising from zero slowly up to $U - U_{mf}$ (where almost all the orifices were operative, indicated by consistent bubbling on the top surface of the bed) and then falling slowly to zero again indicated that channelling could effectively be eliminated at a particular fluidizing flow rate. This may be done by over-running the desired rate and then decreasing the gas supply to the desired rate after obtaining full operation of the orifices. Full operation was maintained until the gas flow rate was reduced to a certain level when some of the orifices stopped bubbling and became inoperative.

(2) The lowest bed height according to prior theory for studying bubble sizesapproximates to the maximum spoutable bed height for a given solid-distributor system. The maximum spoutable bed height (the minimum above which bubbles may be observed or complete fluidization in a two-dimensional bed) was calculated from the expression given by Lefroy and Davidson(107) as

$$H_m = 0.68 \; D^{4/3} \cdot D_p^{-1/3} \quad , \tag{4.18}$$

where H_m = maximum spoutable bed height, cm.

D = column diameter, cm.

D_p = mean particle diameter, cm.

For multi-orifice distributor the appropriate parameter for the column "diameter" in (4.18) is the orifice spacing.

4.9.1 Bubble Diameters

The experimental results are presented in Tables (4.2) - (4.3). In figures (4.4) - (4.5) are plots of true bubble diameter D_B vs. excess gas velocity above incipient fluidization $U - U_{mf}$ for each bed height in the range $U - U_{mf}$ = 0.5 - 7.0 cm./sec. for a multi-orifice distributor having free area $\phi = 29 \times 10^{-4}$.

The data in Figures (4.4) - (4.5) have been cross-plotted to show how increases in bed height bring about increases in the diameter of bubbles bursting the top surface of the bed(Figures (4.6) - (4.7)). Similar plots are also shown in Figure (4.8) for a multi-orifice distributor having free area $\phi = 74 \times 10^{-4}$.

As predicted, the diameters observed within the range of gas flow rates and bed heights studied increased linearly as both bubble flow and initial bed height increased. Moreover, the rate of increase of bubble diameter with bed height increases as $U - U_{mf}$ increases. Another important feature is the effect of increasing particle size and density on the size of bubbles. This is apparent when Figures (4.4) and (4.5) are compared at the same values of $U - U_{mf}$. It shows that glass which has a larger mean particle diameter (237 μ) and higher density (2.93 gm/cm^3) produced larger bubbles than sand which has a mean particle diameter and density of 224 μ and 2.64 gm./cm^3 respectively. Although the effect is not pronounced in view of the smaller difference in particle size and density between sand and glass, the results appear to confirm the trend indicated by equation (4.3).

An inspection of Figure (4.6) shows that with silver sand and for an initial bed height H_{mf} = 25 cm. the data seem to deviate from the "least square" lines drawn through the rest of the points. This has not been observed with glass beads, but it would appear that with beds deeper than

30 - 40 cm. the bubble size is no longer a linear function of bed height. Private communication(108) suggests that this might be the case with deeper beds. Observations(108) with beds higher than 40 cm indicated a non-linear dependence of bubble size on bed height. Thus suggesting that (4.3) might be apolicable only to shallow beds. However, the data reported by Cooke et al.(102) for bed depths up to 80 cm. show a linear relationship between bubble diameter and bed height and fit (4.3) reasonably well (see section 4.9.3.).

Significant differences were found when comparing results from two multi-orifice distributors; (i) distributor A having high pressure drop with $\phi = 29 \times 10^{-4}$ and (ii) distributor B having low pressure drop with $\phi = 74 \times 10^{-4}$. As can be seen from figures (4.7) and (4.8), the rate of growth of D_B with bed height is greater with distributor B although it appears that the initial bubble sizes obtained by extrapolating the data to zero bed height are little bigger with distributor B. It clearly shows that the effect of a reduced distributor pressure drop is to produce larger bubbles and therefore in agreement with the discussion earlier. This situation has reflected in the smaller number of bubbles observed on the top surface of the fluidized bed with distributor B.

These results may be explained quantitatively by the theoretical model presented by Fakhimi and Harrison(64) for multi-orifice distributors. The theory suggests that for a given distributor design there should be a minimum gas velocity above which all the orifices are operational. Applying their model (see Chapter 5) - to predict the fraction of operative orifices under given conditions - reveals that the experimental results refer to conditions for which only 10 - 90% of the total number of orifices on distributor B are operative, whereas orifices on distributor A are almost fully operative. This suggests that there was a maldistribution of gas through distributor B and this could partly explain why larger bubbles

were observed with distributor B (low Δp_D) than with distributor A (high Δp_D).

At higher gas flow rates, when $U - U_{mf} = 9.5$ cm/sec, almost 100% of orifices on distributor B can be expected to be operational. At this gas flow rate the two distributors are expected to operate similarly. This can be seen from Figure (4.9) which compares distributor A and B at the same initial bed height. It shows that the rate of increase of D_B with $U - U_{mf}$ was greater with distributor B with the result that both distributors produced similar sized bubbles at high gas flow rates.

In order to examine the effect of orifice diameter on the size of bubbles whilst maintaining the distributor free area constant, distributor C was used. This, in fact, was distributor B with some of its orifices being sealed with Plasticine so as to make its free area equal to that of distributor A (i.e. $\phi \simeq 29 \times 10^{-4}$).

Figure (4.9) compares distributor A and C and shows that both distributors produced similar sized bubbles, confirming the prediction that a change in orifice diameter would not affect the operational effectiveness of the distributor provided the gas is well distributed across it.

4.9.2 Bubble Sizes at the Distributor

Since it was evident from Figures (4.6) - (4.8) that for any given bubble phase flow rate $U - U_{mf}$ the diameter of bubbles increases linearly as the bed height, "least squares" straight lines have been drawn through the points and extrapolated to zero bed height in an attempt to estimate the initial bubble size D_{Bo} on the distributor surface. If the extrapolations are valid, then a comparison with the theoretically predicted values from (4.2) can be made.

Assuming that n represents the number of orifices producing bubbles, then from (4.2) the initial bubble diameter D_{Bo} is given as

$$D_{Bo} = \left(\frac{6A_o (U - U_{mf})}{\pi N_o \left(\frac{n}{N}\right)} \right)^{0.4} \Big/ g^{0.2} , \qquad (4.19)$$

where $\frac{n}{N}$ represents a correction factor introduced to allow for non-bubbling orifices under certain operating conditions and can be predicted from (5.25) (Chapter 5). Bubble diameters calculated from (4.19) agree reasonably well with the extrapolations of observed bubble diameters to zero bed height indicating that expression (4.19) is satisfactory for the prediction of bubble size at the distributor surface.

Comparison between extrapolated and calculated values is as follows:

Solid	224 μ silver sand					237 μ glass beads				
$U - U_{mf}$ (cm./sec.)	1.0	3.0	4.0	5.1	6.0	1.0	3.0	4.1	5.4	6.0
D_{Bo} (cm) calc.	0.76	0.74	0.85	0.92	1.0	0.77	0.74	0.86	0.97	1.06
D_{Bo} (cm)extrapolated	0.36	0.73	0.87	0.99	1.22	0.49	0.70	0.97	1.28	1.65

4.9.3 Bubble Size Correlation

As stated earlier, one of the aims of this work was to evaluate the usefulness of equation (4.3) in predicting the bubble size along the bed height from a multi-orifice distributor. A computer program was prepared for calculating bubble diameters from (4.3). The results of calculation were then compared with actual experimental values obtained from the present study. A number of experimental points from previous investigators are also included. The degree of comparison is shown in Figure (4.10) and the complete results are given in Table (4.4).

It will be noted that almost all the points fall within the range $\pm$ 20% which, allowing for the assumptions, approximations and imprecise nature of bubble data, is not large. However, (4.3) would lead to estimates of bubble size that are probably precise enough for most practical purposes.

4.9.4 Number of Bubbles

The number of bubbles N_B counted on the surface of the bed at any instant is seen from Figure (4.11) to increase rapidly to a maximum before decreasing steadily with the excess gas velocity. The gas velocity at which the maximum number of bubbles occurs appears to be influenced by the bed height; as the bed height increases the peak occurs at low values of $U - U_{mf}$. At the maximum point, bubbles were seen to be evenly distributed across the bed surface indicating a stable fluidization. The influence of distributor pressure drop and in particular the ratio of distributor pressure drop to bed pressure drop ($\Delta P_D / \Delta P_B$) on bed stability has been investigated already (see Chapter 3).

The general shape of the curves shown in Figure (4.11) can be partially explained as follows:

(1) When the gas flow rate is just greater than the incipient fluidizing flow rate, a small number of distributor orifices are operative. Further increase of gas flow rate allows more orifices to become operative, the bubble size increases little or not at all, and little or no coalescence takes place. At about $U - U_{mf}$ = 2.0 cm./sec. the number of bubbling orifices is at a maximum which is not necessarily the total number of orifices in the distributor. The reason seems to lie in the non-uniformities in the distributor gas supply which may occur in practice.

(2) The decrease in the number of bubbles with further increase in $U - U_{mf}$ is due to the increase of rate of coalescence whilst the total number of operative orifices remains the same, resulting in fewer and

larger bubbles at the distributor. It is also likely that the number of bubbles decreases due to the interaction of gas jets emerging from the distributor. Observations in a two-dimensional bed (see Chapter 5) have indicated that adjacent jets tend to interact at higher gas velocities and larger bubbles, which subsequently coalesce, are produced at the distributor. A similar phenomenon could exist to an extent depending on the orifice spacing in a three-dimensional bed when a multi-orifice distributor is used.

4.10 Bubble Coalescence Model

As already pointed out, the "bubble assemblage model" proposed by Kato and Wen(101) may be used to predict the number of bubbles and the volume of the bubble phase along the bed height. This model was developed particularly for beds operating with multi-orifice distributors. However, its applicability to multi-orifice distributors has not been examined and it is not known whether its application can be extended to other types of distributor (e.g. bubble-caps). The purpose of the following investigation is, therefore, to evaluate its usefulness in predicting the number of bubbles as they grow and coalesce within the fluidized bed and its relevance to distributor design.

Earlier we indicated that the model is convenient for computer use; thus equations (4.6) - (4.14) were simulated on the digital computer for calculation. The calculational procedure is given below when the following operating conditions are known: superficial gas velocity U, incipient fluidizing velocity U_{mf}, incipient bed height H_{mf}, void fraction at U_{mf}, e_{mf}, number of orifices per unit surface area of distributor, particle size D_p and particle density ρ_s.

(1) Equations (4.6) and (4.7) are used to compute the expanded bed height H.

(2) Using (4.11), the height of the i-th compartment is calculated.

(3) The calculations are repeated from the distributor surface until the bed height corresponding to H_{mf} is reached. For height above H_{mf}, the voidage is given by (4.9) and the number of bubbles N_B is obtained using the same procedure as that shown for the height below H_{mf}. The calculation is repeated until the bed height reaches $H_{mf} + 2(H_f - H_{mf})$ depicted in Figure (4.1).

The calculational procedure outlined above was carried out on the ICL 1905 computer in the University Computing Centre. The program used to make these calculations was written in ALGOL and can be found in Appendix A4. The computer logic diagram illustrating the steps outlined above is shown in Figure (4.17).

The results of calculation are presented in the form of a histogram in Figure (4.12) for a distributor having 0.37 orifices/cm^2. using 224 μ sand as the solid phase. The bubble phase velocity and the initial bed height selected for this study are 3 cm./sec. and 25 cm. respectively. The histogram shows the change in the size of compartments with height above the distributor. The population of bubbles within a compartment is shown to decrease as the size of the compartment increases. Calculations for other gas velocities indicate that the number of compartments decreases as the gas velocity increases resulting in fewer and larger bubbles within each compartment. A decrease in the number of compartments with gas velocity suggests that the distributor is behaving as a perfect mixer. In Figure (4.12) the curve passes through the mid points demonstrates that the rate of growth of bubbles with bed height follows an exponential-type curve, and bubbles coalesce very rapidly near the distributor. The dotted part corresponds to the extrapolation to zero bed height, since it is reasonable to assume that the theoretical number of bubbles at the surface of the distributor is that equivalent to the total number of orifices on the distributor.

4.10.1 Comparison With Experiments

In order to compare the model with actual experimental data, three multi-orifice distributors having 0.37 orifices/cm^2. on each of them were used. The centre-to-centre orifice spacing was constant and the orifice diameter was variable, giving fractional free areas of 29×10^{-4}, 74×10^{-4} and 166×10^{-4}. These were considered respectively as high,

medium and low pressure drop distributors. The experimental procedure was to count the number of bubbles appearing on the top surface of the bed. The initial bed height was varied between 3 - 25 cm. in approximately 3-cm. increments.

The experimental results are presented in Figure (4.13) as plots of N_B (number of bubbles) vs. h(height above the distributor) along with the theoretically predicted values from the model for a bubble phase velocity $U - U_{mf} = 3$ cm/sec.

A study of Figure (4.13) shows a close agreement between the theoretical model and experiments only for the distributor with the high pressure drop. Results from the remaining distributors show considerable deviation with the trend towards the distributor having low pressure drop. This clearly shows the effect of a reduced pressure drop ΔP_D in producing fewer and larger bubbles, which subsequently coalesce, at the surface.

The model put forward by Kato and Wen disregards the effect of distributor pressure drop or flow maldistribution. Probably they presumed that all orifices should operate in a similar way regardless of distributor design, although the authors cited used data from porous distributors to examine their model.

In a commercial fluidized bed reactor, most of the reaction takes place at the distributor where the gas is jetted into the solids and where the bubbles are still small. Flow maldistribution normally leads to fewer and larger bubbles at the distributor level and these coalesce further up the bed, eventually forming slugs in a deep bed. Under such conditions, the "bubble assemblage model" presented by Kato and Wen cannot be used for the prediction of catalytic conversion in a fluidized bed reactor operating with a distributor of the one likely to be used

in practice (e.g. a multi orifice distributor). It is, therefore necessary that the model should include the distributor pressure drop to account for flow maldistribution which, inevitably, occurs under certain operating conditions.

4.10.2 Formulation of the Model in Terms of Distributor Pressure Drop

When there is maldistribution of gas through the distributor, i.e. shortcircuiting due to some orifices ceasing to operate, we commonly have the situation as depicted in Figure (4.14). Visual observations of the distributor from below showed that some of the orifices were not bubbling at all. These were either blocked up with particles or overwhelmed by intermittent dumping of particles. Dumping is a phenomenon occurring at low gas rates and normally associated with non-bubbling orifices, whereas on the other hand weeping is a phenomenon occurring at high gas rates where presumably all the orifices are operational. (These phenomena are considered in Chapter 6 in work on solids flowback through multi-orifice distributors).

Now for the situation shown in Figure (4.14), we have

(1) Bubbling/spouting orifices operating temporarily with superficial gas velocity U_n, where $U_n > U_{mf}$ and pressure drop

$$\Delta p_{D,n} = \frac{\rho_f \cdot U_n^2}{.2g \cdot \phi^2} \qquad (4.20)$$

for turbulent orifice flow (see Chapter 3).

(2) Non-bubbling orifices operating temporarily with superficial gas velocity at incipient fluidization U_{mf}, and pressure drop

$$\Delta p_{D,mf} = \frac{\rho_f \cdot U_{mf}^2}{2g \cdot \phi^2} \qquad (4.21)$$

assuming particles covering the orifices will remain in the incipiently fluidized state.

If n = number of bubbling orifices at a superficial velocity U, with $U_{mf} < U < U_n$, then (N - n) orifices are non-bubbling (i.e. those either blocked or overwhelmed by particle dumping).

Now it is possible to estimate the amount of maldistribution through the distributor in terms of pressure drop across the distributor for the situation described above and this may be applied to the "bubble assemblage model" to account for non-bubbling orifices.

Following the approach of Zabrodsky(73) and the analysis of Fakhimi(74), the flow of gas through the bubbling orifices and those closed by solid particles leads to a balance of pressures expressed as

$$\Delta P_{D,m} = \left(\frac{n}{N}\right). \Delta P_{D,n} + \left(\frac{N - n}{N}\right). \Delta P_{D,mf} \quad , \tag{4.22}$$

where $\Delta P_{D,m}$ = measured pressure drop across the distributor when only n orifices are bubbling.

Substituting (4.20) and (4.21) into (4.22), we obtain

$$\Delta P_{D,m} = \frac{\rho_f}{2g.\phi^2}. \left(\frac{n}{N}. U_n^2 + \left(\frac{N - n}{N}\right). U_{mf}^2 \right) \tag{4.23}$$

At the normal operating velocity U all orifices are supposed to be bubbling and the pressure drop across the distributor is

$$\Delta P_{D,N} = \frac{\rho_f U^2}{2g.\phi^2} \quad , \tag{4.24}$$

where $\Delta P_{D,N}$ = the theoretical pressure drop across the distributor when N orifices are bubbling (N being the total number of orifices in the distributor).

The amount of maldistribution, therefore is given by the difference

$$\varepsilon_D = \Delta P_{D,m} - \Delta P_{D,N} \tag{4.25}$$

or $$\varepsilon_D = \frac{\rho_f}{2g.\phi^2} \cdot \left[\left(\frac{n}{N}\right). U_n^2 + \left(\frac{N-n}{N}\right). U_{mf}^2 - U^2 \right] \tag{4.26}$$

A mass balance on the distributor plate gives

$$\left(\frac{n}{N}\right). \rho_f. A.U_n + \left(\frac{N-n}{N}\right). \rho_f. A.U_{mf} = \rho_f.A.U \tag{4.27}$$

Equation (4.27) suggests that when $U = U_{mf}$ none of the orifices is bubbling. This is true, because at the point of incipient fluidization the bed is quiescent and is allowing just enough gas to pass to keep it buoyant.

Rearranging (4.27) and substituting for U_n in (4.26), we have

$$n = \frac{N}{1 + \frac{2g.\phi^2}{\rho_f} \cdot \frac{\varepsilon_D}{(U - U_{mf})^2}} \tag{4.28}$$

or $$n = \frac{N}{1 + \frac{2g.\phi^2}{\rho_f} \cdot \frac{(\Delta P_{D,m} - \Delta P_{D,N})}{(U - U_{mf})^2}} \tag{4.29}$$

Where n is the number of bubbling orifices expressed in terms of observed pressure drop across the distributor at a gas flow rate U (i.e. $\Delta P_{D,m}$) and pressure drop across the distributor at the same flow rate when all orifices are bubbling (i.e. $\Delta P_{D,N}$).

The boundary conditions are

$$\text{if} \quad \Delta P_{D,m} = \Delta P_{D,N} \quad , \quad n = N \tag{4.30}$$

$$\text{and} \quad \text{if} \quad \Delta P_{D,m} \gg \Delta P_{D,N} \quad , \quad n \to 0 \tag{4.31}$$

Values of $\Delta P_{D,m}$ can be obtained experimentally, and $\Delta P_{D,N}$ is the theoretical pressure drop for turbulent flow and may be calculated from (4.24), U_{mf}, ρ_f, ϕ are known quantities for a given solid-distributor system. Therefore, for a given operating conditions, n can be predicted from (4.29). In the "bubble assemblage model", n is the relevant parameter for the multi-orifice distributor and this should be used under such conditions. In other words, (4.29) provides a factor to be applied to the model to allow for non-bubbling orifices under certain conditions.

Inserting this factor into (4.11) and (4.12), new expressions are then obtained. These are respectively as

$$\Delta h_i^* = 2\, D_{Bo} \cdot \frac{(2+m)^{i-1}}{(2-m)^i} \left[\frac{1}{1 + \frac{2g.\phi^2}{\rho_f} \frac{(\Delta P_{D,m} - \Delta P_{D,N})}{(U - U_{mf})^2}} \right]^{-0.4} \tag{4.32}$$

and

$$N_{Bi}^* = \frac{6A}{\pi(\Delta h_i)^2} \frac{e - e_{mf}}{1 - e_{mf}} \left[\frac{1}{1 + \frac{2g.\phi^2}{\rho_f} \cdot \frac{(\Delta P_{D,m} - \Delta P_{D,N})}{(U - U_{mf})^2}} \right]^{0.8} \tag{4.33}$$

for $\Delta P_{D,m} \geq \Delta P_{D,N}$, i.e. excess pressure drop due to maldistribution. $\Delta P_{D,m}$ was fed to the computer as an input variable because, it is a measurable quantity. At a given gas flow rate, $\Delta P_{D,m}$ was found to decrease with bed height. However, the decrease was small and, therefore, in a particular run $\Delta P_{D,m}$ was taken as the everage of those observed with different bed heights. Unfortunately, consistent results were only obtained with some difficulties, i.e. experiments had to be repeated several times in order to obtain reproducible values of $\Delta P_{D,m}$. This

can be expected with distributors operating at low gas rates and having large plate characteristics and as indicated earlier maldistribution would lead to the orifice behaviour described by Figure (4.14).

A new plot of N_B vs. h on the lines of Figure (4.13) is now possible (see Figure (4.15)). The results of calculation from the modified model show good agreement with experiments and it should be noted that the closeness between the model and results from the high pressure drop distributor is obtained without the need for a correction factor, since at this flow rate (i.e. $U - U_{mf} = 3$ cm.sec^{-1}) pressure maldistribution was negligibly small. This may also be seen from Figure (4.13) which shows the deviation between experiments and the model for the high pressure drop distributor is small.

However, using high enough gas flow to make all orifices operational in the other distributors (i.e. the medium and the low pressure drop distributors) would not necessarily lead to an agreement with the model, but can reduce the displacement of experimental points from the theoretical curve. With distributors having large plate characteristics ϕ, large values of $U - U_{mf}$ are required to bring about full operation, and as shown earlier, higher velocities would result in fewer bubbles at the surface. In Figure (4.16) the experimental results are compared with the theoretical model for a gas velocity high enough (i.e. $U - U_{mf} =$ 9 cm./sec.) to overcome maldistribution through the distributor having medium ΔP_D and shows that the experimental points fall below the theoretical curve, but their displacement is largely reduced.

This suggests that the "bubble assemblage model" is, probably, satisfactory for the prediction of the extent of chemical reaction in beds operating with high gas rates or with distributors having small plate characteristics. But in some systems (e.g. with low U_{mf} values and large

plate characteristics) high values of $U - U_{mf}$ are required to eliminate maldistribution and bring about fully bubbling orifices, and may be undesirable to operate at higher gas rates because of particle attrition, entrainment or slugging of the bed, then operation at low $U - U_{mf}$ necessitates the use of the correction factor to allow for non-bubbling orifices. This, of course, requires the knowledge of pressure maldistribution across the distributor which may be obtained experimentally.

CONCLUSIONS

Bubble sizes and the effect of the distributor on bubble formation have been investigated in gas fluidized beds using multi-orifice distributors:

1. The diameter of bubbles obtained from this work as well as from others is within $\pm$ 20% of values predicted by equation (4.3). This equation implies the existence of a bubble at the surface of the orifice and its growth by the addition of excess gas from the bed.

2. Flow maldistribution is important in influencing the operational effectiveness of the distributor. It is more likely at low gas rates and with distributors having large plate characteristics (i.e. having low pressure drops).

3. The "bubble assemblage model" presented by Kato and Wen(101) for predicting the extent of chemical reaction taking place in a fluidized bed is also useful for the prediction of the number of bubbles and their size in other situations where the fluidized bed is not necessarily a chemical reactor. However, its application becomes invalid at low fluidizing velocities or with distributors having large plate characteristics due to the influence of maldistribution across the distributor plate.

Methods available in the literature have been used for the prediction of pressure maldistribution across the distributor in terms of distributor pressure drop and this has been applied to the model to allow for non-bubbling orifices. Consequently, closer agreement between experiments and the model has been obtained.

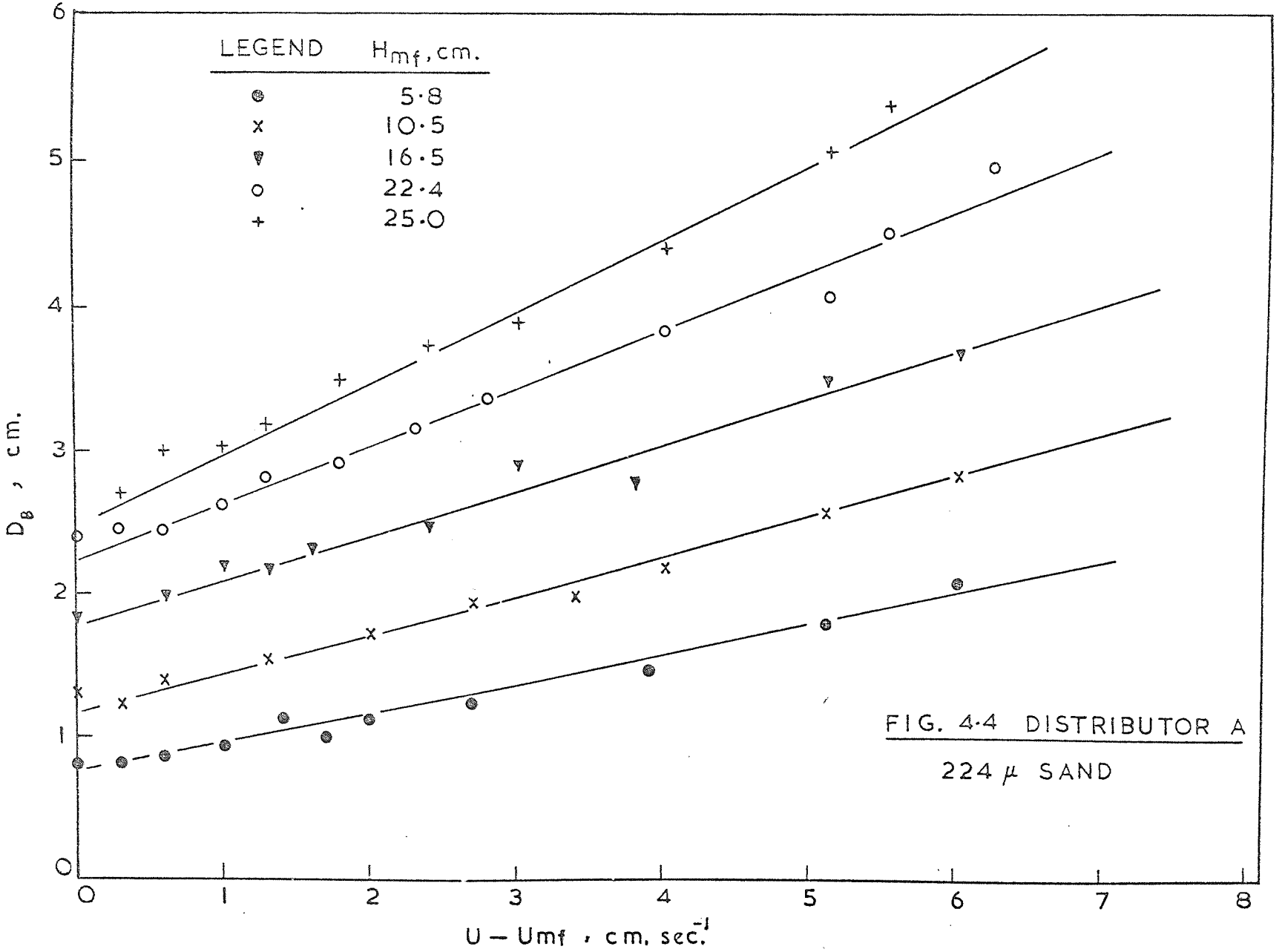

FIG. 4·4 DISTRIBUTOR A

224 μ SAND

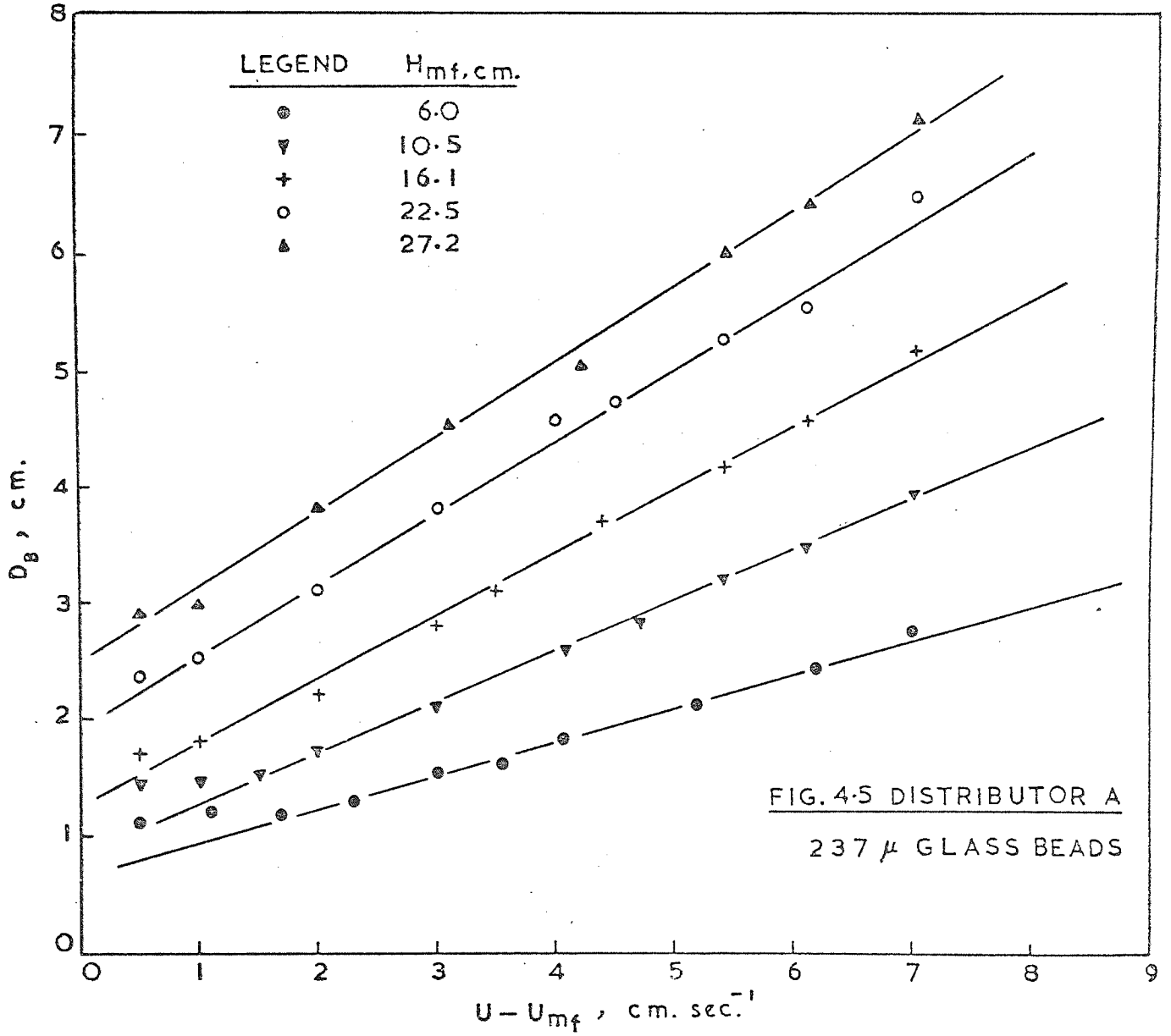

FIG. 4·5 DISTRIBUTOR A

237 μ GLASS BEADS

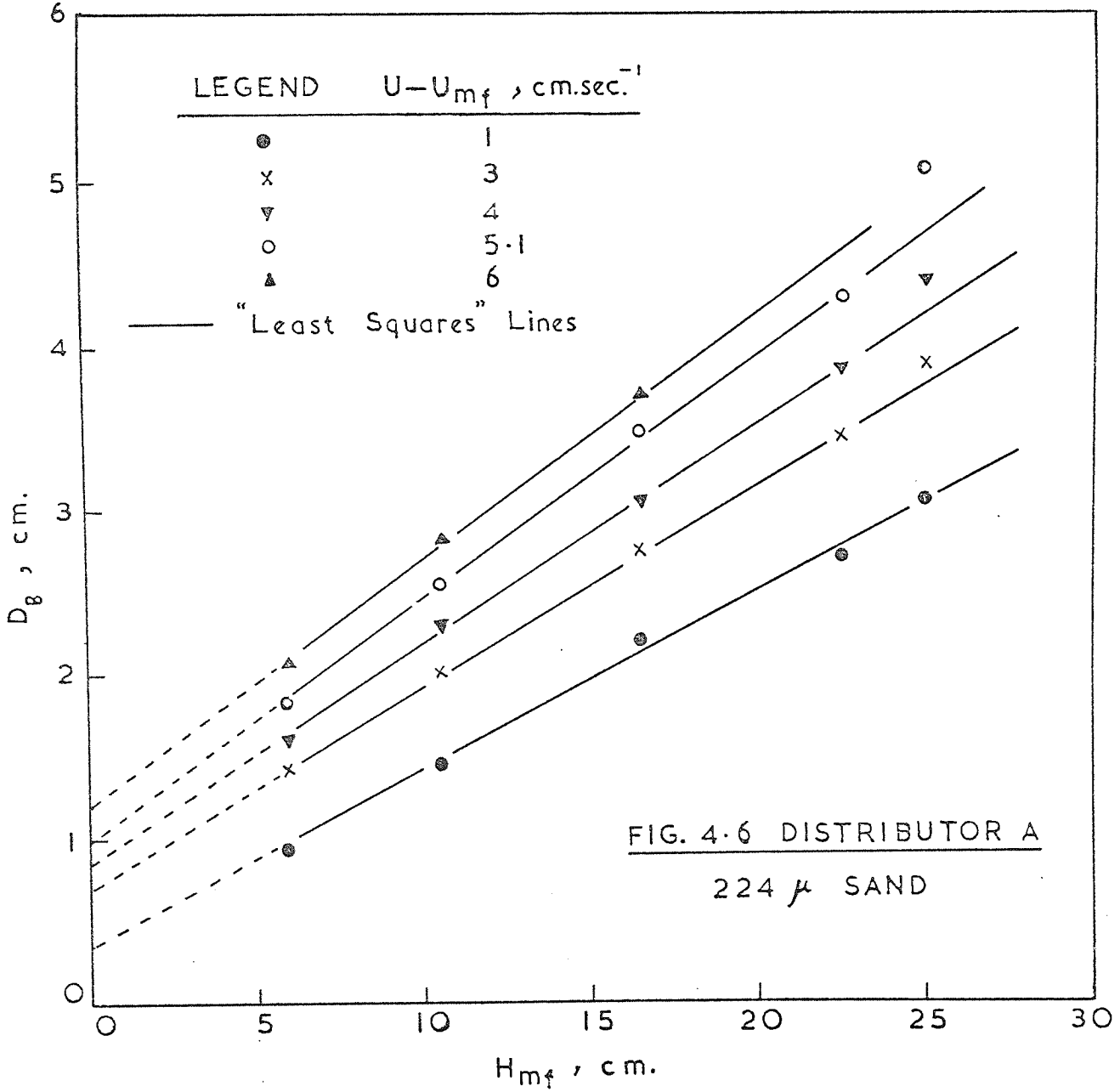

FIG. 4·6 DISTRIBUTOR A

224 μ SAND

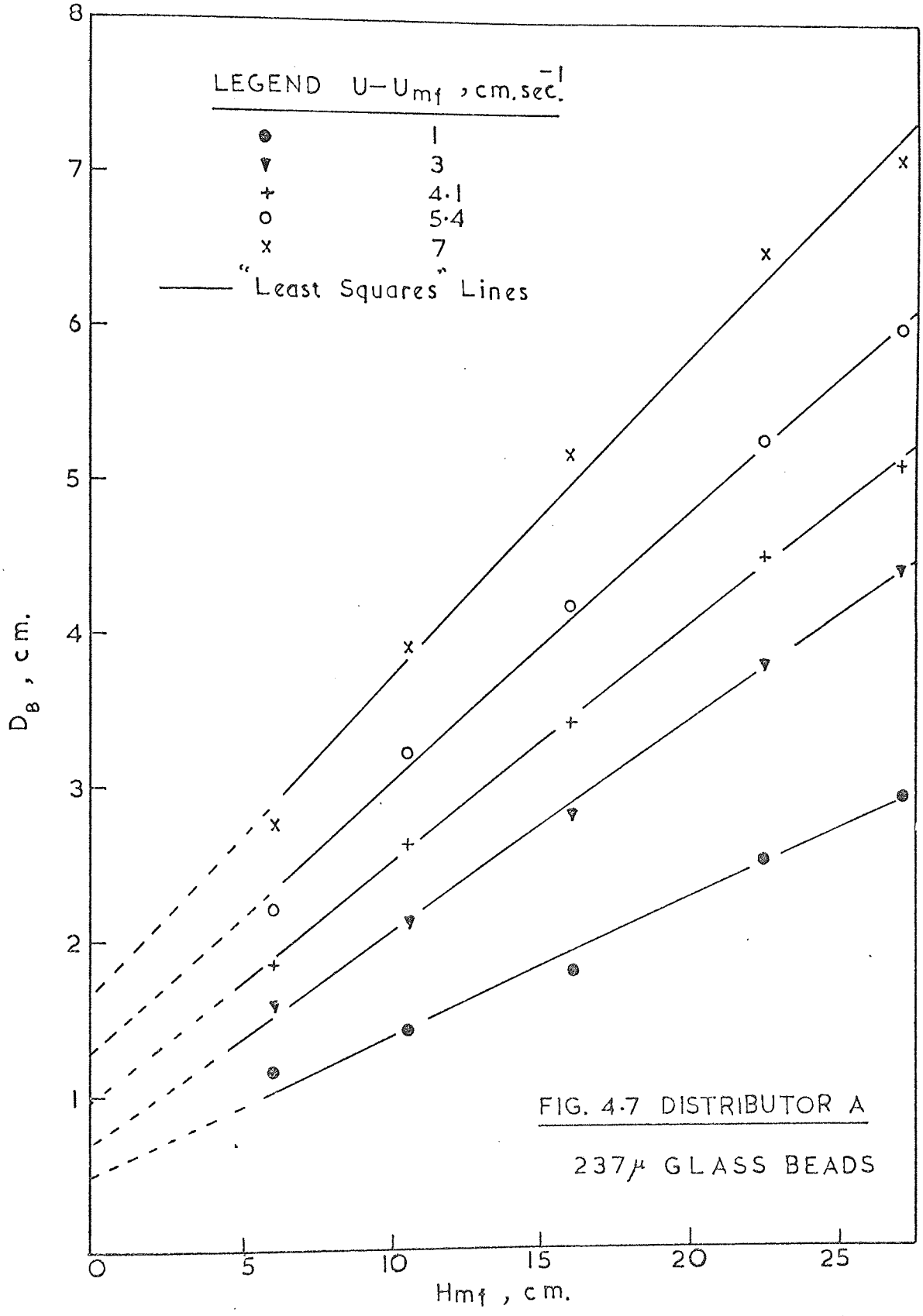

FIG. 4·7 DISTRIBUTOR A

237μ GLASS BEADS

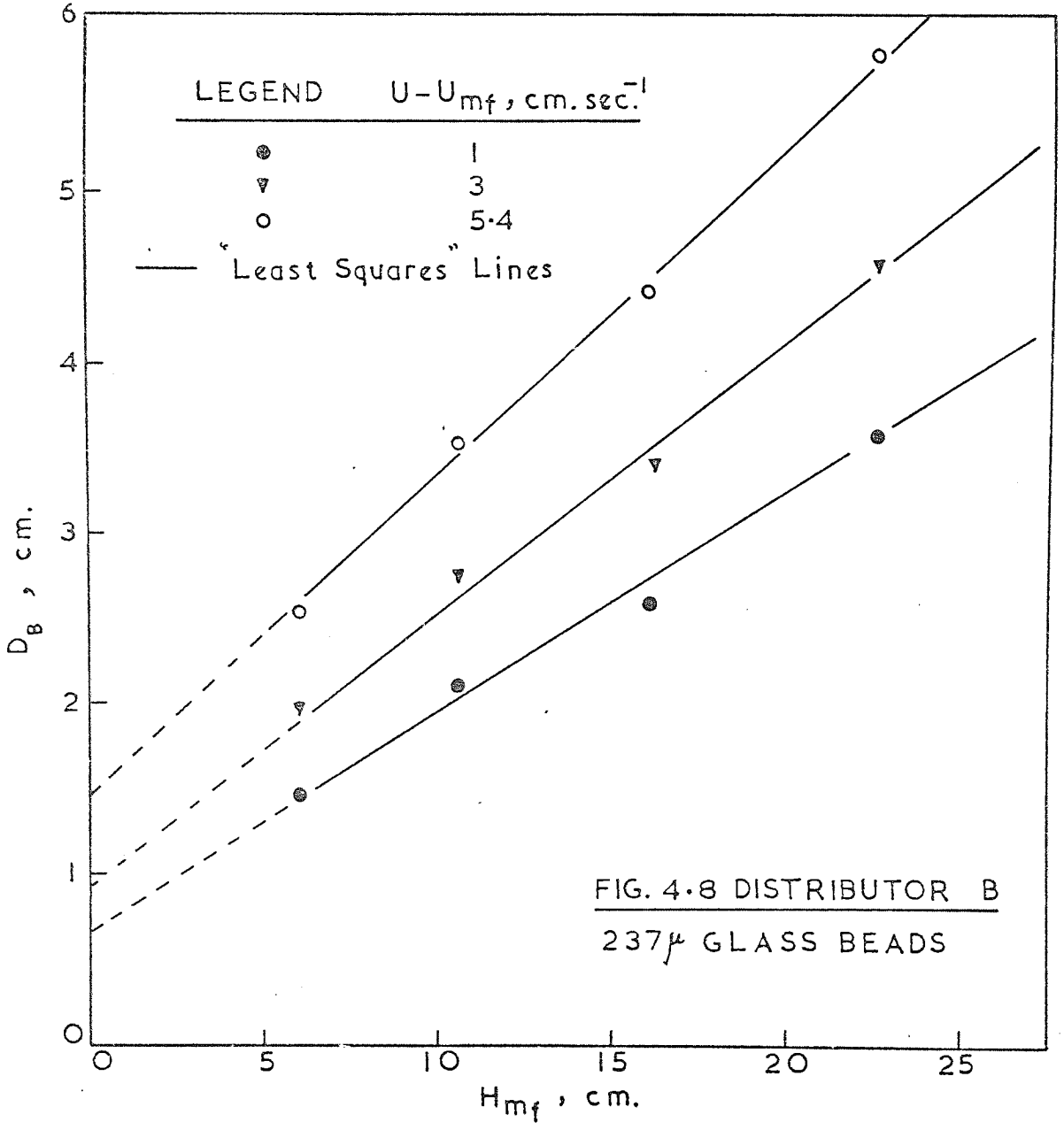

FIG. 4·8 DISTRIBUTOR B

237μ GLASS BEADS

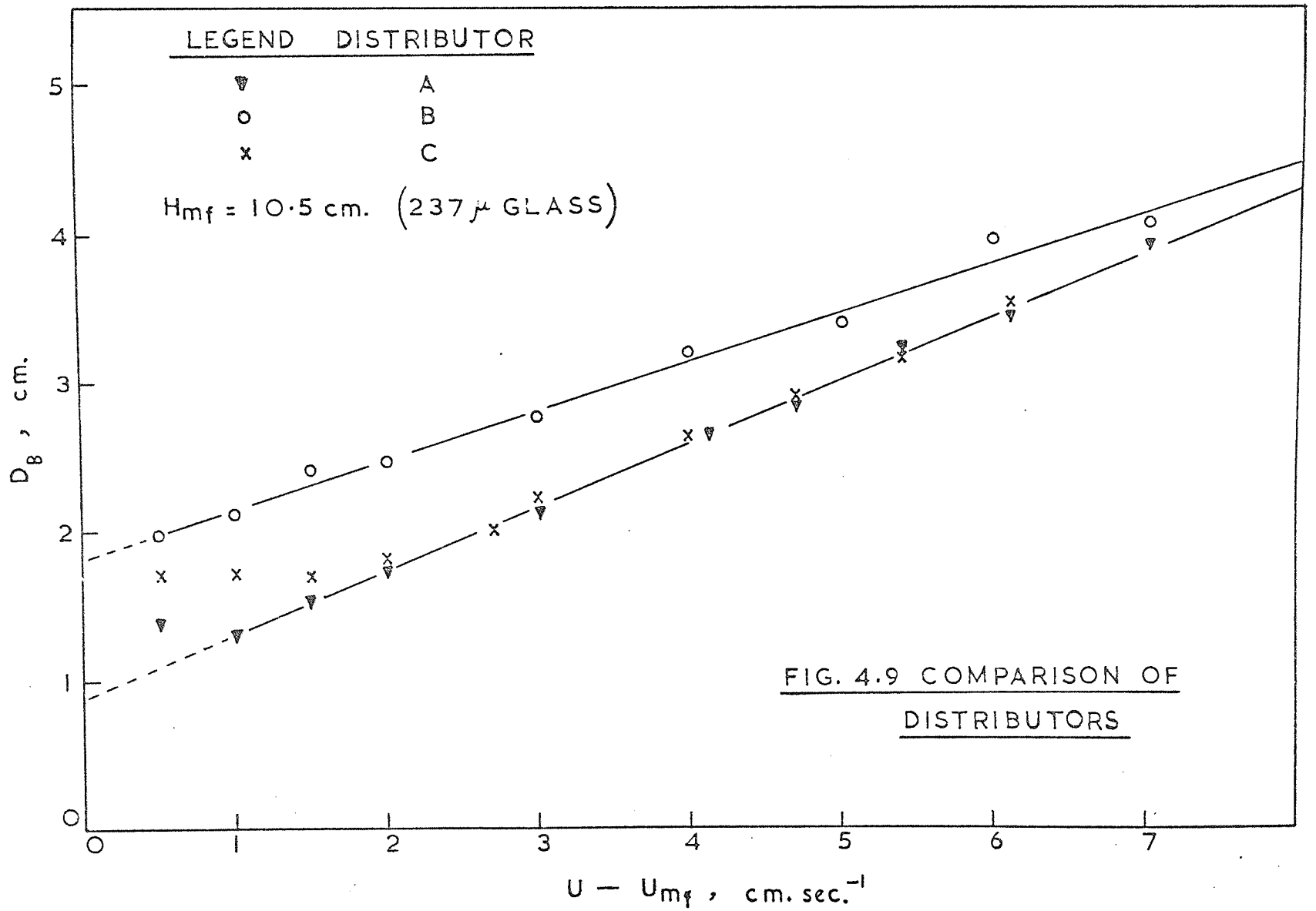

FIG. 4.9 COMPARISON OF DISTRIBUTORS

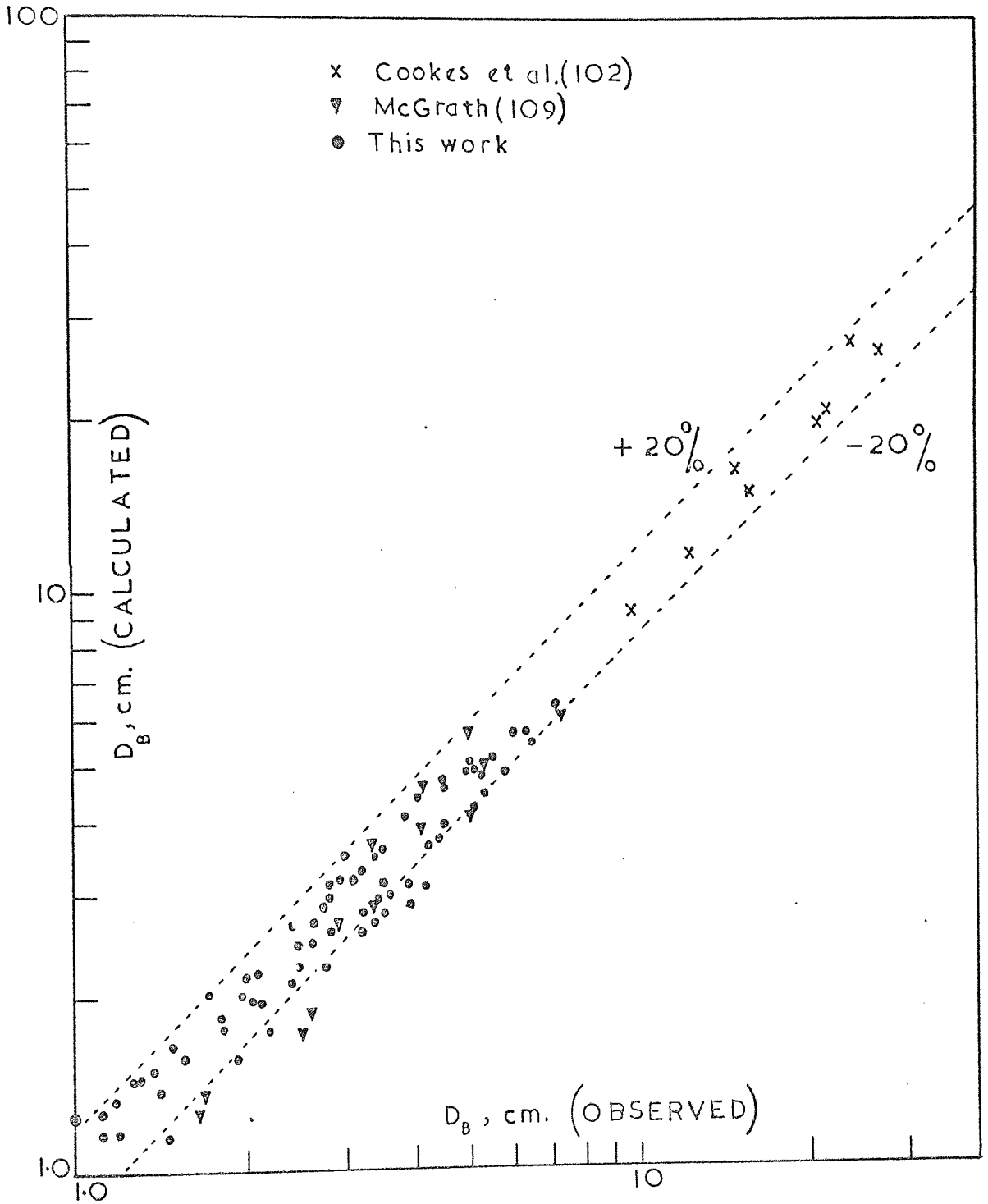

FIG. 4·10 Correlation of Experimental and Calculated Bubble Diameters

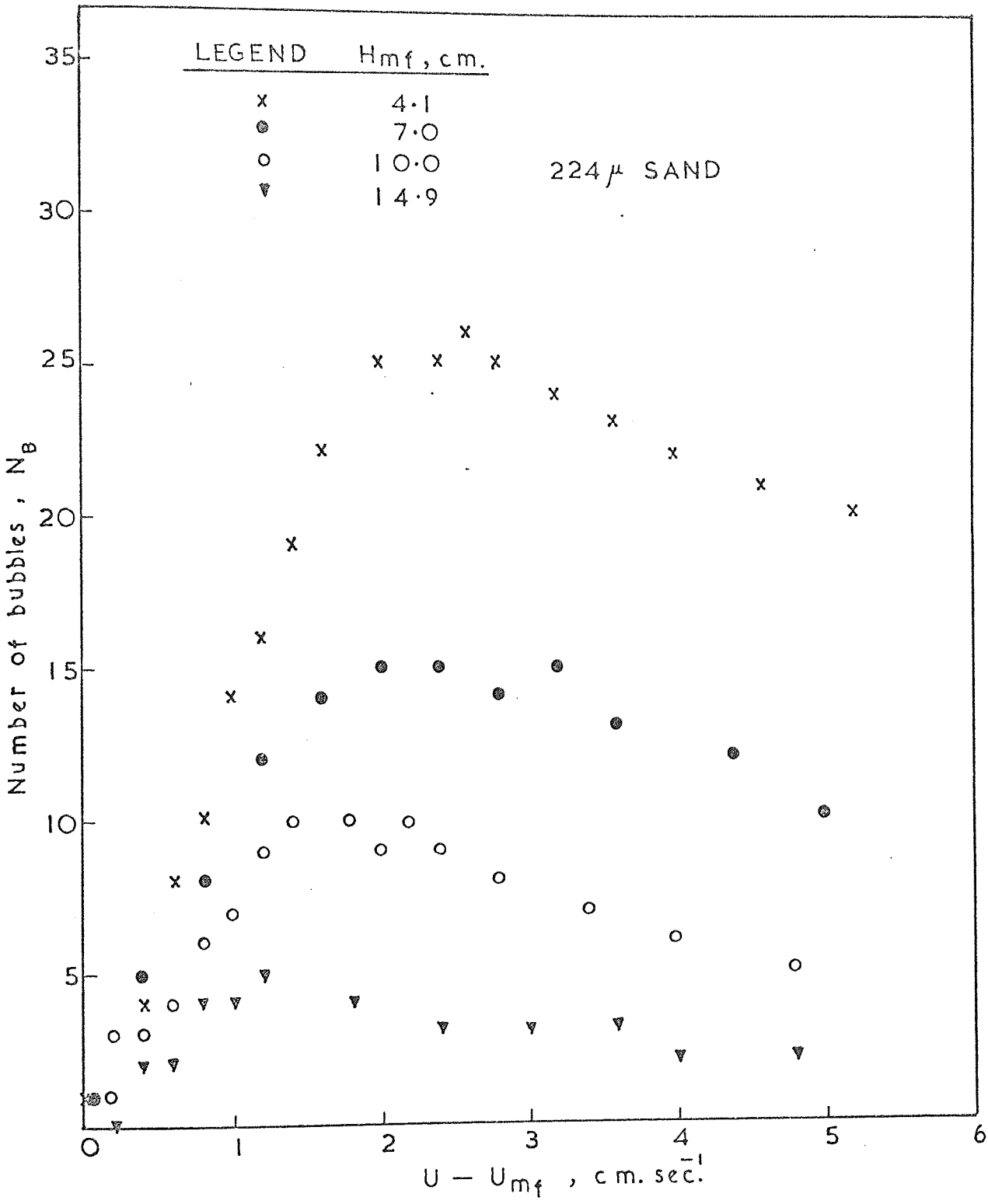

FIG. 4·11 DISTRIBUTOR A

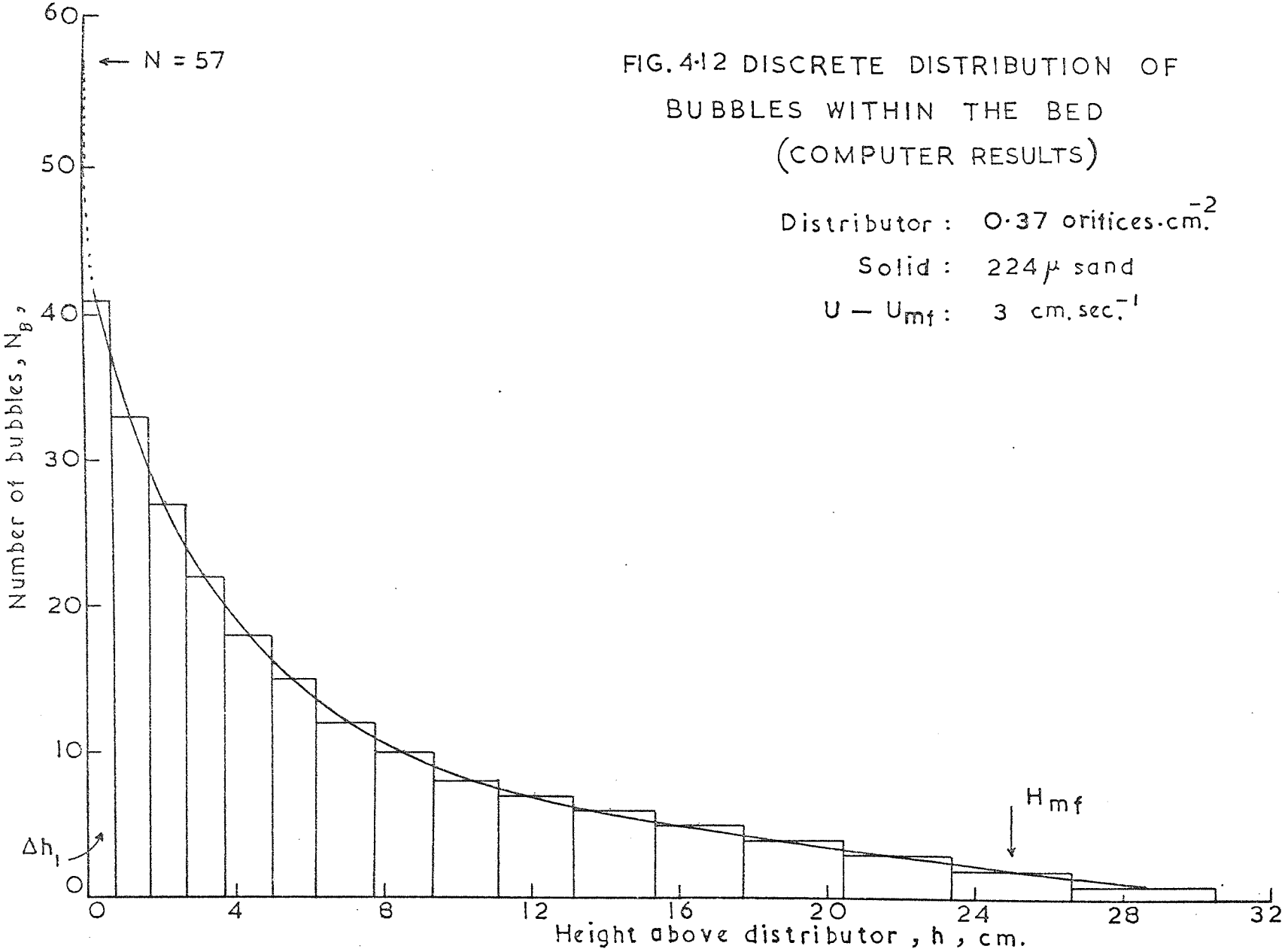

FIG. 4·12 DISCRETE DISTRIBUTION OF BUBBLES WITHIN THE BED (COMPUTER RESULTS)

Distributor : 0·37 orifices·cm.$^{-2}$

Solid : 224 μ sand

$U - U_{mf}$: 3 cm. sec.$^{-1}$

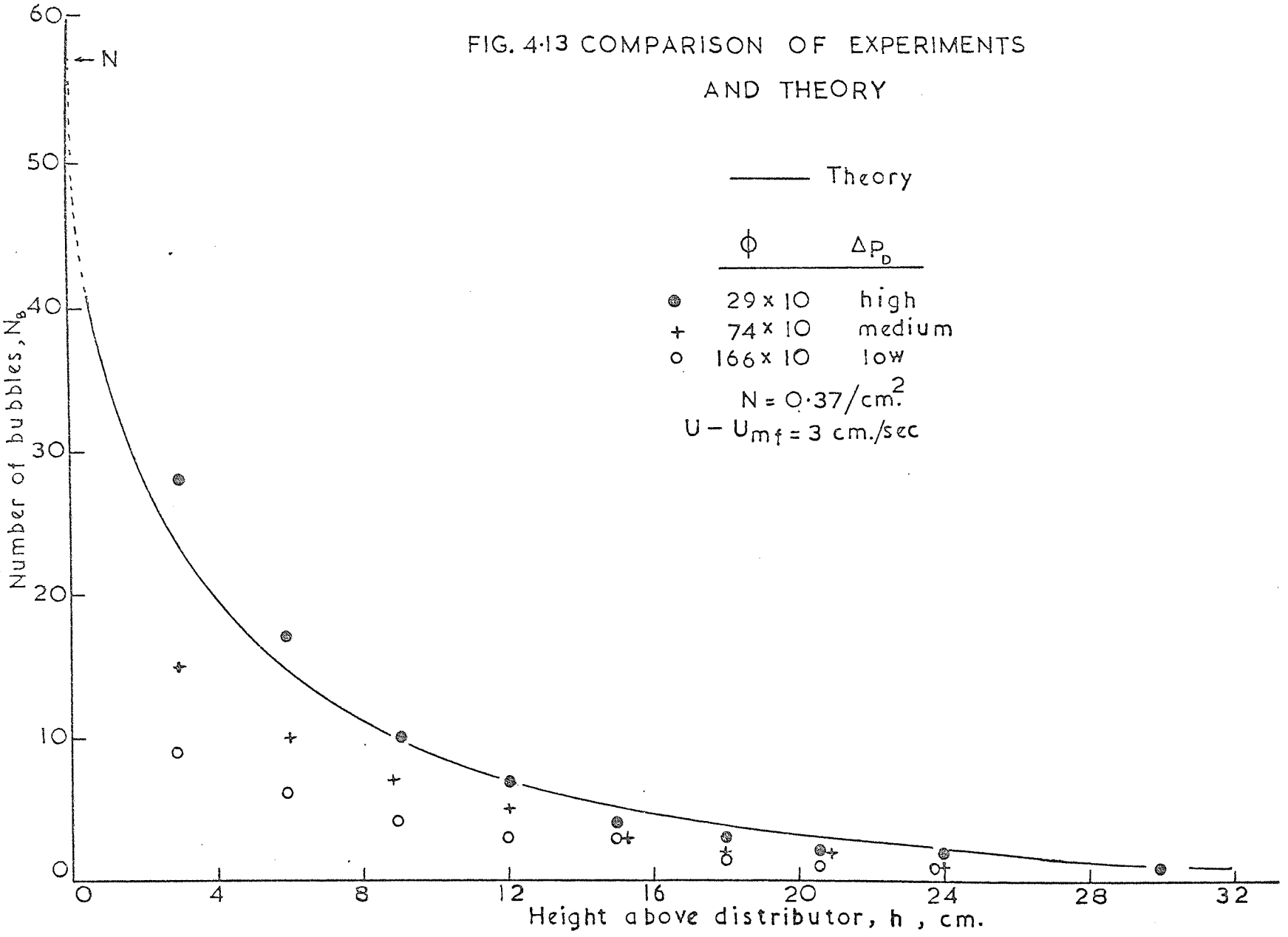
FIG. 4·13 COMPARISON OF EXPERIMENTS AND THEORY
Theory
ϕ ΔP_D
29 x 10 high
74 x 10 medium
166 x 10 low
N = 0·37/cm.^{2}
U − U_{mf} = 3 cm./sec
N
Number of bubbles, N_a
Height above distributor, h , cm.
0
10
20
30
40
50
60
0
4
8
12
16
20
24
28
32

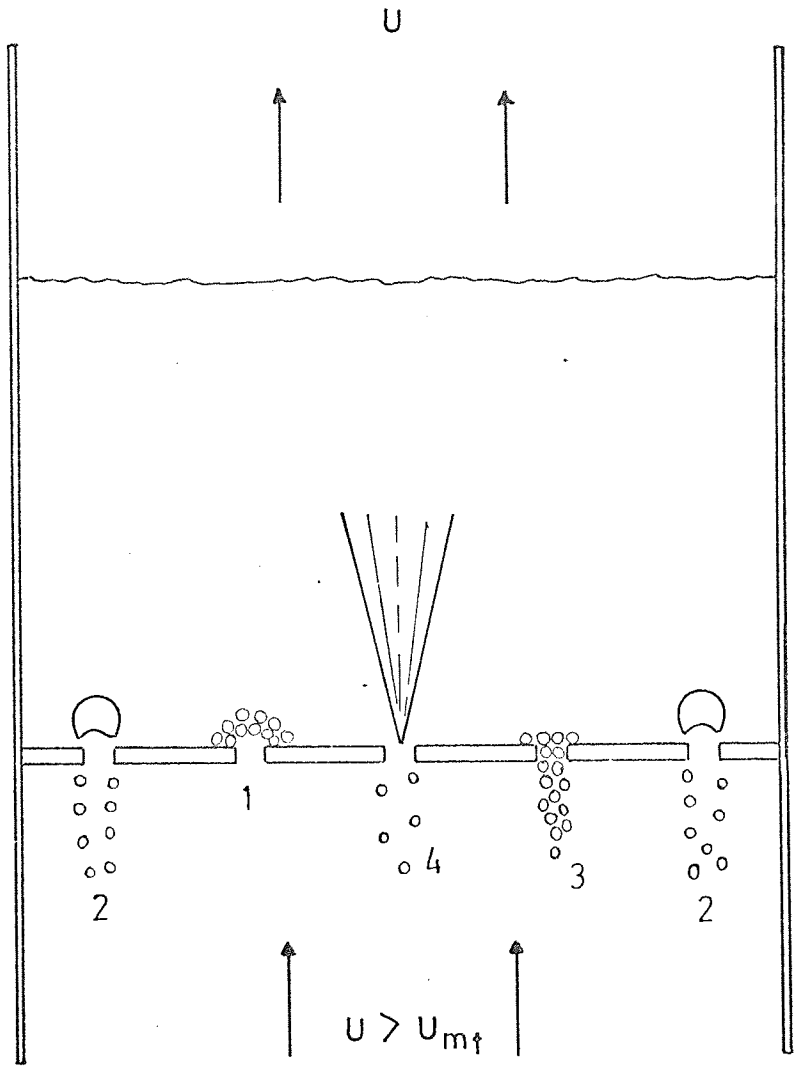

FIG. 4·14 EFFECT OF MALDISTRIBUTION ON THE OPERATIONAL EFFECTIVENESS OF THE DISTRIBUTOR

1 Non-bubbling orifice due to bridging
2 Bubbling orifice with weeping flowback
3 Non-bubbling orifice due to dumping flowback
4 Spouting orifice with weeping flowback

FIG. 4·15

ΔP_D	EXPEPRIMENTS	THEORY
high	●	line 1
medium	+	line 2
low	o	line 3

$U - U_{mf} = 3$ cm. sec^{-1} 224 μ sand

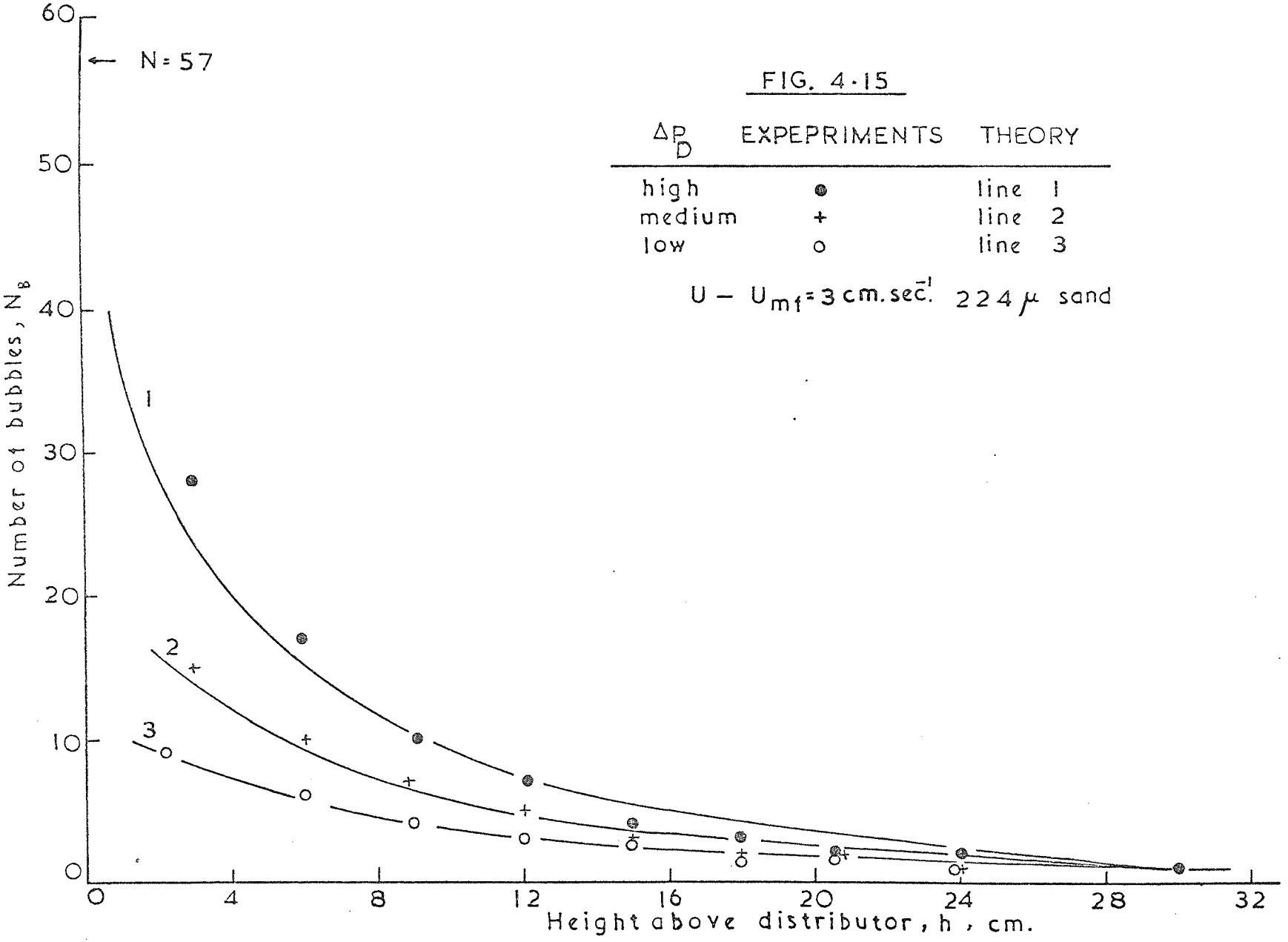

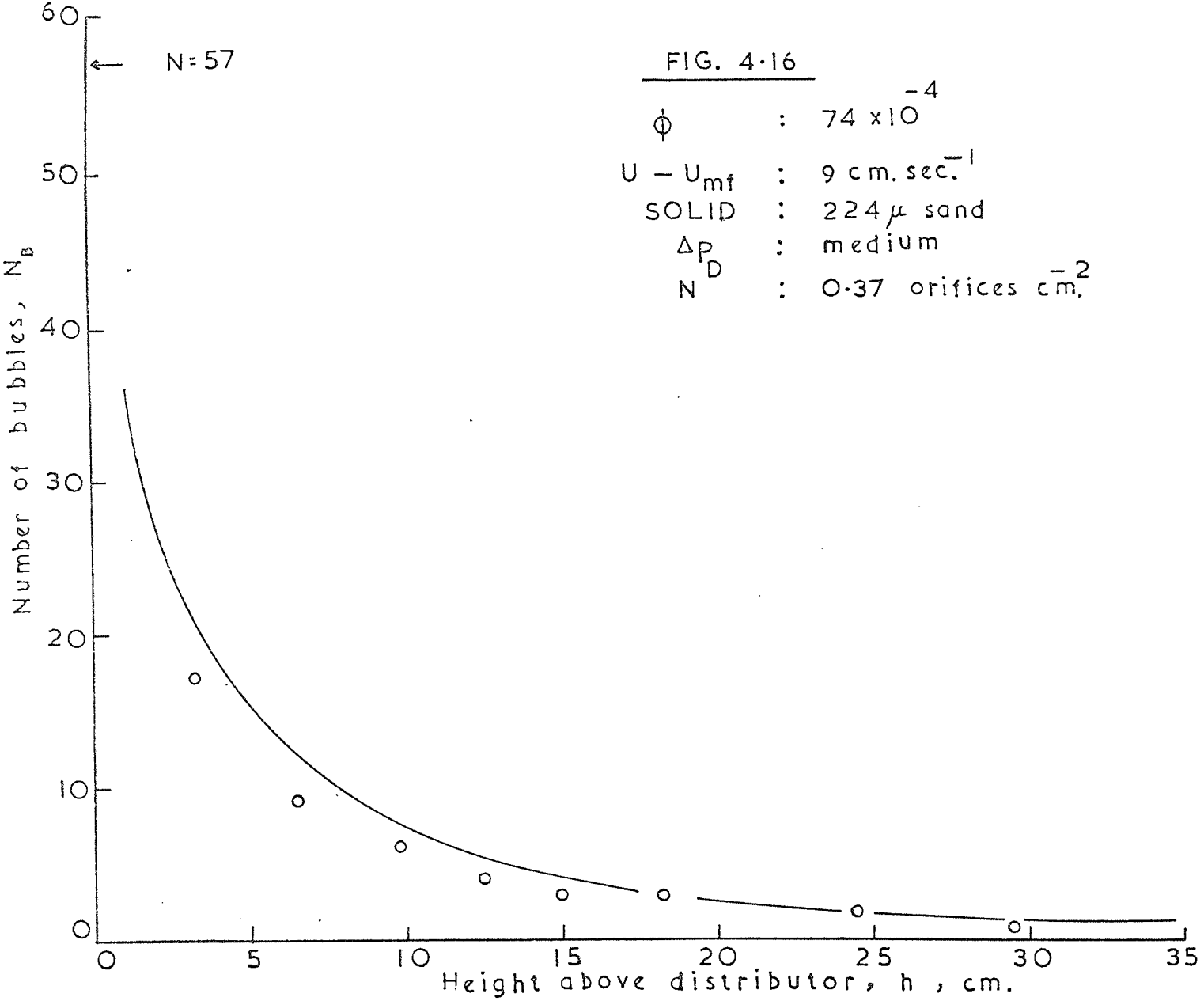

FIG. 4·16

ϕ	:	74×10^{-4}
$U - U_{mf}$	:	9 cm. $sec.^{-1}$
SOLID	:	224 μ sand
ΔP_D	:	medium
N	:	0·37 orifices $cm.^{-2}$

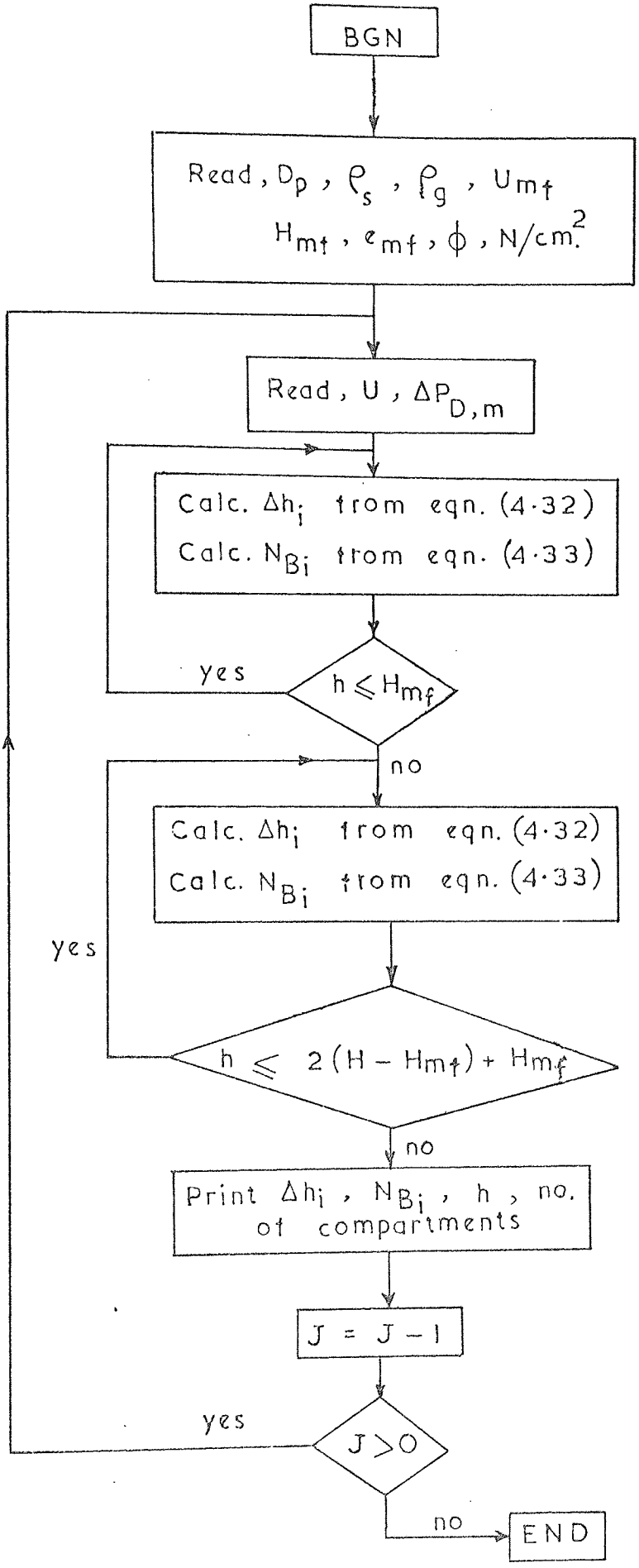

FIG. 4·17 COMPUTER LOGIC DIAGRAM

CHAPTER FIVE

5. DEFLUIDIZED ZONES ON MULTI-ORIFICE DISTRIBUTION PLATE

5.1 Introduction

This chapter provides a study on one of the important aspects of distributor design in a gas fluidized bed, namely the formation of defluidized zones in the spaces between the orifices.

In a commercial fluidized bed, the presence of defluidized or semi-fluidized particles on the distributor in between the gas inlet points is very undesirable. The solid phase in these regions remains completely immobile. For materials that tend to agglomerate on these zones even when small may grow after prolonged operation resulting in distributor blockage and thereby hindering fluidization. Agarwal et al.(24) and Pictor and Robinson(21) attributed coal ignition and plate fires to the existence of defluidized zones in their pilot plants. They were able to eliminate fires by reducing the spacing between the orifices and raising the pressure drop across the distributor. When the fluidized bed is a catalytic reactor, defluidized zones are particularly serious for the following reasons:

1. if the reaction is highly exothermic, there is a probability that defluidized heaps could lead to hot spots on the distributor with a possible loss of product selectivity and catalyst activity, and

2. catalyst particles are not used for reaction, hence a possible decrease in the efficiency.

An understanding of this phenomenon is vitally important for the rational scale-up and design of large fluidized bed reactors. In these units, little reaction occurs in the bed once the bubble is fully grown. Most of the reaction takes place at the distributor where the gas is jetted into the catalyst particles and where the bubbles are still small. Most large scale units are therefore said to be "distributor controlled". Unfortunately, little work has been done on the formation of defluidized zones on the distributor despite its importance. For this reason, the present work has been undertaken.

5.2 Previous Work

Fraiman et al.(91) have studied the problem of defluidized zones on multi-orifice distributor plates in a two-dimensional bed. They found that the formation of defluidized heaps in the spaces between the orifices was influenced by the type of solid, initial bed height and to a certain degree the gas velocity. In order to avoid the formation of defluidized zones, they suggested a grid consisting of conical elements, whose upper widened ends overlap. Obviously, the construction of this type of grids is rather difficult and expensive.

Fakhimi (74) has recently carried out similar studies in a two-dimensional bed. A theoretical model for the prediction of the amount of solids stagnating on the distributor plate has been derived. The model indicates that for a multi-orifice distributor, the height of a defluidized zone is related to the orifice spacing, the gas flow rate and the incipient fluidizing velocity of the solid particles. No quantitative agreement has been found, but theory and experiments show similar trends and thus agree qualitatively. This will be discussed later.

A more recent study comes from Ukhlov and Volkov(92) who also investigated the problem in a two-dimensional bed system using multi-orifice distributor plates. They used a peculiar design consisting of a downwardly pointing cone with a dished apex and perforations in the sides of the cone but not at the apex.

Their results show that the height of the defluidized zone increases with the width of the undrilled (dished) part of the distributor, but decreases with an increase in the gas flow rate. The effect of the particle size has also been observed. A decrease in the mean particle size caused a decrease in the height of the defluidized zone, apparently due to the greater mobility of the particles. In agreement with Fakhimi(74), they too found that the initial bed height had no effect on the height of the

defluidized zone. These observations are in line with those of Fakhimi. However, it is shown that the height of the defluidized zone decreases with a decrease in the fractional free area ϕ , presumably due to the lateral mixing of particles, but it should be recognised that they used a more complex type of multi-orifice distributors than in the present studies.

The work of this chapter examines how defluidized zones on a multi-orifice distributor are influenced by the distributor geometry (particularly the orifice spacing), solid properties and gas flow rate. The effect of bed diameter is also considered.

It should be mentioned here that the work of Fakhimi(74) was published during the course of the present work.

Therefore, the opportunity is taken to compare our results with his theory and experiments.

The study of defluidized zones on multi-orifice distributors may give an insight to the likely behaviour with other types of distributing device (e.g. bubble-caps or nozzle grids) and may be extended to other practices of fluidization technology where defluidized zones inevitably occur (e.g. bed internals, such as baffles and heat transfer tubes).

5.3 Qualitative Observations

The development of defluidized zones has been observed in a two-dimensional gas fluidized beds using a multi-orifice distributor. The observations show that when the superficial gas velocity U is just equal to or little above the incipient fluidizing velocity of the particles U_{mf}, the bed has the appearance shown in Figure (5.1). At this point the bed is quiescent the particles allowing just enough gas to pass through them, and the volumetric rate of flow through each orifice may be equal to the total volumetric rate of flow divided by the total number of orifices in the distributor (i.e. $q = q_{mf} = Q_{mf}/N$). At this point only the upper part of the bed seems to be fluidized. It is suggested that segregation is the cause of this behaviour which has also been observed by Fakhimi(74). This would result in fine particles settling above a packed bed of large particle.

A further increase in the gas flow above incipient fluidization (i.e. $q > q_{mf}$) causes some of the orifices to spout (see Figure (5.2)). With gradual increase of the gas flow rate, the number of jetting orifices also increases until eventually at some value of gas flow all the orifices are spouting. At this point the bed becomes mobile and the only stationary particles are those in the pyramids of fixed beds in between the adjacent orifices. With further increase of the gas flow rate, the height of these pyramids decreases and the bottom part of the bed becomes more fluidized.

Qualitatively these observations revealed three distinct regions of flow (see Figure (5.3)).

(I) A zone directly above the distributor plate and in between the orifices having height Z_R in which the solids settled in advance at the angle of repose. This can be easily observed with widely spaced orifices.

(II) A zone in which particles settled down and stagnated in a heap over zone one. In this zone particles were not mobilized by the fluidizing

gas. Therefore, the overall height representing this zone plus that of zone one was taken as the height above the distributor Z for which the defluidized zone extends.

(III) Fully fluidized zone, which was often washed away by intensive agitation in a short time interval.

In zone three the jets issuing from the distributor often interact when a certain gas flow has been reached (depending on the orifice spacing) resulting in larger bubbles and pressure surges at the distributor. This led to the suggestion that jet interaction is also important in influencing distributor design. Consequently, the height Z_j above the distributor at which jet interaction occurs has also been measured and this has been related to the orifice spacing. It should be emphasised that the data concerning jet interaction are only preliminary, because of the difficulty experienced in locating visually the point of intersection.

5.4 Fakhimi's Theoretical Model

In the previous section, we have indicated that at incipient fluidization the particles in the bed are essentially immobile and allow just that quantity of gas to pass that can readily seep through them (Figure (5.1)). At this point the bed voidage can be considered uniform and the gas issuing from each orifice percolates through the bed above the orifice in equal amounts along radial paths, symmetrical in all directions (i.e. possessing spherical symmetry, the orifice being the origin of symmetry). This is the basic assumption put forward by Fakhimi(74) in deriving his model. However, this is not the physical situation once the gas flow exceeds the incipient fluidizing velocity U_{mf}. In this case the gas flow pattern above each orifice is no longer symmetrical and somewhat as shown in Figure (5.2), i.e. some orifices are spouting. The spout effectively becomes a two-phase jet of gas and solids and for this reason his experiments were at variance with theory.

His analysis is based on the idea that an orifice may be regarded as a simple source situated in a solid plane surface from which fluid seeps symmetrically through a porous medium having uniform voidage and resting on the distributor plate, as shown in Figure (5.4). Hence the lines of flow in this case will be straight radial lines and the strength of the source is, therefore given by:

$$q = 2\pi.r.v_r \tag{5.1}$$

where v_r is the velocity component in the direction of the radius vector r for the two-dimensional flow case. Then he goes on to show that

$$U_y = \frac{v_r}{r} y = \frac{q}{\pi r^2}.y \tag{5.2}$$

$$U_x = \frac{v_r}{r} x = \frac{q}{\pi r^2}.x \tag{5.3}$$

These are the components of gas velocity at the point P (Figure (5.4)) whose polar co-ordinates are r,θ. Since the velocity component relevant to the present problem is the vertical component U_y. Thus (5.2) gives

$$U_y = \frac{q}{\pi r^2}.Z. \tag{5.4}$$

where Z represents the height of defluidized zones measured above the distributor plate. Finally, he shows that

$$\frac{Z}{S} = \frac{\pi}{\sum_{n=1}^{N} \frac{1}{n}} \cdot \left(\frac{U_{mf}}{U}\right) \tag{5.5}$$

for a two-dimensional bed system, and

$$\frac{Z}{S} = \frac{\pi}{\sum_{n=1}^{N} \frac{1}{n^2}} \cdot \left(\frac{U_{mf}}{U}\right) \tag{5.6}$$

for a three-dimensional bed system. Where N is the total number of orifices in the distributor plate.

Thus (5.5) and (5.6) show that the height of the defluidized zone

Z is a function of the orifice spacing S and the gas flow rate U. The effect of the physical properties of the particles and the fluid find expression more or less in the value of U_{mf}.

As can be seen from above, equations (5.5) and (5.6) show a linear relationship between $(\frac{Z}{S})$ and $(\frac{U_{mf}}{U})$ with a slope varying according to the number of orifices in the distributor plate. For the three-dimensional bed system, provided the number of orifices in the plate is large enough, equation (5.6) can be written with adequate accuracy as

$$(\frac{Z}{S}) = \frac{1}{2} (\frac{U_{mf}}{U}) \qquad (5.7)$$

Results obtained from the present work will be correlated in the way suggested by equation (5.5) for the two-dimensional bed system so that a comparison with Fakhimi's theory can be made.

5.5 Equipment and Experimental Procedure

A schematic diagram of the experimental equipment is shown in Figure (5.5). This consisted of a two-dimensional air fluidized bed, 35 cm x 1.27 cm in cross section and 85 cm high, constructed from 1/4" thick Perspex sheet. The wind box was 15 cm deep and 35 cm x 3.5 cm in cross section, also constructed from Perspex.

Table (5.1) gives details of the multi-orifice distributors used. These were 1/8" thick aluminium plates which had a single row of orifices drilled on a line mid-way between the transparent walls of the two-dimensional bed. The diameter of the orifices and their spacing were variables. Also by stopping up orifices with Plasticine the number of orifices and their spacing could be varied as desired. As can be seen from Figure (5.5), the air supply was connected to the wind box via two air feed points, placed opposite each other on the wind box sides. At each feed point, a deflector plate inclined with respect to the gas stream was installed inside the wind box. These had orifices drilled on them in a single row and they were covered with a strip of nylon filter cloth to prevent flowback of particles. This arrangement was intended to provide an even velocity profile to the underside of the distributor plate supporting the fluidized bed. It also served as a collecting funnel for particles falling back through the distributor plate during operation and stoppage.

The fluidizing air was taken from the laboratory main, reduced to a pressure of 20 p.s.i.g. and metered through calibrated rotameters at room temperature. Needle valves were used for flow regulation. The inside walls of the column were sprayed with antistatic cleaner and the air was slightly humidified. These measures were taken in the attempt to reduce electrostatic effects in the bed. Four types of solids were used in the experiments and their properties are specified in Table (5.2). Figure (5.6) shows an overall view of the experimental equipment.

5.6 Experimental Procedure

A known weight of solids was charged in the column, fluidized gently to avoid static build-up, and then allowed to settle under a slowly decreasing air flow. With zero air velocity the height of the settled bed was measured and the air flow rate was then increased gradually up to U_{mf}. At a flow rate a little above U_{mf}, some of the orifices began to spout and stagnant heaps, the boundaries of which were sharply defined, formed in the spaces between the orifices. The height of the defluidized heaps Z was measured visually with the aid of a battery operated magnifying glass (it illuminates and magnifies), this enabled particle movements along the boundaries of the defluidized heaps to be observed and followed clearly and accurately.

The air was then gradually increased, and after each increase the height Z was observed, but the measurement was taken after allowing equilibrium conditions to be attained. This was continued as long as accurate measurements could be made visually. However, this was found rather difficult to achieve at higher gas rates because the upper portion of the stagnant heaps started to erode away and became distorted.

The above procedure was repeated at least three times to be sure of the reproducibility of the results. Z was quite reproducible when measured at increasing and decreasing flow rates and could be estimated to within 0.5 cm. ($\pm$ 0.25 cm.).

In agreement with earlier workers, preliminary experiments showed that the bed height had no influence on Z provided it was deep enough (presumably not to be shallower than the maximum spoutable bed height). Therefore, the experimental procedure was restricted to the same initial bed height of 40 - 50 cm.

It should be noted that the curtaining effects produced by particles either sticking to or raining down the column walls had largely influenced the accuracy of measurements at higher gas rates despite the precautions

taken to reduce it. In addition the use of higher gas flow rates, particularly with sand and with plates having low free areas ϕ , caused a considerable pressure drop in the system. Similar difficulties were also experienced by Fakhimi(74). Consequently most of the experiments were confined to gas flow rates up to 4 - 5 times U_{mf}.

Additional experiments were carried out in order to demonstrate the existence of defluidized zones on the distributor plate. This was done as follows: a batch of 177 μ silver sand particles was dyed with blue colour by dipping the particles in a concentrated solution of methyl blue and allowing them to dry in a hot oven. Then, a layer of blue particles was first charged in the column followed by another layer of undyed (white) particles.

Figures (5.7) and (5.8) are a sequence of two photographs taken at low (U not much above U_{mf}) and high fluidizing velocities respectively. In each case the bed was allowed to fluidize for about five minutes, defluidized gently, and then photographed with a still camera through the transparent Perspex wall.

It should be emphasised that these pictures are of qualitative nature, they are presented here solely for demonstration. As is evident from these pictures, at higher fluidizing rates the heaps of the defluidized particles take the form of a trapezoid whose upper angles are rounded (i.e. a parabola) whereas at low fluidizing rates the heaps take the form of a pyramid. The observed effect at higher gas rates is probably due to the side impact of particles during lateral mixing of the material in the bed. Erosion of the upper regions of the defluidized heaps at higher gas rates has been reported by Ukhlov and Volkov(92), but it is not known whether Fakhimi(74) has also observed a similar sort of behaviour.

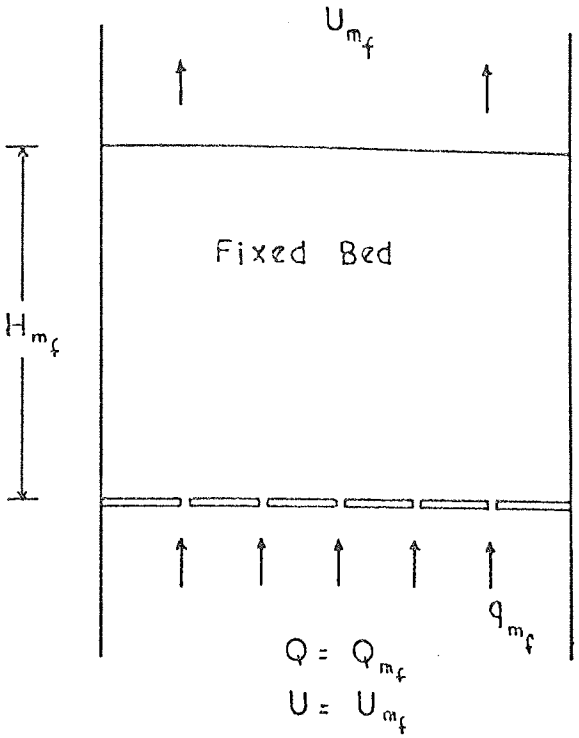

FIG. 5·1

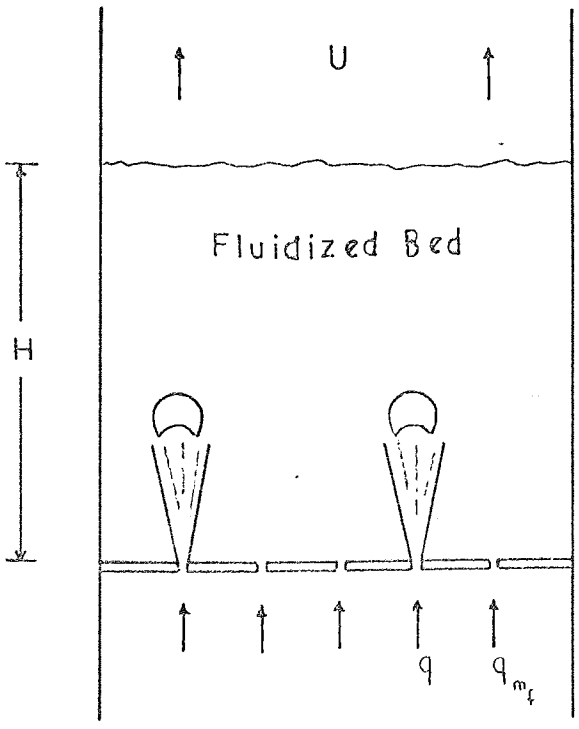

FIG. 5·2

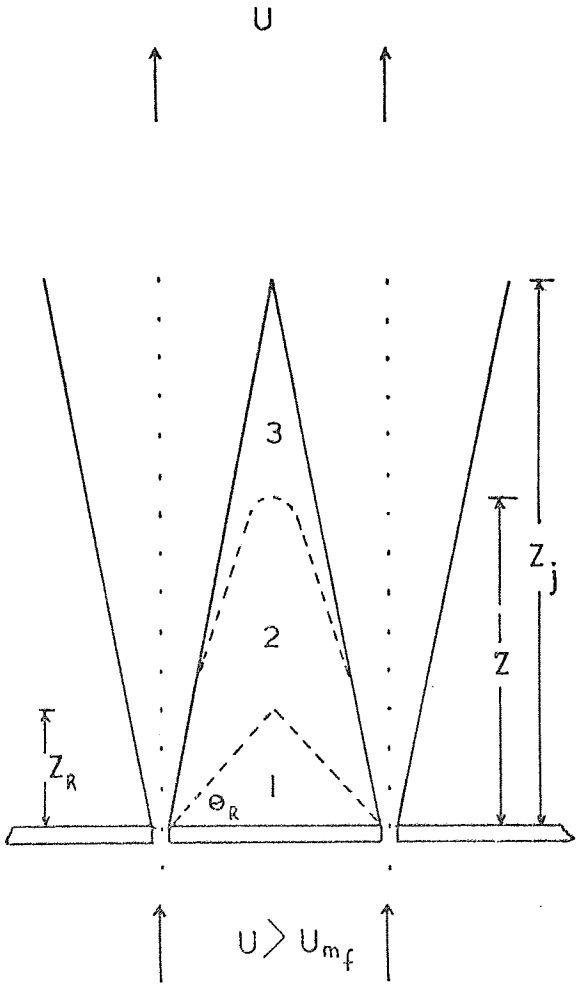

1 — zone I

2 — zone II

3 — zone III

FIG. 5·3

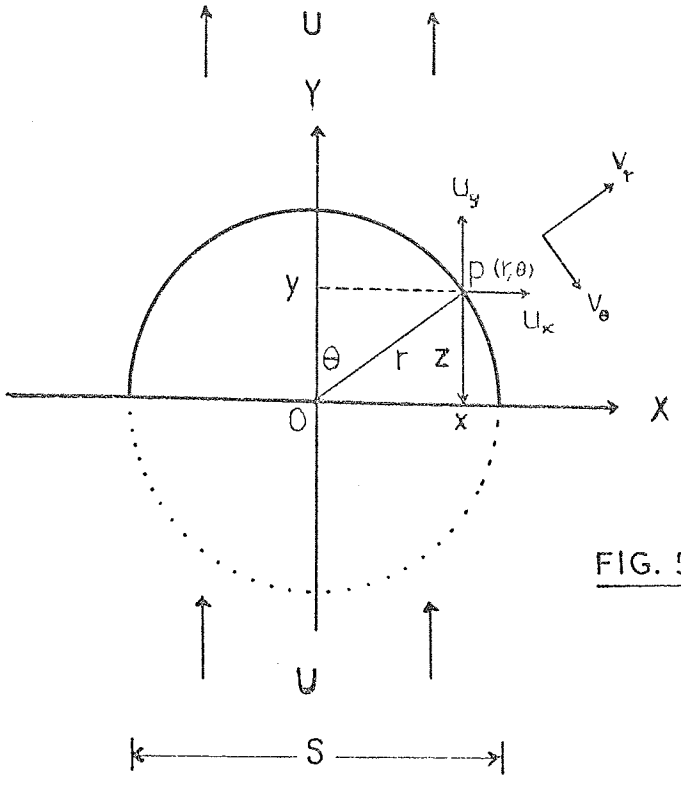

FIG. 5·4 FAKHIMI'S MODEL

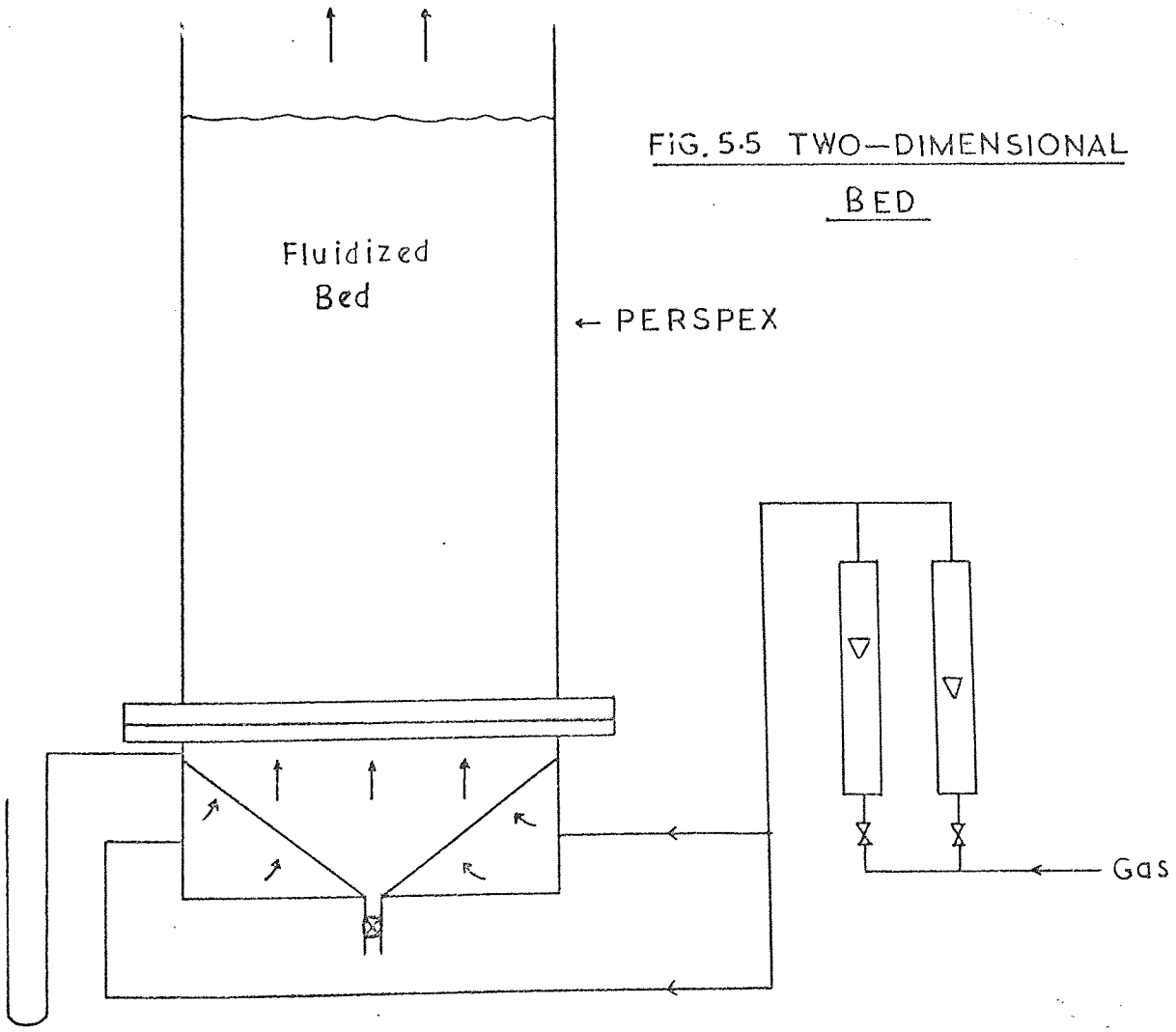

FIG. 5·5 TWO-DIMENSIONAL BED

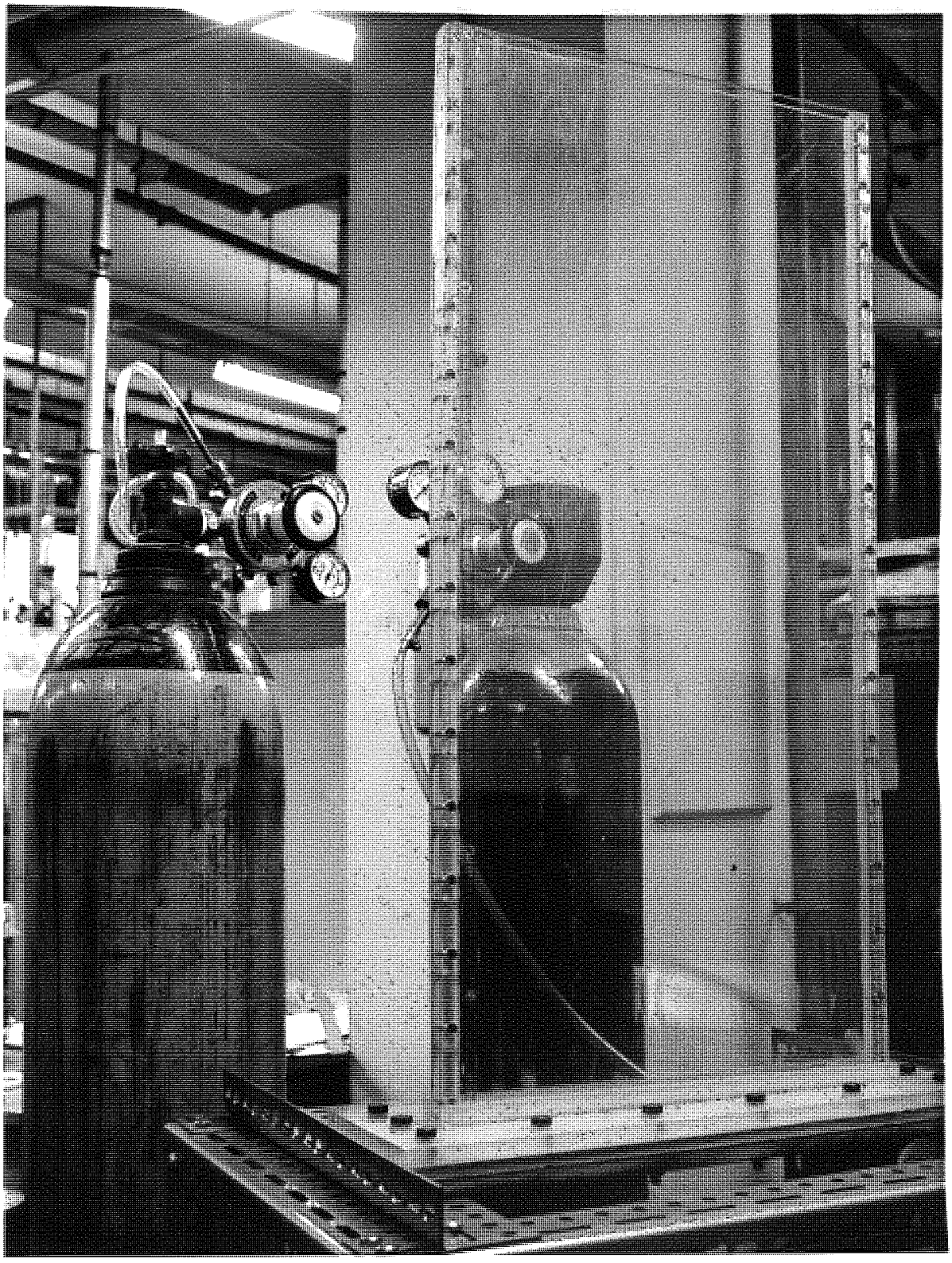

FIG. 5.6 Two-dimensional Perspex column.

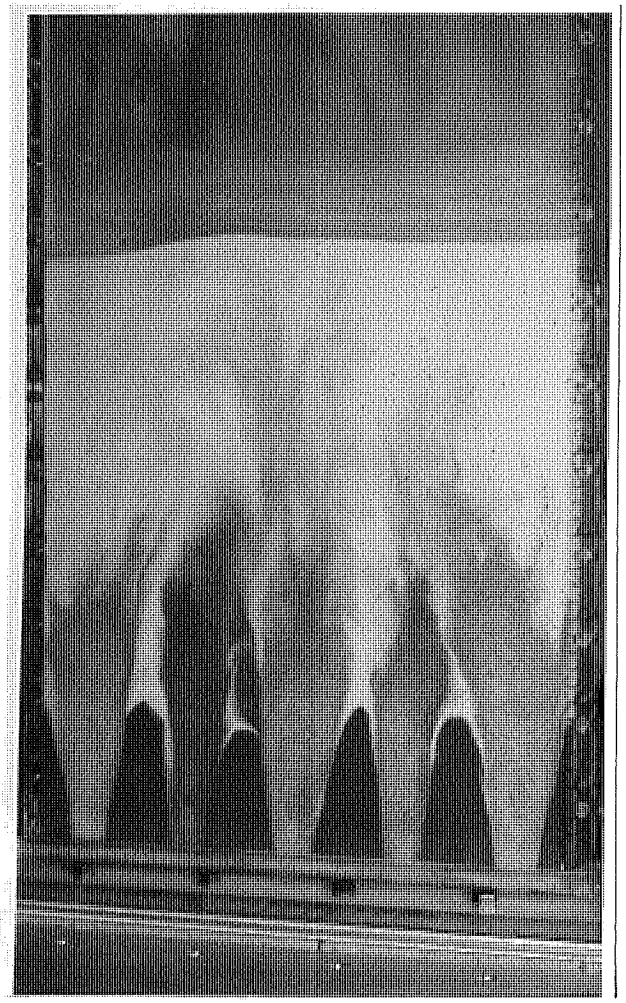

FIG .5.7 Defluidized zones on multi-orifice distributor plate.

$U = 2\ U_{mf}$ solid: 177 μ silver sand.

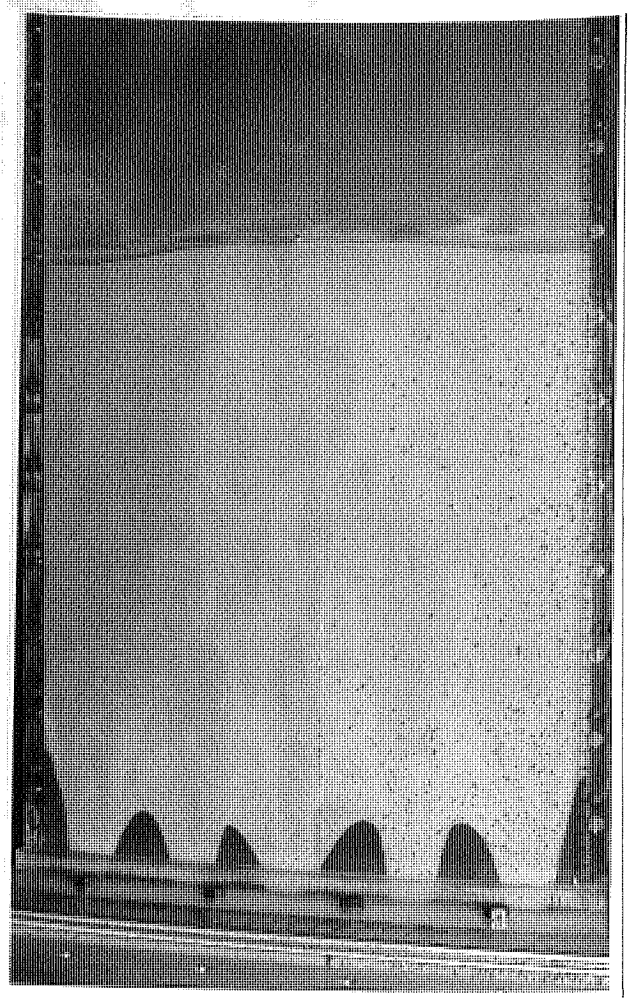

FIG .5.8 Defluidized zones on multi-orifice distributor plate.

$U = 4.8\ U_{mf}$ solid: 177 μ silver sand.

5.7 Experimental Results

The experimental results are given in Tables (5.3) - (5.5) and as plots of $(\frac{Z}{S})$ vs. $(\frac{U_{mf}}{U})$ in the way suggested by (5.5) in Figures (5.9) - (5.11). In figure (5.9), the experimental results are compared with the theoretically predicted line from (5.5).

As can be seen, the experimental results show a linear relationship between $(\frac{Z}{S})$ and $(\frac{U_{mf}}{U})$ and the line drawn through the experimental data passes through the origin as (5.5) predicts. However, the egreement between (5.5) and experiments is not good, but the two sets of results exhibit a similar trend. Similar discrepancy has been observed by Fakhimi(74), and as shown in Figure (5.9) the theoretical line falls below the experimental line with slope of 1.38 (for N = 5).

An important feature of the results is apparent from Figures (5.9) - (5.11). The experimental lines exhibit slopes of the same magnitude (i.e. around 4.0) regardless of the type of solid used. Fakhimi who carried out experiments with sand particles found a slope of similar value (i.e. about 3.8). This clearly demonstrates the closeness of our observations with the recently published work.

5.8 Discussion of Experimental Results

A study of the formation of defluidized zones on multi-orifice distributors and in between the orifices was made in a two-dimensional bed. As can be seen from the plots, the line drawn through the experimental results passes through the origin. The slopes of these lines are approximately similar (i.e. about 4.0) although Diakon exhibits slightly lower slope than sands. This may be attributable to the lower angle of repose obtained with Diakon (spherical). In all the cases studied the height of the defluidized zones decreased with increasing gas flow rate and increased with increasing orifice spacing. Hence for a given orifice diameter and column, a decrease in the fractional free area ϕ would cause an

increase in the amount of defluidized solids stagnating on the distributor plate.

In Figure (5.9) we present a comparison with the recently published theory(74). Only qualitative agreement exists between the two sets of results. This discrepancy was expected and mainly due to two factors given already by Fakhimi.

1. As explained earlier, in the formulation of equation (5.5) (for the case of the two-dimensional bed system), Fakhimi considered a bed of uniform voidage resting on the distributor plate through which gas is percolating (see Figure (5.4)). But this is valid only when the gas flow rate is equal to or less than U_{mf}; a higher gas rate will obviously lead to the spouting situation shown in Figure (5.2). The spouts effectively become two-phase jets of gas and solids of high voidage which, of course, is contrary to what has been assumed in deriving(5.5). This is probably the main reason for the deviation shown between the theoretical model and the experimental results. This discrepancy has been anticipated by Fakhimi himself in the first place and, as can be seen from his results, the experimental line exhibits a slope about twice as much as that of the theoretical line.

2. The experiments were conducted in a two-dimensional Perspex column, chosen particularly to facilitate visual observations at the bed walls. The possible influence of the bed walls and the curtaining effect produced by particles sticking on the Perspex walls may lead to values of Z higher than expected. But it is doubtful whether static effects can lead to unreasonable results because (i) these were completely absent at low gas rates and (ii) rounded sand which showed little tendency to stick on the column walls produced results not different from those of the other solids.

Measurements in a three dimensional bed system cannot be made visually

unless some kind of measuring device is used (e.g. a capacitance probe). However the insertion of a probe in the bed will inevitably disturb the stagnant heaps and may lead to erroneous results. The wall effects in a commercial bed are normally less pronounced, and therefore it is expected that the quantity of defluidized solids stagnating on a unit area of a commercial distributor would be less than that on a laboratory distributor. Obviously, the model presented by Fakhimi cannot be used for design purposes and the only way to obtain Z accurately is to measure it.

Ukhlov and Volkov(92) who experimented with different type of distributors and also observed the effect of gas flow rate and plate geometry on the height of the defluidized zones which appears to be in line with our observations. It is interesting to note that Glass(93) who studied the formation of defluidized zones on the upper surface of a cylindrical baffle immersed in beds of sand and glass beads fluidised with air also shows similar results. He found that the amount of defluidized solids settling on the baffle was governed by the gas flow rate and baffle diameter, i.e. the weight of defluidized solids decreased with gas flow rate and increased with baffle diameter.

5.9 Application of Experimental Results

The study of defluidized zones can now be applied to some aspects of distributor design and fluidized behaviour at the bottom of the bed.

5.9.1. Calculation of the Total Amount of Defluidized Solids Stagnating on the Distributor Plate for a Three-Dimensional Bed System

The results from the present work will be applied directly to a three-dimensional bed system, although the possible influence of the bed walls makes the interpretation of experiments in a two-dimensional bed to be somewhat different from that in a three-dimensional bed system.

Now considering the experimental results, the height Z may be related to the orifice spacing S and gas flow U by:

$$\frac{Z}{S} = 4 \left(\frac{U_{mf}}{U}\right) \qquad (5.8)$$

(i) Orifices with square-pitch arrangement

As may be seen from the photographs, at higher fluidizing rates the curve bordering the stagnant zones is almost a parabola. At lower fluidizing rates the heaps take the form of a pyramid. To simplify the calculations we may assume that each stagnant heap is a pyramid having a base area S^2 and volume

$$V_n = \frac{1}{3} \cdot S^2 \cdot Z \,,$$

$$\text{or} \qquad V_n = \frac{4}{3} \cdot S^3 \left(\frac{U_{mf}}{U}\right) \,, \qquad (5.9)$$

where V_n is the volume of a heap of defluidized solids stagnating on a square accommodating the n-th orifice. If N = total number of orifices on the distributor, then the total volume of defluidized solids stagnating on the distributor plate is

$$V = \sum_{n=1}^{N} V_n \qquad (5.10)$$

$$\text{or} \qquad V = \frac{4}{3} \cdot N \cdot S^3 \left(\frac{U_{mf}}{U}\right) \tag{5.11}$$

If D is the distributor (or column) diameter, then

$$N = \frac{\pi}{4} \cdot \frac{D^2}{S^2} \tag{5.12}$$

Combining (5.11) and (5.12), we obtain

$$V = \frac{\pi}{3} \cdot D^2 \cdot S \cdot \left(\frac{U_{mf}}{U}\right) \tag{5.13}$$

Therefore, the total mass of defluidized particles settling on the distributor is given by

$$M_s = \rho_s \cdot (1 - e_{mf}) \cdot V \quad , \tag{5.14}$$

$$M_s = \frac{\pi}{3} \cdot \rho_s \cdot (1 - e_{mf}) \cdot D^2 \cdot S \cdot \left(\frac{U_{mf}}{U}\right) \tag{5.15}$$

which shows that the amount of defluidized solids is a function of bed diameter, orifice spacing, and gas flow rate.

(ii) Orifices with triangular-pitch arrangement

For a triangular pitch, the base area of the defluidized heap of solids is $\frac{1}{4} \cdot S^2\sqrt{3}$, and therefore its volume is

$$V_n = \frac{\sqrt{3}}{3} \cdot S^3 \cdot \left(\frac{U_{mf}}{U}\right) \quad , \tag{5.16}$$

where V_n is the volume of a heap of defluidized solids stagnating on a triangle accommodating the n-th orifice. For N orifices, the total volume of defluidized solids on the distributor plate is

$$V = \frac{\sqrt{3}}{3} \cdot N \cdot S^3 \cdot \left(\frac{U_{mf}}{U}\right) \tag{5.17}$$

But we have

$$N = \frac{\pi}{\sqrt{3}} \cdot \frac{D^2}{S^2} \tag{5.18}$$

Combining (5.17) and (5.18), we get

$$V = \frac{\pi}{3} \cdot D^2 \cdot S \cdot \left(\frac{U'_{mf}}{U}\right) \qquad (5.19)$$

and

$$M_s = \frac{\pi}{3} \cdot \rho_s \cdot (1 - e_{mf}) \cdot D^2 \cdot S \cdot \left(\frac{U_{mf}}{U}\right) \qquad (5.20)$$

It can be seen that expressions (5.15) and (5.20) are identical confirming that the amount of defluidized solid stagnating on the distributor plate and in between the orifices is independent of the type of orifices pitch

5.9.2. Calculation of Height of Defluidized Zone at the Angle of Repose

As already pointed out, solids settle in advance at the angle of repose (zone I). As this zone is a constant feature in the system it is of interest to relate its extent to the height Z. The slope of the surface of the defluidized zones to the horizontal can exceed the angle of repose only under conditions when the hydrostatic pressure of the fluidized bed is greater or at least equal to the pressure acting from within the defluidized zone. This in effect will prevent particles from rolling down and being swept into the fluidized bed. Thus solid particles at the boundary of the stagnant zone undergo pressure from both sides and under steady conditions these pressures are equal.

In the present work no attempts have been made to reach the angle of repose due to the considerable pressure drop in the system caused by the higher gas rates required.

Consider Figure (5.3), the height of the defluidized zone at the angle of repose of solid particles is given by

$$Z_R = \frac{1}{2} \cdot S \cdot \tan\theta_R \qquad (5.21)$$

where θ_R is the angle of repose of solid particles. Combining (5.8) and (5.21) we have

$$\frac{Z}{Z_R} = \frac{8}{\tan\theta_R} \cdot \left(\frac{U_{mf}}{U}\right) \qquad (5.22)$$

and the gas flow rate necessary to reduce the height Z to Z_R is

$$U = \frac{8}{\tan\theta_R} \cdot U_{mf} \qquad (5.23)$$

Since for most solids θ_R is around 40^o, therefore the superficial gas velocity necessary to reduce Z to the angle of repose should be at least 8 times U_{mf}.

5.9.3. Prediction of Performance of Multi-Orifice Distributors

This follows from the earlier discussion presented in Chapter One concerning the theory of Fakhimi and Harrison(64) with respect to multi-orifice distributor design. These authors have derived a theory for predicting the number of operative orifices n on a multi-orifice distributor as a fraction of the total number of orifices N supported by experimental work on sand particles only (see Chapter One), i.e.

$$\frac{n}{N} = \frac{\left(\frac{U}{U_{mf}} - 1\right)}{\left[1 + 0.727.(1-e_{mf}).g.\left(\frac{\rho_s}{\rho_f . U_{mf}^2}\right).\phi^2.Z\right]^{\frac{1}{2}} - 1} \qquad (5.24)$$

Here Z is the height above the distributor for which the defluidized region extends and above which the superficial velocity U may be considered as uniform. The height Z is related to the orifice spacing and the gas velocity and the relationship $Z = 4\ S.\left(\frac{U_{mf}}{U}\right)$ has been obtained from the present work for different solid systems. Fakhimi and Harrison used Z = 3.8S in the above model, i.e. for a given solid-distributor system Z has been treated as a constant in their model, hence giving a linear relationship between $\left(\frac{n}{N}\right)$ and $\left(\frac{U}{U_{mf}}\right)$. Results from the present work indicate a non-linear dependence of $\left(\frac{n}{N}\right)$ on $\left(\frac{U}{U_{mf}}\right)$ and the possible reason

is that Z was varying with gas flow rate, i.e. for a given solid-distributor system Z = f(U). Their expression is then modified, in the light of experimental evidence indicated by our results, viz

$$\frac{n}{N} = \frac{\left(\frac{U}{U_{mf}} - 1\right)}{\left[1 + 0.727(1 - e_{mf}).g.\left(\frac{\rho_s}{\rho_f . U_{mf}^2}\right).\phi^2.\left(4.S.\frac{U_{mf}}{U}\right)\right]^{\frac{1}{2}} - 1} \qquad (5.25)$$

The purpose of the following work is to examine the applicability of the above models with regard to different solids, as the work of Fakhimi and Harrison was confined to sand particles only.

The experiments were carried out in a two-dimensional column similar to that already described. The characteristics of the solids used are given in Table (5.2): these consisted of particles having different shapes and densities. Following the same experimental procedure as that described by Fakhimi and Harrison(64), the fraction of operative orifices on the distributor $\frac{n}{N}$ as a function of gas flow rate was obtained. The experimental results are presented in Tables (5.6) - (5.8). Plots of $(\frac{n}{N})$ vs. $(\frac{U}{U_{mf}} - 1)$ obtained from these results are compared with the theoretical models (i.e.equations (5.24) and (5.25) in Figures (5.12) - (5.14).

As shown in the plots, the experimental points show a non-linear relationship between $(\frac{n}{N})$ and $(\frac{U}{U_{mf}} - 1)$, i.e. in accord with the modification introduced to the original model. A study of Figure (5.14) shows that with cracking catalyst (having very low U_{mf}) the deviation between experiments and (5.24) is considerable. Unlike the other solids, the points are scattered and Figure (5.14) clearly demonstrates the repeatability of the results, the experimental results show closer agreement with the modified model than with (5.24). It seems clear that this might arise from the fact that cracking catalyst is difficult to defluidize due to the greater

mobility which usually obtained with small particles, and this probably caused Z to decrease very rapidly over the range of gas flows.

In Chapter One we have pointed out the peculiar behaviour found with cracking catalyst and in particular with the unsieved catalyst. In conclusion some doubt may be felt over this theory with respect to its application to solids with low U_{mf}, but the matter still remains to be clarified. In fact (5.25) was relied on in predicting the performance of multi-orifice distributors encountered throughout the work of this thesis.

5.9.4. Distributor Design Variables and Jet Interaction

With multi-orifice distributors and similar devices, adjacent jets issuing vertically through the fluidized bed tend to interact with each other at a certain gas velocity for a given orifice spacing. Visual observations have indicated that jet interaction often leads to larger bubbles and these may coalesce further up the bed, eventually forming slugs. This, of course, is undesirable and can lead to unstable operation of the fluidized bed. The height above which jet interaction occurs is largely governed by the orifice spacing. For example, a small orifice spacing causes neighbouring jets to intersectone another at smaller heights above the distributor with gas velocity not much above U_{mf}.

Little work has been done on this problem previously. As already indicated in Chapter One,Zenz(70) made a study of single vertical jets issuing into a two-dimensional bed of cracking catalyst. As a first approximation, to provide a basis for calculating the orifice spacing in an industrial distributor, he measured the penetration by visual observation and found the following relationship

$$p_j = 2 D_B \qquad (5.26)$$

where p_j is the penetration depth and D_B is the bubble diameter representing the penetration volume.

In order to avoid premature bubble growth, he suggested a minimum orifice spacing given by

$$S_{min} = \frac{3}{4} \cdot p_j \qquad (5.27)$$

Here p_j is not necessarily the height where the boundaries of neighbouring jets intersect one another. From our visual observations, jet intersection occurs at heights much greater than that predicted by (5.27).

Theoretical Analysis

The purpose of the following analysis is to determine the height where the boundaries of adjacent jets intersect one another and this will be related to the design variables of the distributor. With the aid of concepts on the stability of a submerged round fluid jet above a single orifice in the distributor and from a balance of the flow of momentum we shall determine the maximum volume concentration of solid particles which either remain in the same position or are carried off in the direction of flow of the fluid. This limiting concentration is that which can be attained in the effective volume of the jet without destroying its stability. Abramovich(94) analysed a two-phase jet in air by assuming that the motion of admixed particles approximated the local air velocity, and that the solid concentration in a transverse cross-section of the jet was similar to the temperature profile in a jet of non-uniform temperature. Abramovich's analysis applies to small liquid droplets and dust in a jet, where the relative velocities between gas and particles are assumed to be negligible. He also assumed that, even if the particles were initially at rest in the jet stream, they would be instantaneously accelerated to the local gas velocity. This is not the situation in a fluidized bed, because solid particles are large in comparison; those swept into the jet region are accelerated from rest in the gas stream, and whether their velocities can ever reach the local gas velocity will depend on their

size and density. However, the analysis to be pursued here will be based on Abramovich's work, but some simplifying assumptions are necessary.

Now consider a multi-orifice distributor having orifices of constant diameter D_o and centre-to-centre orifice spacing S. The arrangement of the orifices is arbitrary (square or triangular). Slotted distributors giving vertical jets can also be considered, but other types of distributors giving horizontal jets are excluded (e.g. bubble caps). The fractional free area of the distributor plate ϕ is taken as small. The fluid of density ρ_f is assumed to be incompressible and the flow is isothermal and uniformly distributed across the distributor. It may be assumed that at the surface of the orifice the fluid velocity U_o is constant. The solid particles of density ρ_s are of uniform size and shape. It will be assumed that their volume is negligible in comparison with the effective volume of the jet. It is further assumed that all particles in the fluidized bed which have entered the jet region above the orifice either remain in their position or are carried out in the direction of flow. At the distance Z_j above the distributor plate, where the boundaries of adjacent jets intersect one another, the velocity of solid particles in the jet is zero.

Consider Figure (5.15), and under these assumptions make a balance of flow of momentum in the jet in the direction of flow of fluid, between the plane of area a_o at the surface of the orifice and by the plane perpendicular to the axis of flow in the jet and limited by the jet boundary at the distance Z_j above the distributor. Then

$$\rho_f . U_o^2 . a_o = (1 - e_j) . V_j \, g . (\rho_s - \rho_f) \qquad (5.28)$$

Where V_j is the effective volume of the jet, e_j is the average maximum voidage of solid particles in the jet and $(1 - e_j)$ is the maximum volume concentration of particles contained in the effective volume of the jet.

In view of the assumed small free area ϕ of the distributor, we have neglected in (5.28) the flow of momentum in the jet at the distance Z_j from the distributor, further we have neglected the loss of momentum due to changes in momentum of the solid particles and fluid, and the additional turbulence due to the presence of solid particles and their collisions.

Calculation of V_j

From Figure (5.15), if the angle of the jet is considered constant, then it can be shown that

$$X_j = S \tag{5.29}$$

Where X_j is the width of the jet at height Z_j. Thus we have

$$V_j = \frac{1}{3}\cdot\frac{\pi}{4}\cdot\left(Z_j + \frac{Z_j D_o}{S - D_o}\right).S^2 - \frac{1}{3}\cdot\frac{\pi}{4}\cdot\left(\frac{Z_j D_o}{S - D_o}\right).D_o^2 \tag{5.30}$$

Simplifying (5.30), we have

$$V_j = \frac{1}{3}\cdot\frac{\pi}{4}\cdot Z_j\left(\frac{S^3 - D_o^3}{S - D_o}\right) \tag{5.31}$$

Now using (5.31) in (5.28) and considering that for gas-solid systems $\rho_s \gg \rho_f$, we obtain

$$Z_j = \frac{\rho_f \cdot U_o^2 \cdot a_o}{\frac{1}{3}\cdot\frac{\pi}{4}\cdot(1-e_j).D_o^2\left[\frac{\left(\frac{S}{D_o}\right)^3 - 1}{\left(\frac{S}{D_o}\right) - 1}\right].\rho_s \cdot g} \tag{5.32}$$

For square-pitch arrangement, we have

$$\phi = \frac{\pi}{4}\cdot\frac{D_o^2}{S^2} \tag{5.33}$$

Also, we have

$$U = U_o\cdot\phi \quad \text{and} \quad a_o = \frac{\pi}{4}\cdot D_o^2 \tag{5.34}$$

Using (5.33) and (5.34) in (5.32) simplify and rearrange, we have

$$Z_j = \frac{\rho_f . U^2}{\frac{1}{3}.(1-e_j).\left[\phi^2 + \gamma.\phi^{\frac{1}{2}} + \gamma.\phi\right]^{3/2}.\rho_s.g} \qquad (5.35)$$

where $\gamma = 4/\pi$.

Thus (5.35) relates, for a three-dimensional bed system, the height Z_j at which adjacent jets intersect one another to the plate characteristics, solid and gas properties and the gas flow rate. It also shows the conditions under which the volume concentration $(1 - e_j)$ of particles in the effective volume of the jet above the distributor of a fluidized bed will attain its maximum value. It should be noted that Z_j for a triangular pitch arrangement of orifices is also given by (5.35)

Unfortunately, knowledge of $(1 - e_j)$ is not available and its estimation is rather difficult due to the complexity of the situation. Another problem encountered in this study is the difficulty in locating visually (using the two-dimensional column) the height Z_j, because of the uncertainty of jet interaction. Values of Z_j as a function of orifice spacing for the distributors used are plotted in Figure (5.16) and this may be demonstrative of the reproducibility of the results. Nevertheless, from these preliminary observations we find

$$\frac{Z_j}{S} = 4.4 - 5.7 \qquad (5.36)$$

when experimenting with (281μ) graded Diakon. (With this material (Perspex) clearer vision of jets has been obtained compared with other solids). Equation (5.36) implies that for a given orifice spacing there exists a definite height above the distributor at which jets intersect one another and this intersection takes place at a certain gas flow rate. It should be noted that Z_j is always greater than Z, the height of the defluidized heaps

stagnating on the distributor plate. However, for smaller values of S, the gas flow rate needed for jet intersection is equal to or little above U_{mf} and in this case Z_j would approach Z.

If it is required that the distributor should not cause irregular behaviour in the fluidized bed over the entire range of concentration, i.e. not even at the point of incipient fluidization U_{mf} when the voidage of spherical particles is approximately 0.40 (see Chapter Two), we have for the height Z_j the relation

$$Z_j = \frac{\rho_f . U^2}{0.2\left[\phi^2 + \gamma^{\frac{1}{2}}\phi^{3/2} + \gamma.\phi\right].\rho_s.g} \qquad (5.37)$$

With the aid of (5.36) and (5.37), it is possible to estimate the design parameters for a multi-orifice distributor able to avoid irregularities at incipient fluidization.

It should be realised that the complexity of the problem has forced a number of drastic assumptions to be made. The purpose of the above analysis can be accomplished if the problem is pursued more rigorously and this, of course, requires a separate study. Investigation of this problem together with study on the nature of voidage in the effective volume of the fluid jet above the orifice would be useful subjects for future research and would give results of design interest.

CONCLUSIONS

1. The study of this chapter has shown that the amount of defluidized particles stagnating on the distributor plate is influenced by the orifice spacing, column diameter, gas flow rate and incipient fluidizing velocity of the solid particles, but independent of the pitch arrangement of the orifices. The experimental results agree only qualitatively with Fakhimi's model(74), but in excellent agreement with his experiments.

The experimental results indicate that the minimum gas flow rate necessary to reduce the height of the defluidized zones to the angle of repose of solid particles should be at least 8 times U_{mf}.

2. In the light of the experimental evidence it is suggested that the theory of Fakhimi and Harrison(64) for predicting the performance of multi-orifice distributors might break down with solids having low U_{mf} values (e.g. cracking catalyst). A modification to the original model has been proposed and this modification has resulted in closer agreement with experiments.

3. A simple relationship has been derived for predicting the conditions under which adjacent fluid jets issuing vertically through a fluidized bed interact with each other, and this has been considered in particular with regard to distributor design. The conclusions which can be drawn from the analysis are qualitative in nature. This follows from the fact that no information is available about the nature of the voidage within the fluid jet above the orifice. It is therefore, suggested that this subject is a useful field for further research.

4. Judging from our observations, the fluidized bed in the region close to the distributor surface or close to an obstacle placed in the bed should not be treated as an ideal inviscid fluid for its analysis but as a more complex system.

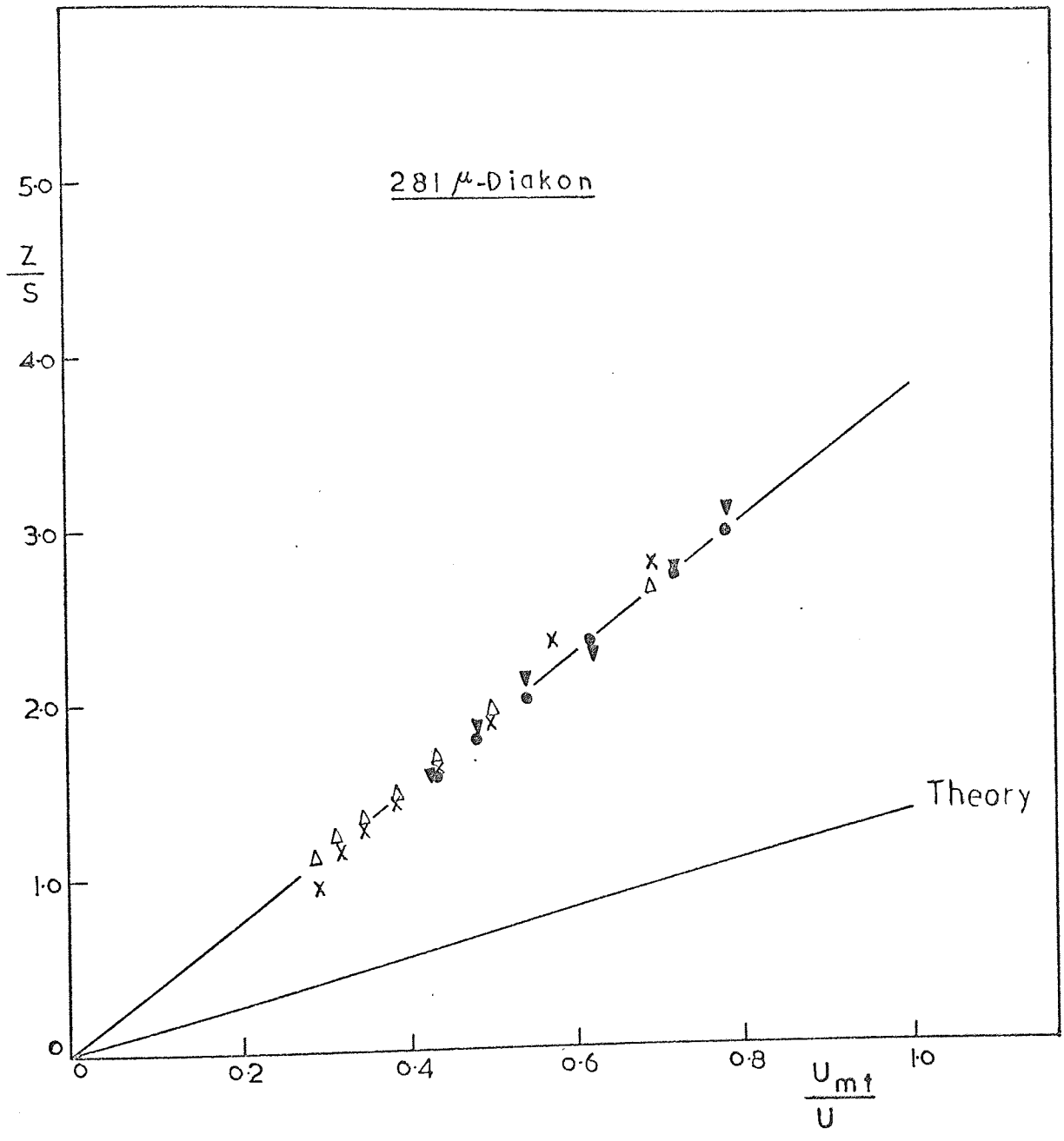

Legend	S, cm	N
●	3·3	11
X	4·8	3
▼	6·6	5
Δ	7·2	5

FIG. 5.9

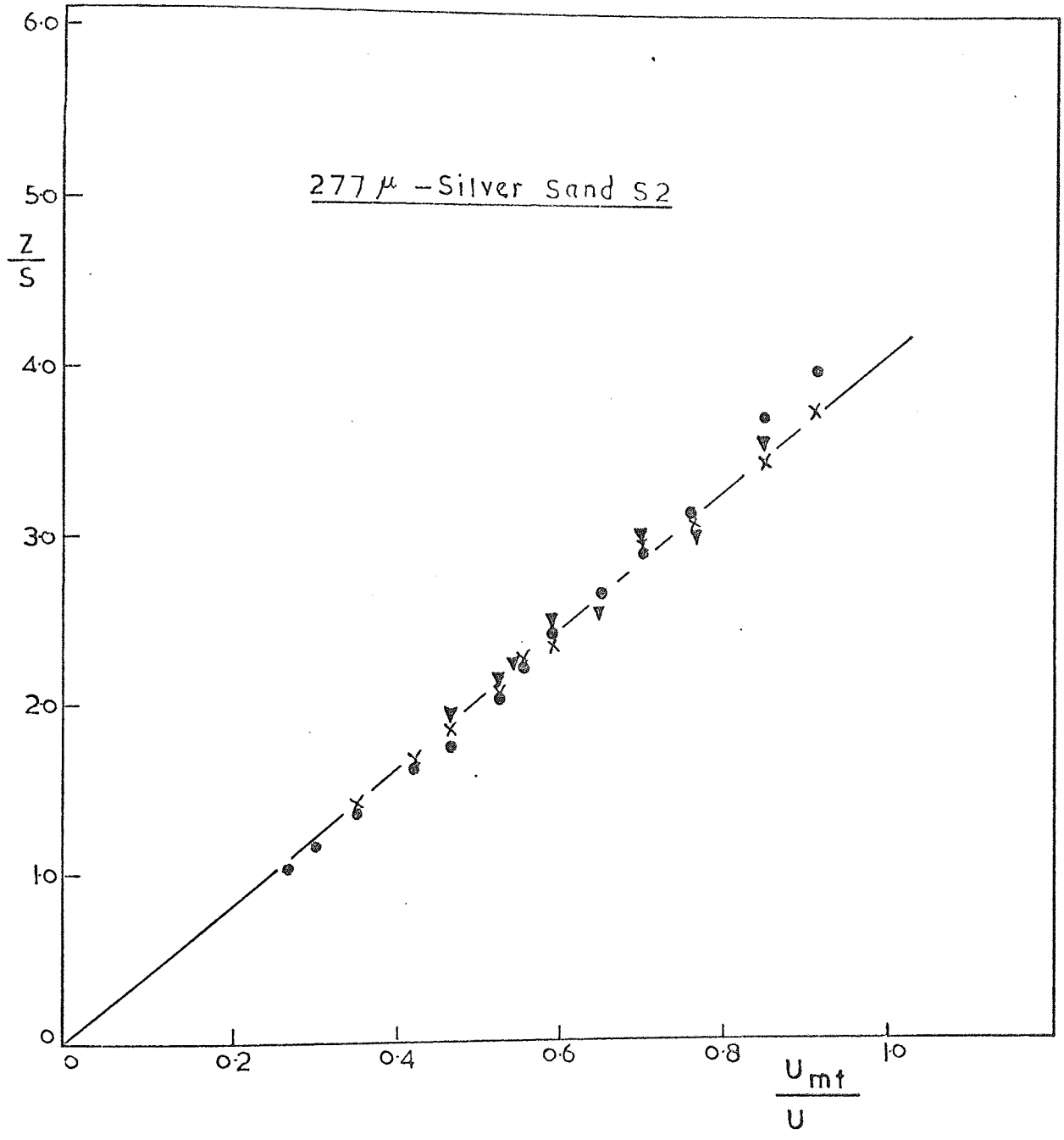

Legend	S, cm	N
●	2·4	15
X	4·8	8
▼	7·2	5

FIG. 5·10

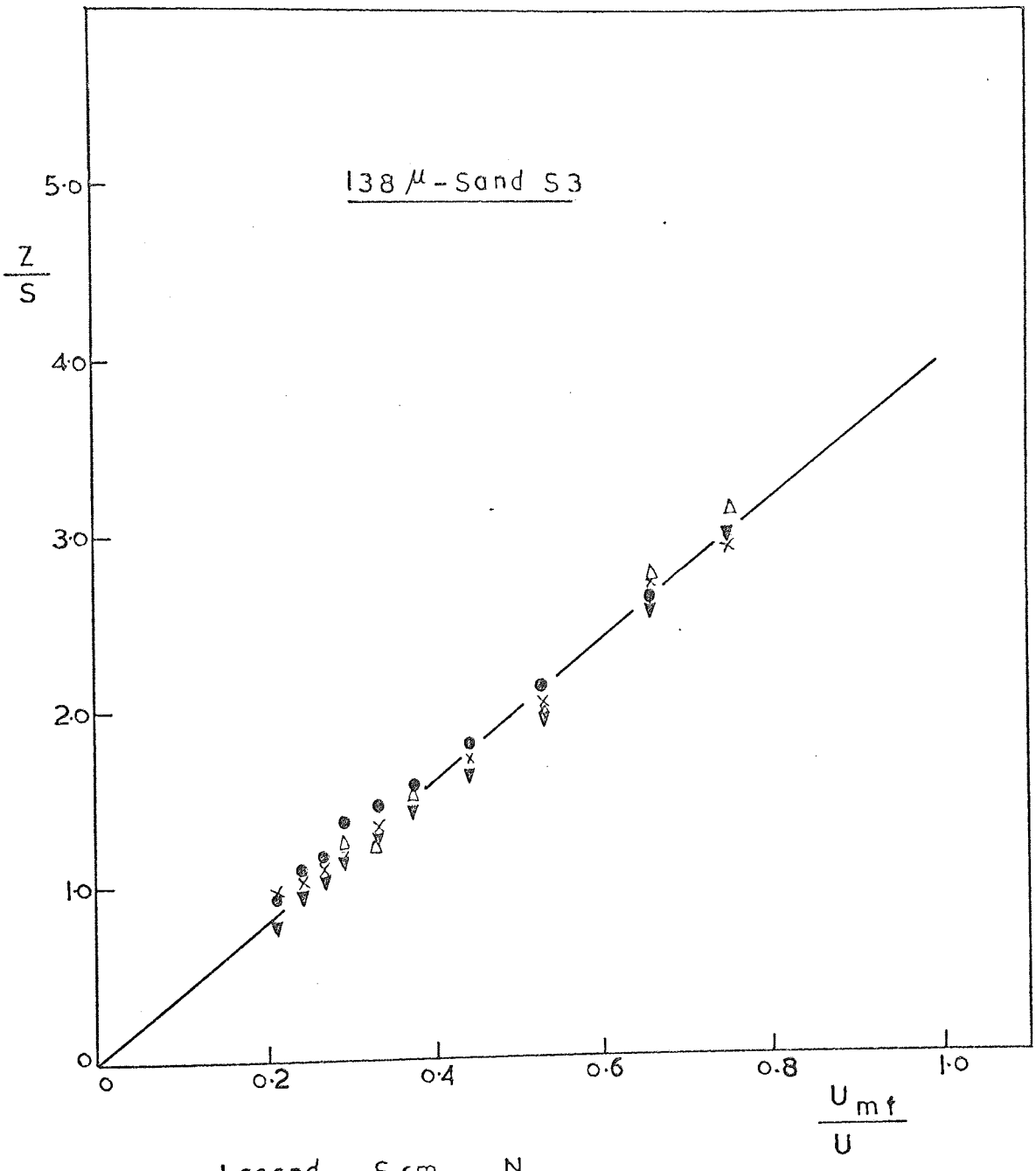

Legend	S, cm	N
●	2·4	15
X	4·8	8
▼	7·2	5
Δ	9·6	3

FIG. 5·11

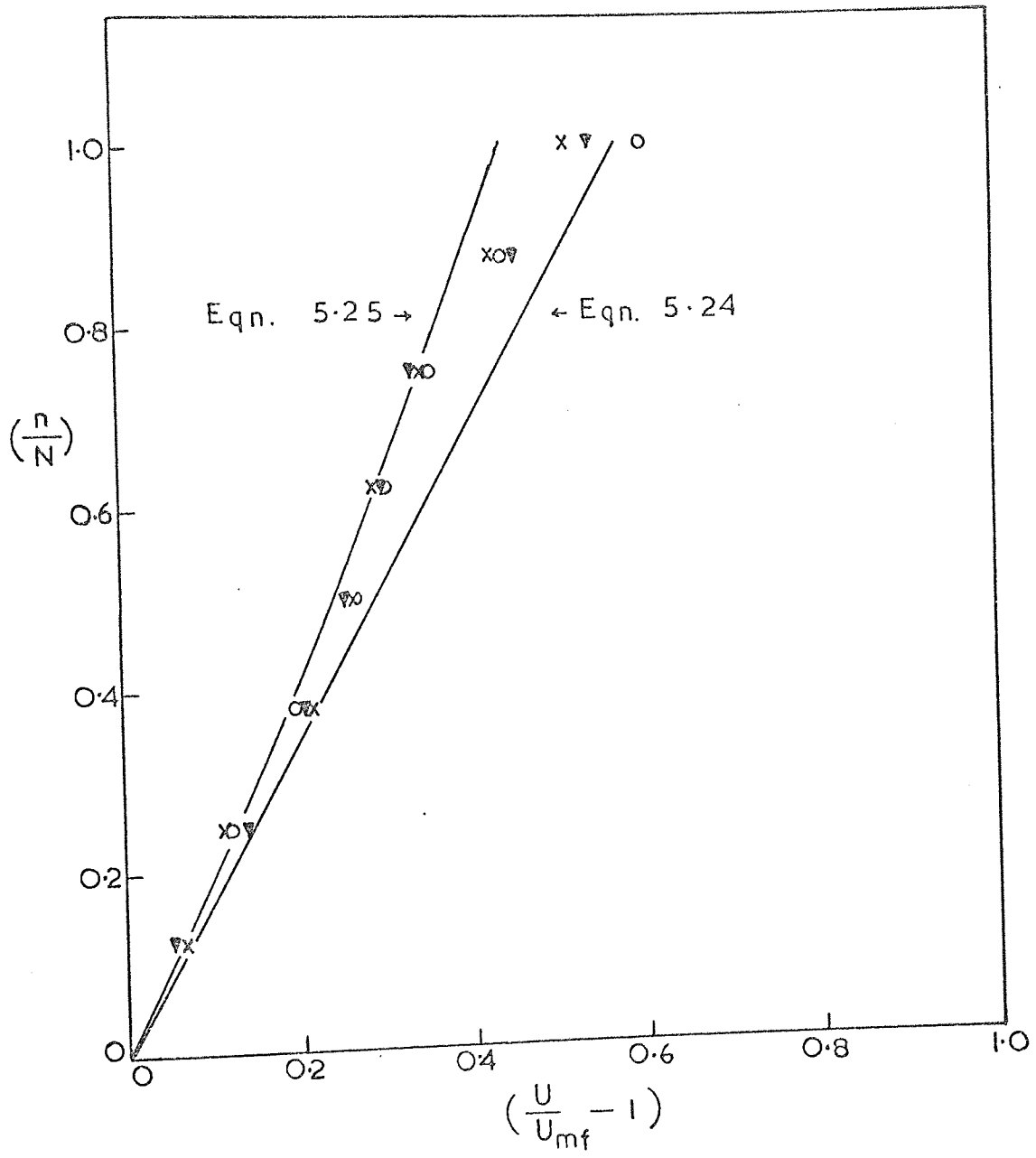

DISTRIBUTOR 5 231 μ DIAKON

LEGEND	Hmf
o	21·5
▽	46·5
x	66·6

FIG. 5·12

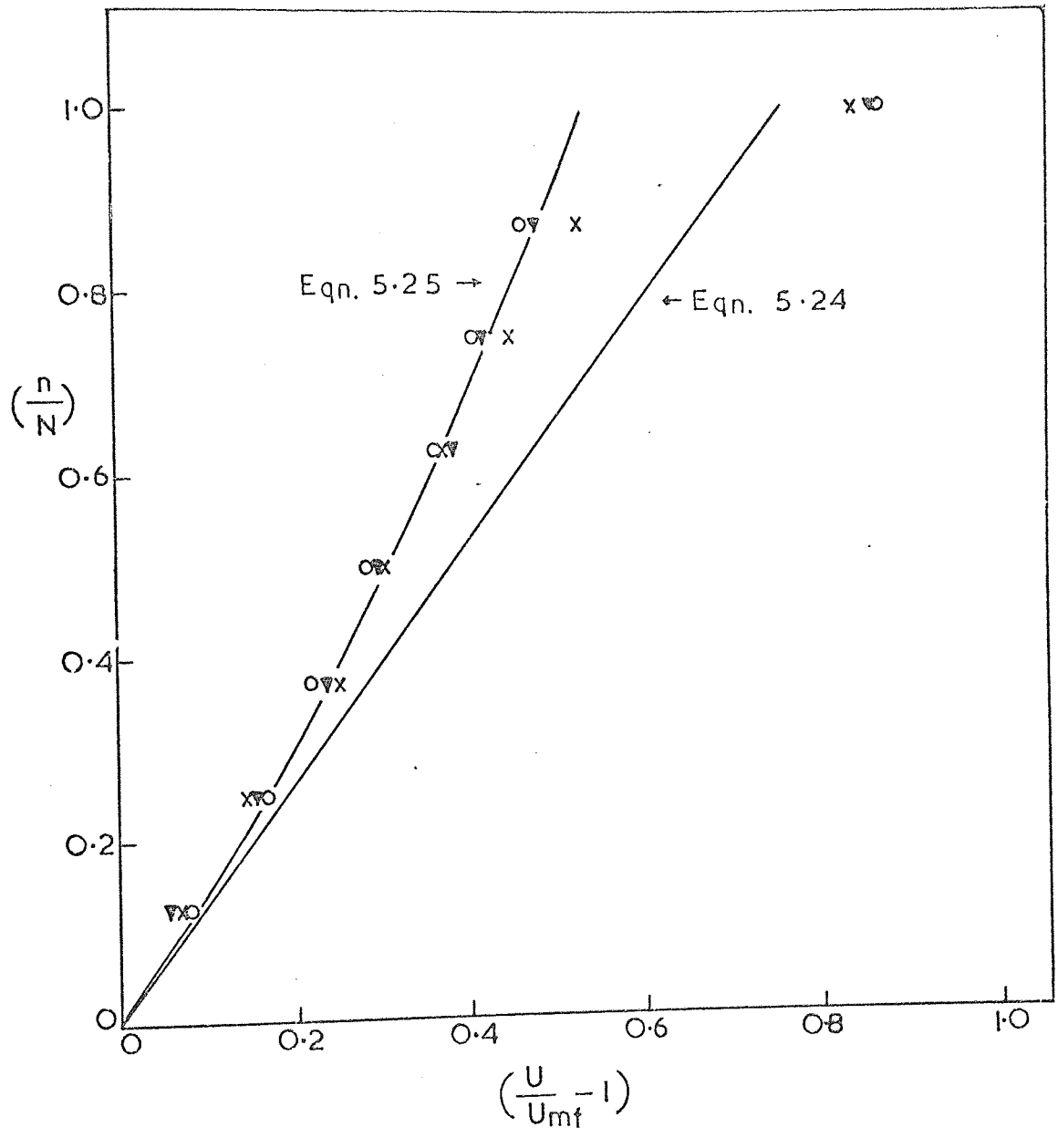

DISTRIBUTOR 5 177 μ SAND S1

LEGEND Hmf, cm.

o	21·7
▼	36·4
x	56·2

FIG. 5·13

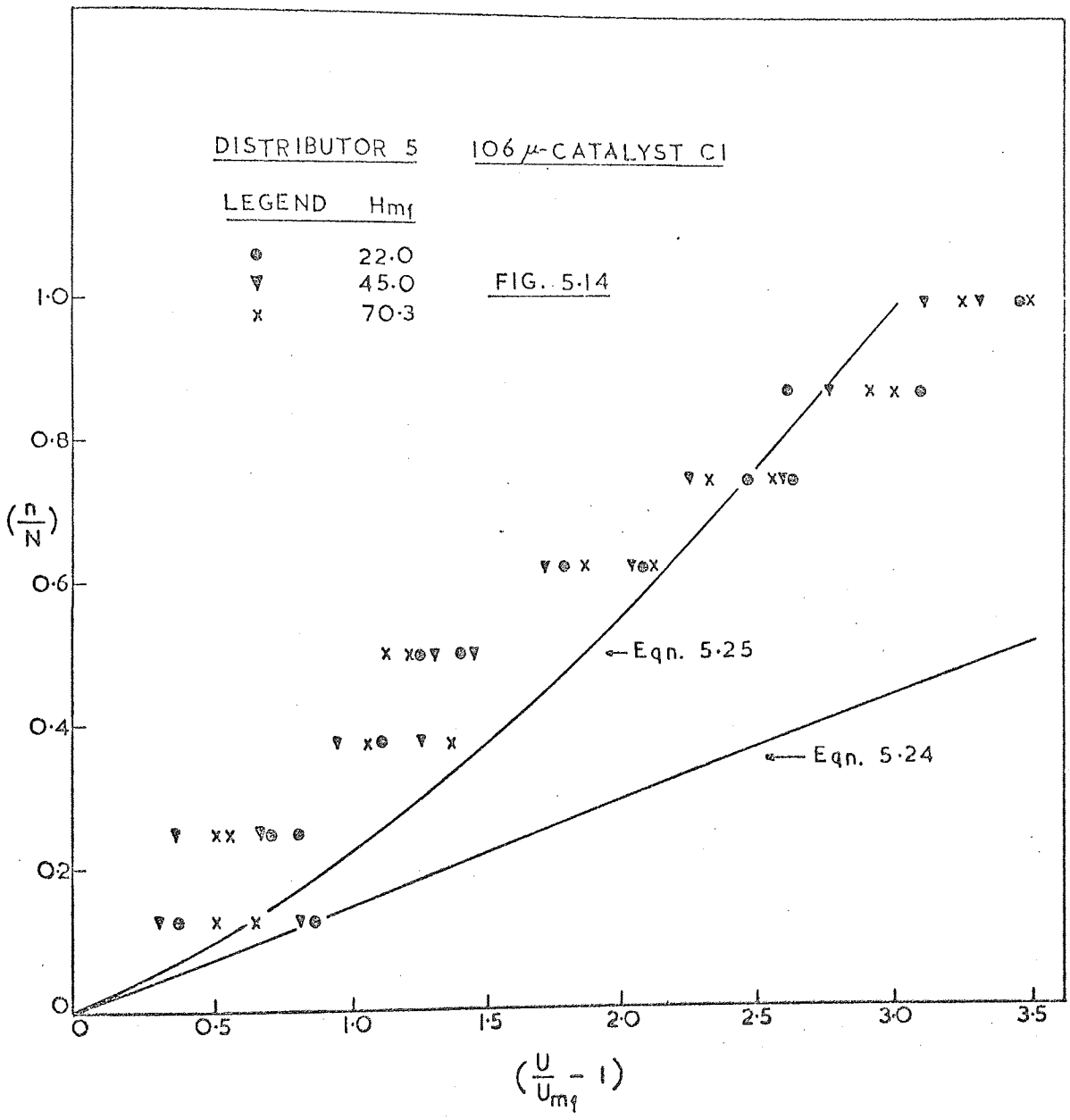
DISTRIBUTOR 5
106 μ-CATALYST C1
LEGEND Hmf
22·0
45·0
70·3
FIG. 5·14
Eqn. 5·25
Eqn. 5·24
(n/N)
(U/Umf − 1)
0
0·2
0·4
0·6
0·8
1·0
0·5
1·0
1·5
2·0
2·5
3·0
3·5

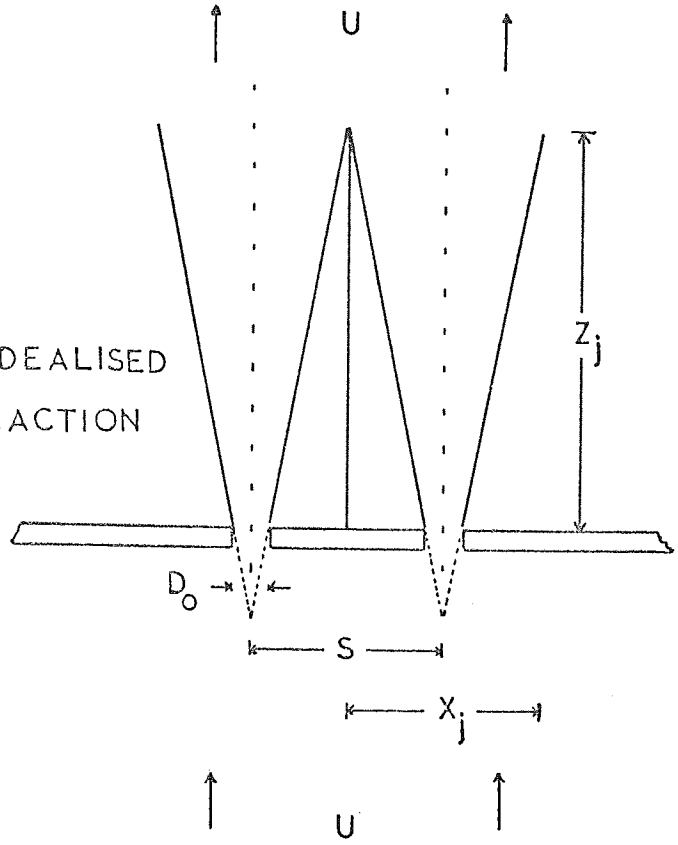

FIG. 5·15 IDEALISED JET INTERACTION

FIG. 5.16 JET INTERACTION ABOVE MULTI-ORIFICE DSTRIBUTOR

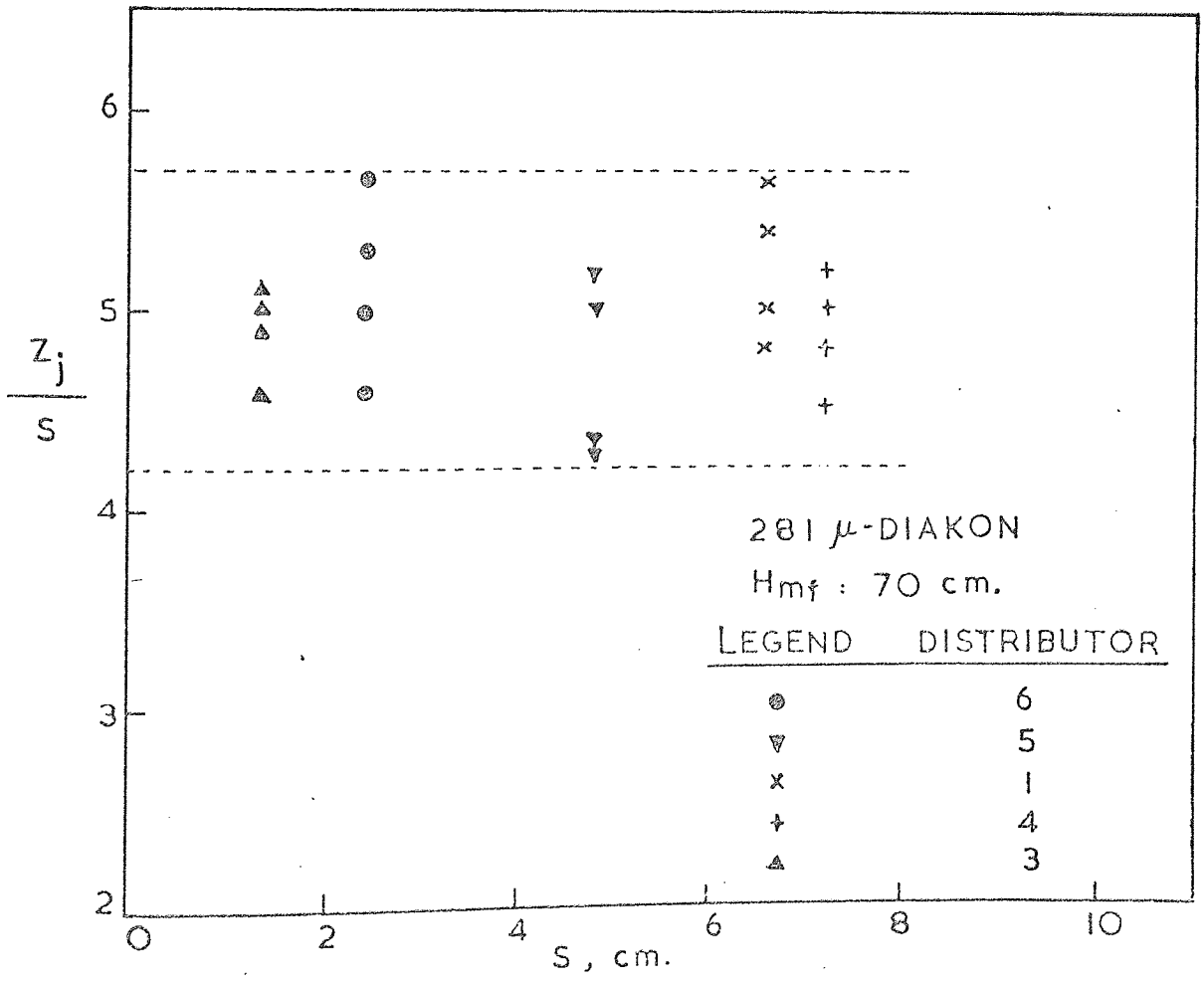

CHAPTER SIX

6. FLOWBACK OF SOLID PARTICLES ACROSS THE DISTRIBUTOR PLATE

6.1 Introduction

The study presented in this chapter is concerned with a phenomenon that occurs at perforate distributors of gas fluidized beds, namely the flowback (or leakage) of solid particles through the distributor orifices into the wind box. This flowback can easily be observed with multi-orifice distributors where it has been reported even at average orifice velocities one hundred times greater than the particle free fall velocity (15). Excessive flowback of solids quite often results in the destruction of the distributor, especially when the fluidized bed is a catalytic reactor, for the following reasons:

1. Particle reentrainment at high velocity into the fluidized bed causes erosion of the distributor orifices.

2. If an exothermic reaction is carried out in the bed, the reaction will start inside the wind box due to the presence of catalyst particles under the distributor plate and submit the distributor to temperatures for which it has not been designed. The presence of solids below the distributor implies that some of the catalyst particles are unavailable for reaction in the bed.

Despite its adverse effects on fluidized bed reactors, flowback is actually required during the operation of multi-stage systems where multi-orifice plates act both as gas distributors and downcomers.

An understanding of flowback behaviour is vitally important for the rational design of fluidized beds. As noted by Gregory(2), flowback of particles through the distributor in gas fluidized beds has not been studied theoretically. To date, only little work has been reported, and more systematic work remains to be done. For this reason, the present study has been undertaken.

6.2 Previous Work

Information on flowback derived partly from the patent literature and partly from reported investigations can be found in the literature survey presented in Chapter 1. Gregory(2) stated the problem and gave two curves of distributor flowback plotted against the fluidizing velocity. He postulated that surges associated with bubble growth and activity may be significant in influencing flowback. The present author(77) has also carried out preliminary investigations on solids flowback through multi-orifice distributors. The distributors were constructed from Perspex plates and silver sand (irregular) was used as the fluidized solid. However, blockage of some of the orifices with sand particles during operation led to some difficulties and made the interpretation of the experimental results rather ambiguous. But nonetheless, the study gave an insight to the important variables in the problem.

Recent work by Serviant et al.(76) on flowback through orifices in gas fluidized beds revealed two different types of flowback: dumping and weeping. Dumping is a phenomenon associated with low gas flow rates causing particles to fall through the entire area of the orifice. Whereas weeping is associated with high gas flow rates causing particles to fall by the periphery of the orifice. Weeping and dumping are phenomena observed with sieve trays in distillation columns, and, since the incipiently fluidized bed behaves so much like an inviscid liquid, it seems reasonable to suppose that the rate of flowback of solid particles through the orifices of the distributor should occur in the same way as for liquid on sieve trays. However, the analogy between gas-solid systems and gas-liquid systems may not be justified for reasons stated in Chapter 1. We may nevertheless gain some partial insight into the likely behaviour by considering the analogy. Unfortunately the work of Serviant et al.(76) has been confined mainly to plates with single orifices with

little work done on multi-orifice distributors using one solid only (i.e. unsieved cracking catalyst). It should be noted that data obtained from a single-orifice experiments cannot be used to interpret the behaviour of a multi-orifice distributor. As the present work shows, maldistribution of the gas flow through the distributor which usually occurs in practice may cause the flowback behaviour of an orifice on a multi-orifice distributor to be different from that with single-orifice distributor.

In a closely related problem, Bulove and Tyuryaev(110) have given two design equations to compute solids flowback through perforated baffles. Baffles are used in staging fluidized beds and differ from distribution plates mainly because of higher values of their relative free areas, ϕ (Bulove and Tyuryaev studied baffles with values of ϕ as high as 16%). The free areas of commercial distributors hardly exceed 4% otherwise proper fluidization cannot be achieved.

In this study we consider the flowback behaviour of multi-orifice distributors in more detail. Plates having single orifice and distributors equipped with long cylindrical nozzles are also included in the study.

The distributor design variables under consideration in this study are: the distributor plate characteristics ϕ (or fractional free area), orifice diameter D_o and spacing S, distributor thickness or nozzle length ℓ and wind box volume V_w.

The following work consists of two types of investigations:

1. Investigation of solids flowback across the distributor plate under free-flow conditions (i.e. gravity flow), without gas being blown into the bed (i.e. U = 0).
2. Investigation of solids flowback through the distributor plate

under fluidized conditions (i.e. $U \geqslant U_{mf}$), and this can be divided into two types of investigations:

(a) Determination of the limiting gas velocity $U\ell_o$ (in the distributor orifices) at which the particles cease entirely to fall through the orifices (i.e. weep point).

(b) Determination of solids flowback through the distributor plate over the entire range of fluidizing velocities from $U = U_{mf}$ to $U = U\ell$, where $U\ell$ is the limiting superficial velocity of gas.

6.3 Flowback Through the Distributor Under Free-Flow Conditions (Gravity Flow)

Numerous equations have been published for the gravity flow of solids through circular orifices. The summary of some of these can be found in a short review paper by Pilpel(111) who classifies them into (a) empirical equations (b) those derived from dimensional analysis and (c) those derived from theoretical analyses based on analogies with fluids. Empirical equations usually take the form $W = \rho_B . D_o^n . f(D_P)$, where n varies between 2.5 and 3 and ρ_B is the bulk density of solids in the bed. Instead of D_o the so-called effective diameter $(D_o - 1.5\ D_P)$ is sometimes used as well as $(D - k)$, where k is a factor depends upon the size and shape of the solid particles. In general these empirical relationships imply some analogy with fluid flow either through orifices or over weirs. Empirical equations such as that of Gregory(53):

$$W = 0.278\ D_o^{2.5} \tag{6.1}$$

which is related to stick-slip downflow of solid particles in pipes. Gregory(53) also suggested some rules for the flow of particulate solids in pipes.

Beverloo et al.(112) published for the flow of granular solids through circular orifices, the following equation:

$$W = 35\ \rho_B . \sqrt{g} . (D_o - 1.4\ D_P)^{2.5} \tag{6.2}$$

Using the effective hydraulic diameter D_e so that $D_e = D_o - 1.4\ D_p$ and the effective orifice area A_e calculated from D_e, (6.2) can be replaced by the equation

$$W = 45\ \rho_B . A_e . \sqrt{g\ D_e} \tag{6.3}$$

Some workers have included the bed height in their correlations,

for example Newton et al.(113) found

$$W = 213\, D_o^{2.96} \cdot H^{0.04} \qquad (6.4)$$

where H is the height of the bed of solids standing above the orifice. However, the influence of bed height is usually negligible when it is higher than several times D_o. This is because friction between particles prevents the transmission of pressure forces. Unlike a liquid where the rate of discharge varies as the square root of the height of liquid standing above the orifice (proportional to the pressure). Also the fluid-flow analogy is only valid to any extent when the particles are fluidized, i.e. when the particles are no longer in contact with each other. It was ascertained in this study that the discharge rate of solid particles under free-flow conditions was independent of bed height with both single-orifice and multi-orifice distributors.

Dimensional analysis yields equations such as that of Jones and Pilpel(114) and Brown and Richards(115):

$$D_o = \frac{1}{m} \left(\frac{4\,W}{60\,\pi \cdot \rho_B \cdot \sqrt{g}}\right)^{0.4} + k \qquad (6.5)$$

which is of the same form as

$$D_o = A \left(\frac{4\,W}{60\,\pi\,\rho_B \cdot \sqrt{g}}\right)^{1/n} , \qquad (6.6)$$

where A, m, n and k are all functions of particle size and shape.

The most satisfactory theoretical study of the problem has been that of Brown and Richards(115) who considered the variation of the total (potential + kinetic) energy of a granule as it approached the orifice. Their treatment of the problem postulated radial flow and a progressive decrease of the total energy of a moving column in a "stream tube" approaching the orifice. This led to the minimum energy equation

at $R = R_m = \frac{D_o - k}{2 \sin \alpha}$:

$$\frac{d}{dR} (PE + KE) = 0 \qquad (6.7)$$

Where R is the radius of surface of minimum energy and α is the angle of approach (included $\frac{1}{2}$ angle of flow of channel). By neglecting any change in the bulk density of the granule-fluid mixture, they were able to show that the discharge rate could be expressed as:

$$\frac{4 W}{\pi \rho_B . \sqrt{g} . (D_o - k)^{2.5}} = \frac{1 - \cos\alpha}{\sqrt{2} \sin^{1.5}\alpha} \qquad (6.8)$$

Thus, the above theory shows that the flow through a circular orifice of diameter D_o is also represented by an equation of the form:

$$W = \text{constant} \times f(\alpha) . \rho_B . (D_o - k)^{2.5} \qquad (6.9)$$

Flow rates computed from (6.8) have been shown to be remarkably accurate if the particles are coarse and in practice the only difficulty encountered concerns the value of the angle α, if a non-mass flow hopper is used(116).

As the particle size decreases, however, flow rates computed from Brown and Richards' approach invariably exceed the experimental values, as noted by Miles et al.(116). By considering kinetic and potential energies Brown and Richards have examined the role of inertial and gravitational forces and, in the case of coarse particles, the success of their equation would suggest that these forces dominate when the particle diameter is large. In general terms, the effects which are neglected in the analysis may be described as fluid drag forces and interparticle forces.

Holland et al.(117) have studied the effects of fluid drag on the discharge of particles from orifices. They showed that fluid drag forces become significant as the particle diameter is reduced. These forces act

against the gravitational forces and thus retard the flow. Miles et al. (116) also carried out similar studies and found that fluid drag effects are associated with a negative pressure gradient in the orifice region and this pressure gradient is responsible for the lower discharge rates obtained with fine particles.

The above analyses refer to flows through single orifices only. From the distributor point of view it would be relevant to have a flow equation that could be equally applied to a single orifice and a multiplicity of adjacent orifices (i.e. a multi-orifice plate). The free flowback of particles through multi-orifice plates has not been studied before and it is not known whether the presence of neighbouring orifices would cause the flow from an orifice to be different from that in isolation.

In the present work, therefore, a study has been made of the flow behaviour of both single and multi-orifice plates using a variety of solids. One objective has been to derive an equation which can be used to predict the flow rate through multi-orifice distributor plates.

6.3.1 Formulation of the Proposed Equation

General consideration and analysis of experimental data published on the gravity flow of solids through circular orifices suggests that the rate W of free flowback of solid particles through multi-orifice distributor plates can be expressed as:

$$W = f(\rho_B, D_o, N, g) \quad , \tag{6.10}$$

where

D_o = orifice diameter,

g = acceleration due to gravity,

N = number of orifices on distributor,

ρ_B = bulk density of solids.

Equation (6.10) contains four dimensional quantities and three principal dimensions; by the similarity theory, the number of dimensionless groups determining the given effect is 4 - 3 = 1. If ρ_B, D_o, and g are chosen as the principal quantities, equation (6.10) may be written as

$$\frac{W^a}{\rho_B^b \cdot D_o^c \cdot g^d} = f(N) \tag{6.11}$$

where the left-hand side is the required dimensionless group.

Dimensional analysis gave the following values for the indicies:

$a = 1$, $b = 1$, $d = 0.5$, $c = 2.5$.

Therefore,

$$\frac{W}{\rho_B \cdot D_o^2 \cdot \sqrt{g\, D_o}} = f(N) \tag{6.12}$$

or

$$W = K \cdot \rho_B \cdot D_o^2 \cdot N \cdot \sqrt{g\, D_o} \tag{6.13}$$

where K is a constant.

But we have $N.D_o^2 = \frac{4}{\pi} . A_o$, where A_o is the total orifice area on the distributor, therefore

$$W = K. \rho_B. A_o. \sqrt{g D_o} \qquad (6.14)$$

6.3.2 Effective Orifice Area

As pointed out by previous investigators, the effective diameter of the orifice is less than the actual orifice diameter D_o, because of the existence of an empty annulus just inside the orifice where no particles pass or where the concentration of particles is low. Analogous to the expression of Beverloo et al.(112) for the flow through circular orifices:

$$W = K_1. \rho_B. A_e. \sqrt{g(D_o - \beta D_p)} \quad , \quad \beta \geqslant 1 \qquad (6.15)$$

Where $A_e = \frac{\pi}{4}.(D_o - \beta D_p)^2. N$ (the total effective area of orifices on the distributor) and β is an empirical coefficient. Brown and Richards (115) found that β is independent of the orifice size and flow rate, varies with the particle size and other solid properties. Beverloo et al. (112) found $\beta = 1.4$ for spherical particles. In the present work β was determined from experiments with solids having different size and shape and found to be approximately constant (i.e. $\beta \sim 1.42$).

6.4 Equipment and Experimental Procedure

6.4.1 Single-Orifice Experiments

These were carried out in a cylindrical column made of Perspex, having inside diameter of 10 cm. and 50 cm high, fitted with a base plate of Perspex. This held a shutter and a sliding aluminium plate, 1/8" thick, into which had been accurately drilled seven smooth orifices with diameters D_o of 0.238, 0.3175, 0.4762, 0.635, 0.873, 1.1112 and 1.27 cm.

The solids used are specified in Table (2.3) (Chapter 2). These were sand fractions, glass beads, cracking catalyst, Diakon and Coal. All these materials are closely graded and may be regarded as monodispersed particles.

Experimental procedure was as follows: known weights of particles were placed in the column so as to give static beds of various heights. The flow rates W in gm/min. were determined three times by collecting the material that discharged through the orifice during a definite time, after the flow had become steady, and weighing the quantity collected.

6.4.2 Multi-Orifice Experiments

For an investigation of the gravity flow of solids through multi-orifice distributor plates use was made of two cylindrical columns originally designed for the study of flowback under fluidized conditions. One column was made of standard Q.V.F. glass, having inside diameter of 7.9 cm. and 60 cm. high. It was connected at the base to a conical inlet, also made from Q.V.F. and had the same diameter as the column. The second column used in the experiments was identical to that described in Chapter 3 or 4 (i.e. a Perspex tube of 14 cm. diameter and approximately 100 cm. high). The multi-orifice distributors were made of 1/8" thick aluminium plates, with orifices drilled either on a square-pitch or on a triangular-pitch array depending upon the number of orifices.

The number of orifices drilled on a particular plate was varied between 2 to 14 according to the orifice size (see Tables (6.4) - (6.8)). Preliminary experiments showed that orifices had to be drilled within 0.8D diameter circle in order to eliminate the wall effects, where D is the bed diameter.

The experimental procedure was essentially the same as that with single-orifice experiments. However, loading the column and starting up the experiments required a more laborious procedure owing to the difficulty of preventing the bed from discharging into the wind box while solids were being added. A typical run was, therefore, started as follows: before introducing solids into the column, the discharge exit E (see Figure (6.1)) of the wind box was closed with a tightly fitting rubber stopper S. Then a gentle current of air of about 9 $cm.^3$/ sec., regulated via needle valve V, was passed upwards through the distributor. With this air flow, solids discharge was effectively prevented without fluidizing the bed. As shown in Figure (6.1), the column was filled from a Hopper H through a glass standpipe of 2 cm. diameter. Preliminary experiments showed that the height of the bed had no influence on the flow rate W. Therefore, the bed height selected for the study was maintained within 50 - 60 cm. The flow rate W (gm/ min.) was measured shortly after closing the air valve and removing the rubber bung. The measurements were repeated at least three times to be sure of the repeatability of the results.

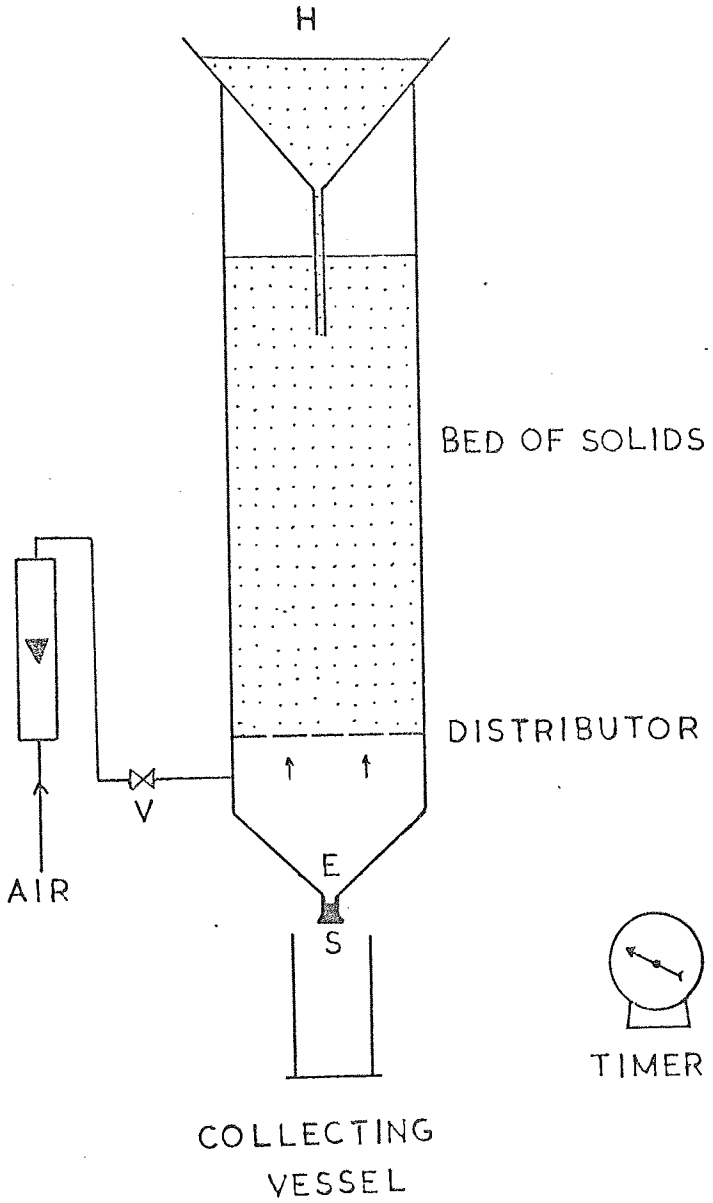
H
BED OF SOLIDS
DISTRIBUTOR
V
AIR
E
S
TIMER
COLLECTING
VESSEL

FIG. 6·1

6.5 Experimental Results and Discussion

The experimental results obtained from the single-orifice studies are presented in Tables (6.1) - (6.3), and as plots of W (flow rate) vs. D_o^2 (square of the orifice diameter) on a log scale in Figures (6.2) - (6.3). The flow rates obtained with multi-orifice plates can be found in Tables (6.4) - (6.8), these will be dealt with later. The examples given in Table (6.1) may be demonstrative for the repeatability of the results. From Table (6.2) it appears that the bed height, within the range investigated (H = 10 - 30 cm. for a single-orifice flow), has no influence on the flow rate W, and therefore is in agreement with those of earlier workers.

In agreement with previous investigations it is found that W plotted on a log-log scale as a function of the square of the orifice diameter D_o^2 gives straight lines.

A dimensional analysis (refer to equation (6.14)) suggests that for a given orifice, W should be proportional to $\rho_B . \sqrt{g} . D_o^{2.5}$. However, the plots shown in Figures (6.2) - (6.3) give exponents of D_o greater than 2.5, viz:

glass beads	W	α	$D_o^{3.36}$
sand	W	α	$D_o^{3.35}$
Diakon	W	α	$D_o^{3.32}$
coal	W	α	$D_o^{3.28}$
cracking catalyst	W	α	$D_o^{3.0}$

This clearly indicates the existence of a zone, around the edge of the orifice, empty of solids. This zone is useless or less fit for use for flow. Its size varies with particle size but is independent of the orifice diameter, so that the equation $W = K_1 \rho_B . \sqrt{g} . (D_o - \beta D_p)^{2.5}$ is valid.

However, it may not be valid for fine particles where the drag forces are significant compared with the inertial and gravitational forces. As can be seen from above, the catalyst has, in fact, exhibited a flow rate lower than that of the other solids. This discrepancy is believed to be due to the effects of fluid drag forces which become significant as the particle size is decreased. The particle size of both grades of catalyst used in the experiments is small in comparison with other solids, but the most notable difference is their porosity. Cracking catalyst is a porous material with pore volume about 0.68 cm^3./gm., whereas other solids are non-porous. It is not known whether its porosity has anything to do with the drag forces. In this work no attempts have been made to investigate the effect of fluid drag on the flow rate, since it required a separate study. Miles et al.(116) have discussed the effect qualitatively; a quantitative treatment has just been published recently by Holland et al.(117). However, visual observations with catalyst revealed some interesting features:

1. When a batch of catalyst particles was placed in the column, the bed immediately became full with air and had the property of a semi-fluidized bed. Unlike the other solids, a metal rod met no resistance when it was pushed down the bed (reminding of a quicksand).

2. A periodically varying flow rate and intermittent break-up of the column of discharging catalyst from the orifice. This has been observed particularly with larger orifices, but subsided with smaller orifices. It was believed to be due to the effects of fluid drag which, according to Miles et al.(116), were associated with negative pressure gradient in the region close to the orifice. Fluid tended to flow into the bed and this probably was responsible for the break-up of the column of discharging particles. For larger orifices the area available was sufficient for simultaneous discharge of solids and counterflow of air.

6.5.1 Determination of the Coefficient β

Consider the equation $W \alpha \rho_B . \sqrt{g} . (D_o - \beta D_p)^{2.5}$ for the flow through a single orifice, then by plotting D_o vs. $W^{0.4}$ the value of β can be determined from the intercept. In Figure (6.4) are shown plots of D_o vs. $W^{0.4}$, whose intercepts $\beta . D_p$, on the ordinate have been used to calculate β . For the catalyst, however, β has been determined by plotting D_o vs. $W^{0.5}$. The reason for this can be seen from Figure (6.5). Contrary to the indications of dimensional analysis we found that D_o plotted against $W^{0.4}$ on a log scale yields a straight line with slope of 1.25, whereas a plot of D_o vs. $W^{0.5}$ yields a straight line with slope of 1.0. This suggests that the flow of cracking catalyst through a circular orifice of diameter D_o would follow the relationship,

$$W = K_2 . \rho_B . \sqrt{g} . (D_o - \beta . D_p)^2 \quad , \tag{6.16}$$

rather than that derived by dimensional analysis. (This behaviour might be associated with absence of a 'breaking arch' as might be expected from the quicksand-like characteristics.)

Applying this result to a multi-orifice plate system, we have

$$W = K_2 . \rho_B . N . \sqrt{g} . (D_o - \beta . D_p)^2 \tag{6.17}$$

or

$$W = K_3 . \rho_B . A_e . \sqrt{g} \tag{6.18}$$

The values of β determined from Figure (6.4) are as follows

glass beads	$\beta = 1.443$
sand	$\beta = 1.407$
Diakon	$\beta = 1.423$
coal	$\beta = 1.410$
cracking catalyst	$\beta = 1.408$

For all the solids examined we can therefore assume for β an average value of 1.42.

It appears, therefore, from these results that the drag forces which are considered to be of influence on the flow of catalyst have no effect on the coefficient β.

6.5.2 Flow Through Multi-Orifice Distributor Plates

A large number of observations were made on the gravity flow of solid particles through multi-orifice plates. For a particular solid, the flow was directly proportional to the number of orifices N on the distributor. The same was found with all solids investigated and the complete results are presented in Tables (6.4) - (6.8). Suffice, therefore, to give one example, viz of Diakon (see Figure (6.6)). It can be seen that with orifices of the same diameter, the flow increases linearly with N, i.e. in accord with equation (6.17). An interesting feature of the results is also apparent from Figure (6.6). This shows that orifices were discharging solids at equal rates, thus confirming that there was little or no interference between adjacent orifices. It is evident, therefore, that the flow rate obtained from a single-orifice plate can be used directly to predict the flow through an array of orifices.

The results obtained from multi-orifice plates have been finally correlated as shown in Figure (6.7). Results from single-orifice studies are also included in the correlations.

As shown in Figure (6.7), two sets of results have been correlated individually: (i) by plotting W vs. $\rho_B \cdot A_e \cdot \sqrt{g(D_o - 1.42\ D_p)}$ in the way suggested by equation (6.15) for the non-porous (or coarse) particles, and (ii) by means of equation (6.18) as a plot of W vs. $\rho_B . A_e \sqrt{g}$ for the porous (or fine) particles, i.e. the catalyst. In each case a straight line correlation is obtained, and the best lines drawn through

the points are those obtained by method of "least squares". For the latter purpose, a computer library subroutine available from the University Computing Centre was used. The equations of the best lines are

$$W = 47\ \rho_B .\ A_e .\ \sqrt{g(D_o - 1.42\ D_P)} \mp 5\%\ (gm./min.) \qquad (6.19)$$

$$W = 23\ \rho_B .\ A_e .\ \sqrt{g} \qquad \mp 4\%\ (gm./min.) \qquad (6.20)$$

Where $$A_e = \frac{\pi}{4} .\ (D_o - 1.42\ D_P)^2 .\ N$$

It seems remarkable from the above equations that the particle shape appears to be of no significance. However, the influence of the shape factor finds expressions more or less in the values of both ρ_B and D_P, so that it is admissible to drop the shape factor.

A comparison of our equation $W = 47\ \rho_B .\ A_e .\ \sqrt{g \cdot (D_o - 1.42\ D_P)}$ with that inferred by Beverloo et al.(112)(i.e. $W = 45\ \rho_B . A_e \sqrt{g.(D_o - 1.42 D_P)}$ shows that the two correlations are remarkably close, noting that Beverloo's work was based on large spherical particles (i.e. a number of seeds) with ρ_B about 0.7. From this we may conclude that our correlation can be used to predict the free flowback of coarse particles and is equally valid for both single and multi-orifice systems.

Unfortunately, the second correlation has been derived from results obtained with cracking catalyst only where the influence of fluid drag is believed to be significant. Therefore it is hoped that future research in this field may add further support to the correlation.

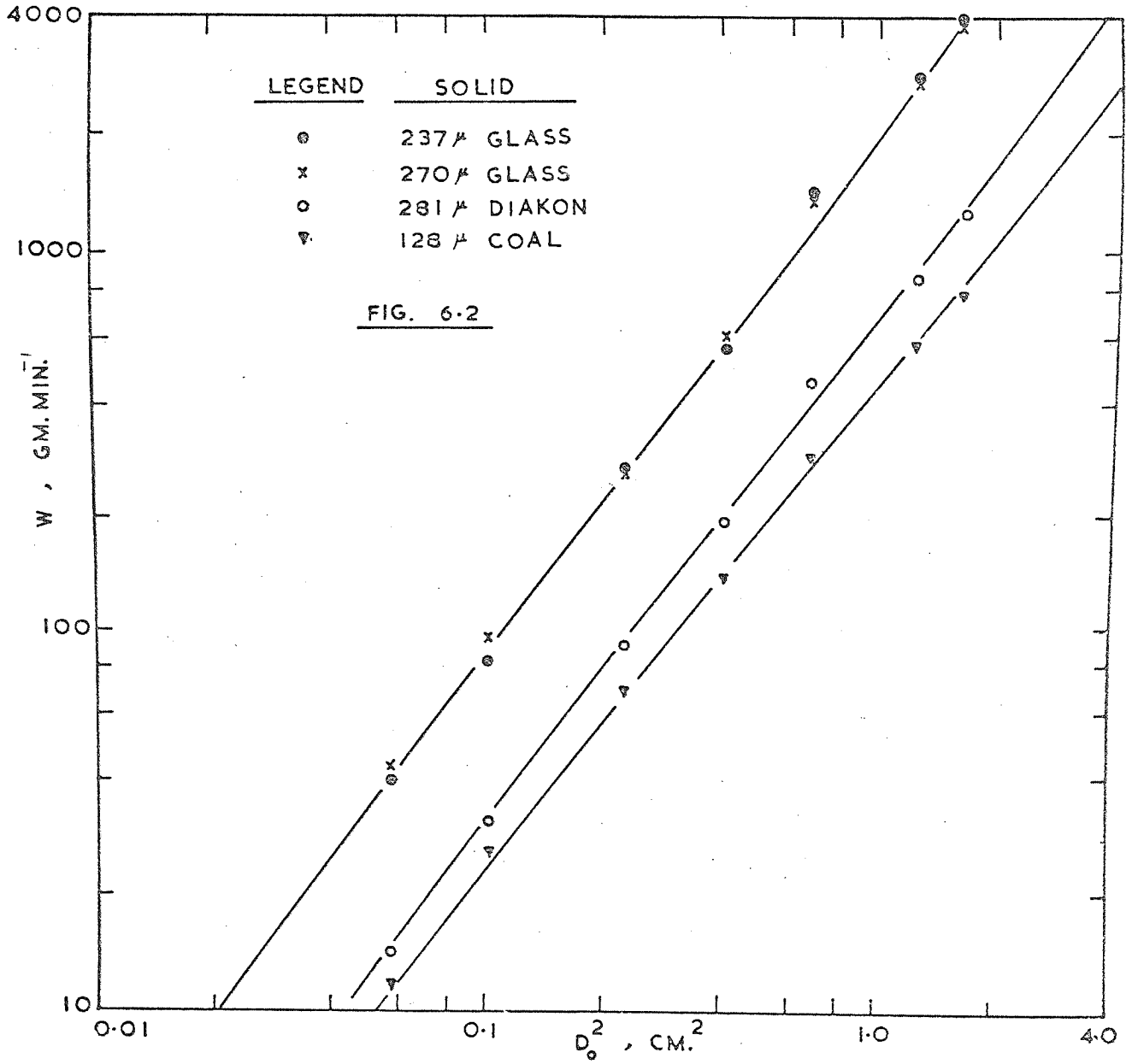
4000
1000
100
10
W , GM. MIN.$^{-1}$
0·01
0·1
1·0
4·0
D_o^2 , CM.^{2}
LEGEND
SOLID
237 μ GLASS
270 μ GLASS
281 μ DIAKON
128 μ COAL

FIG. 6·2

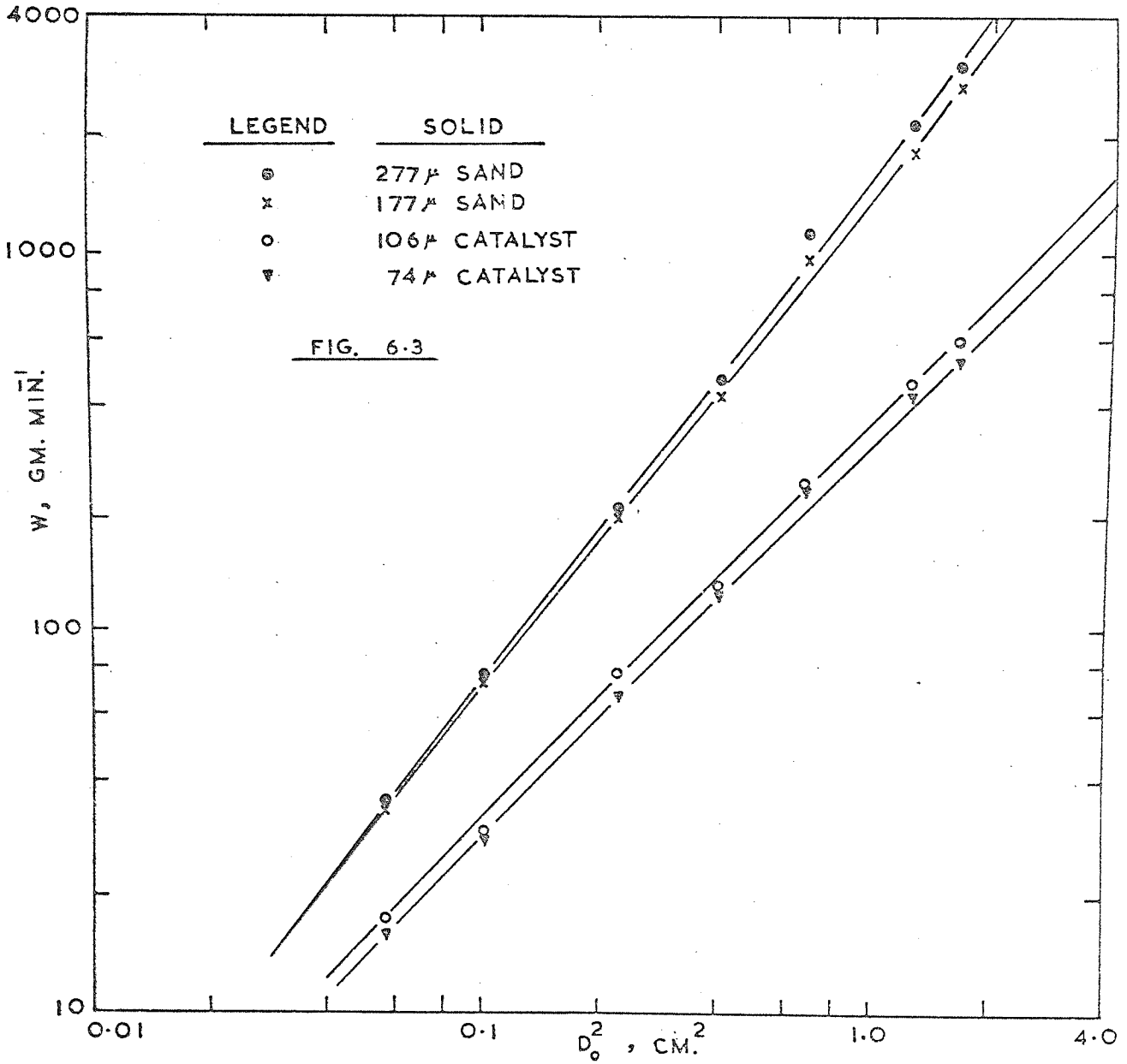
4000
1000
100
10
0·01
0·1
1·0
4·0
W, GM. MIN.⁻¹
D_o^2, CM.²
LEGEND
SOLID
277μ SAND
177μ SAND
106μ CATALYST
74μ CATALYST

FIG. 6·3

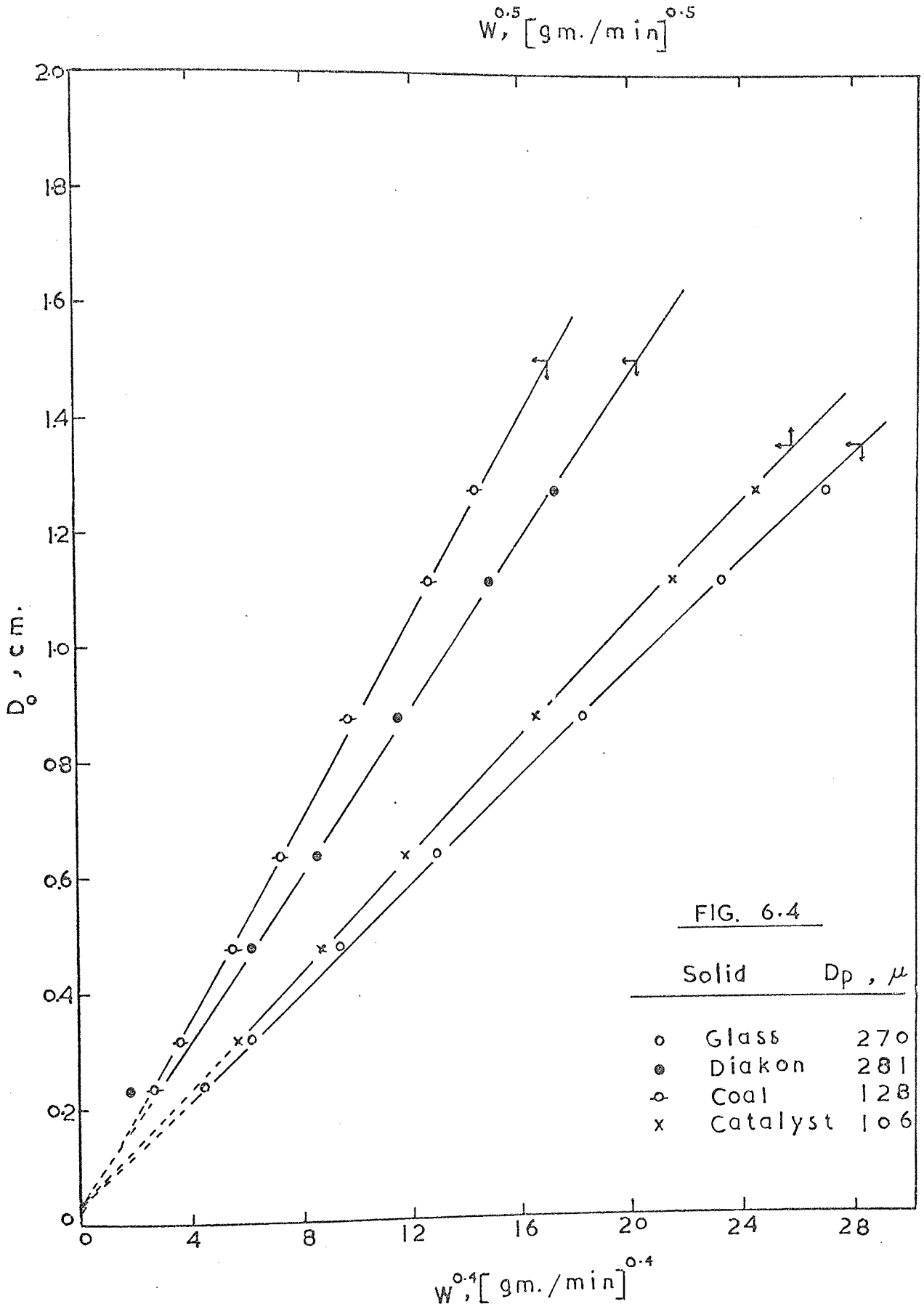
W, 0.5 [gm./min] 0.5
2.0
1.8
1.6
1.4
1.2
1.0
0.8
0.6
0.4
0.2
0
D°, c.m.
0
4
8
12
16
20
24
28
W 0.4 [gm./min] 0.4
Solid
Dp, μ
o Glass 270
Diakon 281
Coal 128
x Catalyst 106

FIG. 6.4

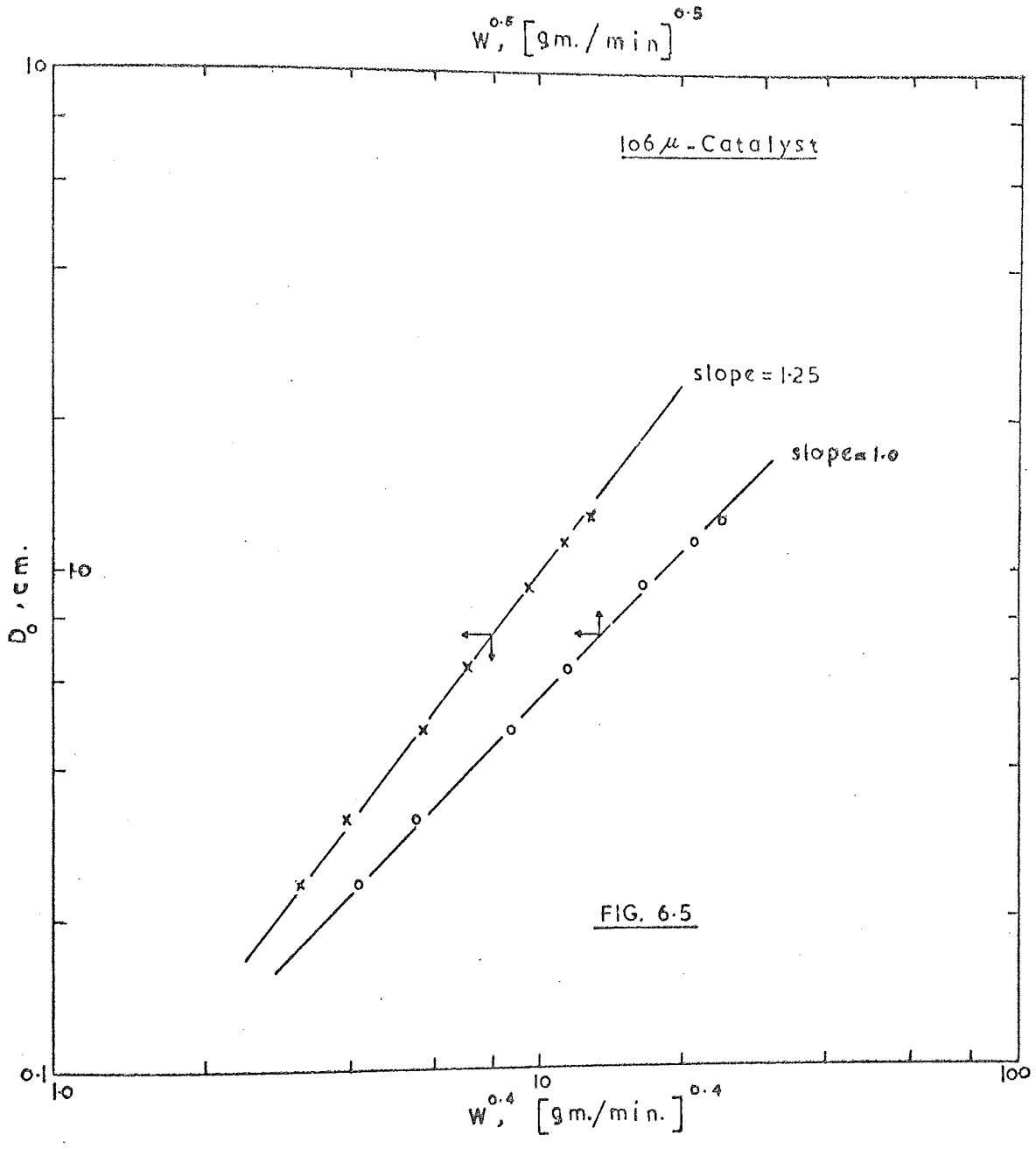
$W_1^{0.5}$ [gm./min]$^{0.5}$
10
106 μ - Catalyst
slope = 1·25
slope = 1·0
D_0, c.m.
1·0
0·1
1·0
10
100
$W_1^{0.4}$ [gm./min.]$^{0.4}$

FIG. 6·5

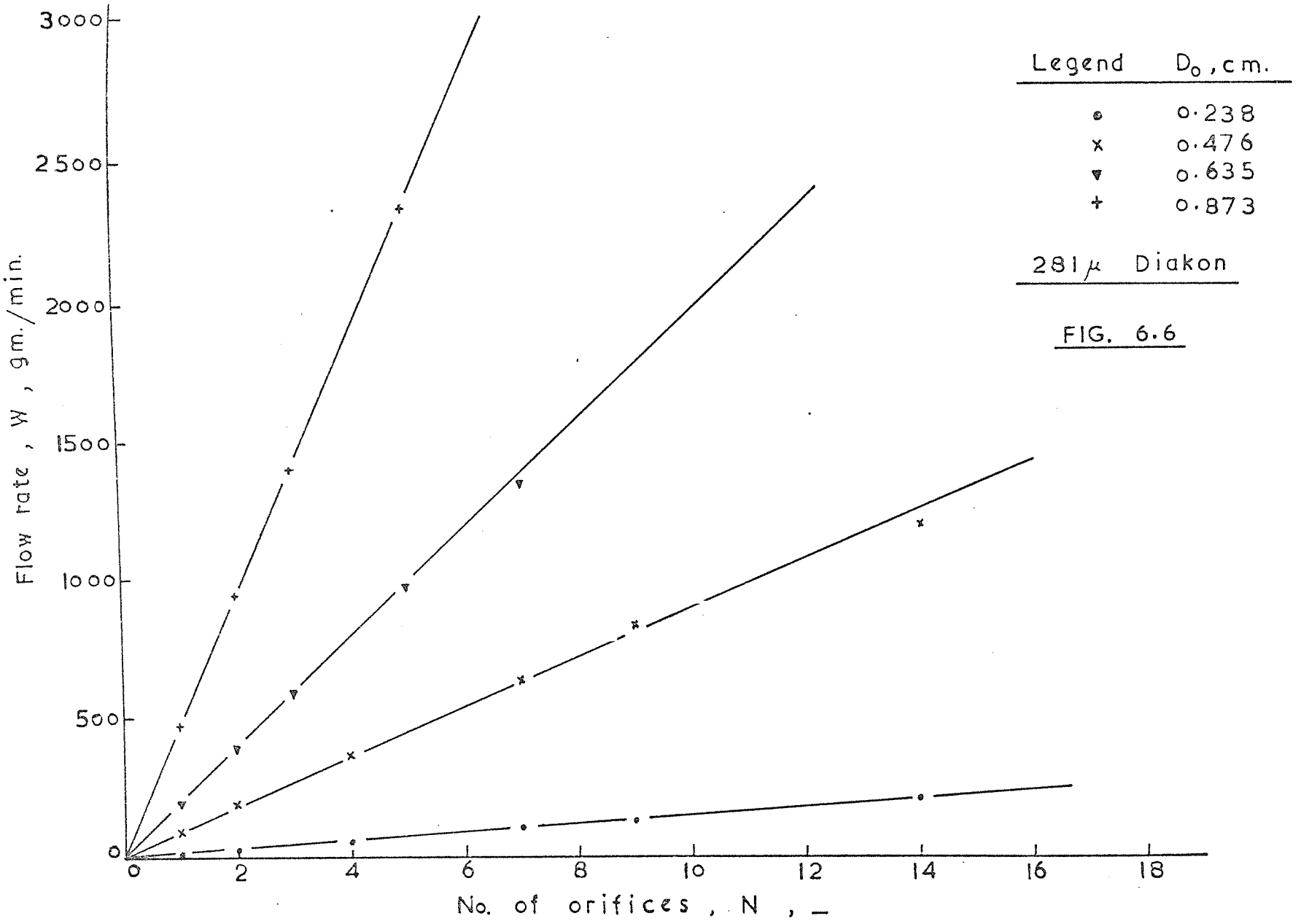

Legend	D_o, cm.
•	0.238
×	0.476
▼	0.635
+	0.873

281 μ Diakon

FIG. 6.6

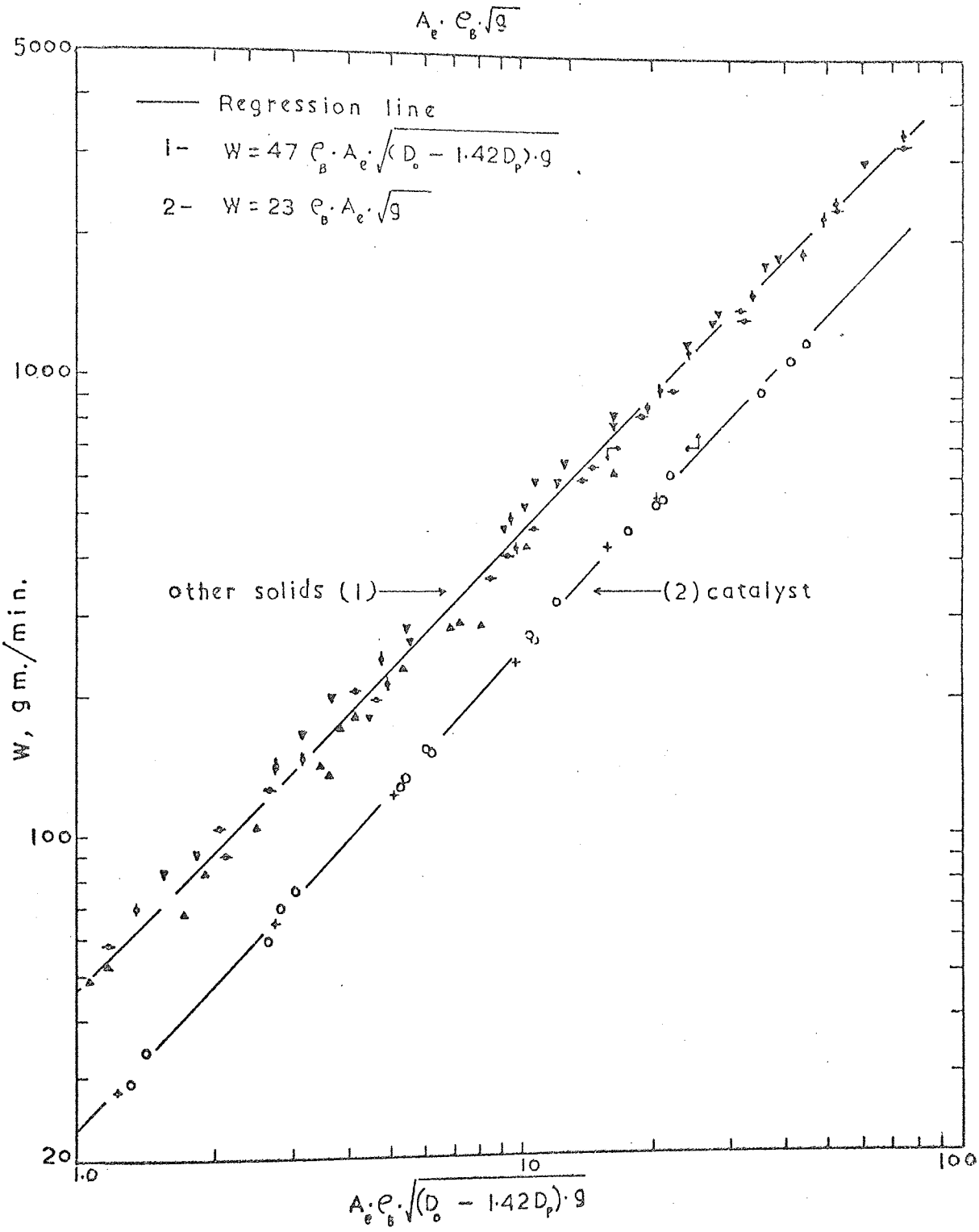

Fig. 6·7 Gravity Flow Through Multi-orifice Distributors

6.6 Flowback of Solids Through the Distributor Under Fluidized Bed Conditions

The objective of the following work is to obtain more extensive data on flowback of particles in gas fluidized beds and in particular to determine the conditions under which flowback of solids is completely excluded.

In this work, the flowback of solids through single and multi-orifice distributor plates has been investigated in two-dimensional and cylindrical beds of solids fluidized with air. Single and multi-nozzle distributors have also been included in the study. The two-dimensional bed has been used mainly for the experiments with single-orifice plates. The initial objective was to obtain visual observations of the flowback behaviour of the orifice. However, some experiments have also been conducted in the cylindrical column so that a comparison with the two-dimensional column can be made.

6.7 Equipment and Experimental Procedure

6.7.1 The Cylindrical Beds

Two cylindrical columns were employed in the experiments:

1. A 7.9 cm. diameter Q.V.F. glass column and about 80 cm. high was used in most of the experiments involving multi-orifice and multi-nozzle distributors. This was connected at the base to a conical inlet (wind box) also made of Q.V.F. glass and had the same diameter as the column. Between the wind box and the column, the metal distributor was tightly bolted with the steel flanges. Above the column was an expansion section about 14 cm. diameter to minimize particle entrainment. Pressure tappings consisted of three holes at 120 deg. to each other were drilled on the glass walls below the distributor. Short pieces of 3/32" I.D. stainless

steel tubing were glued into each of these tappings and then covered with a patch of 350 mesh stainless steel gauze to prevent particles entering the tappings. These tappings enabled the wind box pressure to be determined. The wind box volume was approximately $2 \times 10^3 cm^3$.

It is to be noted that use of this column has already been made in the previous section with experiments concerning the free flowback of solids across multi-orifice distributors. Figure (6.8) shows a schematic illustration of the present arrangement of the column.

As shown in Figure (6.8), particles falling back through the distributor were continuously collected from the bottom of the wind box in a detachable vessel. With this arrangement, it was possible to make several samplings within a run without the likelihood of the wind box pressure altering.

2. The second cylindrical bed used in the experiments was a Perspex tube 14 cm. diameter and 120 cm. high This was, in fact, the same column used in the experiments of Chapters 3 and 4, but they differed only in their respective heights. Here, for example, a taller column was used in order to obtain enough disengaging height.

This column was used to supplement studies made with the two-dimensional bed. This enabled the use of bigger distributor loadings, i.e. it was possible to investigate beds as high as 110 cm.

Unsieved cracking catalyst (size range 20 - 150 μ) was the only material available in bulk quantities and suitable for this type of study. When this was fluidized, its fine particles formed a cloud of dust which discharged from the top of the column and created problems in the laboratory.

These undesirable conditions were overcome by connecting two Q.V.F. cyclones (meant for vapour separation) in series with the top exit of the column. Then, by fluidizing the catalyst for about 1/2 hour at

10 - 15 cm./sec. air superficial velocity, most of the dust was allowed to be carried away by the cyclones. Because the catalyst then lost some of its original volume, its size distribution in the experiments was somewhat different from the one specified in Appendix A2. However, the amount of catalyst lost was very small relative to that in the column. Therefore, no size distribution determination of the treated material was made.

Particles falling back through the distributor plate were collected at the bottom of the wind box as with the smaller diameter column.

Figure (6.8) also shows a schematic diagram of the arrangement of the column described above.

6.7.2 The Two-Dimensional Bed

This was identical to that already used in the investigation of defluidized zones (Chapter 5). It was used primarily for the experiments with single-orifice plates. No expansion section was installed, but a nylon filter cloth was clamped on the top cross-section of the column to prevent particle entrainment which was apparent only with unsieved cracking catalyst.

6.7.3 The Distributors

A large number of multi-orifice and multi-nozzle distributor plates were used in the experiments. Table (6.9) gives details of the various distributors (including single-orifice and single-nozzle plates) used. The multi-orifice distributors were made from aluminium plates with orifices arranged on either a triangular-pitch or a square-pitch array. The centre-to-centre orifice spacing and orifice diameter were variables.

By stopping up orifices with Plasticine, the number of open orifices

on a particular plate could be reduced as desired. This, of course, entailed a change in the orifice spacing and the relative free area. thus a variety of distributor geometries was obtained. Some plates had orifices positioned at the same diameter to pitch ratio, thus keeping the plate free area constant for plates with different sizes of orifices.

The values of the relative free area ϕ used in the experiments were between 0.5 - 5%. These values of ϕ spanned the range used in industrial distributors. The plate thickness was varied between 0.082 cm. (32 Thou) and 1.27 cm. It was felt that with higher plate thicknesses the orifices drilled were not smooth, particularly with small orifice diameters. Consequently, multi-nozzle distributor plates equipped with cylindrical nozzles were introduced to overcome the above difficulties as well as to obtain deeper orifices. These were built by fitting stainless tubes into the orifices of a 1/8" thick aluminium plates, for example a 1/4" outside diameter nozzle was inserted into a 1/4" diameter orifice. The length of the nozzles was varied between 2 cm. and 18 cm. For single-nozzle experiments, the length was varied between 1.3 am. and 10 cm.

6.7.4 The Secondary Distributors

In single-orifice experiments secondary air distributors had to be used to keep the bed well fluidized. Views of these distributors are shown in Figure (6.9). In the two-dimensional bed, two manifolds were placed on each side of the orifice. In the cylindrical bed (14 cm. diameter), an annular distributor was designed to rest on a single-orifice distributor plate. The annular distributor was made from two interconnected circles of 1.27 cm. outside diameter copper tubing having 16 x 1 mm diameter equally spaced orifices drilled on the underside to prevent blockages with particles.

6.7.5 Varying the Wind Box Volume

In order to investigate the effect of the wind box volume on solids flowback a 30.5 cm. (12") Q.V.F. glass column was built in sections. These consisted of a conical (or bottom) section and three lengths of pipe sections, each 30.5 cm.(12") long. When these were assembled together, a wind box volume approximately 86.1 x 10^3 cm^3 was obtained. By mounting the fluidized bed at different levels in the column (see Figure (6.10)), four wind box volumes could be obtained as follows:

Wind Box			Volume, $cm.^3$
$V_{\omega 1}$	=	conical section alone	19.2 x 10^3
$V_{\omega 2}$	=	$V_{\omega 1}$ + a 12" long pipe section	41.5 x 10^3
$V_{\omega 3}$	=	$V_{\omega 2}$ + a 12" long pipe section	63.8 x 10^3
$V_{\omega 4}$	=	$V_{\omega 3}$ + a 12" long pipe section	86.1 x 10^3

The wind box volume may be defined as the volume between the distributor and that first point in the fluidizing gas supply stream where there is a very large pressure drop. In our work, this point occurs at the needle valve placed normally before the wind box.

6.7.6 The Fluidizing Gas

The fluidizing gas was air taken from an 80 p.s.i.g. main, reduced to 20 p.s.i.g. via a pressure reducing valve and fed into an inlet manifold which supplied a bank of variable area flow meters. The outlet manifold was connected via a valve to the wind box of the fluidized bed under study. The flow meters were a range of calibrated metric type rotameters, two of which were of the precision type and suitable for small flow rates. With this set of rotameters it was possible to meter flows between 0.6 - 200 litre/min.(rotameters for metering flows up to 360 litre/min. were also used, but only with

experiments concerning the flow through distributors with long nozzles). The flow to each flowmeter was finely controlled by its own needle valve which also served to isolate any meter not in use.

In the single-orifice experiments, the secondary distributor was fed separately from a small compressor capable of delivering about 70 litre/min. This was intended to avoid interaction between the primary and secondary air flows. The air pressure from the compressor was regulated by a Negretti and Zambra controller which damped out all noticeable fluctuations in the flow. After the controller there was a variable bleed to atmosphere and then a mercury manometer, then came the secondary distributor.

In the determination of the limiting gas velocity at which solids ceased entirely to fall through the orifices, as well as air three additional gases were used. These were compressed carbon dioxide, helium and Arcton 12 ($CC\ell_2F_2$) supplied from high pressure cylinders. The rotameters used to meter the flow of these gases were calibrated according to procedure stated in the manufacturer's manual. The calibration procedure along with the calibration charts can be found in Appendix A6.

Figures (6.11) - (6.13) are photographs showing the general arrangement of the experimental equipment including some of the different distributors used.

6.8 Particles

6.8.1 Required Particle Properties

Shape: Orifices are more liable to blockage with sharp particles than with rounded particles. In general irregularly shaped particles are less free-flowing and less fluidizable than rounded particles. Therefore rounded or spherical particles were preferred for ease of fluidization and correlation.

Size: The particle size is normally chosen according to the size of the orifice. It is recommended(31) that the orifice size should be at least ten times greater than the mean particle diameter, if blockage is to be avoided. In our experiments, the distributors had orifices at least an order of magnitude larger than the mean particle diameter of any of the solids used. Thus blockage was effectively eliminated. Preliminary experiments showed that build-up of static charges in the bed increased with increasing particle size. Thus from this point of view smaller particles were also preferred.

Uniformity of Size: It is inevitable that solids with wide size range tend to segregate on fluidization. Consequently, particles falling through the distributor plate may not be representative of those actually in the bed. Therefore, it was necessary to work with as small a size range of particles as possible, in the attempt to reduce to a minimum the error in measuring flowback.

Density: Materials with a low density were preferred due to the fact that these would require lower gas rates than high density particles for exploring the entire range of fluidizing velocities. Also, pressure drop limitations in the system would not allow the use of high gas rates and from this point of view dense particles were not preferred.

Electrical Properties: In this particular study, static charges are very undesirable. The build-up of static electricity in the bed encourages segregation and can result in blockage of the distributor orifices. The humidification of the fluidizing gas does not solve the problem entirely, but nevertheless, it can reduce static effects to a certain extent as observed with experiments of Chapters 3 and 5. Therefore, in using non-conducting particles those of high surface conductivity particles are preferable (i.e. those with low dielectric constant), since they are less likely to give up static charges.

All metallic surfaces were earthed (e.g. steel flanges and distributors) as an extra measure to reduce static effects in the bed.

6.8.2. Choice of Particles

1. Glass Spheres: These were available in small size and close cuts with densities ranging between 2.70 - 2.95 gm./cm^3. The advantage of the small size available and the spherical shape of the particles was outweighed by the ease with which the particles became charged. Consequently, few experiments were carried out with it.

2. Sand: Two types of sand particles were available: silver sand and rounded sand with density about 2.64 gm./cm^3. Silver sand (sharp) was avoided because of the ease with which the orifices became blocked. Previous work(77) in this field also emphasize on the undesirable characteristics of silver sand. Rounded sand showed no tendency to stick or block up the distributor, and therefore experiments were carried out with it.

3. Coal: This was used with size range 75 - 150 μ (mean particle diameter 128 μ), and particle density 1.35 gm./cm^3. Larger particles were also used, but only with experiments concerning the

limiting velocities. The advantage of the low density was outweighed by the irregular shape of the particles. However, with fine coal (128 μ) orifices showed no tendency towards blockage and values of flowback rate were reproducible to within $\mp$ 5%.

4. Cracking Catalyst (Synclyst - 13% Alumina): This was the most attractive material found among all solids tested. Its advantages were that:

(i) Particles had their corners rounded.

(ii) It was easy to sieve, i.e. no sticking or agglomeration.

(iii) It had a low particle density of about 0.90 gm./cm^3.

(iv) Its dielectric constant was low in comparison with other solids, i.e. it exhibited considerably less static effects in the bed in comparison with other solids.

Therefore, due to the characteristics of this material, most of the experiments were carried out with it.

5. Others: Other materials such as diakon (Perspex) and fire brick were also available as low density solids. However, both had disadvantages which made them far from ideal materials for studying flowback.

Details of particles used in the experiments are specified in Table (2.3) (Chapter 2).

6.9 Variables Studied

6.9.1 Operating Variables

From flow meter readings the time average orifice velocity U_o and superficial velocity U (based on bed cross-section) were calculated in cm./sec. at the pressure just above the distributor. As shown in Chapter 3, the pressure immediately above the distributor plate is practically equal to the weight of the bed divided by its cross-sectional area. This, in fact, is equivalent to the distributor loading (gm/cm^2.) which also determined the bed height.

For a given distributor design the settings of these variables determine the flowback of solid particles through the distributor plate. No hysteresis effect was discernible in the flowback curves.

6.9.2 Distributor Design Variables

Other parameters are known to have an effect on flowback. Among the parameters related to design of a distributor plate, the relative free area ϕ , the orifice diameter D_o, the plate thickness or length of the nozzles ℓ , and the orifice spacing S were studied.

The effect of the wind box volume V_ω was also considered.

6.10 Experimental Procedure

6.10.1 Measurement of Flowback

Flowback rates (gm./min.) across the distributor were obtained from the weight of solids collected under the distributor in a given time.

The experimental procedure was [illegible] as follows: a known weight of solid particles was poured into the column, with the air set at a sufficiently high flow rate to prevent particles from falling into the wind box. In the single-orifice experiments, the secondary air was then adjusted to the desired value. The air supply was then reduced to a pre-determined setting and the timer was started after the system had reached its steady state. The steady state conditions in the system were established by making three preliminary measurements of flowback rates at different time intervals and checking for their reproducibility. The actual sampling time was varied between a few minutes and one hour depending on the flowback rate. Particles were continuously collected at the bottom of the wind box in a detachable vessel (see Figure (6.8)). At the end of the run, the collecting vessel was detached without altering the wind box pressure, and weighed. The solids collected were put back into the bed through the charging hopper.

The measurements were repeated at least three times to be sure of the reproducibility of the results. The values of flowback rate were reproducible within less than 10% (usually 5%) for a given setting of the variables.

For a given solid-distributor system, the measurements were repeated for different gas flow rates and bed heights. In most of these experiments the gas flow was varied between the minimum fluidizing velocity U_{mf} and the limiting superficial gas velocity $U\ell$ at which flowback ceased completely.

However, with some solid-distributor systems, it was not possible to reach U_ℓ because of the considerable amount of gas required and the excessive pressure drop imposed by it.

6.10.2 Determination of the Limiting Gas Velocity

Analogous to gas-liquid systems, this may also be defined as the "weep point", or the point at which flowback of particles diminishes.

In a separate study, the limiting gas velocities through multi-orifice distributors were determined as follows: a known weight of particles was put into the bed, with the gas set at a high flow rate to prevent flowback. The gas supply was then reduced gradually until particles just started to fall through the orifices. At this point the gas flow rate was recorded and the superficial velocity corresponding to this flow was the limiting superficial gas velocity U_ℓ. U_ℓ was also approached by gradually increasing the gas supply from a low value. Almost no difference was detected between the two measurements.

The measurements were repeated at least three times to establish their reproducibility. U_ℓ was quite reproducible when measured at decreasing and increasing fluidizing velocities and could be determined to within 2 - 5%.

The same procedure was carried out with different solids and gases using a variety of distributor geometries. A special feature of our experiments should be noted. The bed height exerted no influence on the value of U_ℓ, and consequently all experiments were restricted to the same initial bed height of 40 - 50 cm.

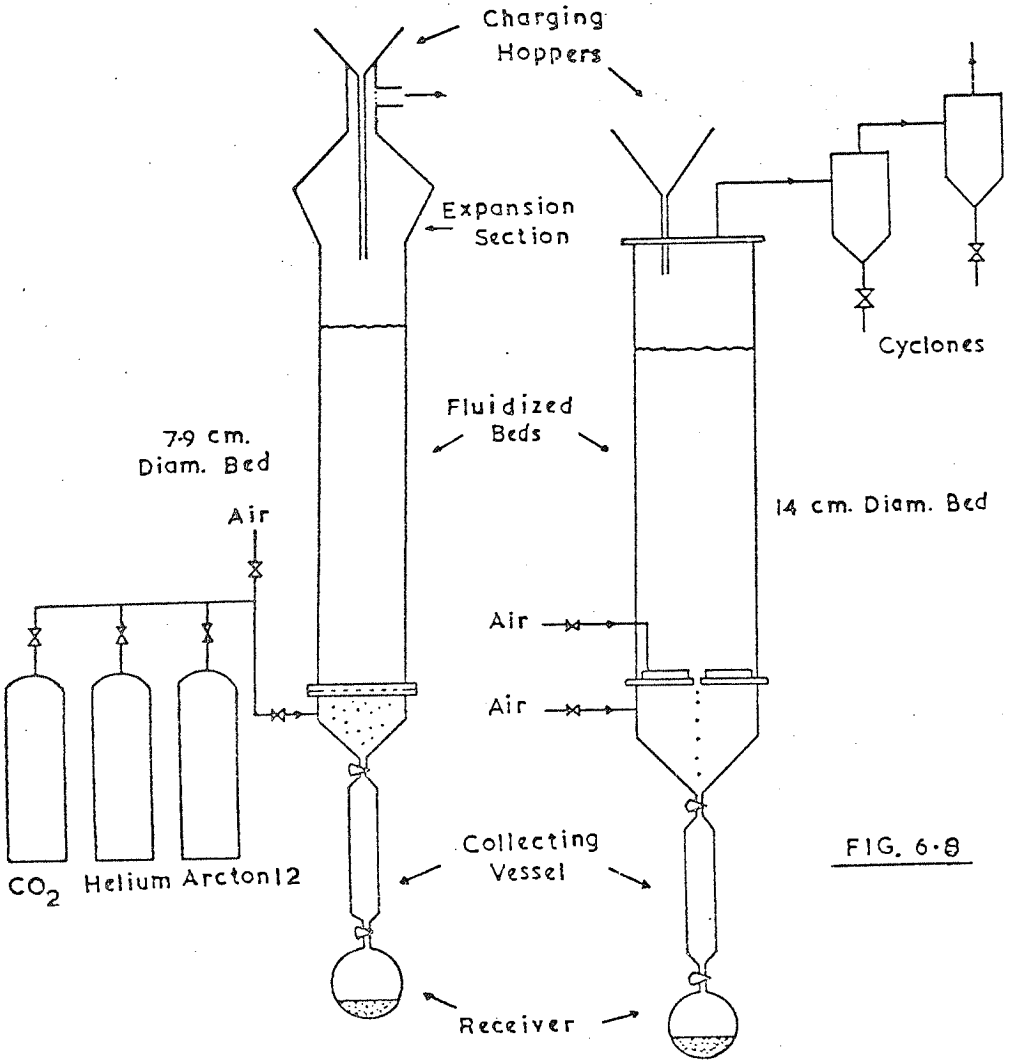

FIG. 6·8

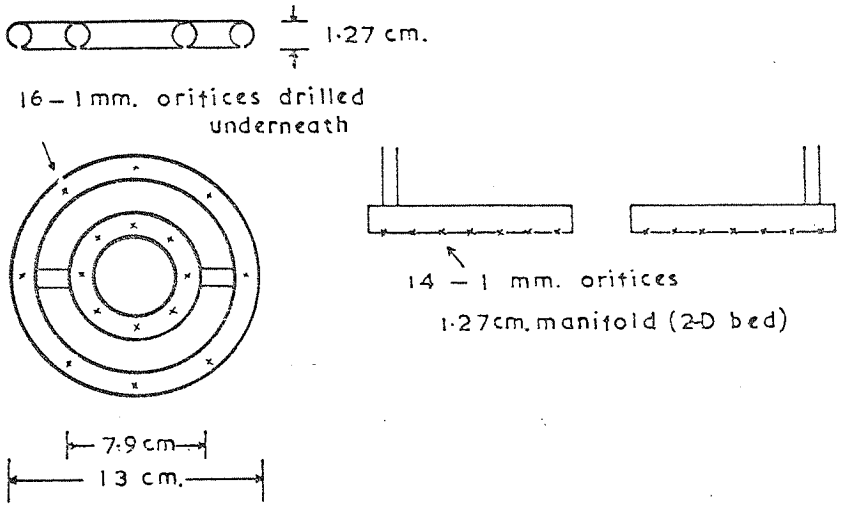

FIG. 6·9 The secondary distributors

II I

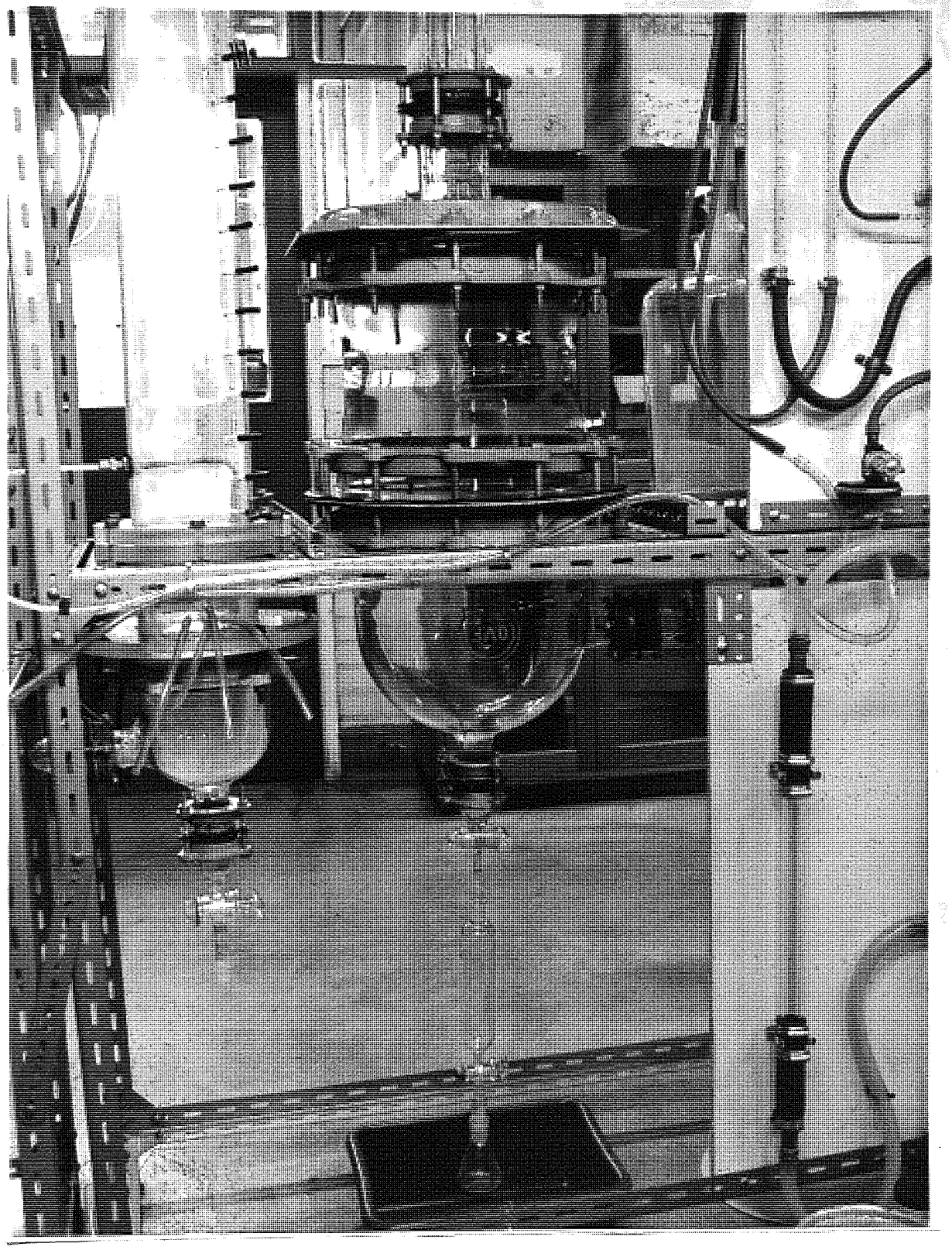

I - FIG. 6.10 7.9 cm. diam. column mounted on 41.5 x 10^3 $cm.^3$ wind box.

II - FIG. 6.11 14 cm. diam. Perspex column.

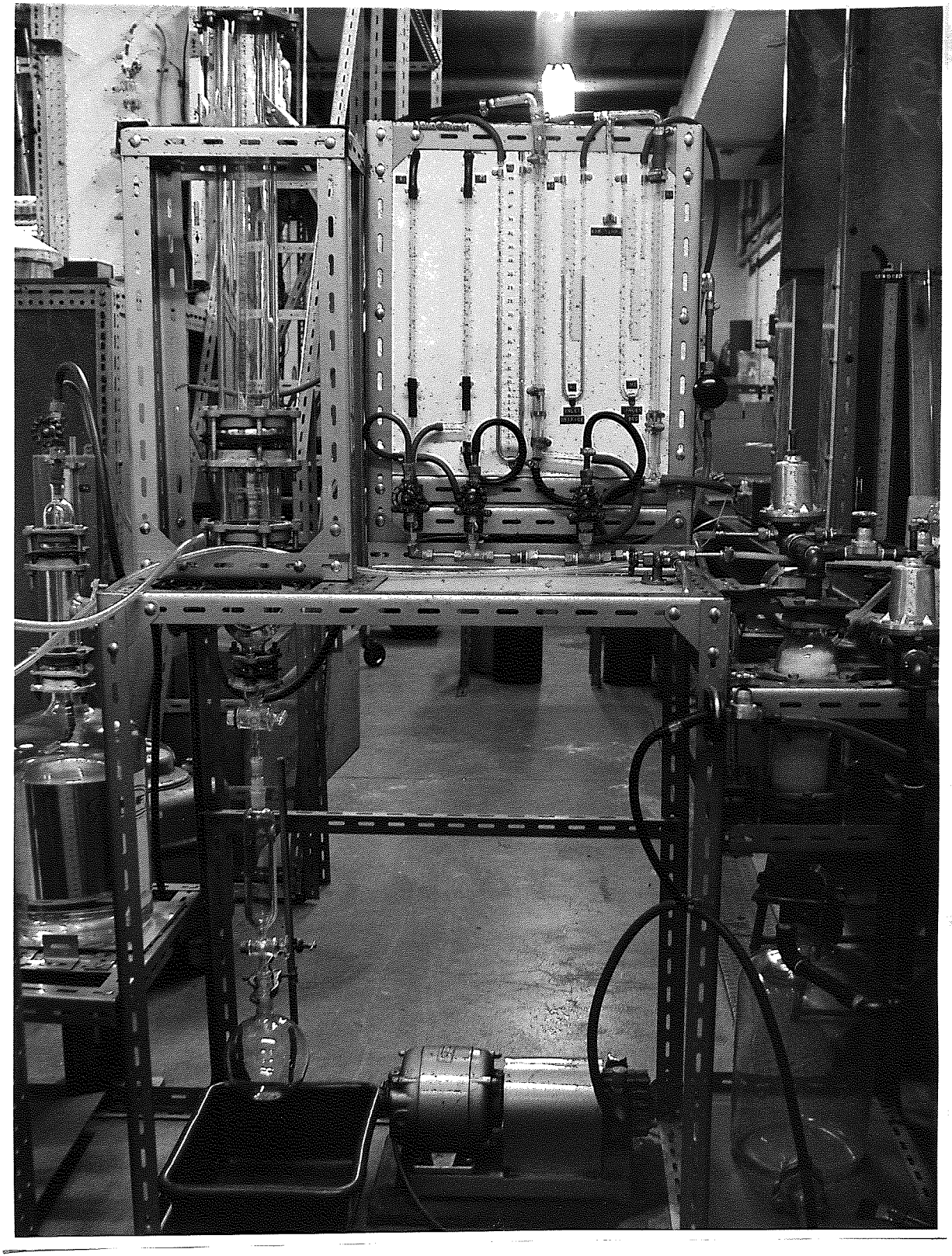

FIG. 6.12 7.9 cm diameter Q.V.F. column.

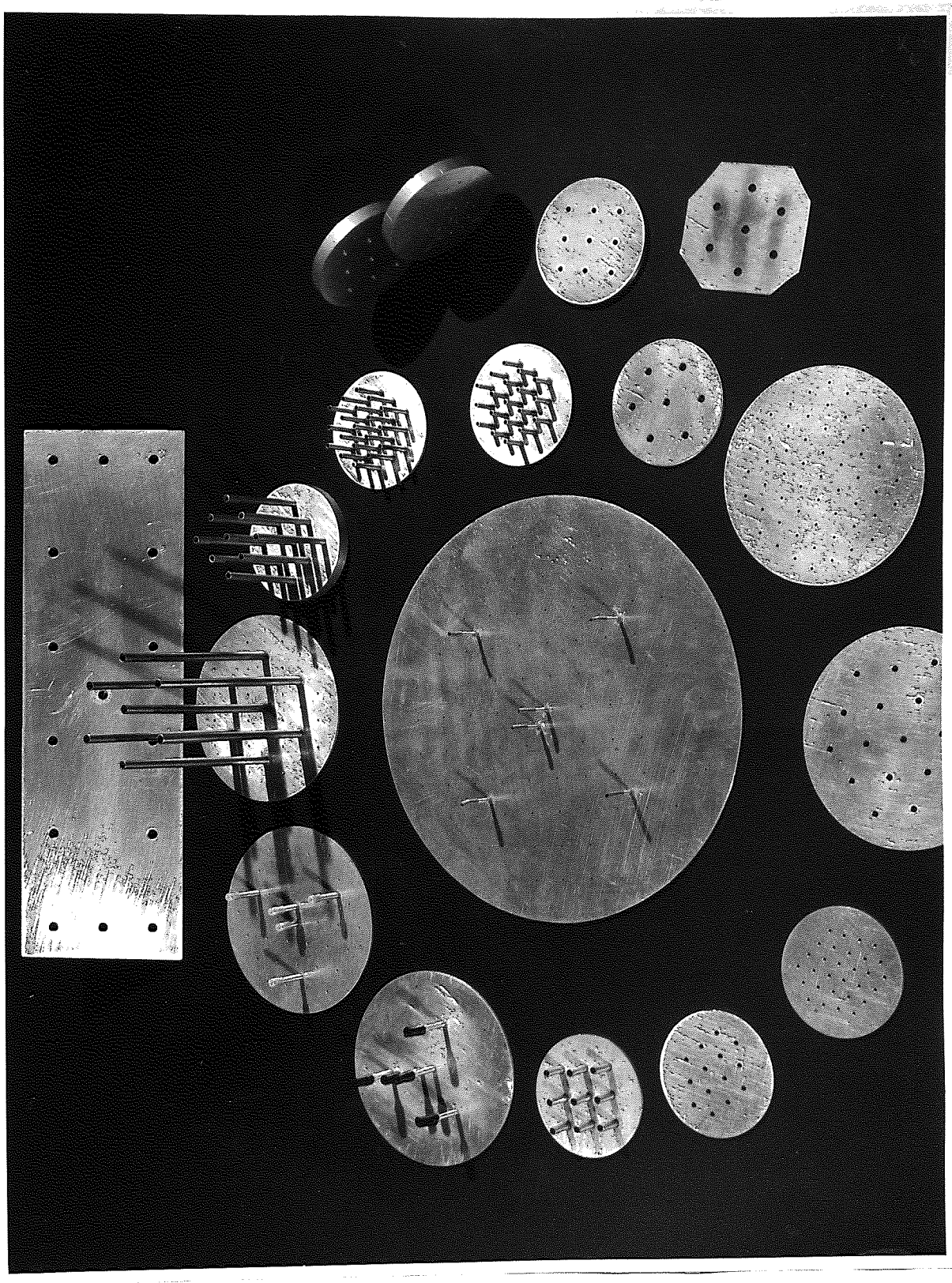

FIG. 6.13 Samples of distributor plates used in the experiments throughout the present work.

6.11 Experimental Results and Discussion

6.11.1 Qualitative Description of the Phenomenon

In agreement with Serviant et al.(76), two phenomena were observed. At high gas velocities, the solids leaked mainly from the periphery of the orifice (cf. weeping). At low gas velocities, the particles fell through the entire area of the orifice in a rhythmical manner (cf. dumping).

As it has been indicated already in Chapter 4, at low gas flow rates maldistribution of flow through the orifices of a multi-orifice distributor often led to two types of orifice behaviour: (i) bubbling/spouting orifices and (ii) non-bubbling orifices. With bubbling orifices particles dumped in a rhythmical manner,, whereas non-bubbling orifices were either jammed or overwhelmed by a heavy, but intermittent, type of dumping (see Figure (4.14)). Thus two types of dumping were recognized. When the gas flow was decreased, more and more orifices started dumping. Simultaneous dumping of all orifices was not observed.

Whan maldistribution was overcome, at higher gas flow rates, the orifices became fully operational and particles often seen falling round the edges of the orifices (weeping).

With single-orifice distributors, the situation was somewhat different in that there existed no maldistribution through the distributor, as we had only one orifice. This, of course, implied that the orifice should be bubbling at all gas rates provided that sufficient secondary air was maintained to keep the bed in a fluidized state.

Visual observations of a single orifice in a two-dimensional bed showed that periodic dumping was associated with orifices producing single bubbles only. Its frequency was consistent with the frequency of bubbles detaching from the orifice and this was, probably, the reason

for the rhythmicity observed. Heavy dumping was observed at very low bubbling rates. This type of dumping was intermittent and usually occurred over a short period of time, stopped and then returned shortly, possibly due to local defluidization and particle bridging above the orifice. No measurements were made under these conditions due to the bad reproducibility of the results.

Weeping, however, was approached at higher bubbling rates, particularly at the transition from single bubble formation to doublet and triplet formation. As the gas flow was further increased, the coalescence point between successive bubbles moved closer to the orifice resulting eventually in jet formation. At this point, weeping could be easily distinguished from the way the particles tended to fall only through the edges of the orifice. This led to the suggestion that weeping was a phenomenon associated with jetting orifices.

It should be borne in mind that these are entirely qualitative observations, but nevertheless these are the phenomena which characterize a multi-orifice distributor operating in the flowback range. To determine the appropriate operating regime of a given distributor it is only necessary to ascertain whether bubbling or jetting occurs at the orifice. The transition from dumping to weeping becomes that point at which a change in the mechanism at the orifice takes place.

6.11.2 Solids Flowback Through Single-Orifice Distributors

All these experiments were conducted with a secondary source of air using mainly the two-dimensional bed. In all the cases studied, the secondary air rate was maintained at or just above the incipient fluidizing velocity of the solid particles. The main objective of this investigation is to simulate as closely as possible the behaviour of an orifice in an actual distributor (i.e. a multi-orifice distributor). But it should be recognized that with multi-orifice distributors the situation is entirely different from that with single-orifice distributors. In the single-orifice experiments, a secondary source of air is necessary to keep the bed in a liquid-like state. The interaction of this secondary air with the main bubbling stream cannot be avoided and its effects are not known. With multi-orifice distributors no secondary air is necessary, but maldistribution at low gas rates and pressure surges and eddies at higher gas rates might cause the flowback behaviour of an orifice to be different from that of a single-orifice distributor. This is evident, as will be shown later, from the higher values of the limiting orifice gas velocity found with multi-orifice distributors in order to overcome solids leakage. Thus, it is expected that results obtained from a single-orifice experiment cannot be applied directly to multi-orifice situations. Nevertheless, we may obtain some insight into the likely behaviour by considering first the behaviour of a single orifice.

The experimental results obtained with single-orifice distributors are presented in Tables (6.10) - (6.13). In all the experiments performed it was found that the rate of solids flowback decreased rapidly with air flow through the orifice in an exponential-type curves. Typical results are shown in Figures (6.14) - (6.15) as plots of flowback rate ω (gm./min.) through the orifice vs. average orifice gas flow rate Q_o ($cm.^3$/sec.) for plates with different orifice diameters using cracking

catalyst as the solid. Similar plots were also obtained with other solids (e.g. rounded sand and coal).

6.11.2.1. Effect of Orifice Velocity and Orifice Diameter

In all the experiments it was found that the flowback of solid particles increased with orifice diameter for a given orifice velocity. The example shown in Figure (6.14) is the results of experiments with ungraded catalyst in the cylindrical bed for three orifice diameters. As can be seen from the plots, at the higher values of ω the data indicate very rapid decrease with orifice flow rate Q_o and at lower values a gradual decrease, hence it would appear, for example, that the ordinate of Figure (6.14) might best be plotted on a logarithmic scale. Preliminary plots of ω vs. Q_o on a semi-log scale produced straight lines almost parallel to each other with the orifice diameter D_o as a parameter. The same is also found with other solids. These lines are brought together by plotting flowback flux ω_o (gm./min.cm^2.) (i.e. ω divided by the surface area of the orifice) against average gas velocity through the orifice U_o (cm./sec.) as shown in Figures (6.16) - (6.17). Orifice velocity appears to be an important correlating factor, and it should be noted that the velocity of falling particles through the orifices has been neglected.

The ordinate of each plot shown in Figures (6.16) - (6.17) represents flowback flux ω_o plus 1.0 so that the line drawn through the points can be represented with an intercept corresponding to zero flowback (or flux) when the abscissa is the limiting orifice gas velocity $U\ell_o$.

With the exception of ungraded catalyst, the scatter of the points in Figures (6.16) - (6.17) is not unreasonable considering that each plotted point depends on the accuracy of three measurements: the time period over which solids were collected, the weight of solids collected and the gas flow rate through the orifice.

The lines drawn through the data in Figures (6.16) - (6.17) can be expressed analytically by the following equations:

106 μ - graded catalyst $$115 \log_{10}(\omega_o + 1) = (U\ell_o)_{\omega_{o\to o}} - U_o \quad (6.21)$$

128 μ - graded coal $$66 \log_{10}(\omega_o + 1) = (U\ell_o)_{\omega_{o\to o}} - U_o \quad (6.22)$$

138 μ - graded rounded sand $$210 \log_{10}(\omega_o + 1) = (U\ell_o)_{\omega_{o\to o}} - U_o \quad (6.23)$$

60 μ - ungraded catalyst $$200 \log_{10}(\omega_o + 1) = (U\ell_o)_{\omega_{o\to o}} - U_o \quad (6.24)$$

Where $U\ell_o$ is the limiting orifice gas velocity which appears to be a function of solid only.

A comparison of the limiting orifice velocity $U\ell_o$ and the particle free-fall velocity U_t based on mean particle diameter for the solids tested (as calculated from the equations given by Jottrand(118)) is as follows:

Solid	ρ_s, gm./cm.^{3}	$U\ell_o$, cm./sec.	U_t, cm./sec.
graded catalyst	0.90	250	25.4
ungraded catalyst	0.90	470	10.8
graded coal	1.35	148	48.6
graded rounded sand	2.63	525	98.6

It can be seen that the limiting velocities are several times greater than the free-fall velocities.

The primary need for such high orifice gas velocities would appear to be to ensure particle conveying and thus preventing flowback. It is significant to note that Zenz(15) has referred to an average orifice velocities one hundred times greater than the particle free-fall velocity being necessary to eliminate solids flowback. He was referring, presumably, to ungraded cracking catalyst. The most likely reason is due to the fact that the flow in the orifice is not well established, and particles fall into the wide boundary layers where eddies force them down into the wind box. With long nozzles, in contrast to that of an orifice, there exists a well established turbulent flow pattern and flat velocity profile. Therefore, lower values of $U\ell_o$ are expected with nozzles or with deep orifices.

A study of the correlations given above shows that the density and the shape of the particles are important in influencing flowback (refer to the graded materials where size effect can be neglected). The higher density of the particles the greater is the rate of flowback and hence the more is the gas required to control it. Particle shape is also important although with gravity flow this appeared to be of no significance. Here, it may influence the flowability of the fluidized particles which is usually characterized by the angle of repose. A free-flowing solid is described as one having low drained angle of repose (e.g. glass spheres). The more shallow the drained angle of repose the more fluid-like its behaviour. A liquid, for example, has a drained angle of repose approaching zero degrees. Thus a fluidizable solid is one which is free-flowing and has a low drained angle of repose. Irregular particles exhibit a higher drained angle of repose than rounded or spherical particles and, therefore, are less free-flowing (i.e. less fluidizable). For example, in the present work, coal particles which are irregular exhibited a drained angle of repose of about 40° when they were allowed

to drain from the two-dimensional bed. Similarly, the catalyst which is more regular exhibited a drained angle of repose of about 33^{o}, whereas rounded sand showed an angle of 31^{o}. The fact that coal appeared to be less flowable than the other solids, and despite the presence of a secondary source of air channelling and rat-holing were often observed. These effects may well result in a lower flowback since particles around the orifice are immobile. However, when the secondary air rate was increased in the attempt to mobilize the bed more particles fell through the orifice. This was also evident from the experiments with multi-orifice distributors which showed a significant increase in flowback of coal at higher gas rates and in particular the limiting orifice velocity was found to be higher than that of the graded catalyst. This is, obviously, not the case with the single-orifice distributor. It should be realised that coal is more dense than catalyst and normally would fall at a greater rate. It would appear, therefore, that the sufficiently high fluidizing velocities used with multi-orifice distributors have enhanced the flowability of coal particles by effectively eliminating channel formation and rat-holing.

In the case of ungraded catalyst (see equation (6.24)), the results seem to be surprisingly high in view of the smaller average particle size. Although, with smaller particles one would expect a lower flowback flux, it was observed that this material, a dusty powder with wide size range (i.e. 20 - 150 μ), had a higher flowback rate than graded catalyst which has a larger particle size. The higher flowback flux exhibited by the unsieved catalyst may be attributed to the following reasons: (i) possible aggregation of its fine particles; (ii) the presence of very fine particles may have a lubricating effect on the larger particles, thus increasing their flowability; and (iii) a combination of (i) and (ii) may be occurring. This is also evident from the significant increase in

the value of W_o observed with this material and the presistence of flowback to low values to a higher gas rate.

The extrapolation of the graphs in Figures (6.16) - (6.17) to zero U_o possibly corresponds to the flow from a defluidized bed into a close chamber (analogous to an hourglass), a phenomenon which to our knowledge has not yet been studied. However, in the present work, some experiments have been carried out and as can be seen from the graphs the experimental results agree reasonably well with extrapolation. In the case of ungraded catalyst a peculiar phenomenon was observed. Qualitative experiments showed that the bed flowed into the wind box by intermittent jets (reminding of a geyser). No measurements were possible at zero U_o due to the high flowback and in particular the intermittent nature of the flow.

The flow from a defluidized bed into a closed chamber should be distinguished from gravity flow (i.e. with open wind box), a study that has already been presented in Section (6.3) of this chapter. For example, the gravity flow of 106 μ catalyst through 0.476 cm. diameter orifice is about 77 gm./min. compared with 22.5 gm./min. obtained from the flow into a close chamber. It is of interest to note that the bed height appeared to be of no significance (see, for example, Table (6.10)) an effect which is also present with gravity flow.

6.1.2.2 Effect of Bed Height

A study of Figures (6.14) - (6.15) show that solids flowback is practically independent of bed height (or distributor loading) and this appears to be so with all solids tested within the range of bed heights studied (i.e. H_{mf} = 25 - 100 cm.). Another important feature of the results is also apparent from the graphs is that the limiting gas velocity through the orifice for a given orifice-solid system is independent of bed height. Similar effects have also been observed with multi-

orifice distributor plates. These results would appear to confirm our visual observations that flowback is associated with bubble growth and activity at the orifice surface. Previous workers(82) and the work of Chapter 4 have shown that bubble formation at an orifice to be independent of bed height, it is a function of gas flow rate only and this seems the most likely explanation.

6.11.2.3 Effect of Wind Box Volume

A single orifice, 0.952 cm.(3/8") in diameter was tested with four wind boxes using the cylindrical bed. Ungraded catalyst and air were used as the solid and gas respectively. The bed height selected for the experiments was about 75 cm. The experimental results are given in Table (6.14) and in Figure (6.18) these are shown as plots of ω vs. Q_o with the wind box volume V_ω as a parameter. Results obtained already from experiments using the original wind box (i.e. $V_\omega = 4.9 \times 10^3$ cm^3.) are also included in Figure (6.18) to complete the range of V_ω.

The same trend of behaviour has been observed, i.e. for a given wind box volume, flowback decreases with gas flow rate in an exponential manner. The effect of the wind box volume V_ω on solids flowback can be seen from Figure (6.18) which shows that at low values of Q_o solids flowback is significantly reduced by increasing the wind box volume. However, the effect seems to diminish rapidly as Q_o increases with the result that flowback becomes virtually independent of the wind box volume at higher values of Q_o. This, of course, suggests that the limiting orifice gas velocity $U\ell_o$ at which solids flowback ceases is also independent of the wind box volume.

These results are particularly interesting because they find a parallel in gas-liquid systems. The strong effect of the wind box volume (or gas chamber volume as noted with gas-liquid systems) underneath

the orifice has been acknowledged by several workers who studied gas-liquid phenomena. McCann and Prince(86) observed a significant decrease in liquid flowback at low gas rates with large wind box volumes. As with this work, the effect decreased rapidly with gas flow rates so that liquid flowback, and hence weep point, became independent of the wind box volume at higher gas rates. The similarity between the two sets of phenomena is remarkable, and in this connection it is noteworthy that from the experimental results of McCann and Prince(86) liquid flowback decreases with orifice gas velocity in the same manner as does solids flowback in gas fluidized beds, i.e. flowback curves in both systems are very similar.

The reduced solids flowback observed at low gas rates and large wind box volumes may be associated with bubble formation in this region. Qualitative experiments showed that for gas flow rates in the range of 40 - 70 cm^3./sec. and for wind box volumes larger than 41.5 x 10^3 cm^3., particles were falling round the edges of the orifice only (i.e. weeping). Visual observations in a two-dimensional bed have shown that in the weeping regime the gas issues from the orifice in the form of a jet, whilst in the dumping regime the primary mechanism at the orifice is one of discrete bubbling.

At the same gas rate, but smaller wind box volumes (e.g. V_ω < 19.2 x $10^3 cm^3$.) particles were observed to fall through the entire area of the orifice in a rhythmical manner, thus indicating that there was a single-bubble formation. Therefore, the important conclusion to be drawn from these observations is that at low gas rates and large wind box volumes jet formation is possible and this could be the reason for the lower flowback obtained with the largest wind box volume. Similar effects have also been observed with gas-liquid systems. Hughes et al.(119) found that at very low gas rates and large wind box volumes, the bubbles

formed in doublet and triplets. This led to the definition of a "capacitance number" which related the acoustical properties of the gas-orifice system to the wind box volume. The wind box volume was used as a parameter in determining the growth rate and ultimate size of a bubble.

It should be borne in mind that the effect of the wind box volume on bubble formation in gas fluidized beds has received little attention in the past. It has been neglected to the same degree that solids flow-back through the distributor has been neglected. However, if the argument based on our visual observations is correct, then it would appear that the wind box design is important in influencing fluidized behaviour particularly at the distributor level.

6.11.3 Solids Flowback Through Single-Nozzle Distributors of Different Lengths

As with single-orifice experiments, a secondary source of air was used to keep the bed minimally fluidized. Preliminary experiments with single cylindrical nozzles showed a significant reduction in solids flowback. Experiments carried out with a single nozzle, 0.794 cm. diameter and 10 cm. long indicated that leakage of solid particles would only occur for values of U_o corresponding to laminar flow in the nozzle. Visual observations suggested that the solids were falling in the boundary layer in a way similar to weeping for single and multi-orifice distributor plates.

Studies have been made on two sets of single-nozzle distributor plates: (i) plates having cylindrical nozzles with 0.794 cm. diameter, 1.36 cm. $< \ell <$ 10 cm., in the two-dimensional bed using the graded catalyst (106 μ) and (ii) plates having cylindrical nozzles with 0.635 cm. diameter, 3.0 cm. $< \ell <$ 8.9 cm., in the cylindrical bed using ungraded catalyst (20 - 150 μ). In both systems air was used as the gas. The experimental results are presented in Tables (6.15) - (6.16) and as plots of flowback rate ω vs. air flow rate through the orifice Q_o in Figures (6.19) - (6.20) with the nozzle length ℓ as a parameter. Results obtained from experiments with single-orifice plates are also included in the plots to complete the range of ℓ.

As shown in Figures (6.19) - (6.20), the curves exhibit similar trends in behaviour as for the single-orifice plates, i.e. flowback decreased rapidly with air flow in an exponential manner. It can clearly be seen that the effect of increasing the nozzle length is to reduce solids flowback, hence resulting in lower values of $U\ell_o$. If ω is cross-plotted against ℓ for constant values of U_o, another interesting

feature emerges. ω decreases exponentially with nozzle length, as shown in Figures (6.21) - (6.22). This effect becomes more pronounced at higher values of U_o and it is so with both grades of catalyst.

As may be seen from Figure (6.21), results from the single orifice with the graded catalyst also fall on the same lines. However, with the unsieved catalyst, the single orifice exhibits a different trend as indicated in Figure (6.22). At Low gas rates the data are considerably lower than those of the nozzles, the difference gradually becoming less pronounced at higher gas rates. This indicates that the advantage of using nozzles to reduce flowback is only apparent at higher gas velocities. The reason for this anomalous behaviour is not clear, but nevertheless trends and effects found with nozzles seem to confirm the behaviour observed with the graded catalyst (refer to Figures (6.21) and (6.22)).

It is interesting to note that flowback of solids through nozzles varies in the same way as does entrainment of solids with freeboard height. As shown in Figures (6.21) - (6.22), for a given orifice velocity U_o, solids flowback varies with nozzle length ℓ by

$$\omega = \alpha \, EXP \, (- \beta \cdot \ell) \quad , \tag{6.25}$$

where α and β are constant. Similar relationship has been found to apply for entrainment at a given fluidizing velocity U (50), and in this case ℓ would be the freeboard height. But for a given nozzle length flowback decreases with gas velocity, whilst for a given freeboard height entrainment increases with gas velocity. Therefore, flowback of solids through nozzles might be referred to as a negative entrainment.

6.11.4 Comments and Conclusions

The study of flowback through a single-orifice distributor has led to a number of conclusions that might be usefully used to interpret the flowback behaviour of a multi-orifice distributor in the next phase of this work. Multi-orifice distributors are of much greater practical interest because, single-orifice distributors are not used in industry. The conclusions are

1. Two regimes of solids flowback, namely dumping and weeping have been differentiated

2. Solids flowback has been found to decrease rapidly with gas flow rate through the orifice in an exponential-type curve and this finds a parallel in gas-liquid systems. Flowback flux has been correlated in terms of orifice gas velocity.

The effect of bed height (or distributor loading) on flowback has been found to be negligible. This is believed to be due to the fact that flowback is a phenomenon associated with bubble formation and activity at the orifice surface.

3. The effect of varying the wind box volume has been observed, particularly at moderate gas flow rates.

4. The advantage of using nozzles in minimizing solids flowback has been observed.

5. The limiting orifice gas velocity at which complete cessation of solids flowback occurs has been found to be independent of orifice diameter, bed height and wind box volume. It is a function of solid properties and orifice depth (or nozzle length).

6. Effects observed in a two-dimensional bed system are also present in a three-dimensional bed system.

FIG. 6.14

Flowback through single-orifice distributors

Legend	H_{mf}, cm.
×	25.2
●	51.3
▼	74.4
⊙	103.0

$V_\omega = 4.9 \times 10^3$ cm.^{3}

20 - 150μ catalyst

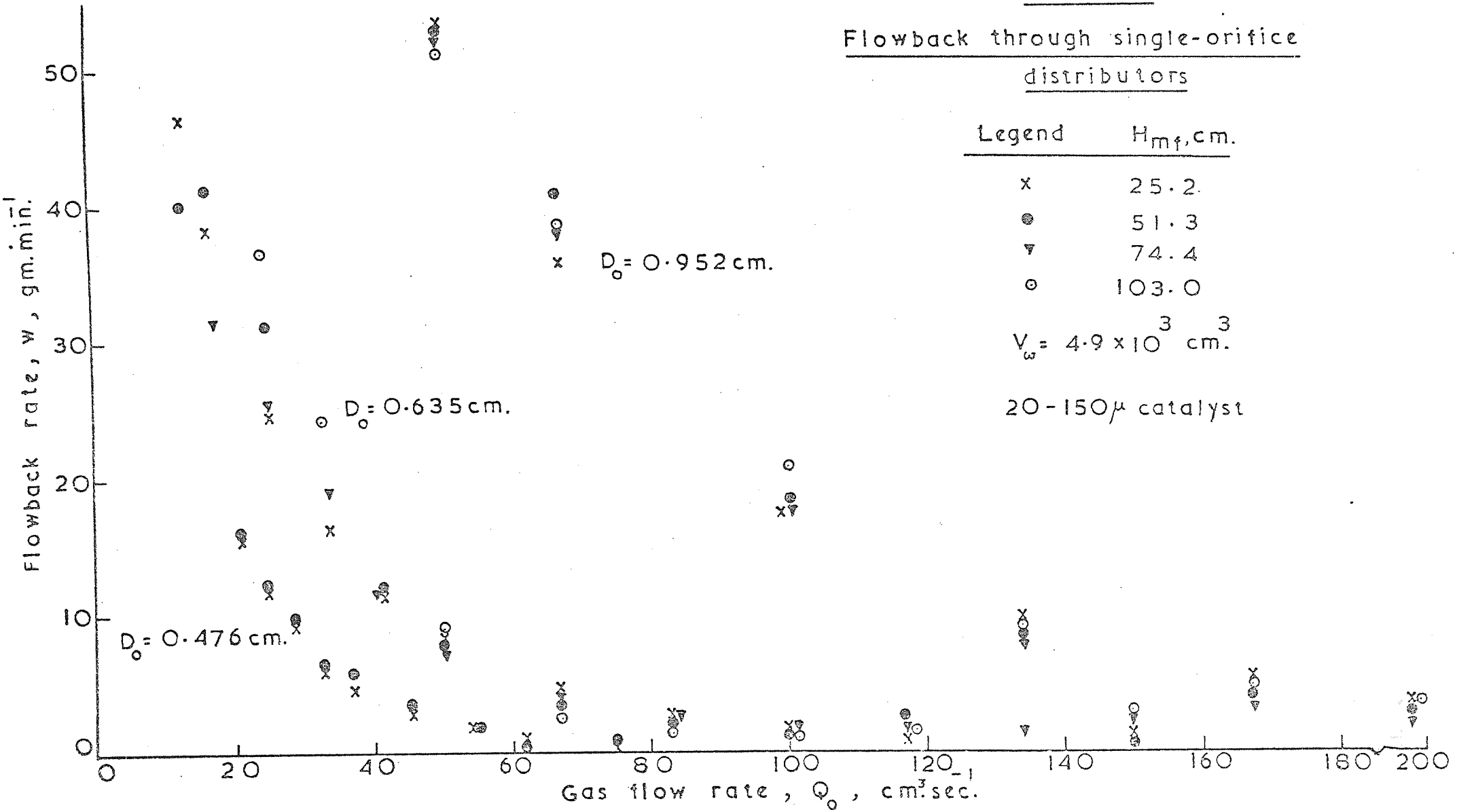

FIG. 6-15

Flowback through single-orifice distributors

Legend	H_{mf}, cm.
×	32·2
●	52·2
▼	70·3

106 μ catalyst, 2-D bed

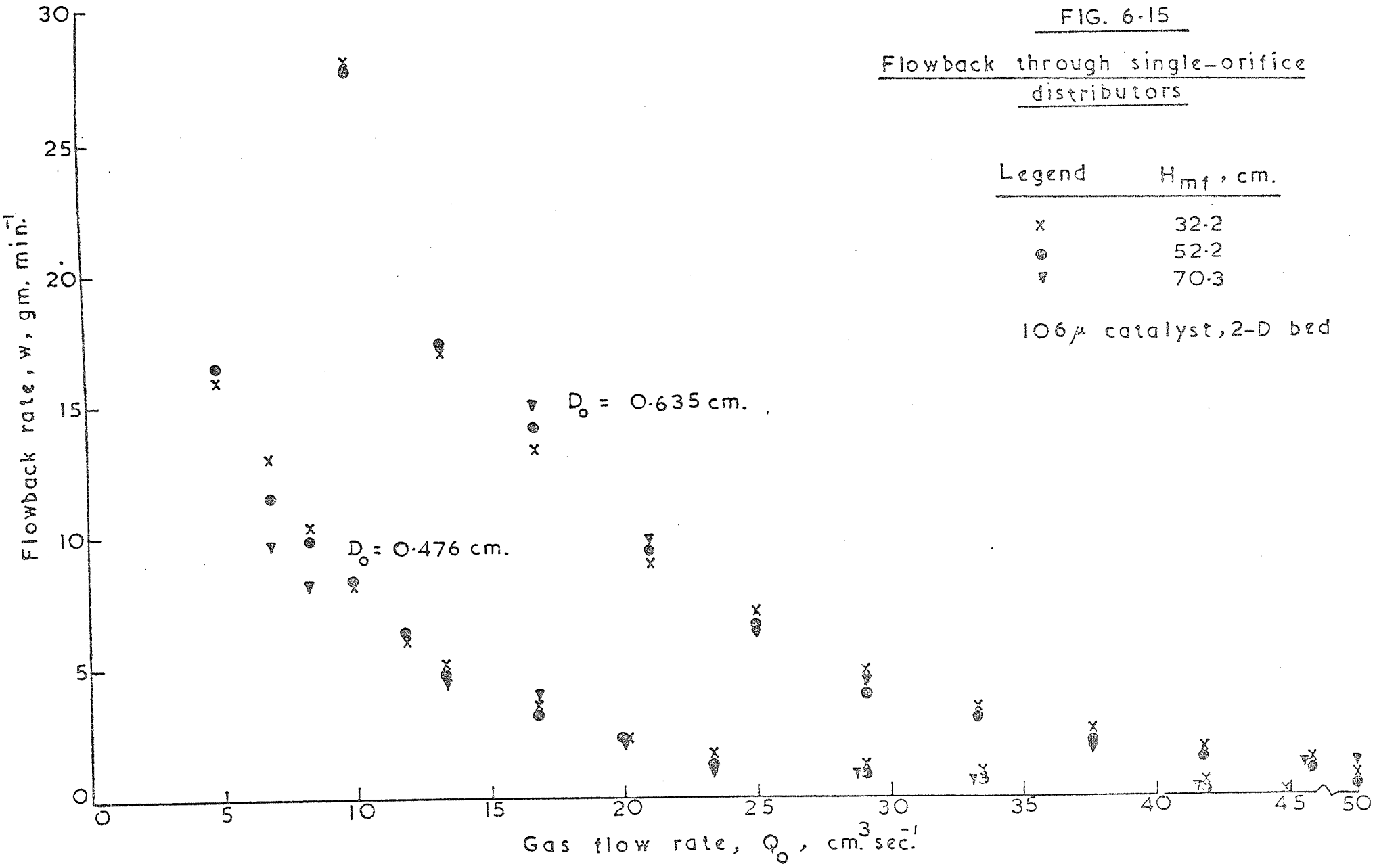

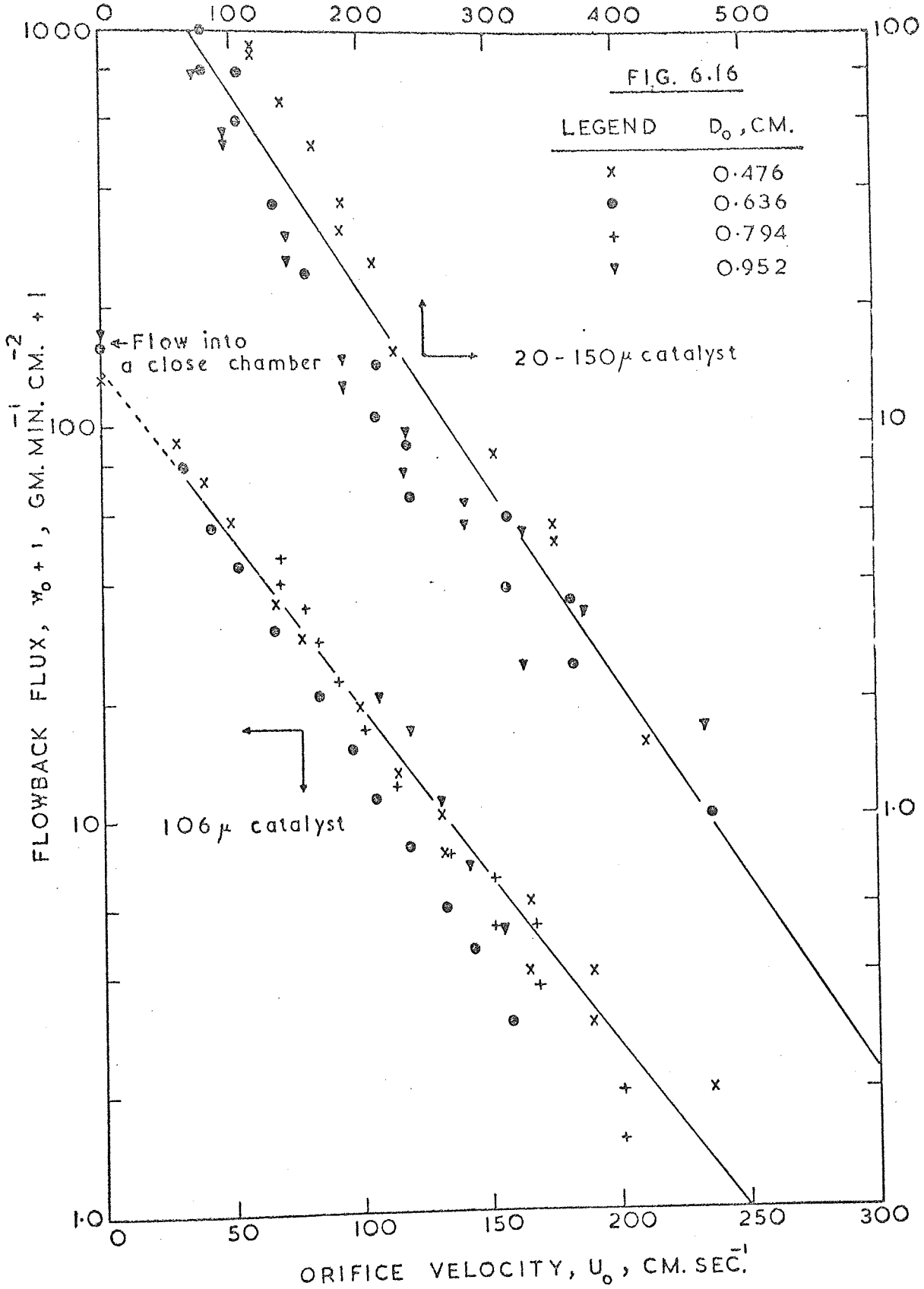
FIG. 6.16
LEGEND
D_o, CM.
0·476
0·636
0·794
0·952
←Flow into a close chamber
20 - 150μ catalyst
106μ catalyst
FLOWBACK FLUX, $w_o + 1$, GM. MIN. CM.$^{-2}$ + 1
ORIFICE VELOCITY, U_o, CM. SEC.$^{-1}$
0
100
200
300
400
500
1000
100
10
1·0
50
150
250

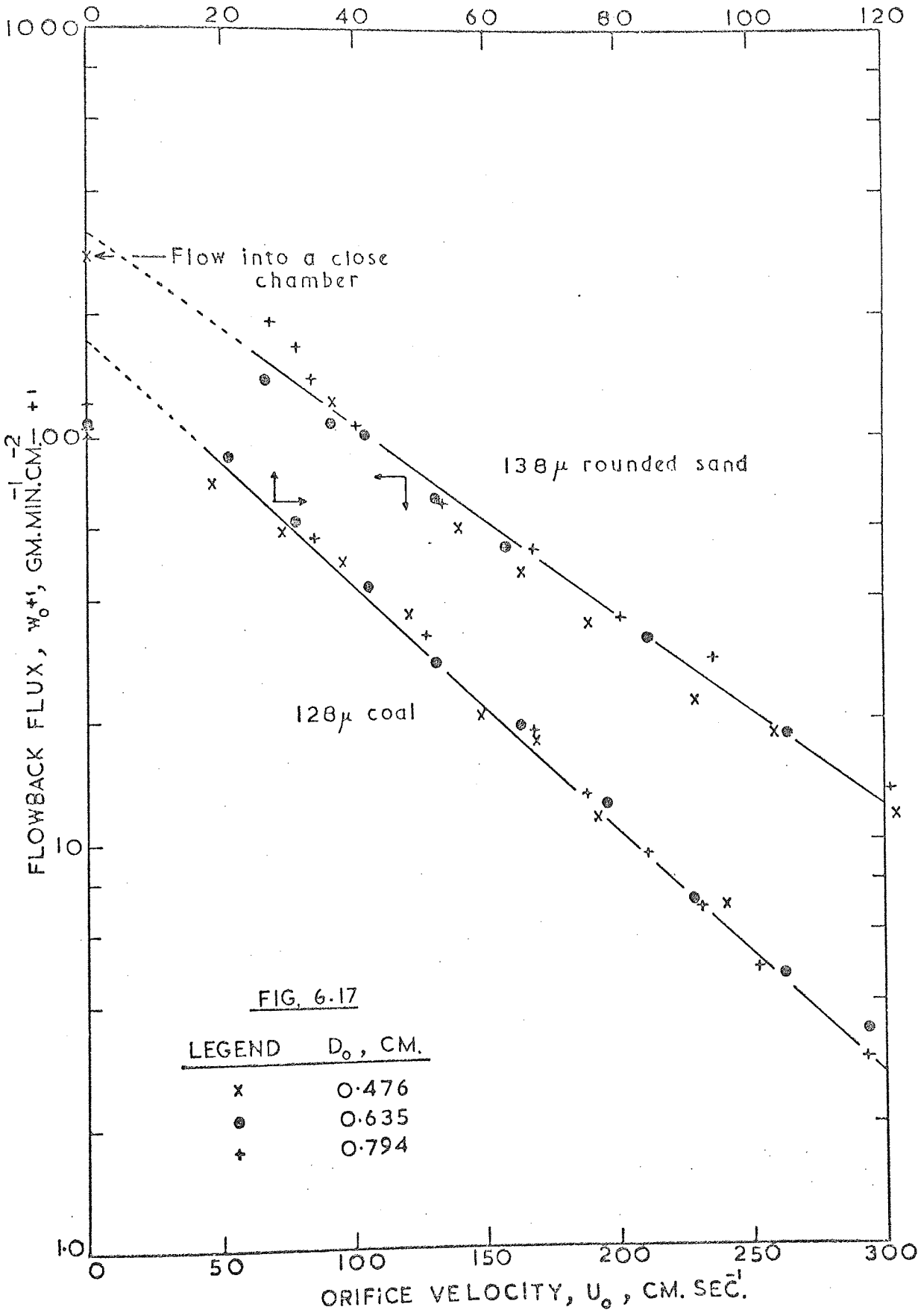
1000
100
10
1·0
0
20
40
60
80
100
120
0
50
100
150
200
250
300
Flow into a close chamber
138μ rounded sand
128μ coal
FLOWBACK FLUX, w_o^{+1}, GM.MIN.CM.$^{-2}$
ORIFICE VELOCITY, U_o, CM. SEC.$^{-1}$
LEGEND
D_o, CM.
0·476
0·635
0·794

FIG. 6.17

FIG. 6·18

Flowback Through Single-Orifice Distributors

LEGEND	V_w, CM.^{3}
▼	4.9×10^3
×	19.2×10^3
●	14.5×10^3
+	63.8×10^3
⊙	36.1×10^3

D_o = 0·952 CM. H_{mf} = 75 CM.
20-150μ CATALYST

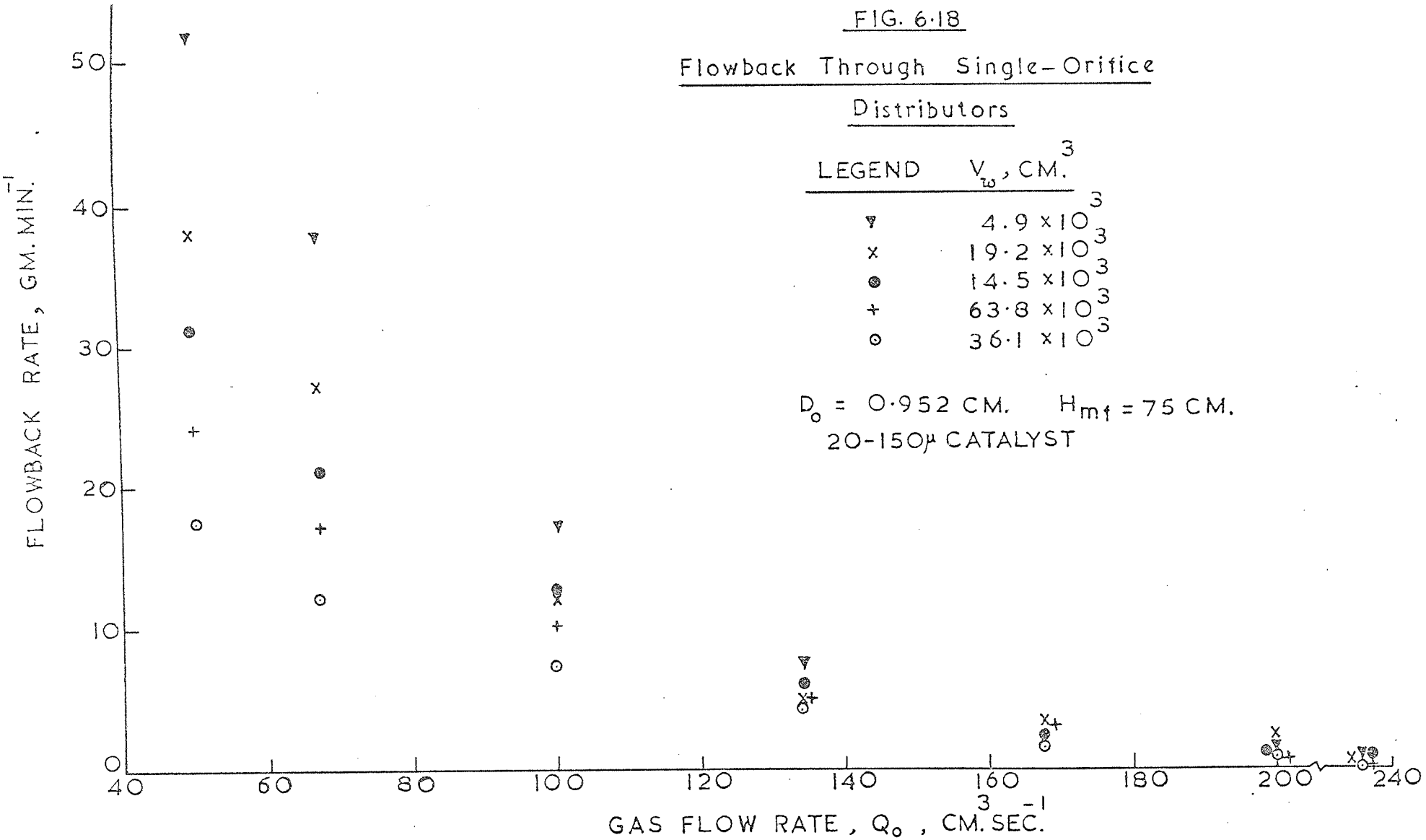

FIG. 6.19

Flowback Through Single-Nozzle Distributors

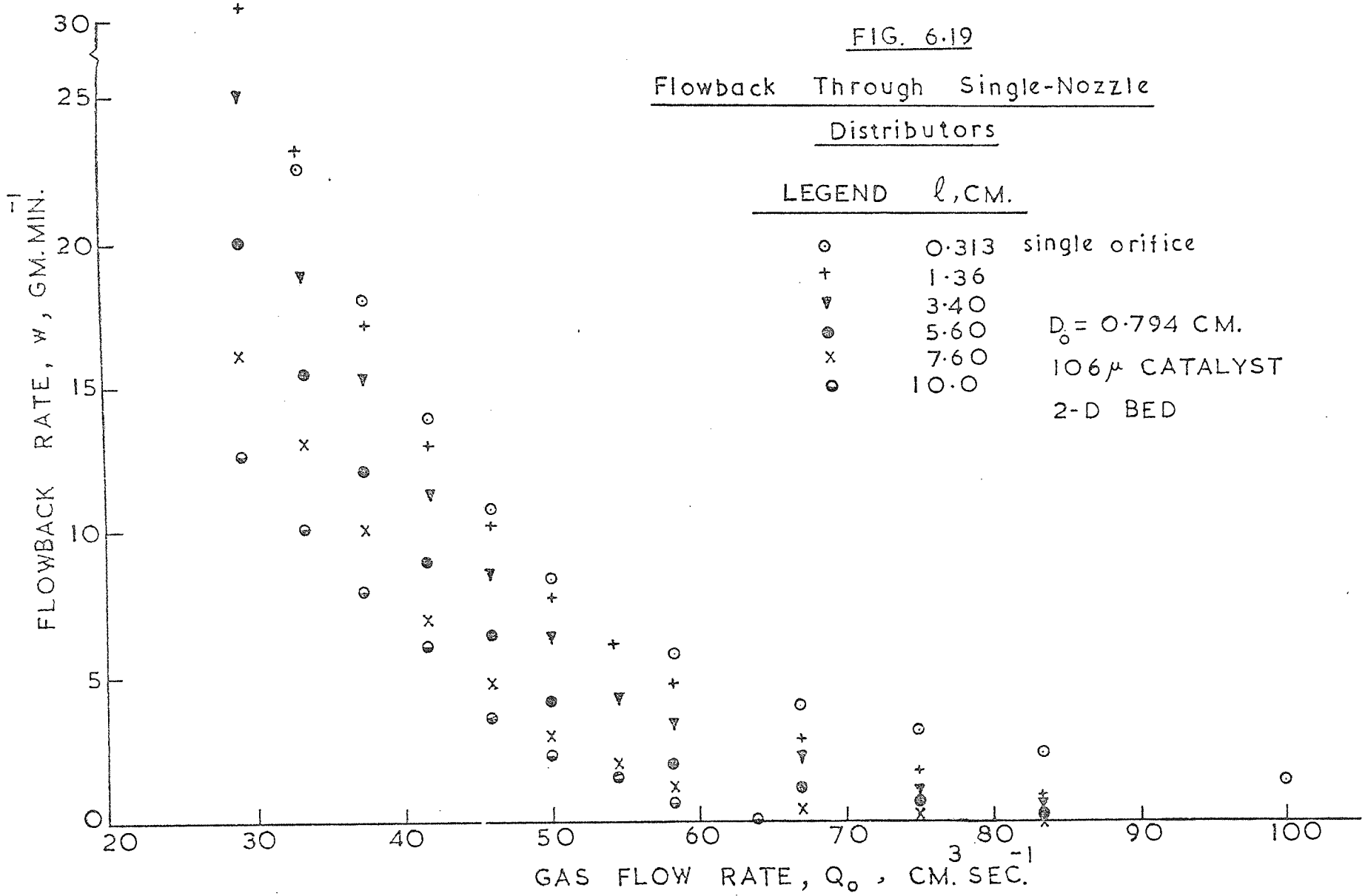

FIG. 6·20

Flowback Through Single-Nozzle Distributors

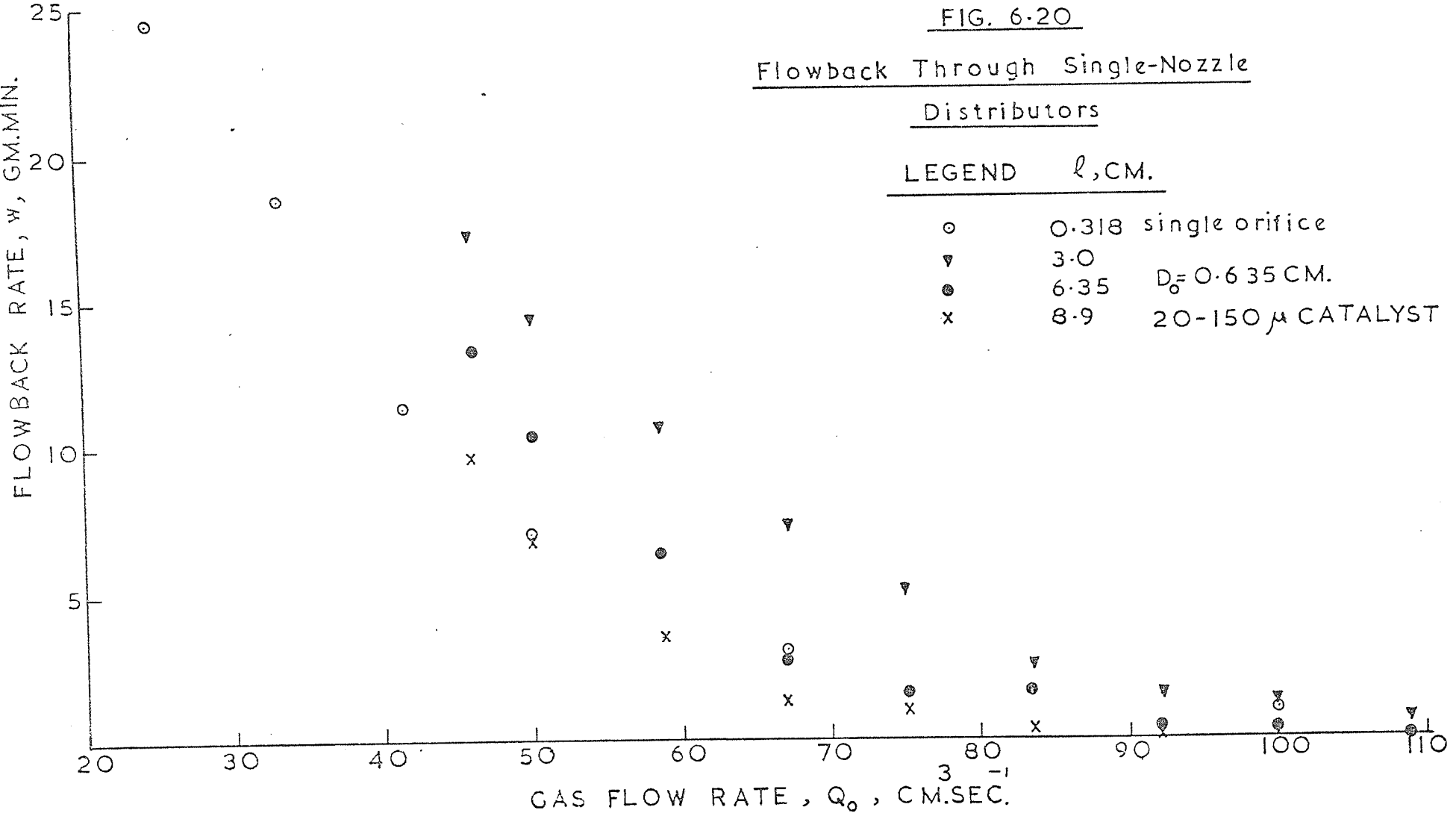

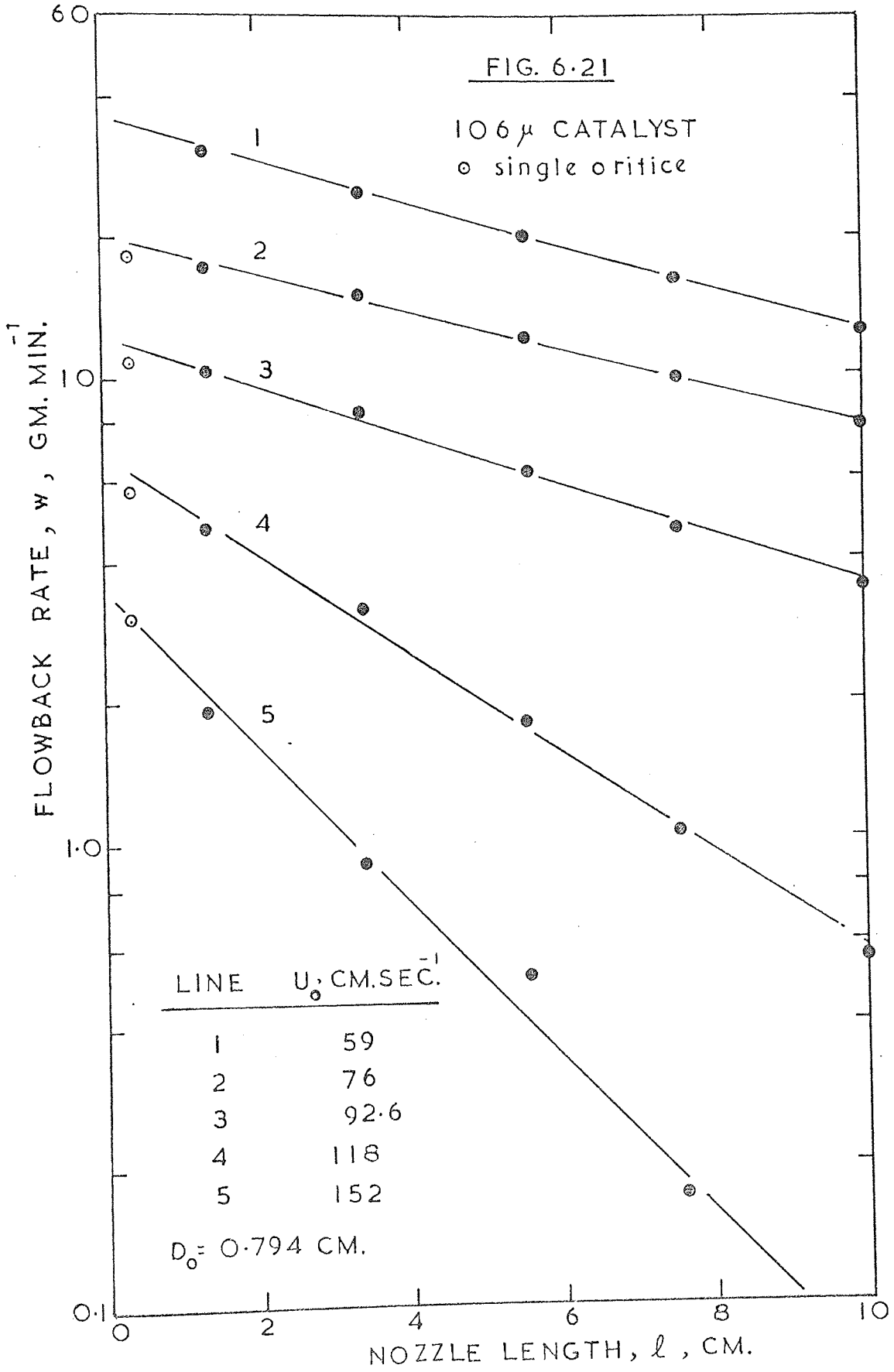
FIG. 6·21
106 μ CATALYST
⊙ single orifice
1
2
3
4
5
LINE U₀, CM.SEC.⁻¹
1 59
2 76
3 92·6
4 118
5 152
D₀ = 0·794 CM.
FLOWBACK RATE, w, GM. MIN.⁻¹
NOZZLE LENGTH, ℓ, CM.
60
10
1·0
0·1
0
2
4
6
8
10

FIG. 6·22 20–150μ CATALYST

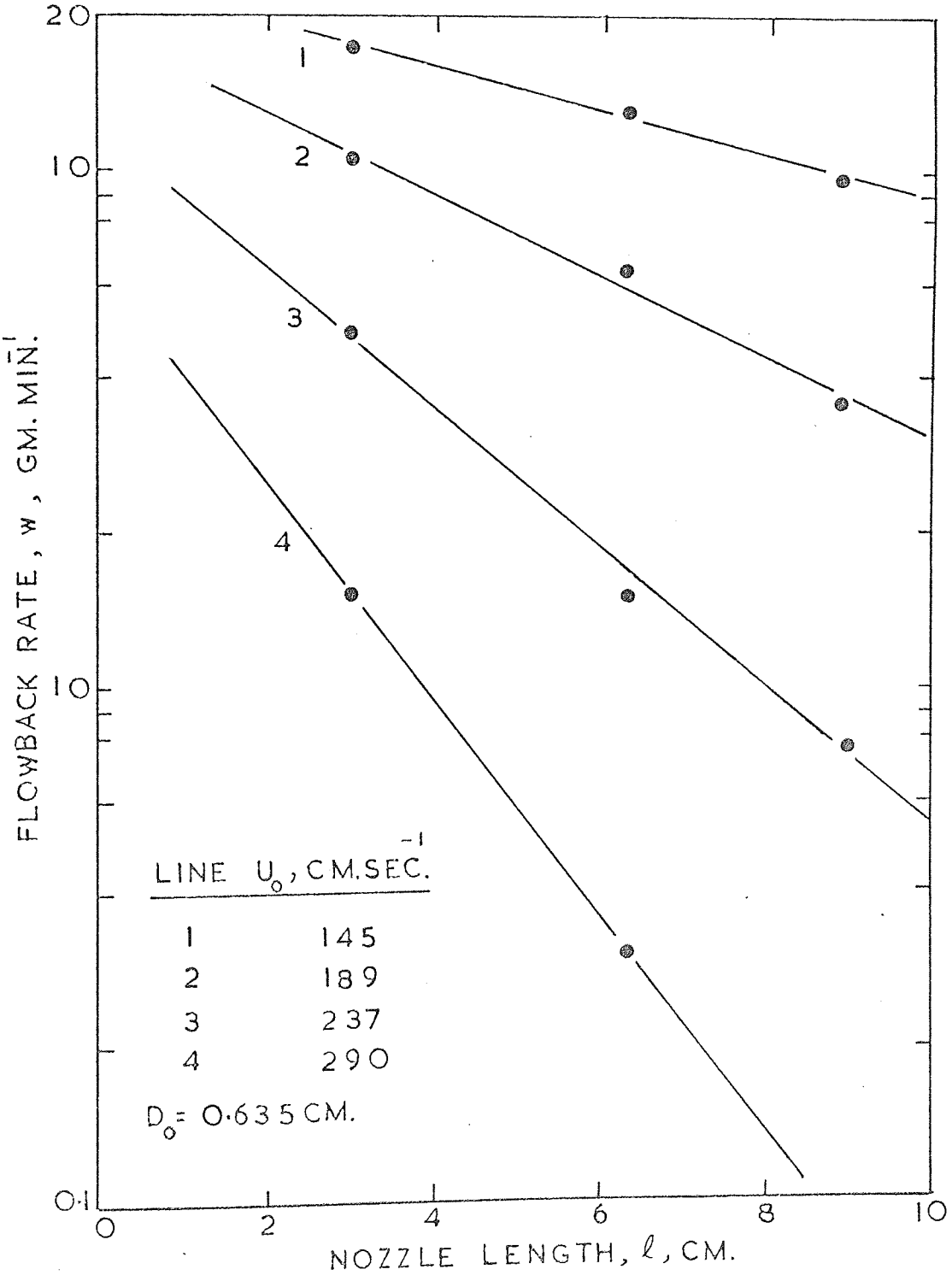

6.11.5 Solids Flowback Through Multi-Orifice Distributors

The experimental work was carried out in the cylindrical column (7.9 cm. diameter) with a wind box volume of about 2×10^3 cm^3. The larger cylindrical column was also used in the experiments, but mainly with distributors equipped with long nozzles. No secondary source of air was used; therefore the superficial gas velocity U (based on bed cross-section) was related to the gas velocity through the orifices by (3.2), i.e.

$$U = \phi . U_o \qquad (cm./sec.) \quad , \tag{3.2}$$

where ϕ is the plate characteristics (or fractional free area).

As explained earlier, there appear to be two causes for solids flowback through a multi-orifice distributor plate. At high gas flow rates, the velocity profile across the orifice of a multi-orifice distributor is peaked and the particles have been observed to fill the thick boundary layer where pressure fluctuations sporadically force them down into the wind box. This phenomenon is referred to as weeping as for single-orifice plates (i.e. particles leaked through the edges of the orifices).

At lower gas flow rates, the pressure drop through the distributor is not sufficient to ensure an equal distribution of the flow through the orifices. Some orifices have been observed to dump particles in a random way (i.e. not together). This phenomenon is referred to as dumping. When the gas flow was decreased more and more orifices started dumping. Simultaneous dumping of all orifices was not observed. However, at a very low gas rate dumping lasted only for a short period of time with the result that most of the orifices became jammed with particles.

6.11.5.1 Solids Flowback Over the Entire Range of Fluidizing Velocities

Tests were made with air fluidized beds of cracking catalyst, rounded sand, and coal, but most of the experiments were carried out with the catalyst. The multi-orifice distributors used in the experiments had free areas ranging between 1.74 - 3.4%, the orifice diameter and the centre-to-centre orifice spacing were variables. Four of the distributors had orifices positioned at the same pitch to diameter ratio ($S/D_o = 5$), thus keeping the free area approximately constant for plates with different sizes of orifices. The fluidizing air was varied between the incipient fluidizing velocity U_{mf} and the limiting superficial velocity $U\ell$ (where $U\ell = \phi\, U\ell_o$) at which solids flowback was completely excluded.

The experimental results are given in Tables (6.17) - (6.26) and as plots of flowback rate ω (gm./min.) vs. superficial air velocity (cm./sec.) in Figures (6.23) - (6.32). These indicate the way in which flowback through a multi-orifice distributor increases rapidly from zero to a maximum and then decreases steadily in exponential manner as with single-orifice distributors. The general trend of the curves can be explained as follows.

1. When bubbling commences at velocities slightly above U_{mf}, a small number of distributor orifices are operative and produce bubbles, and dropping of the particles through the orifices is apparently hindered by the restricted nature of their motion near the orifices. As the gas flow rate is increased more orifices become operational, the mobility of the particles in the fluidized bed also increases, and the number of particles dropping through in unit time increases accordingly. However, the increase of flowback rate of particles with increasing gas velocity continues only up to a certain value. At this point the flowback

rate is at a maximum and the number of operative orifices is also at a maximum but this is not necessarily the total number of orifices in the distributor. Throughout this region, orifices have been observed to dump particles in the manner described earlier and, therefore, it is referred to as the dumping region.

2. The decline in the flowback rate with further increase in U may be explained as follows: on further increase of gas velocity the orifices in the distributor plate become gradually "locked" by the dynamic action of the gas jets in them. The decrease in the flowback rate continues until a certain limiting gas velocity U_ℓ is reached. At this limiting velocity, solids flowback ceases completely.

In this region, particles leaked mainly through at the edges of the orifice and, therefore, it is referred to as the weeping region. In the weeping regime, the flowback does not fall at the same rate as does a single-orifice distributor (as might be expected from the jetting mechanism then prevailing at the orifices). Rather, it continues at a low level until quite high gas rates. This is a result of wave-like oscillations in the bed over the distributor plate which temporarily prevent some orifices from jetting and can cause localised weeping. This is probably the main reason why a multi-orifice distributor requires a much higher limiting orifice velocity than a single-orifice distributor.

As can be seen from the plots, the experimental data obtained in the weeping region show little or no scattering and of the cases studied weeping has always been consistent. The most notable feature of this region is that the flowback rate decreases essentially in the same way as does flowback through a single-orifice distributor. Qualitatively, this suggests that in this respect the single-orifice distributor is simulating the behaviour of an actual distributor. Quantitatively, however,

this is not so for reasons which have been indicated already.

Unlike the weeping data, the points in the dumping region are somewhat scattered and reproduce rather badly. This is attributed to a number of effects which have been referred to earlier, but are mainly due to the effect of flow maldistribution across the distributor which occurs at low gas flow rates. In this region, the orifices dump particles in a random manner and only few orifices are weeping. Therefore, operation of a distributor under these conditions is undesirable and can easily lead to instability in the bed. Provided some relatively low level of flowback is tolerable the weeping region is apparently a stable region because almost 100% of the orifices are operational and weep in a consistent manner. In this region, flow maldistribution is almost negligible, and it can be seen that the single-orifice and the multi-orifice distributors exhibit similar trends of behaviour, confirming a uniformly distributed gas flow through the orifices. At the limiting velocity $U\ell$, the flow through the orifices is high enough to ensure particle conveying and thus preventing flowback.

An inspection of Figures (6.23) - (6.32) shows that the superficial gas velocity at which maximum flowback occurs appears to be a function of solid characteristics and it is interesting to note that of the systems studied this maximum occurs at gas velocities 4 - 8 times U_{mf}. However, this also appears to be influenced, but not considerably, by the plate characteristics and in particular the orifice diameter. The influence of orifice diameter will be referred to later.

6.11.5.2 Effect of Distributor Characteristics

The influence of the geometrical plate parameters (orifice diameter and free area) on solids flowback is clearly evident from Figures (6.23)-(6.32). It should be emphasised that an exact comparison of the various

distributors employed is possible only with results obtained in the weeping regime. A comparison with these obtained in the dumping regime may not be exact due to the bad reproducibility and the considerable scatter observed in this region. The examples shown in Figures (6.23)-(6.25) are the results of experiments with graded catalyst (106 μ) for plates having the same thickness ℓ and orifice diameter D_o but different relative free areas ϕ (orifice spacing S is a variable). It can be seen that the effect of decreasing the relative free area is to decrease solids flowback for a given superficial gas velocity U and consequently the limiting velocities must be decreased. As found with single-orifice studies, the limiting gas velocity through the orifices $U\ell_o$ $(= U\ell \cdot \phi^{-1})$ is independent of the plate free area (or orifice diameter). Hence the flowback flux ω_o must also be independent of the plate characteristics. Effect of plate characteristics on flowback flux will be examined later.

The examples shown in Figures (6.26) - (6.28) are also the results of experiments with graded catalyst which show the effect of orifice diameter on flowback for plates having approximately the same free area $(S/D_o = 5)$. It is apparent that large orifices favour weeping, i.e. it appears that plates with large orifice diameters tend to move into the weeping regime more readily than plates with small orifice diameters. The result is not unexpected. Equations proposed by Kutateladze and Sorokin (120) for gas-liquid systems suggest that the orifice velocity at the onset of jetting has an inverse power dependence on orifice diameter. A similar dependence of the dumping-to-weeping transition on orifice diameter may apply to gas-fluidized beds.

6.11.5.3 Effect of Bed Height

The effect of bed height may also be seen from Figures (6.23)-(6.32) for all solid-distributor systems tested. The bed height was

varied between 20 to 70 cm. It is apparent that for the range of bed heights employed, the bed height has little effect at low gas flow rates and almost no effect at high gas flow rates, particularly in the weeping regime. This is consistent with the results of the single-orifice distributors, but in disagreement with Gregory(2) who shows that solids flowback decreases sharply with bed height and then rises to a local maximum. A bed height effect may be associated with waves traversing the surface of the distributor as the amplitude of these waves will depend on the bed height and it is more likely with large diameter beds. The work of Chapter 3 shows that the larger diameter bed tends to be less stable than the smaller diameter bed when these are operated with shallow beds. Visual observations also show that the larger bed exhibits some degree of pulsation. It is possible that the distributor then undergoes periodically a certain dynamic pressure when the bed (or a part of it) sinks onto the distributor, this pressure being proportional to the bed height. It may be supposed that the flowback rate across the distributor is proportional to this pressure. On further increase of the bed height the pulsating material in the region above the orifices becomes considerably more compact, so that the rate of increase of flowback with bed height diminishes. The current experimental investigation has shown that the bed height does not influence flowback and this is so with both single and multi-orifice distributors. Therefore, further work on deeper and larger diameter beds is necessary to establish whether bed height or bed diameter are actually influencing flowback.

6.11.5.4 Change in Flowback Behaviour With Change in Distributor Thickness or Nozzle Length

In view of the promising results obtained with single nozzles, it was decided to test plates with different thicknesses as well as

plates with cylindrical nozzles of various lengths (i.e. multi-nozzle distributors).

A new phenomenon was observed with long nozzles. At a certain gas velocity the bed would start flowing through one nozzle and flood the wind box. The longer the nozzle, the more difficult it was to control it by increasing the gas flow rate, because of the hydrostatic head in the nozzle. There is a critical nozzle length for a bundle of cylindrical nozzles above which this phenomenon can occur. It would appear, however, that for the range of nozzle diameters and lengths employed this uncontrollable downflow of solids occurs only with nozzles having ratios of length to diameter ℓ/D_o exceeding 12. In other words, the critical nozzle length would exist only with ratios higher than 12, and this is so with all solids tested. Consequently, all experiments concerning the effect of plate thickness (or nozzle length) were restricted to ratios ℓ/D_o equal to or less than 12 in the attempt to prevent the occurrence of this phenomenon. Flowback through distributors equipped with long cylindrical nozzles (i.e. $\ell/D_o \gg 12$) has been considered in a separate study. A theoretical model for predicting the critical nozzle length for a bundle of nozzles in terms of gas velocity through the nozzles has been derived. This will be dealt with later, now we consider distributors with ratios $\ell/D_o \leqslant 12$.

The experimental results are presented in Tables (6.27) - (6.29) and as plots of flowback rate ω (gm./min.) vs. superficial gas velocity U (cm./sec.) with the plate thickness (or nozzle length) ℓ (cm.) as a parameter in Figures (6.33) - (6.35). The distributors selected for the experiments are either flat plates having different thicknesses or plates equipped with short nozzles, so that $\ell/D_o \leqslant 12$. The distributors have approximately the same free area for different orifice diameters, i.e.

pitch to diameter ratio is maintained constant ($S/D_o = 5$).

In the experiments performed it is found that solids flowback decreases with increasing plate thickness (or nozzle length). The effect appears to be most pronounced in the weeping regime, as can be seen in any of Figures (6.33) - (6.35). These also explain the effect of increasing the plate thickness in reducing the limiting gas velocity Ul. It is also clear that the superficial gas velocity at which maximum flowback occurs is not influenced by the plate thickness and so flowback in the dumping regime. We may, therefore, conclude that the decisive advantage of increasing the distributor thickness or using nozzles to minimize flowback in fluidized beds is apparent only in the weeping regime. The observed difference between the effect of plate thickness on weeping flowback and dumping flowback still remains to be explained.

The observed decrease in flowback with plate thickness in the weeping regime may be associated with the type of flow pattern in the orifices (or nozzles). At high gas flow rates, there exists a well established turbulent flow pattern and flat velocity profile in a deep orifice (or a nozzle). In a thin orifice, in contrast to that of a nozzle, the initial velocity profile is not well established and particles fall through the thick boundary layer where pressure fluctuations sporadically force them down into the wind box. Obviously, with nozzles particles have to travel a longer distance in order to fall through (the nozzle length provides 'braking' for incoming particles) and pressure fluctuations would have less effect in forcing them down the wind box. The longer the nozzle the more difficult it is for the particles to fall down the wind box and hence the lower is the gas velocity at which flowback can occur. However, maldistribution which occurs at low gas flow rates would cause the bed to descend through one of the nozzles

and flood the wind box. A further decrease in the gas flow causes more nozzles to flow simultaneously.

Start-up problems can be expected from long nozzles. The start-up from a defluidized bed with defluidized solids filling the nozzles was found very difficult to achieve for nozzles longer than 15 cm. Flowback through long cylindrical nozzles is considered separately in Section (6.11.9).

6.11.5.5 Effect of Wind Box Volume

A multi-orifice distributor with N = 9, D_o = 0.476 cm. and ϕ = 3.3% was tested with four wind boxes using graded catalyst as the fluidized solid. The bed height selected for the experiments was about 50 cm. The experimental results are given in Table (6.30) and as plots of flowback rate ω vs. superficial gas velocity U with the wind box volume V_ω as a parameter in Figure (6.36). Results shown already in Figure (6.27), for a wind box volume $V_\omega = 2 \times 10^3$ cm^3., are also included in Figure (6.36).

The same trend of behaviour has been observed with all wind boxes tested, i.e. two types of orifice mechanisms have been differentiated. In the dumping regime, orifices have been observed to leak and bubble in a random way regardless of the volume of the wind box which appears to be of no significance in this region. It would appear that the wind box volume has an effect in the weeping regime only and in particular on the transition from dumping-to-weeping. Although the superficial gas velocity at which maximum flowback occurs remains unchanged, this maximum appears to decrease with increasing wind box volume. As observed with the single-orifice distributor, the effect of the wind box volume seems to subside rapidly with increasing gas velocity with the consequence that solids flowback becomes independent of the wind box volume at higher gas rates. This is partly due to the improved

gas distribution obtained at higher gas flows which, probably, eliminates the effect of the wind box. This would, obviously, mean that the limiting gas velocity at which flowback diminishes is also independent of the wind box volume.

The observed influence of wind box volume on the flowback rate is in agreement with that found with the single-orifice distributor and that reported by McCann and Prince(86) for gas-liquid system. Despite the subjective nature of visual observations, the agreement with the single-orifice supports the earlier proposition that large wind box volumes favour jetting at the orifice. In general, therefore, large wind box volumes favour weeping flowback.

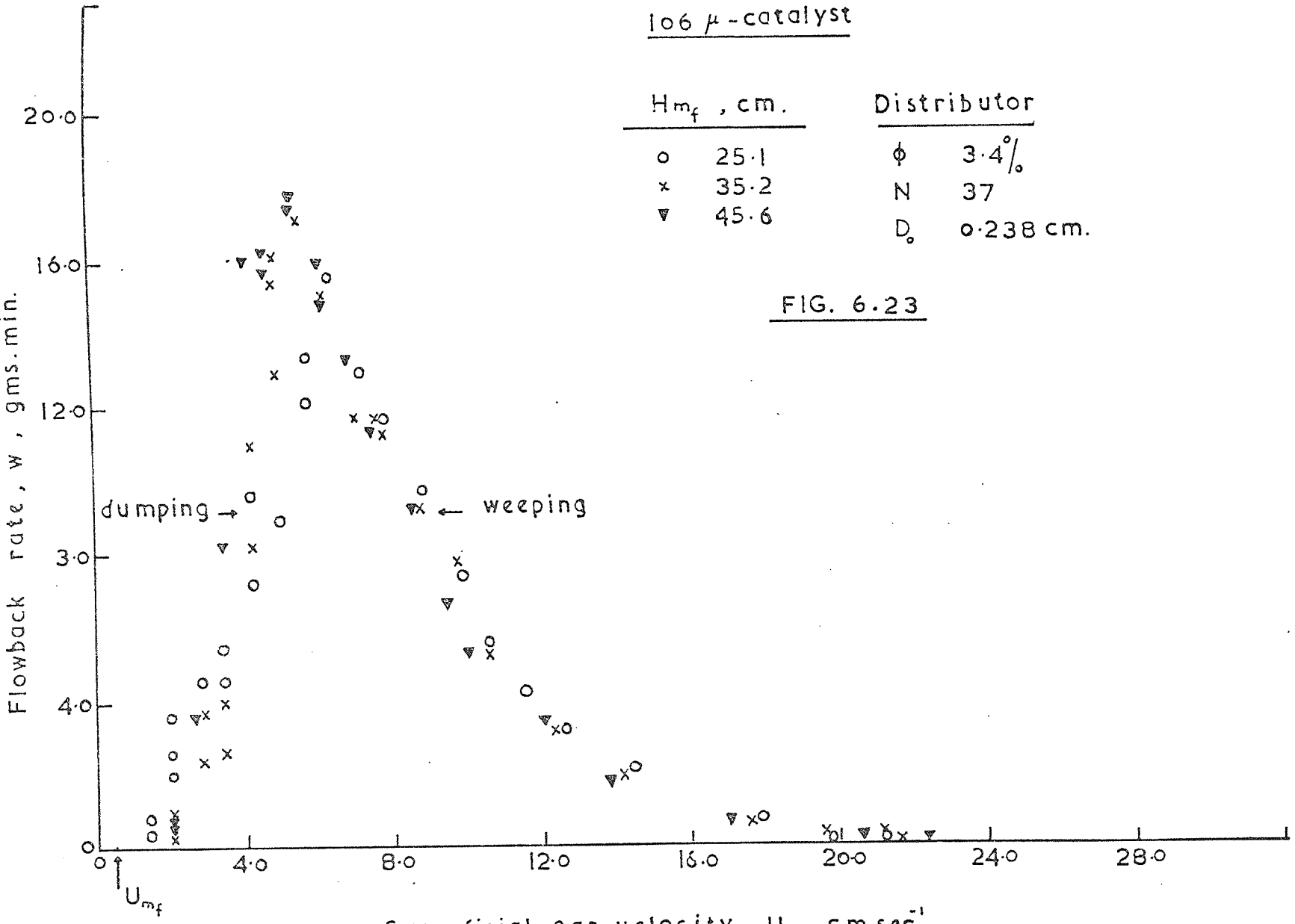
106 μ - catalyst
Hmf , cm.
o 25·1
× 35·2
▼ 45·6
Distributor
ϕ 3·4%
N 37
Do 0·238 cm.
FIG. 6.23
Flowback rate, W, gms. min.-1
20·0
16·0
12·0
3·0
4·0
0
dumping →
← weeping
0
Umf
4·0
8·0
12·0
16·0
20·0
24·0
28·0
Superficial gas velocity, U, cm.sec.-1

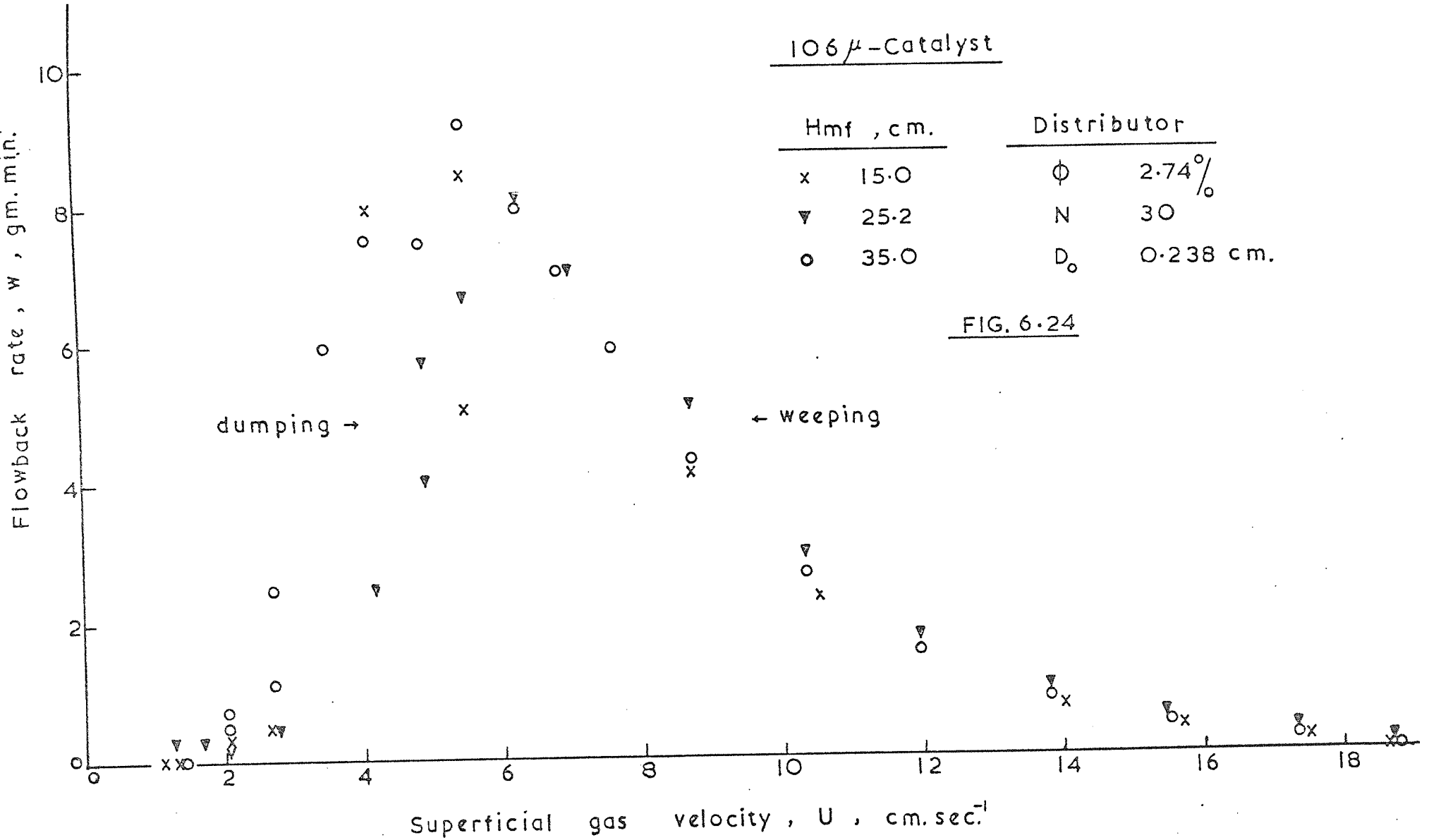
106 μ - Catalyst
Hmf , cm.
x 15·0
▼ 25·2
o 35·0
Distributor
ϕ 2·74%
N 30
D_o 0·238 cm.
FIG. 6·24
dumping →
← weeping
Flowback rate , w , gm. min.$^{-1}$
Superficial gas velocity , U , cm. sec.$^{-1}$
0
2
4
6
8
10
12
14
16
18

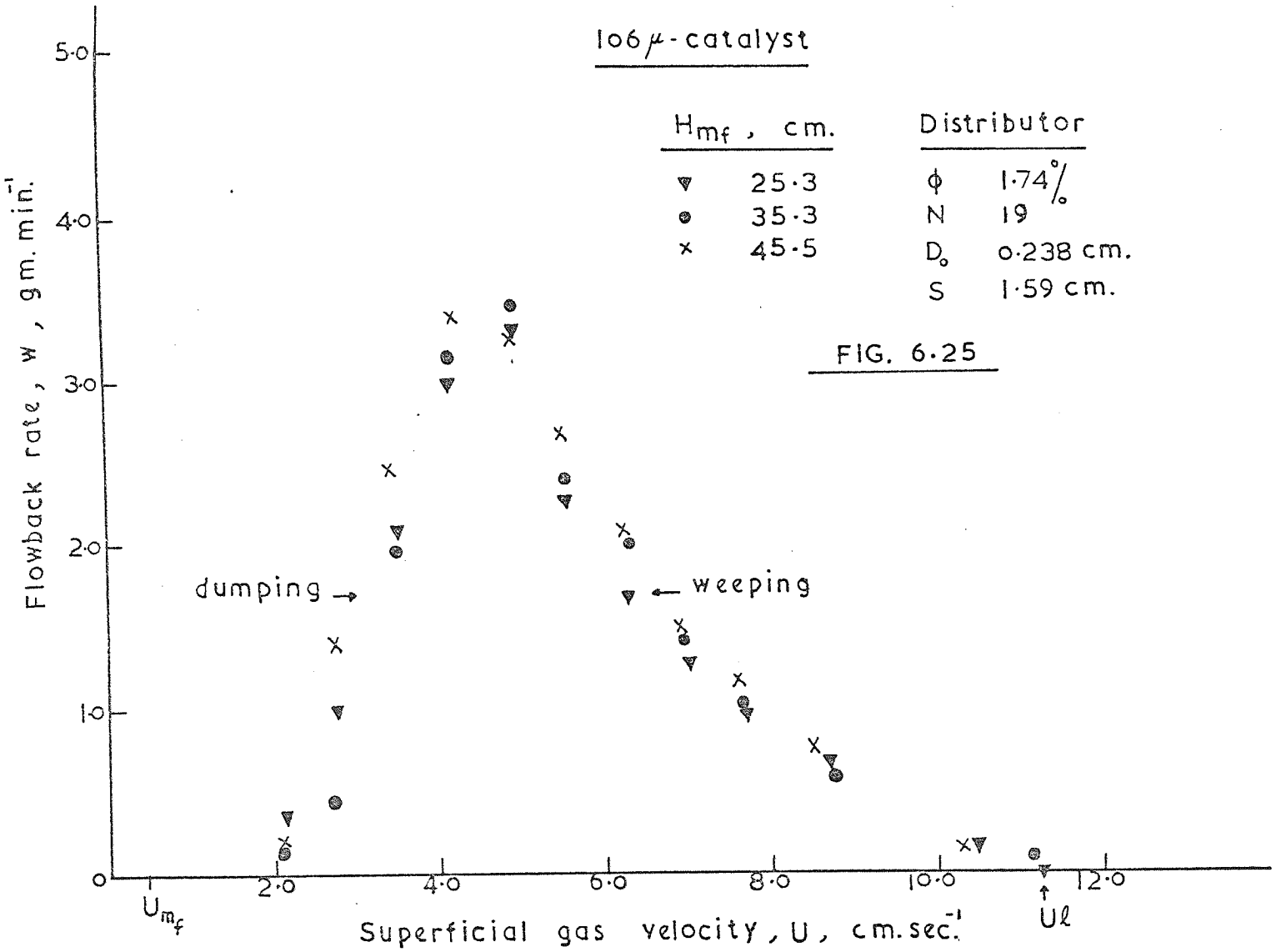
106μ-catalyst
H_{mf}, cm.
25·3
35·3
45·5
Distributor
ϕ 1·74%
N 19
D_o 0·238 cm.
S 1·59 cm.
Flowback rate, W, gm. min.$^{-1}$
5·0
4·0
3·0
2·0
1·0
0
dumping →
← weeping
2·0
4·0
6·0
8·0
10·0
12·0
U_{mf}
Ul
Superficial gas velocity, U, cm. sec.$^{-1}$

FIG. 6.25

106 μ - Catalyst

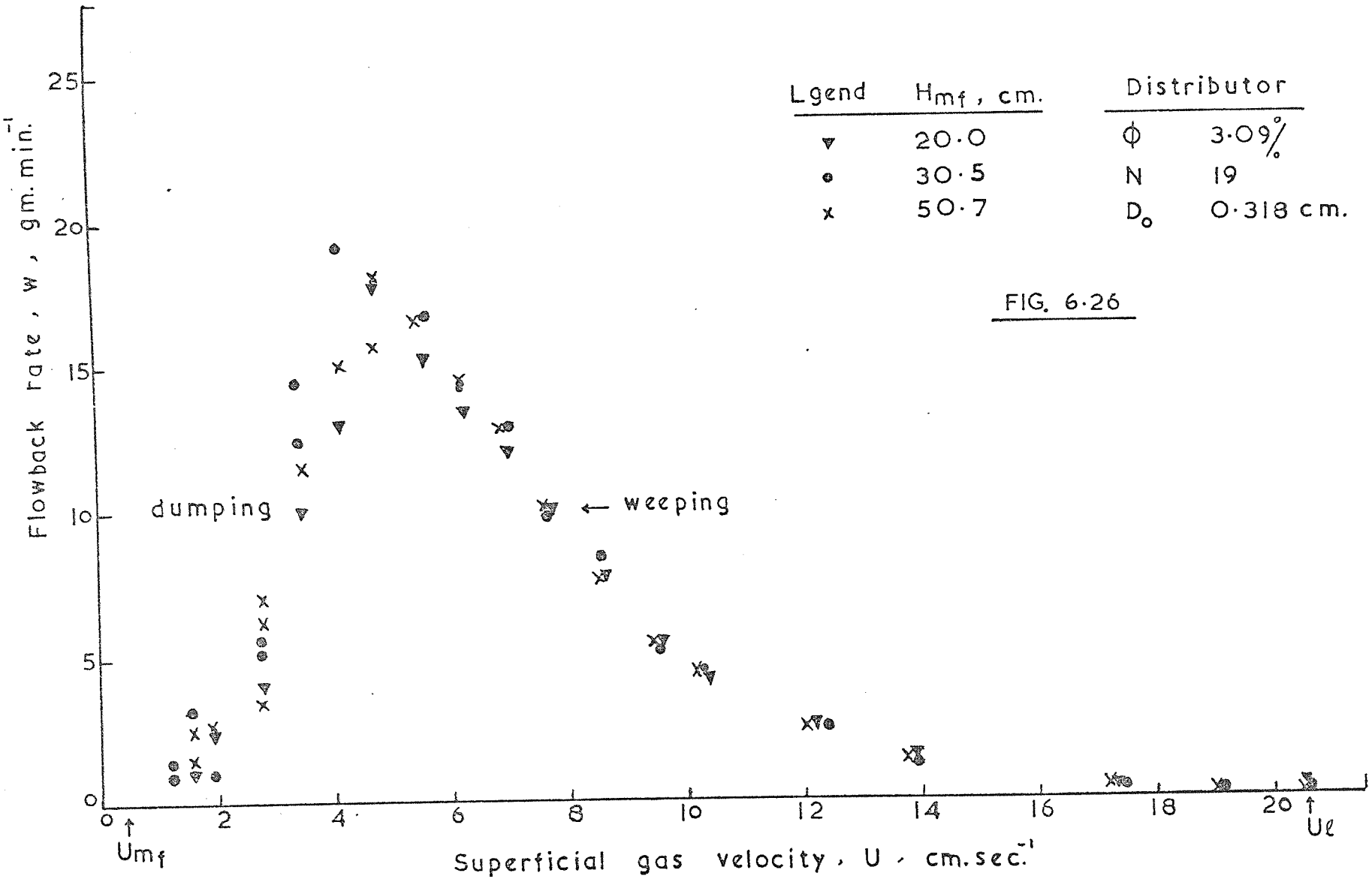

FIG. 6·26

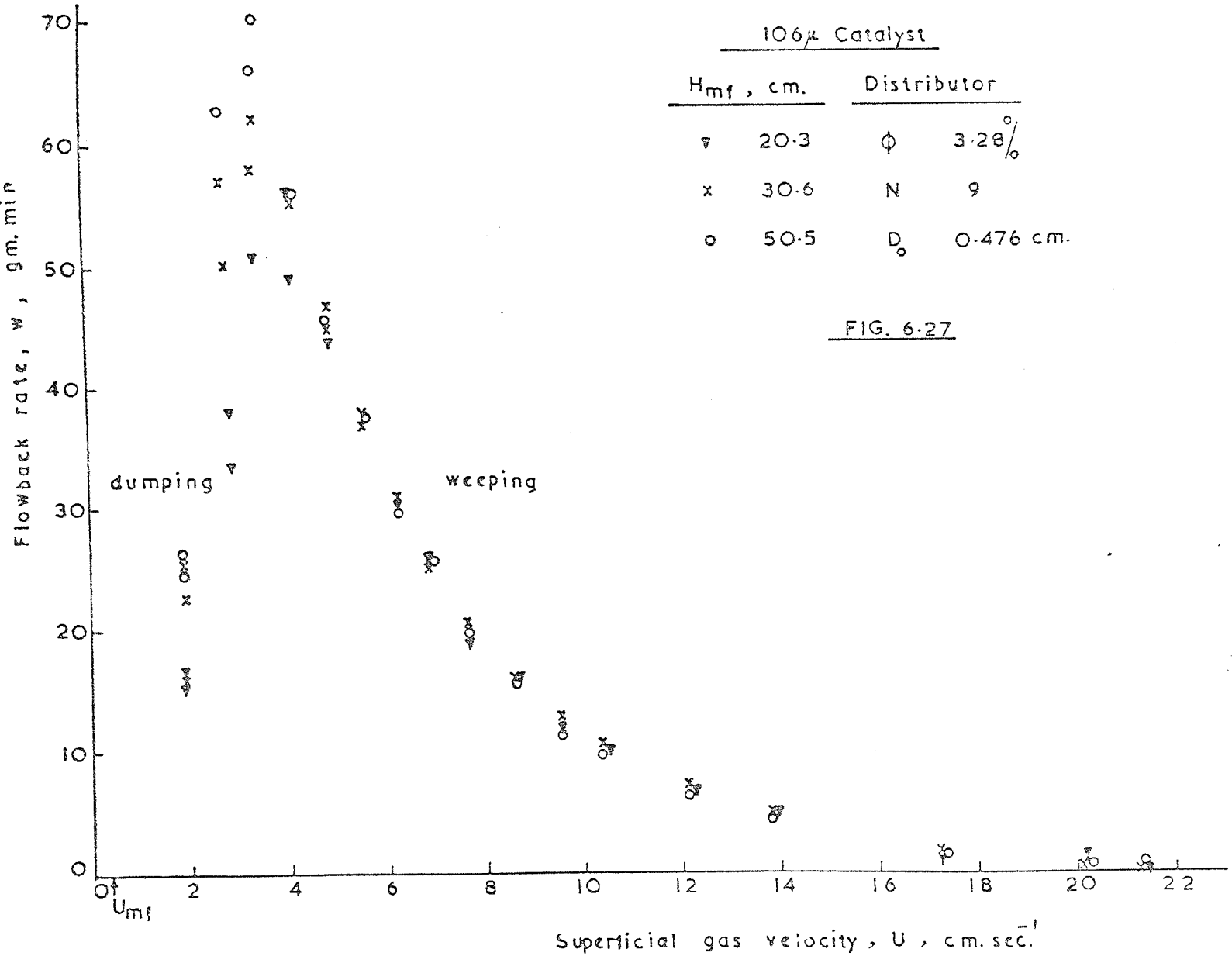
106μ Catalyst
Hmf , cm. Distributor
20·3 Φ 3·28%
30·6 N 9
50·5 D₀ 0·476 cm.
dumping
weeping
Flowback rate, W , gm. min⁻¹
Superficial gas velocity , U , cm. sec⁻¹
Umf
0
10
20
30
40
50
60
70
2
4
6
8
10
12
14
16
18
20
22

FIG. 6·27

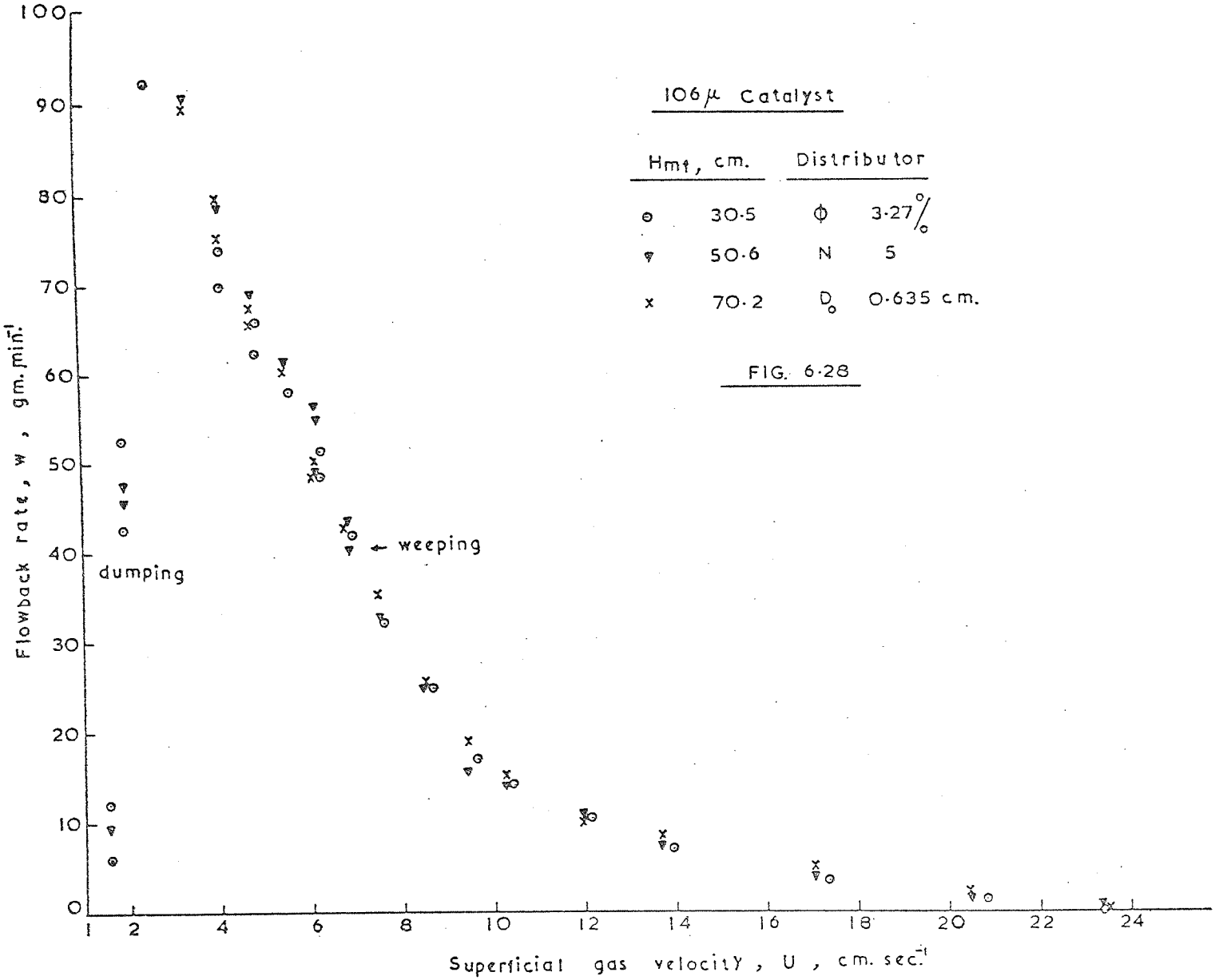
106μ Catalyst
Hmf, cm.
Distributor
30·5
Φ 3·27%
50·6
N 5
70·2
D₀ 0·635 cm.
dumping
weeping
Flowback rate, w, gm.min⁻¹
Superficial gas velocity, U, cm. sec⁻¹
0
10
20
30
40
50
60
70
80
90
100
1
2
4
6
8
10
12
14
16
18
20
22
24

FIG. 6·28

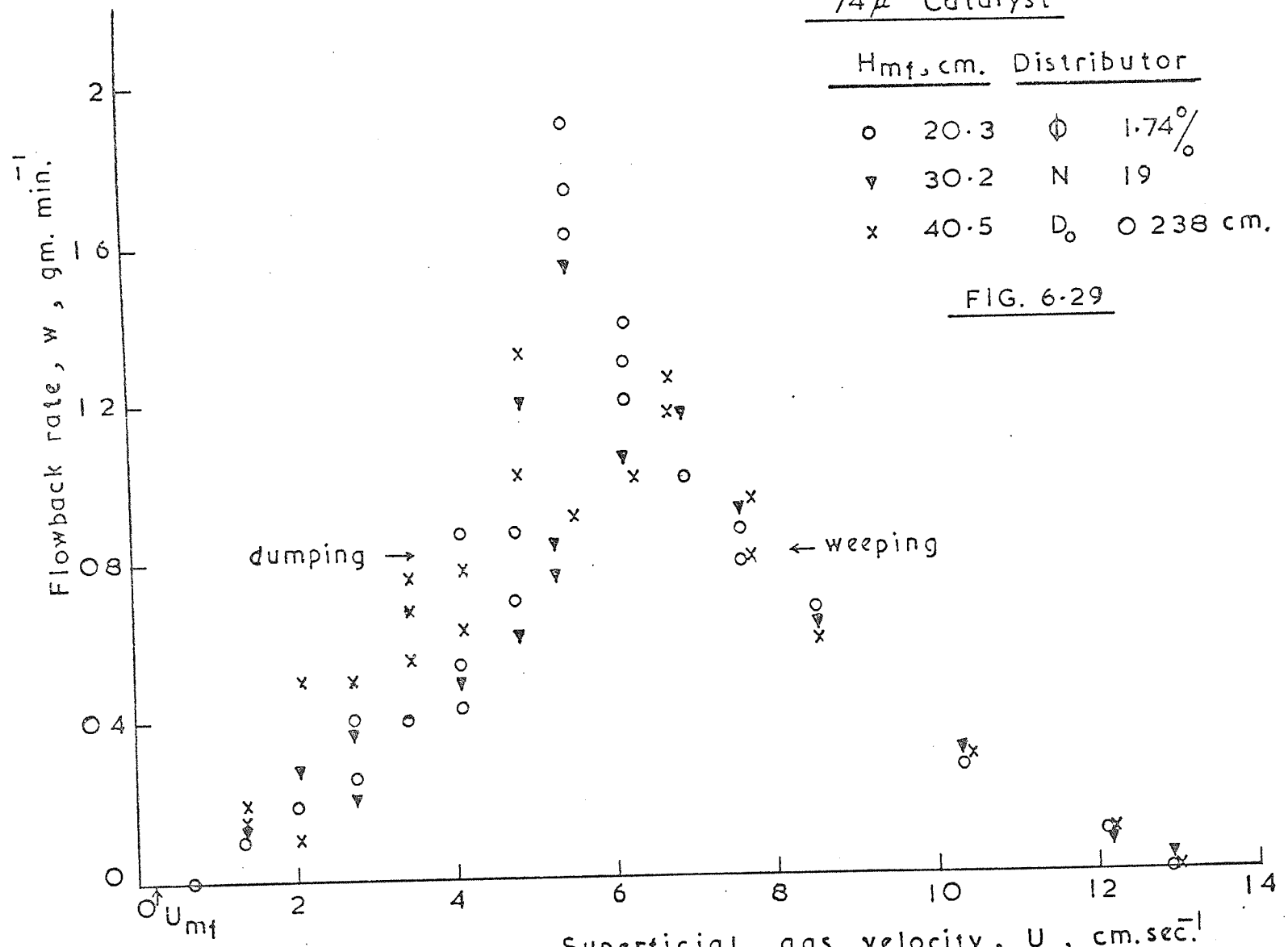
74μ Catalyst
Hmf, cm. Distributor
o 20·3 Φ 1·74%
▼ 30·2 N 19
x 40·5 Do 0 238 cm.
FIG. 6·29
Flowback rate, w, gm. min.⁻¹
dumping →
← weeping
Umf
Superficial gas velocity, U, cm.sec.⁻¹
0
0·4
0·8
1·2
1·6
2
2
4
6
8
10
12
14

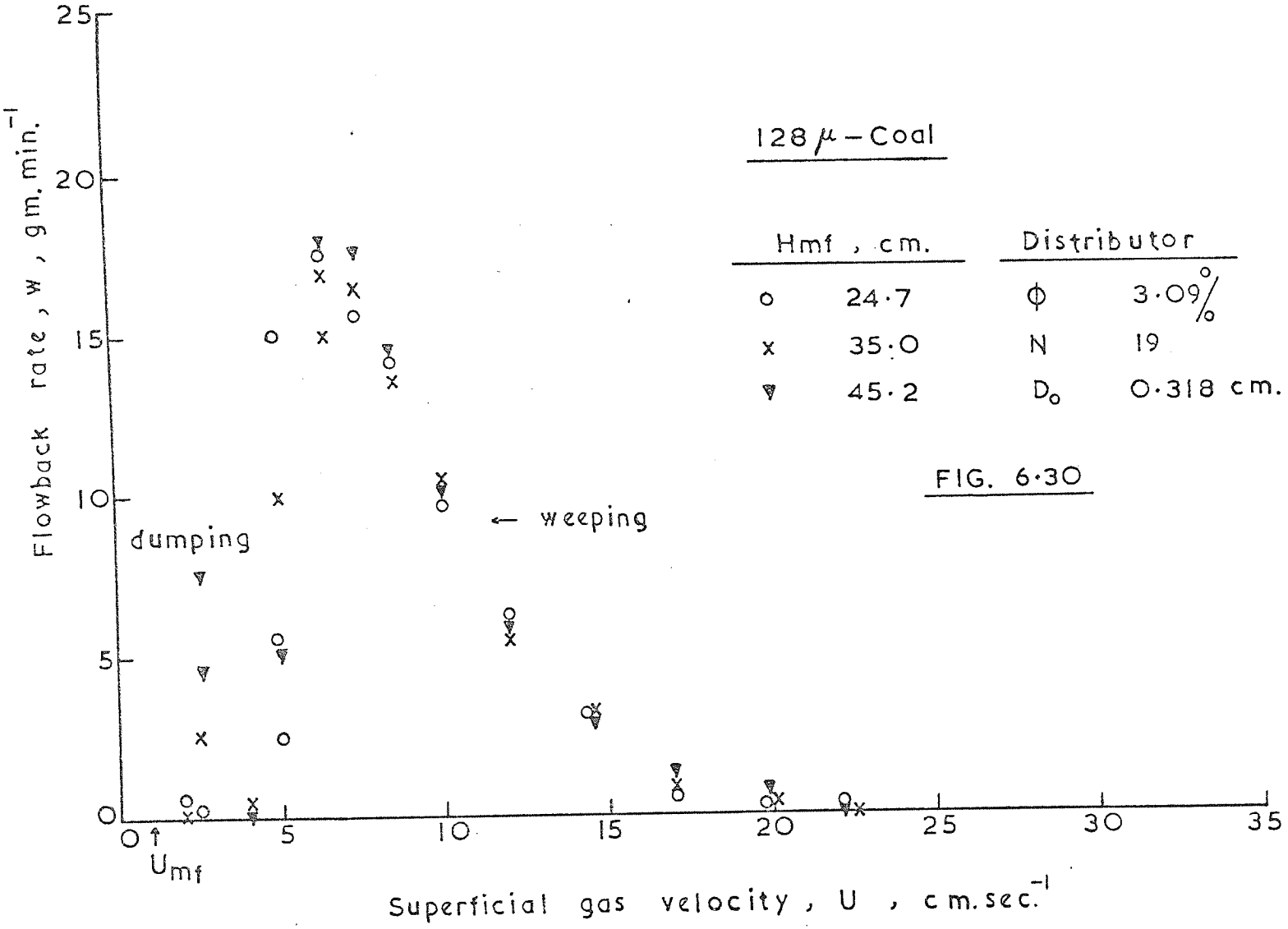
128 μ – Coal
Hmf , cm.
o 24·7
x 35·0
▼ 45·2
Distributor
ϕ 3·09°/°
N 19
D₀ 0·318 cm.
FIG. 6·30
Flowback rate , w , gm. min.⁻¹
dumping
← weeping
Umf
Superficial gas velocity , U , cm. sec.⁻¹
0
5
10
15
20
25
30
35

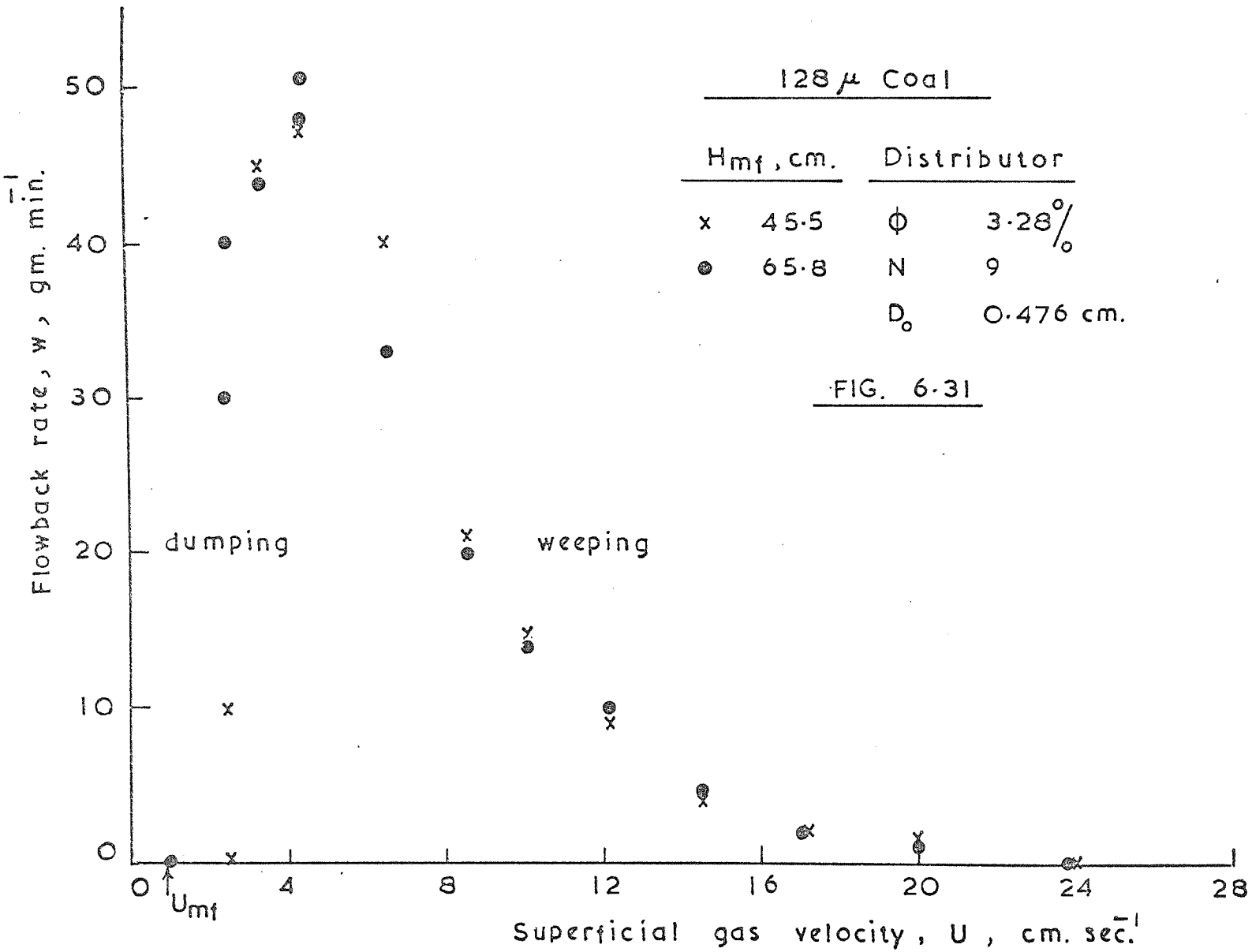
128 μ Coal
Hmf, cm.
Distributor
x 45·5
● 65·8
ϕ 3·28%
N 9
D₀ 0·476 cm.
FIG. 6·31
Flowback rate, w, gm. min.⁻¹
dumping
weeping
Umf
Superficial gas velocity, U, cm. sec.⁻¹
0
10
20
30
40
50
0
4
8
12
16
20
24
28

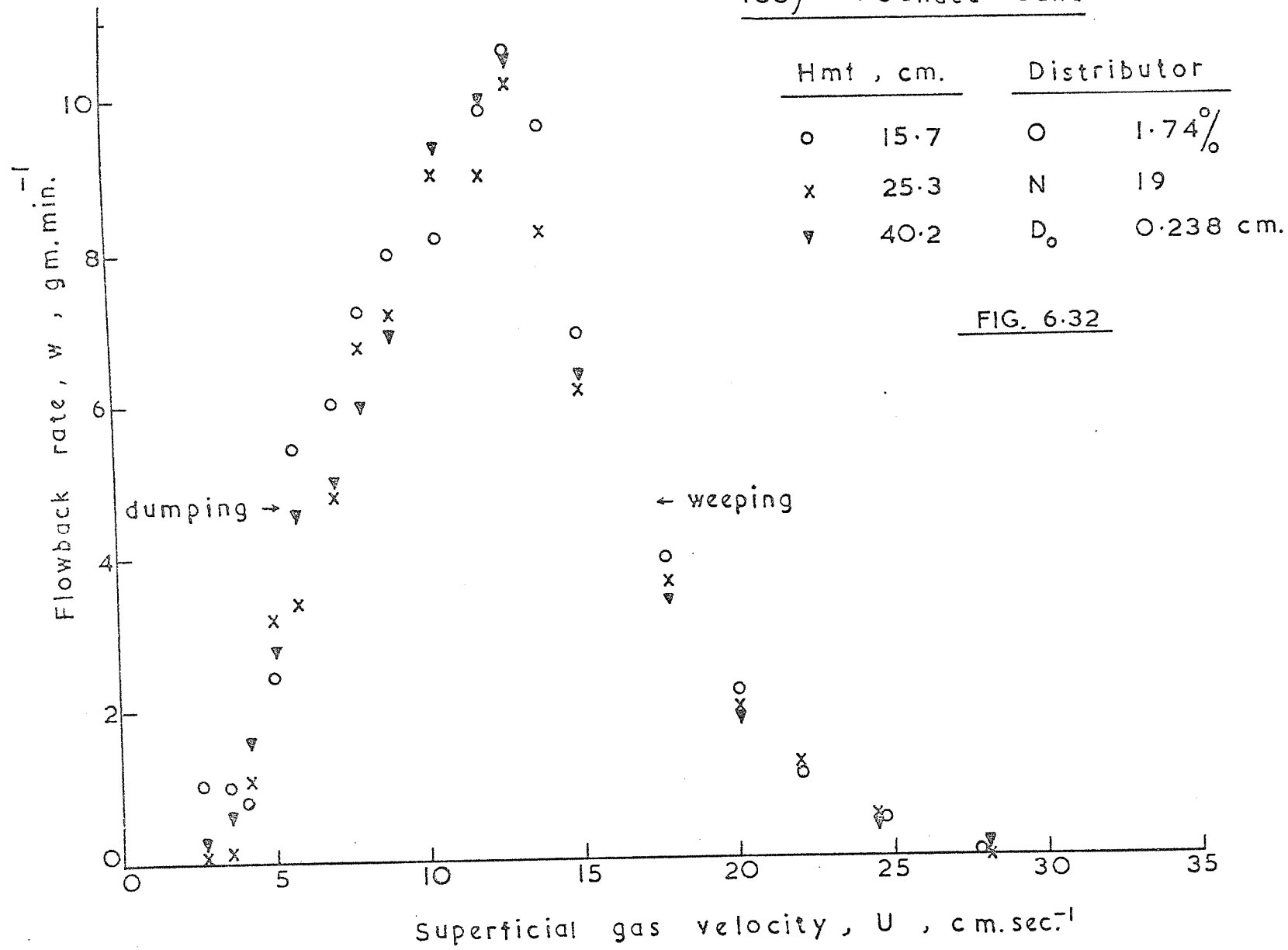
138 μ – Rounded Sand
Hmf , cm.
Distributor
o 15·7 O 1·74%
x 25·3 N 19
▼ 40·2 D_o 0·238 cm.
dumping →
← weeping
Flowback rate , w , gm.min.$^{-1}$
Superficial gas velocity , U , cm.sec.$^{-1}$
0
2
4
6
8
10
0
5
10
15
20
25
30
35

FIG. 6·32

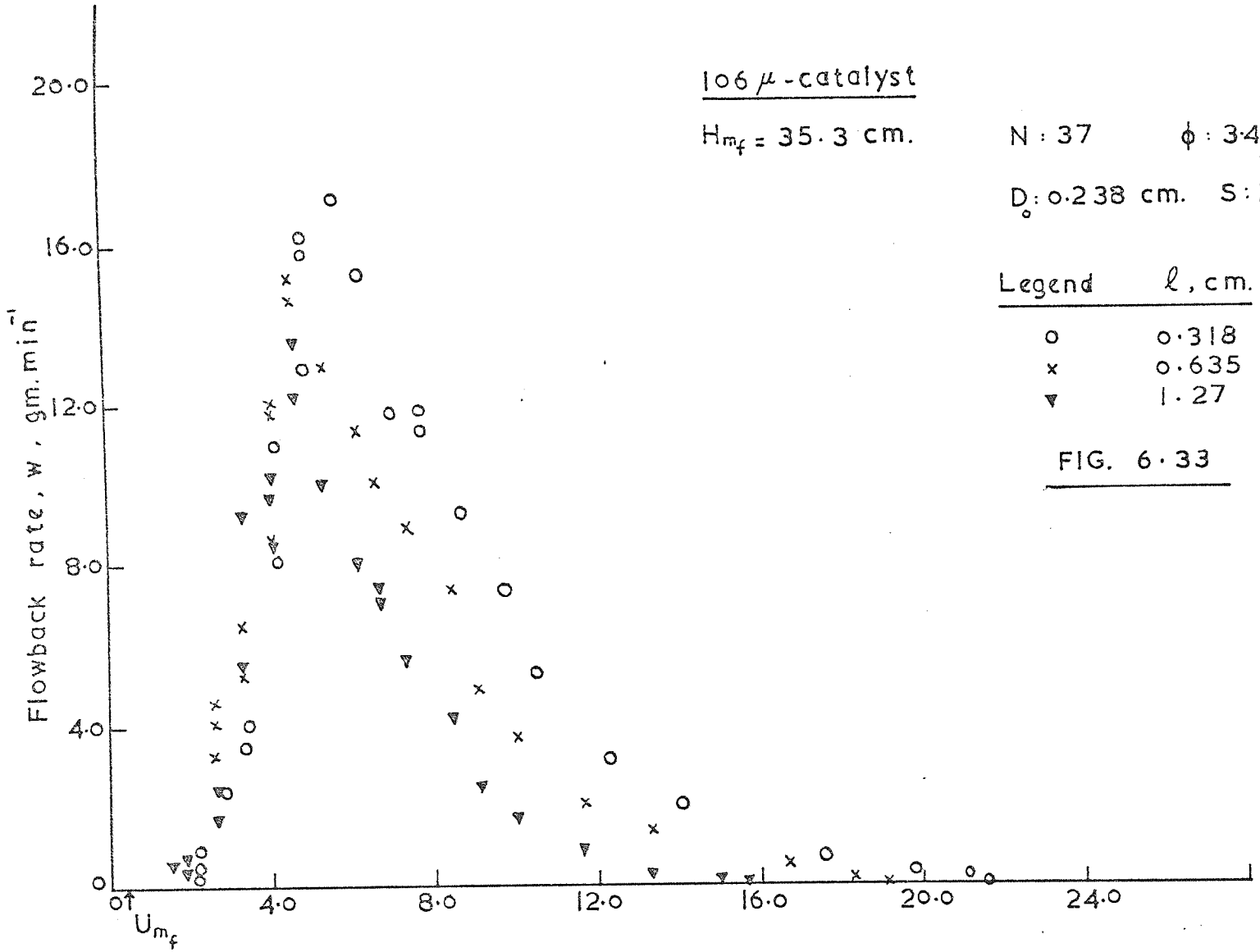
106 μ-catalyst
H_{m_f} = 35.3 cm.
N : 37
ϕ : 3.4%
D_o : 0.238 cm.
S : 1.18 cm.
Legend
ℓ, cm.
o 0.318
× 0.635
▼ 1.27
FIG. 6.33
Flowback rate, W, gm.min⁻¹
Superficial gas velocity, U, cm.sec⁻¹
U_{m_f}
0
4.0
8.0
12.0
16.0
20.0
24.0

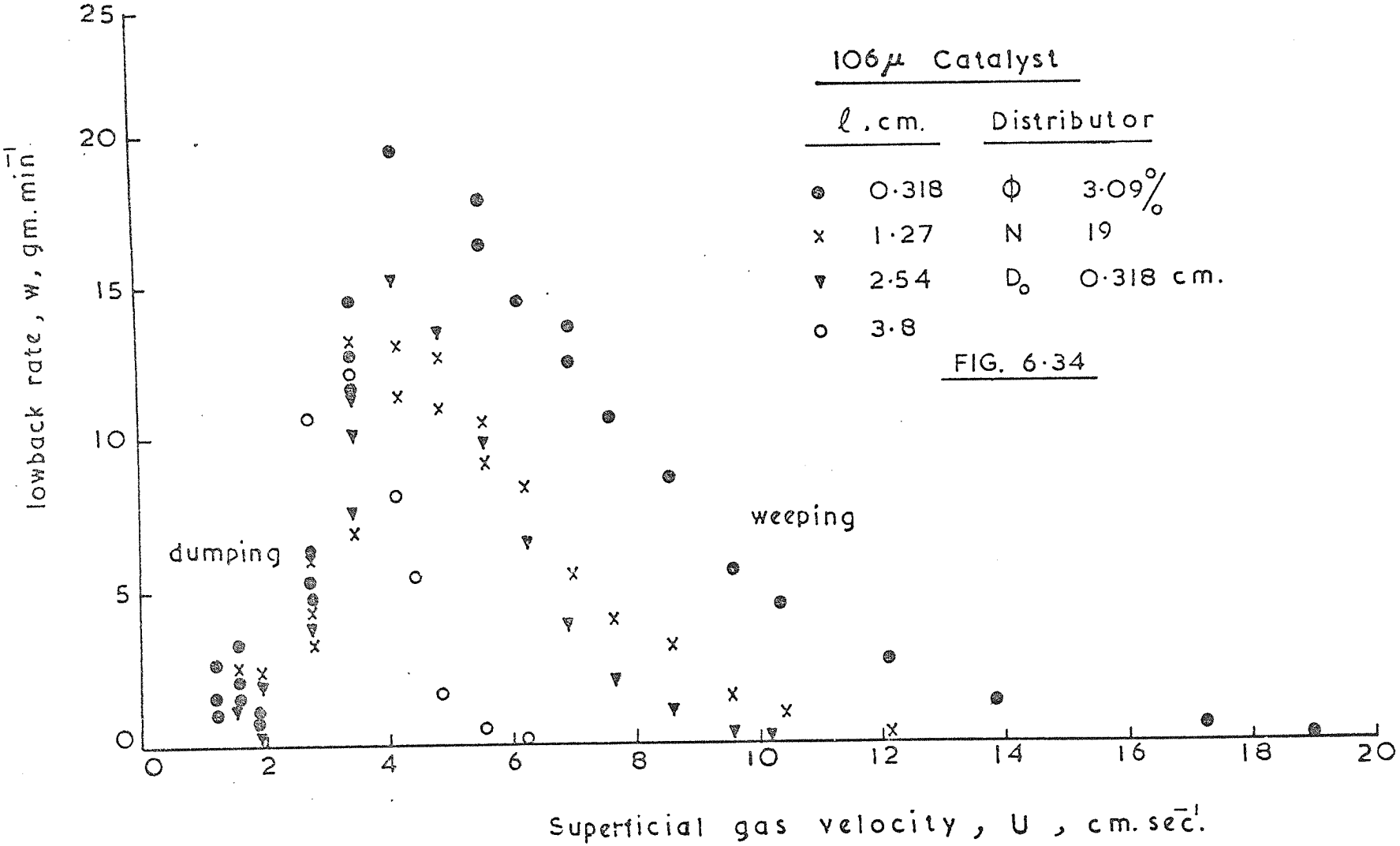
106μ Catalyst
ℓ , cm.
Distributor
0·318
Φ 3·09%
1·27
N 19
2·54
D_o 0·318 cm.
3·8
FIG. 6·34
dumping
weeping
lowback rate , w , gm. min⁻¹
Superficial gas velocity , U , cm. sec⁻¹
0
2
4
6
8
10
12
14
16
18
20
5
15
25

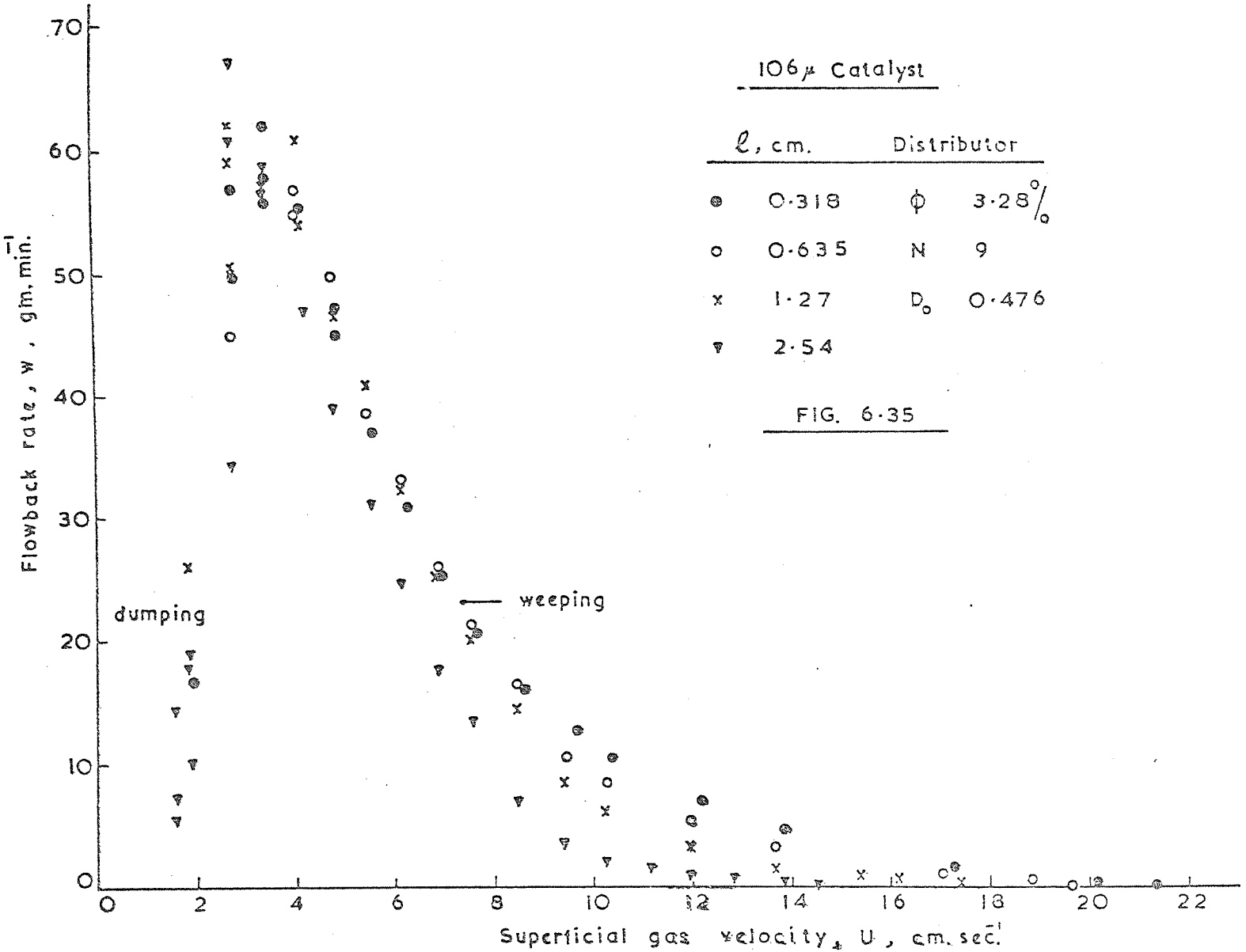
106μ Catalyst
ℓ, cm.
Distributor
0·318
ϕ 3·28%
0·635
N 9
1·27
D₀ 0·476
2·54
FIG. 6·35
Flowback rate, W, gm. min.⁻¹
dumping
weeping
Superficial gas velocity, U, cm. sec.⁻¹
0
2
4
6
8
10
12
14
16
18
20
22
10
20
30
40
50
60
70

FIG. 6·36 EFFECT OF WIND BOX VOLUME.

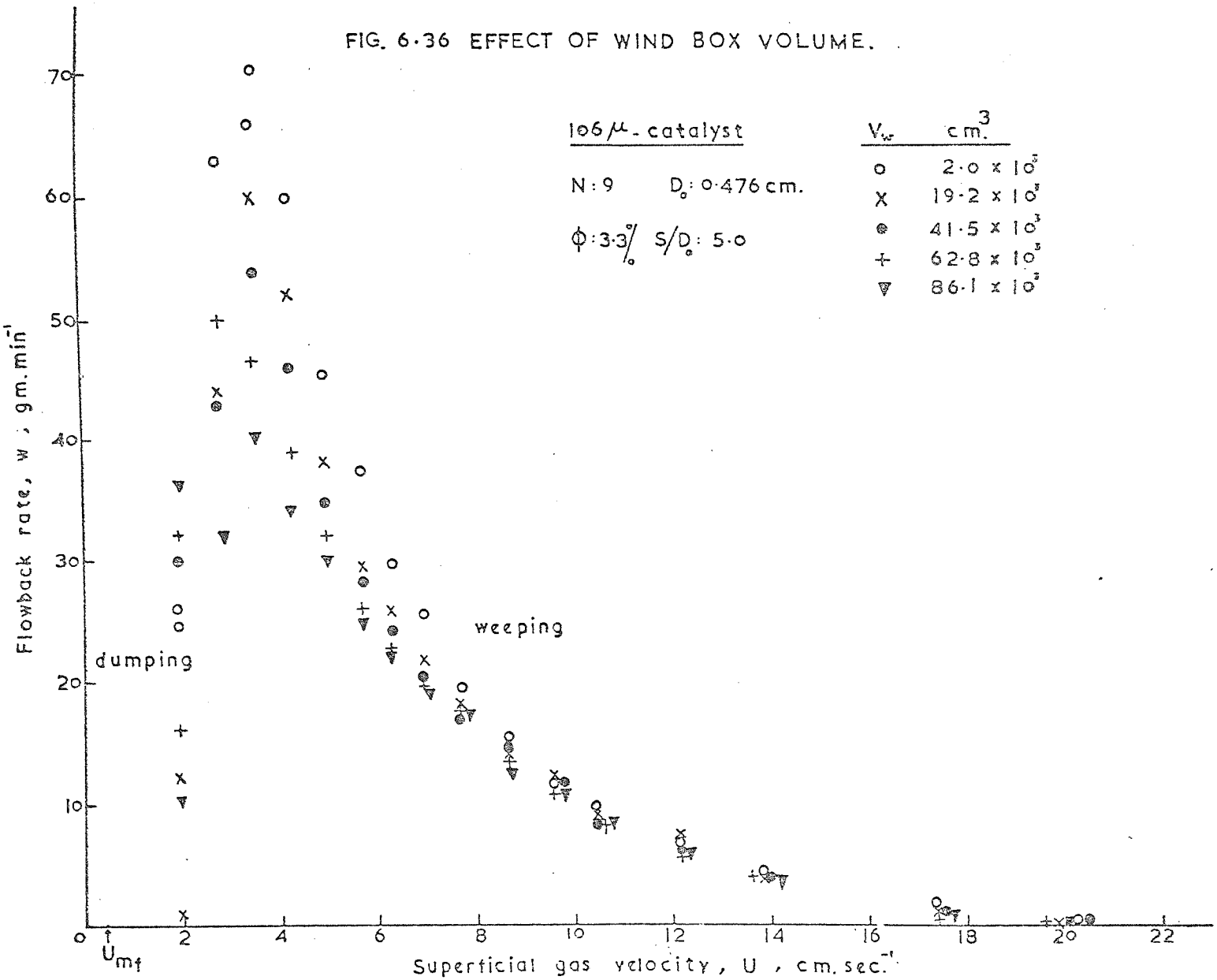

6.11.6 Criterion for the Prevention of Solids Flowback

The following work is an experimental programme aimed at establishing a criterion which can be used to predict the minimum gas flow rate for the prevention of solids flowback (or weeping) through a multi-orifice distributor of a given design.

The gas velocity in the distributor orifices at which solid particles cease entirely to drop through (the limiting orifice gas velocity $U\ell_o$) is, in the general case, determined by the physical properties of the gas (density ρ_g, viscosity μ_g) and of the solid particles (particle diameter D_p, particle density ρ_s, shape factor λ_s), distributor design (orifice diameter D_o, relative free area ϕ, orifice spacing S, plate thickness ℓ), and by the acceleration due to gravity g.

The experimental study of flowback with single and multi-orifice distributors has shown that the depth of the bed and the wind box volume have virtually no effect on the limiting velocity. The shape factor λ_s cannot be varied significantly and, therefore, as with gravity flow the bulk density of the solid phase ρ_B would be the relevant variable in the problem. However, the influence of the shape factor finds expression more or less in the values of ρ_B and D_p, so that it is admissible to drop the shape factor. Therefore,

$$U\ell_o = f(D_o, S, \ell, \rho_g, \mu_g, D_p, \rho_B, g, \phi) \qquad (6.26)$$

Equation (6.26) contains nine dimensional quantities and one dimensionless quantity ϕ, with three principal dimensional units. By similarity theory, the number of dimensionless groups determining the given effect is therefore $1 + 9 - 3 = 7$. Dimensional analysis may be used to arrive at the groups relevant to the problem. See Appendix A6 for detailed account. Evidently one of the required groups is the

Reynolds number for gas flow in the distributor orifices, i.e.

$$Re_{\ell im} = \frac{U\ell_o \rho_g D_o}{\mu_g} \qquad (6.27)$$

The other groups, found by dimensional analysis, may be

$$\frac{\rho_B - \rho_g}{\rho_g} \;,\; \frac{D_o}{D_p} \;,\; \frac{\ell}{D_o} \;,\; \frac{S}{D_o} \;,\; \frac{D_p^3 . \rho_g^2 . g}{\mu_g^2}$$

The number of dimensionless groups can be reduced. We can write

$$\frac{\rho_B - \rho_g}{\rho_g} \cdot \frac{D_p^3 . \ell_g^2 . g}{\mu_g^2} = Ar \;, \qquad (6.28)$$

where Ar is the Archimedes number.

The final criterion form of (6.26) is therefore

$$Re_{\ell im} = \text{const} \left[Ar^a . \left(\frac{D_o}{D_p}\right)^b . \left(\frac{\ell}{D_o}\right)^c . \left(\frac{S}{D_o}\right)^d . \phi^e \right] \qquad (6.29)$$

The inclusion of some of the physical parameters requires explanation. The acceleration due to gravity g will in part determine the rate of falling particles through the orifices and hence, as with gravity flow, is relevant. The effect of the physical properties of gas and solid is linked with the drag forces acting on the falling particles. The Archimedes group which includes these variables is commonly known as the particle Reynolds number (based on the particle free-fall velocity). The Archimedes number could be written as

$$Ar = 18\, Re \quad \text{for } Re \leqslant 1, \left(C_D = \frac{24}{Re} \right) \text{ (Stoke's law)} \;, \qquad (6.30)$$

$$Ar = \frac{1}{3} Re^2 \quad \text{for } Re \geqslant 1000, \left(C_D = 0.44 \right) \text{ (Newton's law)} \;, \qquad (6.31)$$

where R_e is the Reynolds number based on the particle free-fall velocity

$Ut\ (\frac{Ut\ \rho_g\ D_p}{\mu_g})$ and C_D is the single particle drag coefficient.

The effect of gas density on the limiting superficial velocity is shown in Figure (6.37a). Different gases were used to change the density. Cracking catalyst (106 μ) was used as the solid. The distributors were multi-orifice plates having the same orifice diameter (D_o = 0.238 cm) but different free areas. It is clear that the limiting gas velocity increases with decrease in the gas density for a given free area. This also explains the effect of the plate free area on the limiting superficial gas velocity. The linear dependence of $U\ell$ on ϕ confirms that the limiting gas velocity through the distributor orifices $U\ell_o$ is independent of ϕ. Thus the limiting Reynolds number $Re_{\ell im}$ is also independent of ϕ.

The effect of solid density is shown in Figure (6.37b). The distributors with 0.238 cm. diameter orifices were again used. Air was used as the gas. For solids of high density the limiting superficial gas velocity is greater and, therefore, the limiting orifice velocity must be greater. Figure (6.37b) also shows that the limiting superficial gas velocity is a linear function of ϕ. This is consistent with the measurements reported on Figure (6.37a). An inspection of Figure (6.37b) reveals that glass is exhibiting lower values than rounded sand. Although glass has a smaller mean particle diameter, the result was to some extent unexpected, since glass is spherical and more dense than sand. Spherical particles, in particular, are more flowable than non-spherical particles, because they can slip easier. Dense particles would, obviously, fall at a greater rate than light particles. The reason for this discrepancy is presumably due to the jamming of some of the distributor orifices caused solely by static effects in the bed. Visual observations confirmed this. The

development of static charges in the bed was particularly serious with glass beads. Consequently, few experiments were carried out with it.

Some of the geometrical variables in (6.29) are interrelated. For example, for a given orifice diameter D_o the relative free area ϕ is determined by the orifice spacing S. In fact, the free area, the orifice spacing and the orifice diameter are the geometrical variables which do not act independently as far as the surface geometry of the distributor is concerned. As it has been evidenced already, the limiting orifice velocity $U\ell_o$ is not a function of both ϕ and D_o (i.e. $Re_{\ell im}$ is independent of ϕ). Therefore, S can be expected to have no effect on $U\ell_o$. The evidence of this may be seen from Table (6.31) which shows that for a given orifice diameter, the limiting Reynolds number $Re_{\ell im}$ is practically independent of S/D_o. Hence it seems probable that the dimensionless groups ϕ and S/D_o are not significant variables over the wide range of experimental conditions studied (see tables of experimental results). Hence equation (6.29) yields

$$Re_{\ell im} = \text{const} \left[\left(\frac{\rho_B - \rho_g}{\rho_g} \cdot \frac{D_p^3 . \rho_g^2 . g}{\mu_g^2} \right)^a \left(\frac{D_o}{D_p} \right)^b \left(\frac{\ell}{D_o} \right)^c \right] \qquad (6.32)$$

To arrive at the final form of (6.32), about 70 tests were carried out using different gases and solids with distributors of various design (including multi-nozzle distributors). The distributors involved in the tests had Reynolds numbers $Re_{\ell im}$ in the range $0.4 \times 10^3 - 9 \times 10^3$. Archimedes numbers Ar were in the range 3 - 310. It will be shown later that for stability reasons ℓ/D_o should be within the range 0.5 - 12.0.

As explained earlier, data obtained from the single-orifice studies are considerably lower than those obtained with multi-orifice distributors. A comparison of $U\ell_o$ values (cm./sec.) observed with single and

multi-orifice distributors for some of the solids tested is as follows:

Solid	Single-orifice plate	Multi-orifice plate
138 μ - rounded sand	525	1560
128 μ - coal	148	710
106 μ - cracking catalyst	250	650 - 720

The difference is clearly evident and therefore only data from experiments with multi-orifice distributors will be used in establishing the final form of (6.32) as, of course, a multi-orifice distributor is more relevant than a single-orifice distributor.

With the number of experimental data available (see Table (6.32)), equation (6.32) was programmed for a computer analysis so that the best values of the exponents a, b and c could be found. A multiple regression analysis program was used. This program minimized the square of the error between the dependent variable (always $Re_{\ell im}$) and the collection of groups being used to correlate the dependent variable.

The functional relationship between $Re_{\ell im}$ and each of the dimensionless groups are shown in Figures (6.38) - (6.40). In Figure (6.40), $U\ell_o$ is plotted against ℓ/D_o instead of $Re_{\ell im}$ on a semi-log scale to show how increases in ℓ/D_o bring about decreases in the limiting orifice velocities. It can be seen that $U\ell_o$ decreases exponentially with ℓ/D_o and it is true with all solids tested. However, this decrease can only be achieved within the range $0.5 \leqslant \ell/D_o \leqslant 12$. As it has been indicated already, uncontrollable downflow of solids has been observed mostly with ratios higher than 12. With very thin distributor plates (i.e. $\ell/D_o < 0.5$) solids flowback was observed to persist to a considerably

higher gas ratio. The deviation of the experimental data from "least squares" lines drawn in Figure (6.40) is indicative of the behaviour observed with ratios $\ell/D_o < 0.5$. This, of course, is undesirable and therefore operation of a fluidized bed with thin distributor plates should be avoided. Thus, the proposed correlation will be valid only for distributors within the range $0.5 \leqslant \ell/D_o \leqslant 12.0$ where controllable downflow of solids can be achieved.

The best values for the exponents in (6.32), as obtained by computer analysis, are

$$a = 0.43 \qquad b = 0.87 \qquad c = -0.27$$

In Figure (6.41) $Re_{\ell im}$ is plotted against

$$\left(\frac{D_o}{D_p}\right)^{0.87} \cdot \left(\frac{\ell}{D_o}\right)^{-0.27} \cdot \left(\frac{\rho_B - \rho_g}{\rho_g} \cdot \frac{D_p^3 \cdot \rho_g^2 \cdot \rho_g}{\mu_g^2}\right)^{0.43}$$

on a logarithmic base and the linear relationship produced the equation:

$$\frac{U\ell_o \cdot \rho_g \cdot D_o}{\mu_g} = 21.8 \left(\frac{D_o}{D_p}\right)^{0.87} \cdot \left(\frac{\ell}{D_o}\right)^{-0.27} \cdot \left(\frac{\rho_B - \rho_g}{\rho_g} \frac{D_p^3 \cdot \rho_g^2 \cdot g}{\mu_g^2}\right)^{0.43}, \qquad (6.33)$$

$$\text{for } 0.5 \leqslant \ell/D_o \leqslant 12.0$$

Equation (6.33) and the experimental data are shown in Figure (6.41). More than 90% of all the data lies within $\pm$ 25% of values predicted by equation (6.33) which may seem high but leads to estimate that, probably, it is adequate for practical purposes.

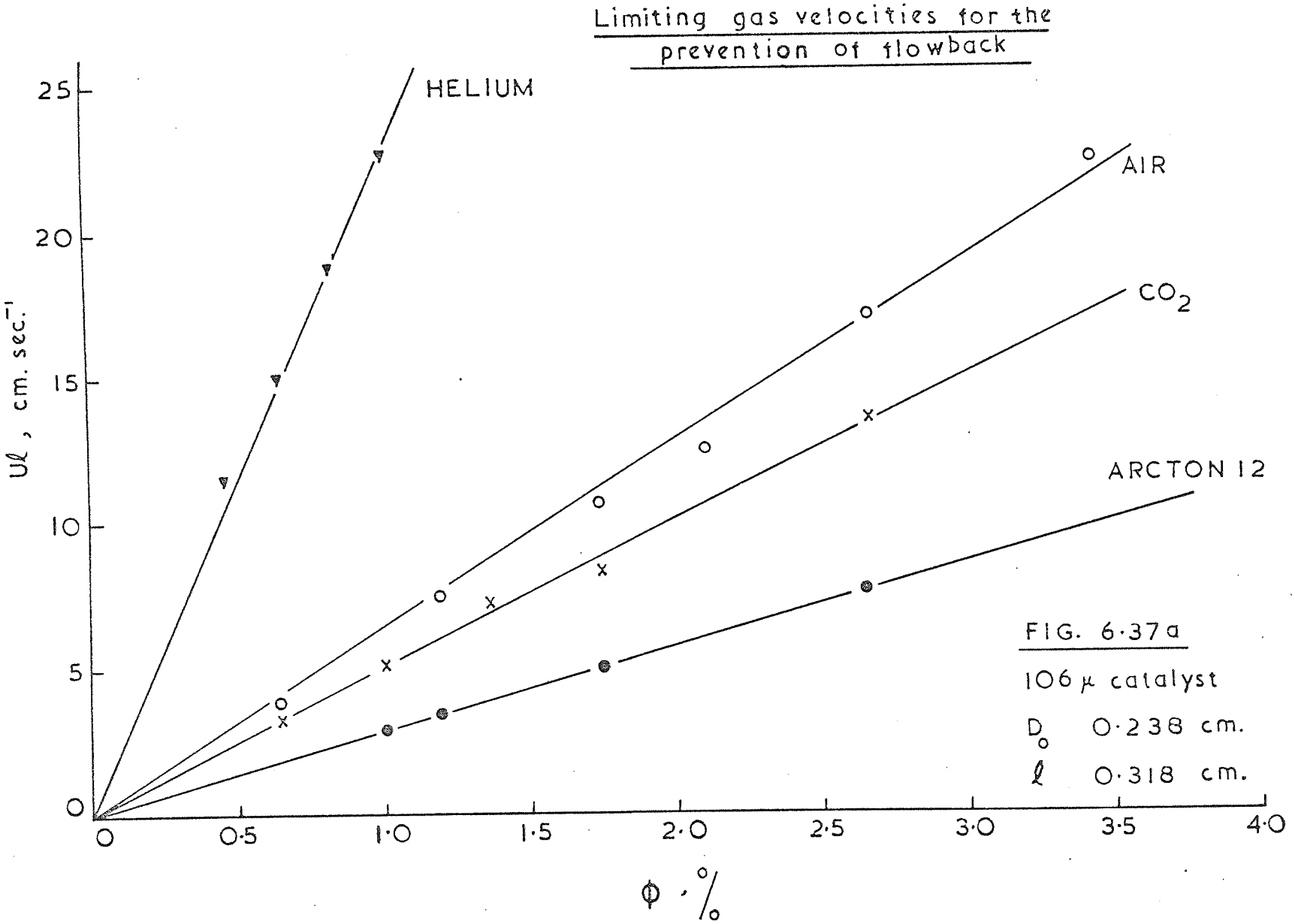

FIG. 6·37a

106 μ catalyst

D_o 0·238 cm.

l 0·318 cm.

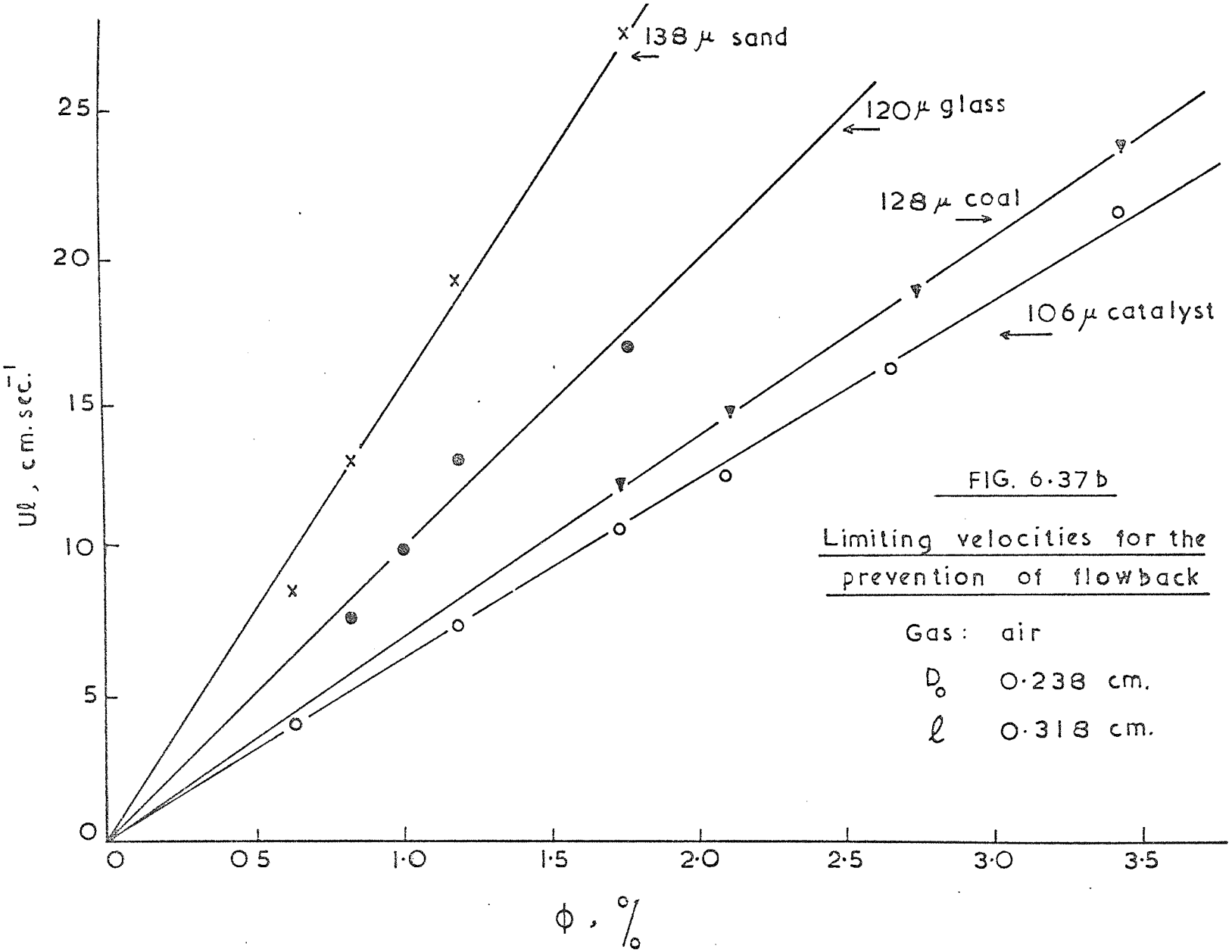

FIG. 6·37 b

Limiting velocities for the prevention of flowback

Gas : air

D_o 0·238 cm.

ℓ 0·318 cm.

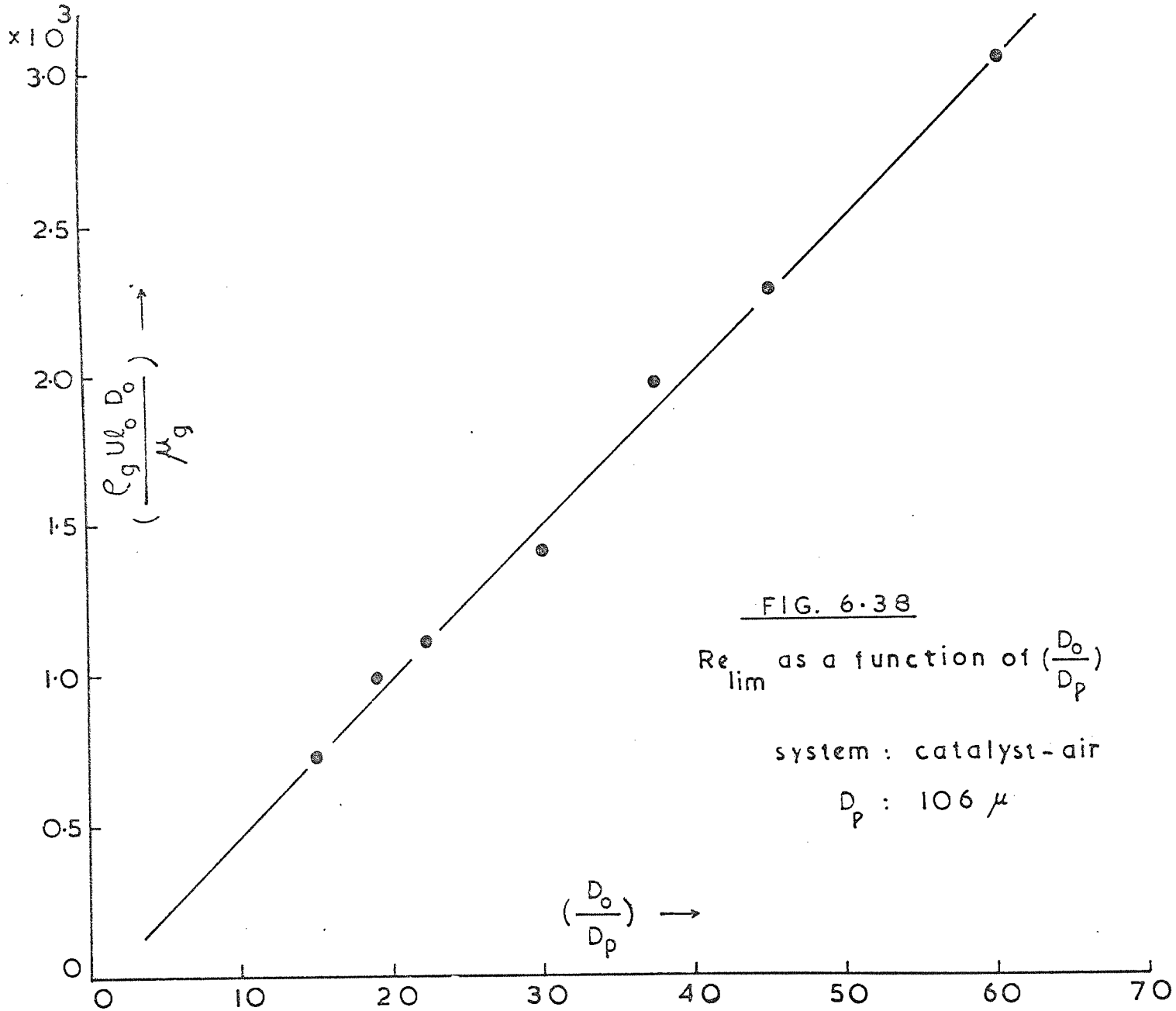

FIG. 6·38

Re_{lim} as a function of $(\frac{D_o}{D_p})$

system : catalyst - air

D_p : 106 μ

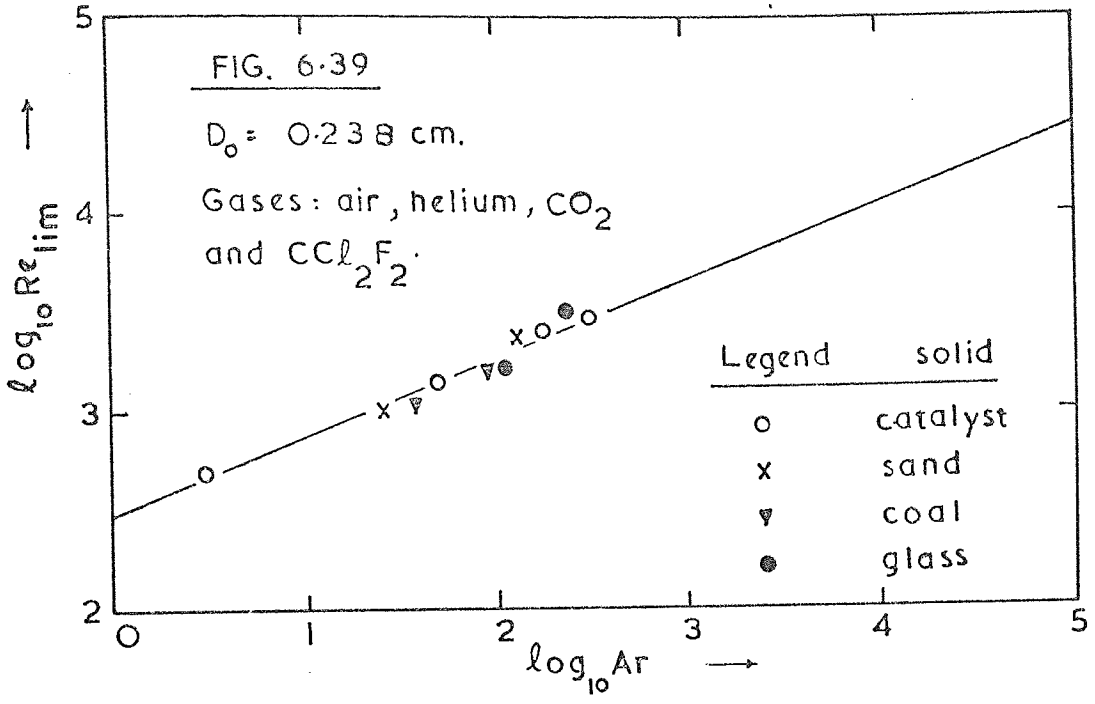
FIG. 6·39
D_o = 0·238 cm.
Gases : air, helium, CO_2 and CCl_2F_2.
Legend solid
o catalyst
x sand
coal
glass
$\log_{10} Re_{lim}$
$\log_{10} Ar$

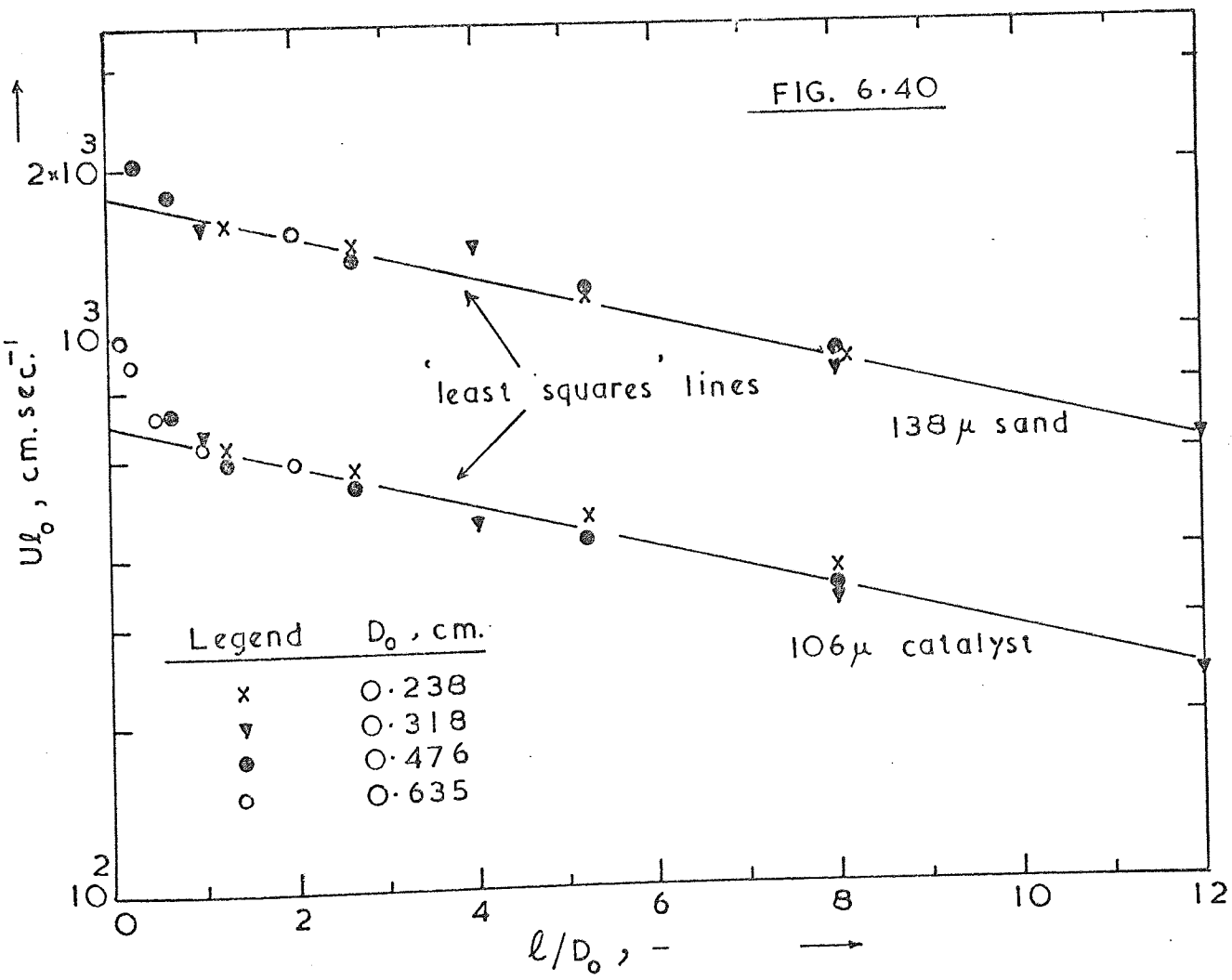
FIG. 6·40
Ul_o, cm.sec.$^{-1}$
'least squares' lines
138 μ sand
106 μ catalyst
Legend D_o, cm.
0·238
0·318
0·476
0·635
l/D_o, –

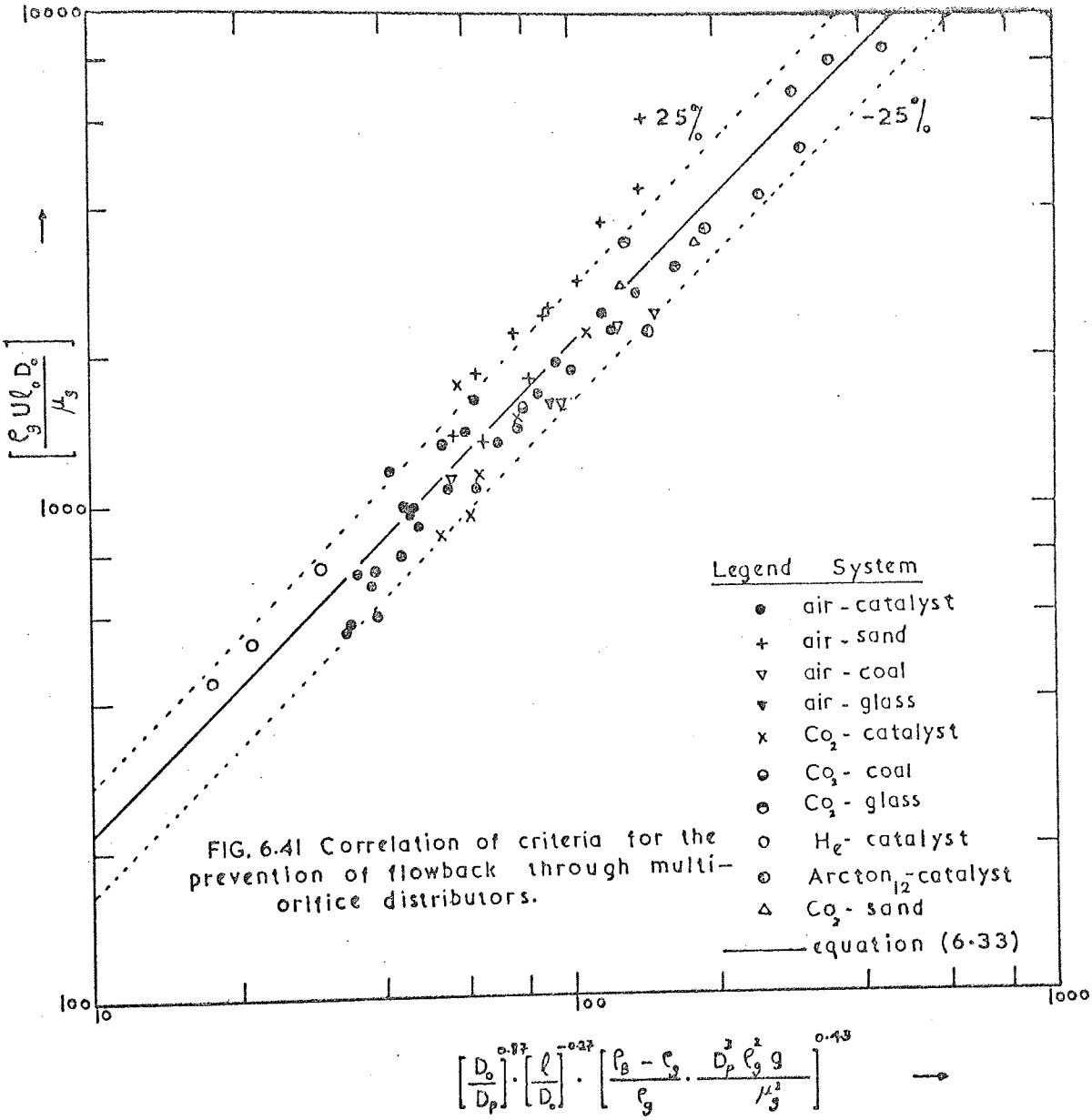

FIG. 6.41 Correlation of criteria for the prevention of flowback through multi-orifice distributors.

6.11.7 Correlation of Weepage Data

This correlation permits calculation of flowback rates when operating multi-orifice distributors in the weeping regime. Normally one would choose to design at some point well above the flowback range so that reduced load operation would also still fall above this range. However, there exist instances in which pressure drop considerations or the need to prevent excessive entrainment force the design point to be quite close to the weeping regime and partial load operation can fall into the weeping regime. An operation in the dumping regime is evidently undesirable and should be avoided.

6.11.7.1 Formulation of the Proposed Correlation

With a gas flowing through the distributor orifices, solids flowback depends on the distributor design, the properties of solid particles, and the characteristics of the gas stream. The effect of the wind box volume may be neglected. If the flowback flux ω_o (i.e. flowback rate ω divided by the total area of the orifices in the distributor) is expressed as a fraction of the maximum flux W_o, then we have

$$\frac{\omega_o}{W_o} = f(U\ell_o \ , \ U_{op}) \ , \tag{6.34}$$

where $W_o = W/A_e$ is the flux due to gravity flow (see equations (6.19) - (6.20)); $U_{op} = U_o + U_p$ is the gas velocity in the distributor orifices relative to particles falling with velocity U_p.

It can be easily shown by dimensional analysis that the effect is determined by two dimensionless groups; one is ω_o/W_o and the other follows from the evident consideration that flowback flux , in the weeping regime, increases with decrease $U_{op} = U_o + U_p$, i.e. with increase of the difference $U\ell_o - (U_o + U_p)$. Therefore the second

dimensionless group is

$$\frac{U\ell_o - U_{op}}{U_{op}} = \frac{U\ell_o - (U_o - U_p)}{(U_o + U_p)}$$

and then

$$\frac{\omega_o}{W_o} = a\left[\frac{U\ell_o - (U_o + U_p)}{U_o + U_p}\right]^b \qquad (6.35)$$

Since the falling velocity of the particles in the distributor orifices is not large, at gas velocities differing considerably from zero (as in this investigation) we may write with adequate accuracy

$$\frac{U\ell_o - U_o + U_p}{U_o + U_p} = \frac{U\ell_o - U_o}{U_o}$$

Then

$$\frac{\omega_o}{W_o} = a\left[\frac{U\ell_o - U_o}{U_o}\right]^b \qquad (6.36)$$

A preliminary plot of weepage data as $(\frac{\omega_o}{W_o})$ vs. $(\frac{U\ell_o - U_o}{U_o})$ on a logarithmic base produced a linear relationship from which we had $a = 8 \times 10^{-3}$ and $b = 1.42$. Therefore equation (6.35) becomes

$$\frac{\omega_o}{W_o} = 8 \times 10^{-3}\left[\frac{U\ell_o - (U_o + U_p)}{U_o + U_p}\right]^{1.42} \qquad (6.37)$$

Now it is possible to calculate U_p from (6.37) as follows:

In the absence of gas flow $U_o = 0$ and $\omega_o = W_o$, i.e.

$$1 = 8 \times 10^{-3} \left(\frac{U\ell_o - U_p}{U_p} \right)^{1.42}$$

and hence

$$U_p = \frac{U\ell_o}{31} \tag{6.38}$$

Substituting the expression for U_p into (6.37), we finally have

$$\omega_o = 8 \times 10^{-3} \; W_o \cdot \left[\frac{U\ell_o - (U_o + \frac{U\ell_o}{31})}{U_o + \frac{U\ell_o}{31}} \right]^{1.42} \tag{6.39}$$

It would appear that correlating the data in the way suggested by (6.35) is unsatisfactory as far as the boundary conditions are concerned. A more satisfactory correlation can be obtained if $\log_{10} (\frac{\omega_o}{W_o})$ is plotted against $(\frac{U_o}{U\ell_o - U_o})$. This follows from the evident consideration that the fractional flux (ω_o/W_o) decreases with increase of the ratio $(U_o/U\ell_o - U_o)$, i.e.

$$\log_{10} (\frac{\omega_o}{W_o}) = a \left(\frac{U_o}{U\ell_o - U_o} \right)^b \text{, with } U_p \sim 0, \tag{6.40}$$

where a is a negative coefficient.

As a large number of weepage data were available, equation (6.40) was programmed for computer analysis so that the best values of a and b could be obtained. For the later purpose, a non-linear regression analysis program was written in FORTRAN 4. The calculational procedure and the computer program can be found in Appendix A6. This program minimized the square of error between the dependent variable $\log_{10}(\frac{\omega_o}{W_o})$ and the group $(\frac{U_o}{U\ell_o - U_o})$. The best values for a and b were -1.91

and 0.4 respectively. Equation (6.40) then becomes

$$\log_{10} \left(\frac{\omega_o}{W_o}\right) = - 1.91 \left(\frac{U_o}{U\ell_o - U_o}\right)^{0.4} \qquad (6.41)$$

The boundary conditions are

$$\text{if} \quad U_o = 0 \quad , \omega_o = W_o \quad \text{(gravity flow)} \quad , \qquad (6.42)$$

$$\text{and} \qquad \text{if} \quad U_o = U\ell_o \quad , \omega_o = 0 \quad . \qquad (6.43)$$

Equation (6.41) and the experimental data are shown in Figure (6.42). A wider scatter exists at higher orifice velocities: this scatter is attributed to the less accurate measurement of flowback which in most cases is found to persist to a higher gas rate.

Two points concerning the results in Figure (6.42) must be commented on.

(i) In this work no information is available regarding gravity flow through deep orifices or nozzles. Brown and Richards(115) have shown that with orifices longer than 1 cm., the flow rate increases linearly with orifice length. However, Private communication(57) suggests that the flow is proportional to $\sqrt{\ell}$. Therefore, in order to avoid error in the correlation presented in Figure (6.42), we have excluded distributors thicker than 1.27 cm.(1/2"). Consequently, it is recommended that further work is necessary to examine the effect of plate thickness on gravity flow through multi-orifice plates.

(ii) The results of a series of air-solid experiments with multi-orifice distributors of various design have shown that the transition from the dumping regime to the weeping regime occurs at superficial

fluidizing velocities 4 - 8 times U_{mf} (typically at $U = 6\ U_{mf}$). It is, therefore suggested that equation (6.41) should be used to predict solids flowback through multi-orifice distributors only at fluidizing velocities $U \geqslant 6\ U_{mf}$.

It is not known whether this applies to all orifice sizes, especially larger than those employed in the present study (i.e. for $D_o > 0.635$ cm.). There appears, however, some evidence that plates with large orifices tend to move into the weeping regime more readily than plates with small orifices. Further work with wider range of orifices is necessary to ascertain our argument.

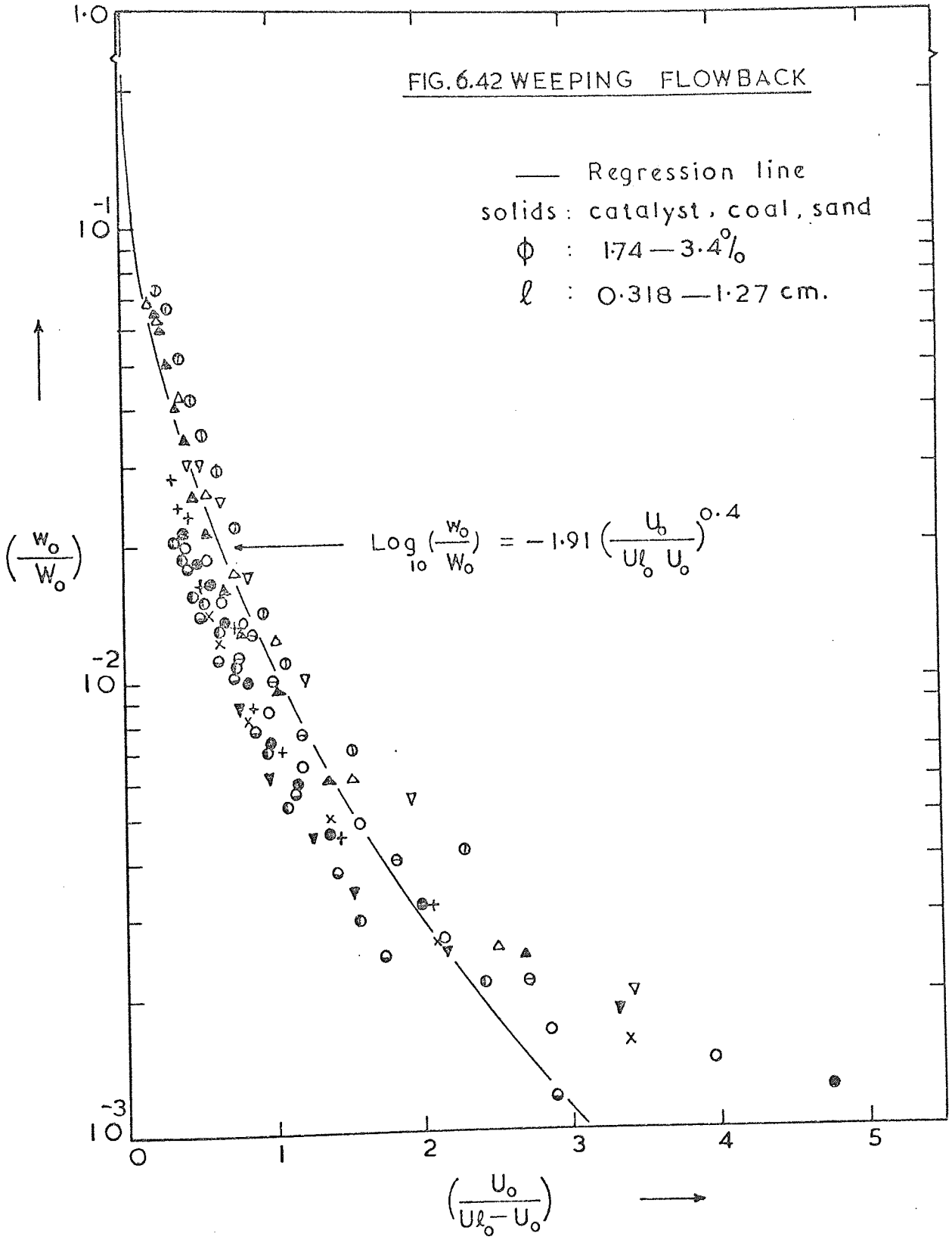
FIG. 6.42 WEEPING FLOWBACK
—— Regression line
solids : catalyst , coal , sand
ϕ : 1·74 — 3·4%
ℓ : 0·318 — 1·27 cm.
$\text{Log}_{10}\left(\frac{W_o}{W_o}\right) = -1.91\left(\frac{U_o}{U\ell_o\ U_o}\right)^{0.4}$
$\left(\frac{W_o}{W_o}\right)$
$\left(\frac{U_o}{U\ell_o - U_o}\right)$
1·0
10^{-1}
10^{-2}
10^{-3}
0
1
2
3
4
5

6.11.8 Recommended Design Equations

The following equations may be used for design calculations relating to solids flowback in gas fluidized beds. For the rate of free flowback of defluidized solids through multi-orifice distributors (gravity flow).

$$W = 47\ \rho_B \cdot A_e \cdot \sqrt{(D_o - 1.42\ D_p) \cdot g}\ ,\ \text{for coarse particles}$$

$$W = 23\ \rho_B \cdot A_e \cdot \sqrt{g}\ ,\ \text{for fine particles}$$

and for the determination of the limiting gas velocity through the distributor orifices $U\ell_o$ at which flowback is completely eliminated

$$\frac{U\ell_o \cdot \rho_g \cdot D_o}{\mu_g} = 21.8 \left(\frac{\ell}{D_o}\right)^{-0.27} \left(\frac{D_o}{D_p}\right)^{0.87} \left(\frac{\rho_B - \rho_g}{\rho_g} \cdot \frac{D_p^3 \cdot \rho_g^2 \cdot g}{\mu_g^2}\right)^{0.43},$$

$$\text{for } 0.5 \leqslant \ell/D_o \leqslant 12.0\ ,$$

and for the determination of the weeping flux

$$\log_{10}\left(\frac{\omega_o}{W_o}\right) = -1.91 \left(\frac{U_o}{U\ell_o - U_o}\right)^{0.4} \text{ for } U \geqslant 6\ U_{mf}$$

where $W_o = W/A_e$ and $A_e = \frac{\pi}{4}(D_o - 1.42\ D_p)^2 \cdot N$

6.11.8.1 Application Where Flowback is Needed

The results obtained may be applied to some practices of fluidized bed technology where flowback is actually required in the process, i.e. in multi-stage systems where multi-orifice plates (or grids) act both as downcomers and stage separators. These results provide an approach to evaluation of the efficiency of grids of a given

design in relation to mixing of the solid phase.

The efficiency of a grid is unity if there is no intermixing of two beds of suspended particles separated by the grid. In this case the flowback rate ω must be equal to the external circulation rate ω_e of the solid phase across the system. In industrial practice $\omega > \omega_e$ under steady conditions, so that the hold-up of the solid phase is avoided. Since under the given conditions the grid lets through an amount ω of the solid phase, and a smaller amount ω_e leaves the system, under steady conditions the excess amount of material $(\omega - \omega_e)$ passing through the grid is carried by the gas stream into the bed above, creating internal circulation of the solid phase. If $\omega < \omega_e$, the grid does not let through the required amount of the solid phase.

Therefore $\frac{\omega_e}{\omega} = \xi$ is a measure of grid efficiency in relation to solid mixing.

6.11.9 Uncontrollable Downflow of Solids Through Long Cylindrical Nozzles

As pointed out earlier, a new phenomenon was observed with distributors equipped with long nozzles. At a certain gas velocity the bed would start flowing through one nozzle and flood the wind box. Simultaneous flow through a number of nozzles was observed, but normally at very low gas rates. The longer the nozzle the more difficult it was to stop the flow by increasing the gas flow rate, because of the hydrostatic head in the nozzle. It is believed that maldistribution through the nozzles is the reason for the occurrence of this phenomenon. There is a critical length for a bundle of cylindrical nozzles above which this phenomenon can occur.

6.11.9.1 Theoretical Prediction of the Critical Nozzle Length

Consider a bundle of N nozzles of length ℓ which initially are all operational (i.e. bubbling). At an orifice velocity U_o, the distributor pressure drop is given by (3.2) and (3.8), assuming a turbulent flow through the nozzles (see Chapter 3), i.e.

$$\Delta P_D = \frac{\rho_g}{2g} \cdot U_o^2 \qquad (6.44)$$

If one nozzle stops bubbling, the velocity through the $N - 1$ remaining nozzles becomes $\frac{N}{N-1} \cdot U_o$ and the pressure drop through each of these nozzles is therefore:

$$\Delta P_D = \frac{\rho_g}{2g} \cdot \left(\frac{N}{N-1}\right)^2 \cdot U_o^2 \qquad (6.45)$$

If an incipiently fluidized bed which has a density ρ_B is treated as a liquid, then the maximum distance z which the bed will be able to descend inside the nozzle, creating a hydrostatic head $\Delta P_z = \rho_B . z$ is given by

$$\Delta P_D = \Delta P_z \qquad (6.46)$$

or $$z = \frac{\rho_g}{\rho_B} \cdot \frac{1}{2g} \cdot \left(\frac{N}{N-1}\right)^2 \cdot U_o^2 \qquad (6.47)$$

For $z > \ell$ the solids start flowing into the wind box and become uncontrollable. Hence for each velocity U_o, there is a critical length for a multi-nozzle distributor given by

$$\ell_c = \frac{\rho_g}{\rho_g} \cdot \frac{1}{2g} \cdot \left(\frac{N}{N-1}\right)^2 \cdot U_o^2 \qquad (6.48)$$

Alternatively, for nozzles of length ℓ there is a critical orifice velocity below which uncontrollable downflow of solids may occur. If n nozzles remain bubbling (i.e. N - n nozzles start flowing simultaneously) a larger value of the critical length, equal to $\left(\frac{N-1}{n}\right)^2 \cdot \ell_c$ is obtained.

Experiments were carried out on three sets of multi-nozzle distributors with 0.318, 0.476 and 0.635 cm. diameter nozzle respectively. The nozzle length was varied between 4-18 cm., so that $\ell/D_o \geqslant 12$ (see Table 6.33). In all experiments, unsieved cracking catalyst (ρ_B = 0.4 gm./cm^3.) was used. The experimental procedure was started as follows: a known weight of catalyst particles was poured into the column, with the air set at a sufficiently high flow rate to prevent the flow of solids. The air supply was then reduced gradually until one of the nozzles started to flow and flood the wind box. At this point the orifice velocity U_o was recorded as the critical velocity at which uncontrollable downflow of solids would occur. This measurement was repeated several times to be sure of its reproducibility. Further decreases in the gas flow rate allowed more nozzles to flow simultaneously. Consequently it became exceedingly difficult to stop the flow by increasing the gas flow rate.

The experimental results are given in Table (6.33) and in Figure (6.43) a plot of ℓ_c vs. U_o^2 shows their comparison with the theoretical

line predicted from (6.48) for the multi-nozzle distributors used. As may be seen, the experimental points fall above the theoretical line.

But the trend of the experimental data indicates a linear dependence of ℓ_c on U_o^2 ; it would appear that the best line through the data passes through the origin, i.e. in accord with the prediction of (6.48). Large pressure fluctuations at low values of ℓ occasionally started the phenomenon and this may explain the deviation observed at low values of ℓ . The deviation disappears at higher values of U_o, probably due to the lack of sufficiently large pressure fluctuations.

Therefore, although there is no quantitative agreement between experiments and theory, there is some agreement qualitatively. However, better agreement is obtained if the right hand side of equation (6.48) is multiplied by an empirical coefficient η . Equation (6.48) then becomes

$$\ell_c = \eta \cdot \frac{\rho_g}{\rho_B} \cdot \frac{1}{2g} \cdot \left(\frac{N}{N-1}\right)^2 \cdot U_o^2 \qquad (6.49)$$

It has been shown(121) that η for a distributor jetting into a fluidized bed is not significantly different from the 'dry' coefficient. η was measured from jetting experiments in an empty bed and was found to be

$$1.55 < \eta < 1.62 \qquad (6.50)$$

The value $\eta = 1.62$ was used to predict ℓ_c from (6.49). It can be seen in Figure (6.43), equation (6.49) compares well with the experimental data. Therefore, (6.49) may be used to predict the critical length for a multi-nozzle distributor plate. Alternatively, it may be used to estimate the critical orifice gas velocity for nozzles of length ℓ .

Start-up problems can be expected from long nozzles. As indicated earlier, the start-up from a defluidized bed with defluidized solids filling the nozzles was found very difficult to achieve for nozzles longer than 15 cm.

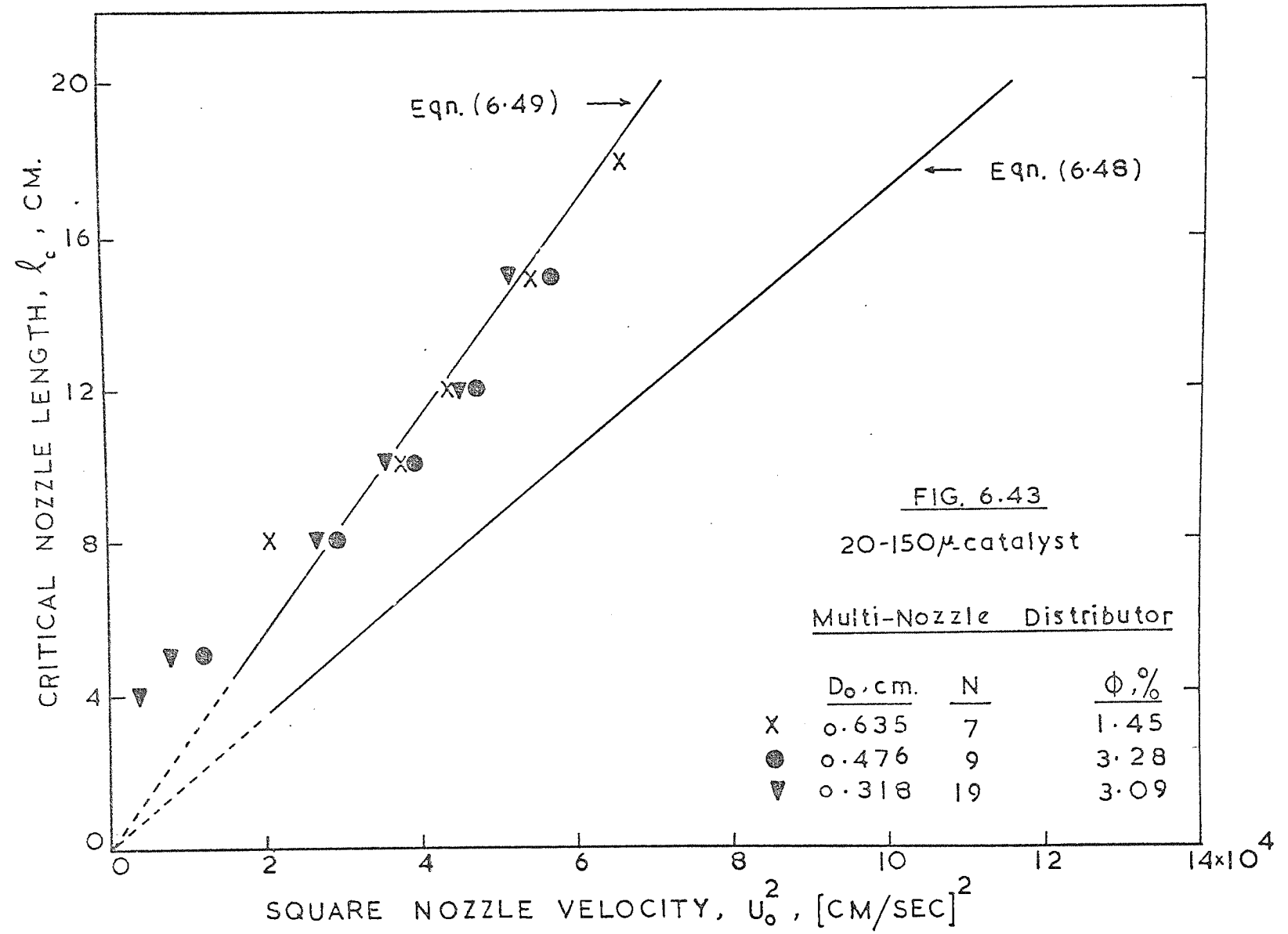
Eqn. (6·49)
Eqn. (6·48)
CRITICAL NOZZLE LENGTH, ℓ_c, CM.
SQUARE NOZZLE VELOCITY, U_o^2, $[CM/SEC]^2$
0
4
8
12
16
20
2
6
10
14×10⁴
FIG. 6.43
20-150μ catalyst
Multi-Nozzle Distributor
D_o, cm. N Φ, %
X 0.635 7 1·45
● 0.476 9 3·28
▼ 0.318 19 3·09

CONCLUSIONS

The findings of the study of solids flowback through distributors in gas fluidized beds can be summarised as follows:

1. Solids flowback across a multi-orifice distributor passes through a maximum with respect to gas velocity. Two regimes of flowback, namely weeping and dumping, have been differentiated. In the weeping regime, the orifices leaked in a consistent manner and almost 100% of orifices were operational. In the dumping regime, however, the orifices leaked and bubbled in a random way. Thus operation of a distributor in this region is highly undesirable and can lead to instability.

2. Data from distributors of various design using different gas-solid systems have been correlated. Three design equations have been derived and these may be used to estimate solids flowback through multi-orifice distributor plates in gas fluidized beds.

3. The decisive advantage of increasing the distributor thickness or using nozzles to minimize flowback has been observed. Cylindrical nozzle-plates reduced solids flowback for nozzle lengths less than a critical value. Above this critical length uncontrollable downflow of solids would occur. A theoretical model for predicting the critical length of a bundle of nozzles in terms of gas velocity through the nozzles has been derived. Experiments showed reasonable agreement with theory.

GENERAL CONCLUSIONS AND RECOMMENDATIONS

The study presented in Chapters (3) - (5) concludes that in the presence of the bed the distributor pressure drop is reduced relative to that without the bed, and this pressure drop in the former condition is the appropriate parameter for distributor design. Further work is necessary to show the precise effect of the bed on the normal pattern of gas flow through the orifices because, it is unlikely that the lowering observed in the distributor pressure drop is due to compression of the gas as suggested by earlier work(74).

There is evidence that larger diameter beds tend to be less stable than small diameter beds when these are operated with shallow beds. It would be useful to extend this study to larger and shallower beds as it is relevant to multi-stage systems.

Jet interaction may be important in influencing the performance of the distributor. Investigation of this problem together with study on the nature of voidage in the jet would be useful subjects for further research.

The work of Chapter 6 is concerned with solids flowback through distribution plates. More work should be carried out on multi-orifice distributors in a larger bed with a wider range of orifice diameters.

Cylindrical nozzle-plates reduced solids flowback for nozzle lengths less than a critical value. Above this critical length uncontrollable downflow of solids would occur. It would be interesting to re-do the study conducted with cylindrical nozzles using convergent conical nozzles. The hydrostatic head is less likely to form with these nozzles which therefore should be more stable. Also they should plug less easily and consequently have less start-up problems. A search for optimal angle of these nozzles would also give results of design interest.

APPENDIX

APPENDIX A2

Determination of Physical Properties of Solid Particles

(properties of particles are specified in Table (2.3)(Chapter 2))

1. Density Determination

(a) Bulk density, ρ_B

An estimate of ρ_B was made by pouring a known weight of particles very gently into a measuring cylinder.

Then

$$\rho_B = \frac{\text{weight of particles}}{\text{volume occupied by particles}} \qquad (A2.1)$$

The above procedure was repeated several times to establish the reproducibility of the measurements and the results were averaged.

(b) Particle density, ρ_s

For non-porous particles, the particle density was determined using the water displacement method. The main disadvantage of this method was that even with a surfactant such as Nonidet P40, minute air bubbles remained trapped between the submerged particles. In some cases, especially with fine glass beads, the density bottle and its contents were heated until the water boiled, in an attempt to drive off all the entrapped air.

Catalyst: It was noted that the catalyst particles were porous and that therefore the particle density required was the value that would be obtained if all the pores could be plugged with a solid of the same density as air and a normal determination in water then carried out. This density value was obtained by measuring the skeletal density of the particles by the water method, and then correcting this value by the pore volume per unit mass determined on a sample of the catalyst, i.e.

$$\rho_s = \frac{\rho_k}{1 + V_p \cdot \rho_k} \qquad (A2.2)$$

where ρ_s = particle density, gm./cm.^{3}

ρ_k = skeletal density, gm./cm.^{3}

V_p = pore volume, cm.^{3}/gm.

The pore volume was determined by the liquid titration method described by Innes(122) and found to be equal to 0.636 cm^3./gm. This figure represents an average of three measurements.

The skeletal density ρ_k = 2.18 gm./cm^3. (using water method)

Therefore particle density $\rho_s = \frac{2.18}{1 + 0.634 \times 2.18} = 0.915$ gm./cm^3.

The supplier (Joseph Crosfield Ltd.) quote 0.68 cm^3./gm. for the pore volume. Using this value in (A2.2), gives 0.88 gm./cm^3. for the particle density. Therefore an average of 0.90 gm./cm^3. was taken as the particle density of cracking catalyst.

2. Estimation of Bed Voidage, e_{mf}

The bed voidage at the point of incipient fluidization was estimated from the bulk density ρ_B and the particle density ρ_s:

$$e_{mf} = 1 - \frac{\rho_B}{\rho_s} \qquad (A2.3)$$

3. Determination of Shape (λ_s) and Roundness (λ_r) Factors

Two-dimensional shape and roundness factors of particles listed in Table (2.3) (Chapter 2) have been determined by visual comparison with charts available in the literature (see Figures (A2.1) - (A2.2)). The method is based on Wadell(123) (shape and roundness of quartz particles).

To determine the shape factor (or sphericity) and the roundness factor by visual comparison, loose particles were magnified by microscope to about 2 - 3 times the size of those in Figures (A2.1) and (A2.2). The shape factor and the roundness factor of each particle was estimated

by comparison with the outlines on the charts. Best results were obtained by first selecting sphericities on the charts that are obviously too high and too low and then narrowing this range.

The visual method permitted sphericities to be determined at the rate of 2 - 3 per minute. The values of λ_s and λ_r presented in Table (2.3) (Chapter 2) were the average of at least 40 estimates. It should be noted that three-dimensional shape factors can be determined with the aid of the Carman-Kozeny equation (i.e. from experiments of fluid flow through fixed beds). However, it would give less consistent results and for this reason it was not used. Considering the rather large sampling errors to which sphericity studies are subject, it seems probably that visual comparisons will yield data of sufficient accuracy for many investigations. Certainly the rapidity of the method will permit shape studies to be made a part of many investigations in which the time available otherwise would be insufficient.

4. Determination of Mean Particle Diameter, D_p

The particle size which is relevant to fluidization studies is the surface/volume diameter D_{sv}. It is the diameter of a sphere having the same surface to volume ratio as the particle. This can normally only be obtained from fluid flow or gas adsorption tests using fixed beds. The sieve diameter D_{pi}, can usually be obtained readily and the mean size of a mixture of particles calculated from:

$$D_{p(mean)} = \frac{1}{\sum \frac{x_i}{D_{pi}}} \qquad (A2.4)$$

where x_i is the weight fraction of material in each size range.

All solids were machine sieved (BS mesh size) and were closely graded. Mean particle diameters determined using (A2.4) for all solids tested are listed in Table (2.3)(Chapter 2). Suffice, therefore, to give a few examples of particle size distributions and mean particle sizes for some of the materials used in the present work.

1. Ungraded cracking catalyst - 13% Alumina

size range (μ)*	%
0 - 20	1.0
20 - 40	9.0
40 - 80	70.0
- 80	20.0
Mean particle size (μ)	60

* As quoted by the suppliers in their data sheet. Size distribution determination carried out in the present work showed a size range of 20 - 150 μ.

2. Graded cracking catalyst C_2

size range (μ)		x_i	x_i/D_{pi}
-150	+125	0.184	0.00132
-125	+106	0.299	0.00257
-106	+ 90	0.375	0.00381
- 90	+ 75	0.076	0.00090
- 75	+ 63	0.061	0.00086

$\sum x_i = 0.995 \quad \sum x_i/D_{pi} = 0.00946$

Therefore $D_p = 106\ \mu$

3. Rounded Sand S_3

size range (μ)		x_i	x_i/D_{pi}
-180	+150	0.653	0.003952
-150	+125	0.091	0.000661
-125	+106	0.059	0.000511
-106	+ 75	0.191	0.002100
		$\sum x_i = 0.994$	$\sum x_i/D_{pi} = 0.007224$

Therefore $D_p = 138\ \mu$

4. Coal

size range (μ)		x_i	x_i/D_{pi}
	+ 150	0.396	0.00264
-150	+125	0.330	0.00240
-125	+106	0.118	0.0010216
-106	+ 90	0.074	0.0007551
- 90	+ 75	0.057	0.0006909
- 75		0.023	0.00030666
		$\sum x_i = 0.998$	$\sum x_i/D_{pi} = 0.00782826$

Therefore $D_p = 128\ \mu$

5. Glass beads G_3

size range (μ)		x_i	x_i/D_{pi}
-300	+250	0.352	0.00130
-250	+212	0.510	0.00223
-212	+180	0.134	0.000705
		$\sum x_i = 0.996$	$\sum x_i/D_{pi} = 0.004235$

Therefore $D_p = 237\ \mu$

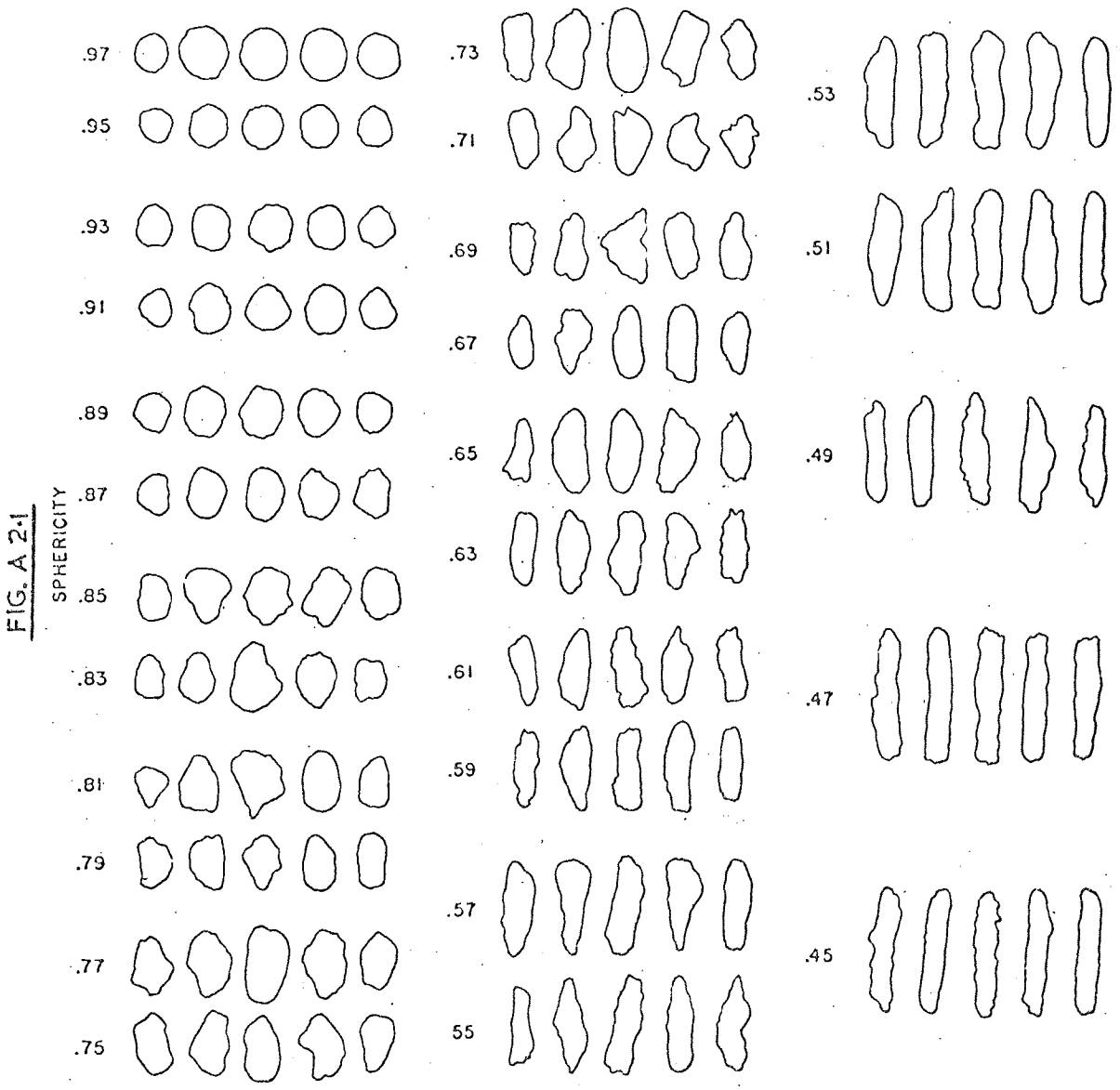
.97
.95
.93
.91
.89
.87
.85
.83
.81
.79
.77
.75
.73
.71
.69
.67
.65
.63
.61
.59
.57
55
.53
.51
.49
.47
.45
SPHERICITY

FIG. A 2·1

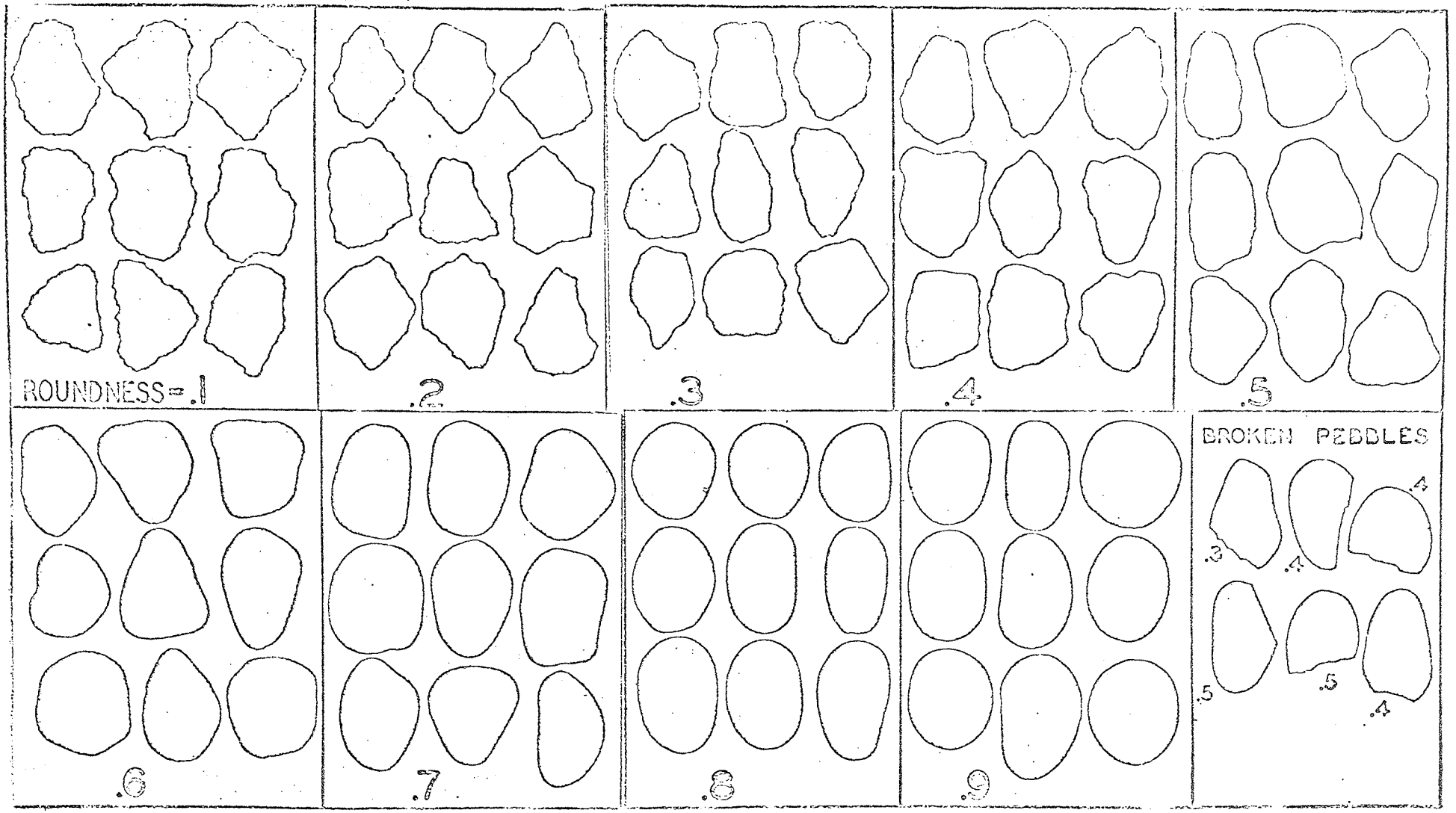

PEBBLE IMAGES FOR VISUAL ROUNDNESS

FIG. A 2-2

APPENDIX A4

Theoretical Prediction of True Surface Eruption Diameter

Zenz(106) approached the problem by considering the annular shell as the region through which the bed solids flow down around the bubble under a fluid head equal to height of the bubble.

From Zenz's analysis the head is related to the solids flow rate by the relationship:

$$W_s = 3.56\ \rho_B\ (\text{height of bubble})^{\frac{1}{2}} \qquad (A4.1)$$

Where W_s = bulk flow of solids, lbs./sec. ft^2.

and ρ_B = bulk density of dense phase flowing solids, lbs./ft^3.

As depicted in Figure (A4.1), the volumetric flow of bulk solids through an area of A_m square feet surrounding the bubble can be equated to volume displaced behind the upwardly rising bubble resulting in the relationship

$$\frac{\pi (\alpha D_B)^2}{4} \cdot U_B = 3.56\ A_m \left[(1 - W_H)\ D_B \right]^{\frac{1}{2}} \qquad (A4.2)$$

Since

$$A_m = \frac{\pi D_c^2}{4} - \frac{\pi D_B^2}{4} \qquad (A4.3)$$

and

$$U_B = 4.01\ K\ D_B^{\frac{1}{2}} \qquad (A4.4)$$

Where K is a constant

Substituting (A4.4) and (A4.3) in (A4.2) results in the relationship

$$\left(\frac{D_c}{D_B}\right)^2 = 1 + \frac{1.13\ K\ \alpha^2}{(1 - W_H)^{\frac{1}{2}}} \qquad (A4.5)$$

Zenz quotes average values for K, α and W_H as reported by other investigators and on substitution in (A4.5) yields

$$\frac{D_c}{D_B} = \sqrt{1 + \frac{(1.13)(1)(0.948)^2}{(1 - 0.34)^{\frac{1}{2}}}} = 1.5 \qquad \text{(A4.6)}$$

or $$D_B = \frac{2}{3} D_c \qquad \text{(A4.7)}$$

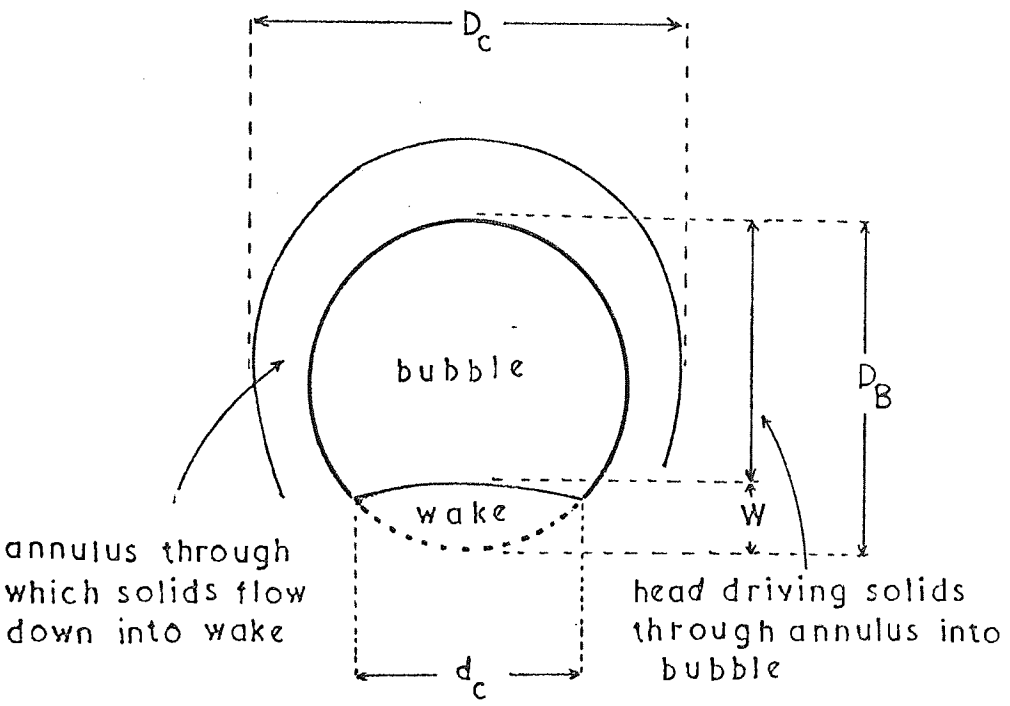

$$W/D_B = W_H$$

$$d_c/D_B = \alpha$$

FIG. A4·1 SOLIDS INFLOW MODEL FOR BUBBLE RISE IN A FLUIDIZED BED ADAPTED FROM ZENZ (106).

BUBBLE ASSEMBLAGE MODEL — COMPUTER PROGRAM

```
'SEND TO' ( ED,ASTD-DEFAULT(0),,PROGRAM)
'WORK' (ED,WORK FILE    )
'BEGIN' 'COMMENT' BUBBLE ASSEMBLAGE MODEL FOR MULTI-ORIFICE
                  DISTRIBUTORS USED IN GAS FLUIDIZED BEDS.
        MODEL IS FORMULATED IN TERMS OF DISTRIBUTOR PRESSURE DROP.;
'BEGIN' 'COMMENT' EQUATIONS ARE BASED ON C.G.S. UNITS.;
'BEGIN' 'REAL' DB,DBO,U,UMF,RHOS,DP,H,HS,HMF,DELTAH,G,PI,NOR,DOR,M,NB,
          A,AF,E,E1,E2,EMF,UB,HB,RHOG,PDN,PDNN,PDB;
        'INTEGER' N,I;
        RHOS:=READ; DP:=READ; G:=READ; UMF:=READ; HMF:=READ; EMF:=READ;
        A:=READ; AF:=READ; DOR:=READ; I:=READ; RHOG:=READ;
        PI:=4*ARCTAN(1);
        NOR:=4*AF*A/(PI*DOR↑(2));
        NOR:=NOR/A;
REPEAT: 'BEGIN' U:=READ; PDN:=READ;
        UB:=U-UMF;  NEWLINE(2); SPACE(5);
WRITETEXT('('BUBBLE%PHASE%VELOCITY(CM/SEC)=')'); PRINT(UB,2,3);
                    NEWLINE(2);
WRITETEXT('('NO%OF%COMPARTMENTS'('3S')'HEIGHT%OF%COMPARTMENT'('3S')
'NO%OF%BUBBLES'('3S')'HEIGHT%ABOVE%DISTRIBUTOR')');
        N:=1;
        HS:=0;
        M:=1.4*RHOS*DP*(U/UMF);
        PDNN:=(RHOG*(U↑2))/(2*G*AF*AF);
         PDB:=(RHOG*(UB↑2))/(2*G*AF*AF);
         NOR:=NOR/(1+(PDN-PDNN)/(PDB));
        DBO:=((6*(U-UMF)/(PI*NOR))↑(0.4))/(G↑(0.2));
        DB:=M*(HMF/2)+DBO;
        H:=HMF*(U-UMF)/(0.711*((G*DB)↑(0.5)))+HMF;
AGAIN:  'BEGIN'
        DELTAH:=2*DBO*(((2+M)/(2-M))↑(N))/(2+M);
        E1:=1-HMF*(1-EMF)/H;
        E2:=1-HMF*(1-EMF)/H+(HMF*(1-EMF)*(DELTAH-HMF))/(2*H*(H-HMF));
        HB:=HMF+2*(H-HMF);
        E:='IF' DELTAH 'LE' HMF 'THEN' E1 'ELSE' 'IF' HB 'GE' DELTAH
           'AND' DELTAH 'GE' HMF 'THEN' E2 'ELSE' EMF;
        NB:=6*A*(E-EMF)/(PI*(1-EMF)*((DELTAH)↑(2)));
        NB:=ENTIER(NB);
                    NEWLINE(2);
SPACE(8); PRINT(N,2,0); SPACE(15); PRINT(DELTAH,2,3); SPACE(13);
PRINT(NB,2,1);
        N:=N+1;
        HS:=HS+DELTAH;
SPACE(9);       PRINT(HS,2,3);          NEWLINE(1);
'IF' H 'GT' HS 'THEN' 'GOTO' AGAIN
        'END';
        I:=I-1;
'IF' I 'GT' 0 'THEN' 'GOTO' REPEAT
        'END';
        'END';
        'END';
        'END';
```

A SAMPLE OF COMPUTER RESULTS

BUBBLE PHASE VELOCITY(CM/SEC)= 3.000

NO OF COMPARTMENT	HEIGHT OF COMPARTMENT	NO OF BUBBLES	HEIGHT ABOVE DISTRIBUTOR
1	0.793	40.0	0.793
2	0.877	32.0	1.670
3	0.971	26.0	2.641
4	1.075	21.0	3.716
5	1.190	17.0	4.906
6	1.317	14.0	6.223
7	1.458	11.0	7.682
8	1.614	9.0	9.296
9	1.787	7.0	11.083
10	1.978	6.0	13.061
11	2.190	5.0	15.250
12	2.424	4.0	17.674
13	2.683	3.0	20.358
14	2.970	2.0	23.328
15	3.288	2.0	26.616
16	3.640	1.0	30.255

APPENDIX A6

Calibration of 'Metric' Series Rotameters for the Flow of Other Gases

In the manufacturer's manual(125), Charts are supplied which can be used for calculating the flow calibration of any 'Metric' Series Rotameter or any 'Metric' tube fitted with a special float the constants of which are known.

Families of curves, expressing the relationship between the variables involved are given in the manual. Using the known meter and fluid constants, the parameters of the curves are evaluated and from these the calibration for the required fluid is established.

Formulae

$$I = \log_{10}\left[K_1 \times \nu. \sqrt{\frac{\rho_F \times \rho_g}{W_F.\ (\rho_F - \rho_g)}} \times 10^4 \right] \qquad \text{(A6.1)}$$

$$F_t = K_2 \times \sqrt{\frac{W_F\ (\rho_F - \rho_g)}{\rho_F \times \rho_g}} \qquad \text{(A6.2)}$$

Where

W_F = weight of float, gm.

ρ_F = density of float, gm./cm^3.

ρ_g = density of gas, gm./cm^3

ν = kinematic viscosity of gas, stokes

F_t = theoretical capacity in litres/min

K_1, K_2 = instrument constants which vary with tube sizes, and are specified in the manual.

Evaluation

Using the appropriate values of K_1 and K_2, I and F_t were calculated using (A6.1) and (A6.2) respectively.

From the characteristic curves the scale readings which correspond to plotted values of f at the calculated value of I were determined and a detailed calibration curve of flow $F(f \times F_t)$ vs. scale reading was plotted. Here f is a parameter as shown on the characteristic charts in the manual.

It should be noted that the flow derived by this procedure was expressed in terms of free volumes ($15^{\circ}C$ and 760 mm Hg). Conversion to mass flow units is effected by multiplying by the free density of the gas. Conversion to volumes at the working conditions is made by dividing the mass flow rate by the working density of the gas.

Example

Calibration of 'Metric' 14 for the flow of Co_2 at $15^{\circ}C$ and 760 mm Hg.

$\rho_g = 1.85 \times 10^{-3}$ gm./cm^3.

$\mu_g = 1.457 \times 10^{-4}$ gm./cm.sec.

Therefore $\nu = \frac{1.457 \times 10^{-4}}{1.85 \times 10^{-3}} = 0.079$ stokes

$\rho_F = 2.80$ gm./cm^3. (for Duralumin float given in manual)

$W_F = 1.77$ gm. (from manual)

$K_1 = 0.379$ (from manual)

$K_2 = 1.316$ (from manual)

Using (A6.1) and (A6.2) and with the aid of the charts supplied in the manual, the following calibration data were obtained.

Scale reading, cm.	0	3.5	6.78	9.9	12.8	15.7	18.35	20.95	23.34	25.9
Free flow rate, litre/min.	4.07	8.14	12.21	16.28	20.35	24.42	28.5	32.56	36.63	40.7

The same procedure was carried out for other gases and for the meters used in the experiments. (The calibration charts produced from the calibration data are not given here).

Construction of (6.29) by Dimensional analysis

The following method of forming the dimensionless groups is adapted from Douglas(124). It is based on the indicial and Buckingham's Pi theorem. The method is to write down all the variables and determine by inspection the least number k of variables in terms of which all the other m-k variables can be described, where m is the total number of variables in the problem. Write down m-k equations expressing the other m-k variables in terms of the selected k fundamental variables. The ratio of the two sides of each of these equations will then form a dimensionless group. There will be a total of m-k dimensionless groups consisting of not more than k+1 variables, namely the k fundamental (or principal) variables, if all are required, together with one of the remaining m-k variables.

Now from (6.26) we have

$$U\ell_o = f(D_o, s, \ell, \rho_g, \mu_g, D_p, \rho_B, g, \phi)$$

Applying the above method, the variables include dimensions of length, mass and time. We therefore require three fundamental variables to include all three of these dimensions.

We have 10 variables, 7 dimensional quantities and three fundamental (principal) dimensions.

Therefore the number of dimensionaless groups is 10-3=7,

$$\text{i.e. } \pi_1 = f_1(\pi_2, \pi_3, \pi_4, \pi_5, \pi_6, \pi_7) \qquad \text{(A6.3)}$$

Selecting D_o, μ_g and ρ_g we express the fundamental dimensions of L, T and M in terms of these:

$$D_o = [L] \quad \text{giving} \quad [L] = [D_o]$$

$$\mu_g = [M\, L^{-1}\, T^{-1}] \quad \text{giving} \quad [M] = [\rho_g\, D_o^3]$$

$$\rho_g = [M\, L^{-3}] \quad \text{giving} \quad [T] = \left[\frac{\rho_g\, D_o^2}{\mu_g}\right]$$

Taking each of the other variables in term we can write down their dimensional formulae in terms of L, M and T and then use the above equations to replace L, M and T by D_o, μ_g and ρ_g.

Group π_1. Selecting $U\ell_o$, the limiting orifice velocity, as the first

of the m-k remaining variables we have, dimensionally,

$$\left[U\ell_o\right] = \left[L\ T^{-1}\right] = \left[D_o\right]\left[\frac{\rho_g D_o^2}{\mu_g}\right]^{-1} = \left[\frac{\mu_g}{\rho_g D_o}\right]$$

whence

$$U\ell_o = \pi_1 \cdot \frac{\mu_g}{\rho_g D_o} \quad \text{and} \quad \pi_1 = \frac{U\ell_o \rho_g D_o}{\mu_g} = Re_{\ell im}$$

By similar procedure, other dimensionless groups can be easily obtained. These are

$$\pi_2 = \left(\frac{D_o}{D_p}\right), \qquad \pi_3 = \left(\frac{\rho_B}{\rho_g}\right)$$

$$\pi_4 = \left(\frac{\ell}{D_o}\right), \qquad \pi_5 = \frac{g\,\rho_g^2\,D_o^3}{\mu_g^2}$$

$$\pi_6 = (\phi), \qquad \pi_7 = \left(\frac{S}{D_o}\right)$$

The number of dimensionless groups can be reduced and since we are concerned with the flow of particles countercurrent to a gas stream, the group of interest would be the Archimedes group (i.e. the particle Reynolds number).

Therefore we may introduce the group

$$\left(\frac{\rho_B - \rho_g}{\rho_g} \cdot \frac{g \cdot \rho_g^2 \cdot D_p^3}{\mu_g^2}\right) = Ar$$

and the final form of the correlation will be:

$$Re_{\ell im} = \text{const} \left[A_r^a \cdot \left(\frac{D_o}{D_p}\right)^b \cdot \left(\frac{\ell}{D_o}\right)^c \cdot \left(\frac{S}{D_o}\right)^d \cdot \phi^e \right] \qquad (6.29)$$

and this equation (6.29) forms the basis of the work presented in Section (6.11.6).

Non-Linear Regression Analysis and the Computer Program

The program is to find the "best" curve describing a set of data which suggests a relationship of the form

$$\log_{10} Z = a X^b \tag{A6.4}$$

Suppose the error lies only in the ordinate Y. The method of "least squares" assumes that the "best" system of values for a and b is the one which renders the sum of the squares of the deviations a minimum, i.e.

$$M = \sum (Y - \log_{10} Z)^2 = \text{Min.} \tag{A6.5}$$

or

$$M = \sum (Y - aX^b)^2 = \text{Min.} \tag{A6.6}$$

where Y is the predicted value of the dependent variable.

The values of a and b may be found by solving the "normal" equations:

$$\frac{\partial M}{\partial a} = \frac{\partial M}{\partial b} = 0 \tag{A6.7}$$

i.e.

$$\frac{\partial M}{\partial a} = -2 \sum (Y - aX^b)X^b = 0$$

giving

$$a = \frac{\sum Y X^b}{\sum X^{2b}} \tag{A6.8}$$

and

$$\frac{\partial M}{\partial b} = -2 (Y - aX^b)aX^b \ln X = 0$$

or

$$\sum Y X^b \ln X = \sum a X^{2b} \ln X$$

Substituting (A6.8) into (A6.9), we have

$$\frac{\sum Y X^b}{\sum Y X^b \ln X} \quad \frac{\sum X^{2b} \ln X}{\sum X^{2b}} = 1 \tag{A6.10}$$

Hence the algorithm is to evaluate (A6.10) for different values of b, then to pick the b value which makes (A6.10) nearest to 1.0 and to evaluate the corresponding a using (A6.8).

The program was written in FORTRAN 4 and can be found in the following pages along with the best values of a and b as obtained from the computer analysis using the experimental data.

The main drawback of this program is the fact that values of b are to be given which suggests that the programmer had to estimate its value in advance.

The other defect is that since the natural log of X is to be evaluated then X cannot have a negative value. However, this may be overcome.

NON–LINEAR REGRESSION ANALYSIS— COMPUTER PROGRAM

```
      MASTER REGRESSION                                                  REG  600
C     NON-LINEAR  REGRESSION  ANALYSIS                                   REG  700
      DIMENSION X(110),Y(110),Z(24),B(24)                                REG  800
      READ (1,10) (B(I),I=1,24)                                          REG  900
   10 FORMAT (24F3.1)                                                    REG 1000
      DO 20 K=1,110                                                      REG 1100
   20 READ (1,30) X(K),Y(K)                                              REG 1200
   30 FORMAT (1X,F5.3,7X,F6.3)                                           REG 1300
      S1=0.                                                              REG 1400
      S2=0.0                                                             REG 1500
      S3=0.0                                                             REG 1600
      S4=0.                                                              REG 1700
      WRITE (2,90)                                                       REG 1750
      DO 40 I=1,24                                                       REG 1800
      DO 50 K=1,110                                                      REG 1900
      S1=S1+Y(K)*(X(K)**B(I))                                            REG 2000
      S2=S2+(X(K)**(2.0*B(I)))*ALOG(X(K))                                REG 2100
      S3=S3+Y(K)*(X(K)**B(I))*ALOG(X(K))                                 REG 2200
      S4=S4+(X(K)**(2.*B(I)))                                            REG 2300
   50 CONTINUE                                                           REG 2400
      Z(I)=(S1*S2)/(S3*S4)                                               REG 2500
      WRITE (2,60) Z(I),B(I)                                             REG 2700
   60 FORMAT (13X,F5.3,10X,F3.1)                                         REG 2800
   40 CONTINUE                                                           REG 2900
      ZZ=1000.0                                                          REG 3000
      DO 70 I=1,24                                                       REG 3100
      IF (ABS(Z(I)-1.0) .GT. ABS(ZZ)) GO TO 70                           REG 3200
      ZZ=Z(I)-1.0                                                        REG 3300
      II=I                                                               REG 3400
   70 CONTINUE                                                           REG 3500
      S1=0.0                                                             REG 3600
      S4=0.0                                                             REG 3700
      DO 80 K=1,110                                                      REG 3800
      S1=S1+Y(K)*(X(K)**B(II))                                           REG 3900
      S4=S4+(X(K)**(2.0*B(II)))                                          REG 4000
   80 CONTINUE                                                           REG 4100
      A=S1/S4                                                            REG 4200
   90 FORMAT (//10X,7HRESULTS,2X,2HOF,2X,10HREGRESSION,2X,8HANALYSIS//15REG 4300
     1X,1HZ,15X,1HB/)                                                    REG 4400
      WRITE (2,100) A,B(II)                                              REG 4500
  100 FORMAT (//12X,12HOPTIMUM A = ,F6.3//12X,12HOPTIMUM B = ,F3.1)      REG 4600
      STOP                                                               REG 4700
      END                                                                REG 4800
```

RESULTS OF REGRESSION ANALYSIS

Z	B
0,381	0,1
0,633	0,2
0,830	0,3
0,991	0,4
1,127	0,5
1,244	0,6
1,345	0,7
1,434	0,8
1,509	0,9
1,572	1,0
1,623	1,1
1,660	1,2
1,685	1,3
1,697	1,4
1,698	1,5
1,689	1,6
1,672	1,7
1,649	1,8
1,620	1,9
1,589	2,0
1,555	2,1
1,520	2,2
1,486	2,3
1,452	2,4

OPTIMUM A = -1,907

OPTIMUM B = 0,4

TABLE (3.1)

Multi-orifice distributors used in the experiments

Orifice diam. D_o, cm.	Orifice Spacing S, cm.	Number of Orifices N, -	Plate free area ϕ
0.10	3.00	19	9.7×10^{-4}
	2.3	37	18.85×10^{-4}
	1.80	57	29.0×10^{-4}
0.159	2.3	37	48.0×10^{-4}
	1.80	57	74.0×10^{-4}
0.200	2.3	37	238×10^{-4}
0.238	1.80	57	166×10^{-4}
	1.59	19	174×10^{-4} *
	1.81	14	127×10^{-4} *
0.318	3.0	19	100×10^{-4}
	1.59	19	310×10^{-4} *

* 7.9 cm. diameter column

TABLE 3.2

Orifice diameter D_o = 0.1 cm.					
N = 57		N = 37		N = 19	
Q_o $cm^3./sec.$	ΔP_D $cm.H_2O$	Q_o $cm^3./sec.$	ΔP_D $cm.\ H_2O$	Q_o $cm^3./sec.$	ΔP_D $cm.\ H_2O$
3.760	0.485	8.05	1.90	11.00	3.30
4.460	0.650	9.20	2.45	13.50	4.80
5.23	0.89	11.50	3.40	17.9	7.45
5.96	1.12	12.60	4.55	22.45	11.35
6.72	1.35	13.70	5.30	26.80	16.30
7.45	1.67	16.20	6.60	36.00	27.50
8.20	2.00	18.20	8.80	44.60	41.00
10.45	3.15	20.60	10.45	54.20	56.50
11.96	3.90	28.20	18.40	62.50	74.00
14.92	5.80	30.60	22.50		
20.80	10.50	36.70	31.80		
23.90	13.70	41.40	40.00		
26.80	16.80	48.40	52.00		
31.30	23.00				
37.95	31.00				

TABLE 3.3

Orifice diameter D_o = 0.159 cm.		Orifice diameter D_o = 0.20 cm.			
N = 57		N = 37		N = 37	
Q_o $cm^3./sec.$	ΔP_D cm. H_2O	Q_o $cm^3./sec.$	ΔP_D cm. H_2O	Q_o $cm^3./sec.$	ΔP_D cm. H_2O
7.10	0.137	13.60	0.44	9.00	0.09
8.87	0.206	19.00	0.85	10.25	0.112
10.80	0.285	21.70	1.090	11.3	0.143
12.56	0.376	27.70	1.72	13.5	0.20
14.30	0.500	33.50	2.47	15.7	0.265
16.10	0.620	42.60	3.90	18.0	0.350
18.20	0.760	52.00	5.65	22.5	0.545
23.70	1.280	62.00	7.90	27.0	0.78
28.0	1.77	73.60	10.55	31.5	1.04
34.10	2.62	80.00	13.00	36.0	1.41
39.60	3.46	91.50	17.80	40.6	1.85
45.30	4.40	100.00	20.40	44.0	2.10
54.00	6.20	109.4	25.50	50.2	2.80
		121.0	30.00	55.0	3.30
				61.0	3.90

TABLE 3.4

Orifice diameter D_o = 0.318 cm.			
N = 19		N = 19*	
Q_o $cm^3./sec.$	ΔP_D cm. H_2O	Q_o $cm^3./sec.$	ΔP_D cm. H_2O
26.3	0.109	19.70	0.07
32.8	0.177	22.00	0.0835
42.2	0.270	26.50	0.117
59.0	0.520	31.00	0.160
71.0	0.730	35.00	0.193
89.0	1.195	39.40	0.244
102.0	1.58	44.00	0.310
118.5	1.90	52.50	0.432
137.0	2.70	61.40	0.595
155.0	3.45	72.0	0.795
172.0	4.14	80.0	0.980
190.0	5.10		
217.0	6.40		

* Data refer to 7.9 cm. diameter column.

TABLE 3.4 (cont'd)

Orifice diameter D_o = 0.238 cm.					
N = 57		N = 19*		N = 14*	
Q_o $cm^3./sec.$	ΔP_D cm. H_2O	Q_o $cm^3./sec.$	ΔP_D cm. H_2O	Q_o $cm^3./sec.$	ΔP_D cm. H_2O
14.0	0.105	13.92	0.110	15.20	0.142
19.60	0.203	16.25	0.143	18.25	0.198
23.4	0.29	18.52	0.180	21.80	0.26
27.4	0.392	21.00	0.225	24.4	0.238
33.6	0.596	23.20	0.27	30.4	0.49
40.5	0.824	25.60	0.33	33.5	0.61
45.0	1.12	27.80	0.382	36.5	0.716
54.5	1.52	32.00	0.500	42.8	0.945
62.0	1.94	37.20	0.650	49.0	1.250
80.0	3.10	46.60	1.080	54.8	1.57
98.0	4.80	56.30	1.600	61.0	2.00
109.0	5.40	66.0	2.150	73.3	2.69
		76.2	2.850		

* Data refer to 7.9 cm. diameter column.

TABLE 3.5

Effect of orifice spacing on distributor pressure drop

(14 cm. diameter column)

D_o = 0.10 cm.		N = 19		$\phi = 9.7 \times 10^{-4}$	
S = 1.27 cm		S = 1.9 cm.		S = 3.0 cm.	
U cm./sec.	ΔP_D cm. H_2O	U cm./sec.	ΔP_D cm. H_2O	U cm./sec.	ΔP_D cm. H_2O
1.50	3.75	1.20	2.54	1.37	3.3
2.20	8.00	1.55	4.0	1.67	4.7
2.78	12.3	1.98	6.6	2.22	7.4
3.00	14.1	2.48	10.0	2.78	11.3
3.65	19.1	3.00	13.4	3.33	16.2
4.56	29.0	3.50	18.0	4.46	27.7
5.36	38.5	3.95	23.8	5.56	40.6
7.00	63.0	3.54	35.4	6.90	56.9
8.00	80.2	5.95	50.0	7.35	74.0
		6.90	60.0		

TABLE 3.6

Comparison of calculated and measured orifice constant

D_o cm.	D_o^2 $cm.^2$	k_o calculated	k_o* measured
0.10	0.01	10	7.08
0.159	0.0253	25.3	20.80
0.20	0.04	40	30.50
0.238	0.0565	56.3	44.00
0.318	0.0101	101.0	82.00

*Is the mean observed orifices coefficient. It was obtained as follows for each distributor

$$k_o = \sum_{1}^{n} \frac{Q_o}{\sqrt{\Delta P_D}} \Big/ n$$

Where n = number of observations.

TABLE 3.7

Distributors used in the experiments (14 cm.diam.bed)

Distributor plates	D_o, cm.	S, cm.	N	ϕ
1	0.1	1.8	57	29.0×10^{-4}
2	0.1	2.3	37	18.85×10^{-4}
3	0.1	3.0	19	9.70×10^{-4}
4	0.159	2.3	37	48.0×10^{-4}
5	0.159	1.8	57	74.0×10^{-4}

TABLE 3.8

Predicted air velocities U required to make all orifices operative for the distributors used in the experiments

Solid	Distributor	U cm./sec.	U/U_{mf}
224 μ silver sand	1	9.133	1.63
U_{mf} = 5.7 cm./sec.	2	7.446	1.33
	3	6.408	1.144
	4	12.474	2.230
237 μ glass beads	1	9.968	1.424
U_{mf} = 7.0 cm./sec.	4	14.680	2.100
	5	16.230	2.320

TABLE 3.9

(Glass Beads)

Distr.	ΔP_B eq. cm.H_2O	ΔP_B obs. cm.H_2O	U cm./sec.	ΔP_1 cm.H_2O	ΔP_2 cm.H_2O	$\frac{\Delta P_B}{\Delta P_1}$	$\frac{\Delta P_2}{\Delta P_1}$
1	37.0	35.8	12.62	27.5	15.8	1.30	0.575
			14.82	37.0	28.2	0.970	0.773
			18.60	56.1	44.2	0.640	0.788
			22.53	78.3	62.2	0.460	0.80
			26.25	105.0	80.0	0.341	0.76
	63.1	61.9	12.22	27.1	15.4	2.285	0.568
			14.5	36.2	23.2	1.71	0.64
			18.86	56.3	42.1	1.100	0.75
			22.86	80.0	57.0	0.774	0.712
			26.0	104.0	84.4	0.595	0.81
	87.9	87.0	12.7	27.7	12.00	3.14	0.433
			14.82	37.0	18.00	2.35	0.487
			18.82	56.1	35.6	1.55	0.635
			22.59	79.0	59.3	1.10	0.747
	107.2	106.	10.75	20.0	6.84	5.30	0.342
			12.44	27.3	10.26	3.90	0.376
			14.40	35.5	17.23	2.986	0.486

TABLE 3.9 (continued)

(Glass Beads)

	ΔP_B eq. cm.H_2O	ΔP_B obs. cm.H_2O	U cm./sec.	ΔP_1 cm.H_2O	ΔP_2 cm.H_2O	$\frac{\Delta P_B}{\Delta P_1}$	$\frac{\Delta P_2}{\Delta P_1}$
4	85.6	83.02	11.80	4.95	1.00	16.80	0.200
		83.65	13.10	6.00	0.82	14.00	0.136
		83.80	15.30	8.00	2.00	10.50	0.250
			17.40	10.50	3.60	7.98	0.343

TABLE 3.9 (continued)

(Glass Beads)

	ΔP_B eq. cm.H_2O	ΔP_B obs. cm.H_2O	gas.ve cm./sec.	ΔP_1 cm.H_2O	ΔP_2 cm.H_2O	$\frac{\Delta P_B}{\Delta P_1}$	$\frac{\Delta P_2}{\Delta P_1}$
5	53.3	51.5	14.00	3.14	0.50	16.40	0.159
			15.40	3.75	0.90	13.74	0.240
			17.10	4.60	1.50	11.20	0.326
			20.00	6.10	2.20	8.44	0.367
	85.25	84.10	17.50	4.80	0.82	17.50	0.170
			19.10	5.65	0.90	14.88	0.159
			20.40	6.30	1.15	13.35	0.182
			21.76	7.10	1.56	11.850	0.220
			24.40	9.00	3.00	9.34	0.334

TABLE 3.10

(Silver Sand)

Distr.	ΔP_B eq. $cm.H_2O$	ΔP_B obs. $cm.H_2O$	U cm./sec.	ΔP_1 $cm.H_2O$	ΔP_2 $cm.H_2O$	$\frac{\Delta P_B}{\Delta P_1}$	$\frac{\Delta P_2}{\Delta P_1}$
1	23.8	22.0	8.62	13.70	11.4	1.61	0.833
			9.71	17.00	15.8	1.29	0.930
			11.0	21.00	18.7	1.05	0.890
			11.8	24.00	21.00	0.916	0.875
			13.36	30.00	27.00	0.734	0.900
			15.6	40.50	35.00	0.544	0.865
	39.7	38.9	9.7	16.70	14.00	2.33	0.840
			11.26	21.40	16.90	1.84	0.79
			13.22	29.60	25.74	1.32	0.87
			15.53	40.00	36.00	0.973	0.90
	68.00	67.3	14.77	36.5	21.90	1.84	0.623
			18.86	56.3	35.7	1.195	0.635
			22.5	78.6	55.7	0.855	0.705
	85	84.0	15.60	40.5	23.6	2.08	0.584
			18.82	56.1	34.0	1.50	0.606
			22.40	78.0	45.0	1.01	0.577

TABLE 3.10 (continued)

	ΔP_B eq. cm.H_2O	ΔP_B obs. cm.H_2O	U cm./sec.	ΔP_1 cm.H_2O	ΔP_2 cm.H_2O	$\Delta P_B/\Delta P_1$	$\frac{\Delta P_2}{\Delta P_1}$
2	16.00	15.10	5.62	13.8	8.8	1.095	0.637
		14.90	6.1	15.7	11.2	0.95	0.720
		15.00	6.637	18.5	13.8	0.812	0.746
			7.735	24.8	19.4	0.605	0.783
			8.87	32.0	25.70	0.470	0.805
			9.98	39.0	33.70	0.385	0.865
			10.55	43.5	37.47	0.345	0.862
			11.65	52.0	46.50	0.289	0.895
	31.8	31.00	5.60	13.65	6.9	2.27	0.504
		30.80	6.00	15.30	8.00	2.00	0.523
			6.64	19.00	10.75	1.62	0.566
			7.725	24.8	16.00	1.24	0.645
			8.87	32.00	23.00	0.963	0.720
			9.94	38.50	29.20	0.800	0.76
			10.51	43.20	33.10	0.713	0.766
			11.60	51.80	43.00	0.595	0.830
	47.70	46.80	6.10	15.70	6.30	2.98	0.400
			6.65	19.00	8.53	2.46	0.950
			7.72	24.7	13.20	1.90	0.535
			8.95	32.2	23.00	1.45	0.715
			9.90	38.0	31.20	1.23	0.82
			10.75	44.0	34.00	1.063	0.773
			11.55	51.5	42.90	0.91	0.834

TABLE 3.10 (continued)

(Silver Sand)

	ΔP_B eq. cm.H_2O	ΔP_B obs. cm.H_2O	U cm./sec.	ΔP_1 cm.H_2O	ΔP_2 cm.H_2O	$\frac{\Delta P_B}{\Delta P_1}$	$\frac{\Delta P_2}{\Delta P_1}$
2	81.7	81.2	6.60	18.40	8.1	4.41	0.44
			7.75	24.5	10.0	3.31	0.408
			8.60	29.5	13.9	2.75	0.472
			10.00	36.8	22.1	2.09	0.570
3	23.8	23.0	5.60	42.00	36.9	0.547	0.88
		23.2	7.35	72.50	71.2	0.320	0.983
			10.00	125.0	118.5	0.185	0.950
			11.20	150.0	145.9	0.155	0.973
			15.23	268.0	265.0	0.0865	0.99

TABLE 3.10 (continued)

(Silver Sand)

	ΔP_B eq. cm. H_2O	ΔP_B obs. cm.H_2O	U cm./sec.	ΔP_1 cm. H_2O	ΔP_2 cm.H_2O	$\frac{\Delta P_B}{\Delta P_1}$	$\frac{\Delta P_2}{\Delta P_1}$
4	23.00	21.8	8.80	2.8	0.66	7.80	0.236
			10.00	3.7	1.15	5.90	0.311
			11.65	4.9	2.20	4.45	0.450
			13.85	6.6	3.70	3.30	0.560
			16.70	9.4	7.00	2.32	0.745
			19.40	12.9	11.30	1.69	0.876
	47.9	45.8	9.95	3.55	0.40	12.9	0.130
			11.60	4.80	1.15	9.55	0.24
			13.80	6.56	2.00	6.97	0.304
			16.60	9.30	4.50	4.93	0.484

TABLE 3.10 continued

(Silver Sand)

	ΔP_B eq. cm.H_2O	ΔP_B obs. cm.H_2O	gas velocity U cm. sec.	ΔP_1 cm.H_2O	ΔP_2 cm.H_2O	$\frac{\Delta P_B}{\Delta P_1}$	$\frac{\Delta P_2}{\Delta P_1}$
4	65.35	64.0	11.10	4.35	0.65	14.70	0.150
			14.00	6.90	1.60	9.30	0.232
			16.65	9.40	3.00	6.80	0.319
			19.00	12.3	4.40	5.20	0.36
	84.70	83.80	11.25	4.4	0.50	19.10	0.114
			13.90	6.8	1.20	12.30	0.176
			16.60	9.3	3.00	9.00	0.323
			19.30	12.7	4.50	6.60	0.354
2	67.0	66.0	6.60	18.00	9.10	3.67	0.505
			7.76	24.60	13.10	2.683	0.533
			8.90	31.50	16.00	2.100	0.507
			9.95	38.00	25.64	1.740	0.675

Pressure drop criteria

TABLE 3.11

(14.0 cm. diam. bed)

	Bed ht. H, cm.	ΔP_B(obs.) cm.H_2O	ΔP_D(obs.) cm.H_2O	H/D	$\Delta P_D/\Delta P_B$
Distributor 4	4.0	6.1	1.28	0.286	0.21
224 μsilver	5.85	8.8	1.80	0.418	0.205
sand	8.10	11.6	1.65	0.578	0.142
	10.0	14.93	1.74	0.715	0.1163
	12.45	18.50	1.45	0.89	0.0785
	16.85	25.50	1.43	1.20	0.0581
	22.40	34.10	1.22	1.60	0.0358
Distributor 5	4.0	6.0	1.40	0.286	0.234
224 μ silver	5.9	6.6	1.22	0.422	0.185
sand	8.5	9.6	1.15	0.608	0.12
	10.5	11.4	1.14	0.750	0.10
	13.8	17.4	1.35	0.985	0.775
Distributor 4	4.1	8.2	1.72	0.293	0.21
237 μ glass	6.5	10.25	2.20	0.465	0.214
beads	10.6	17.10	1.90	0.757	0.111
	13.4	21.40	2.0	0.957	0.0935
	16.4	26.75	1.745	1.171	0.0654
	22.1	36.25	1.90	1.580	0.05245
Distributor 5	5.5	2.70	0.47	0.393	0.174
281 μ Diakon	9.3	6.00	0.61	0.664	0.103
	14.8	8.90	0.52	1.055	0.0585
	18.9	11.15	0.47	1.35	0.0421
Distributor 5	5.5	2.0	0.30	0.393	0.15
106 μ cracking	10.1	4.2	0.42	0.722	0.10
catalyst	15.5	6.3	0.352	1.108	0.056

[illegible] are given in Table (3.7)

TABLE 3.12

(30.5 cm. diam. Bed)

Distributor

N: 97

D_o: 0.159 cm.

ϕ: 26.4×10^{-4}

	Bed ht. H, cm.	ΔP_B(obs.) cm. H_2O	ΔP_D(obs.) cm. H_2O	H/D	$\Delta P_D/\Delta P_B$
.224 μ silver sand	5.8	8.85	2.84	0.19	0.321
	8.6	13.7	3.50	0.282	0.256
	12.2	17.9	4.12	0.40	0.230
	17.4	25.9	4.22	0.57	0.163
	21.4	31.8	3.82	0.70	0.12
	30.5	44.1	3.53	1.0	0.08
237 μ glass beads	6.0	10.2	3.18	0.197	0.316
	8.2	14.2	3.80	0.269	0.268
	12.1	19.9	4.68	0.396	0.235
	16.5	24.7	4.32	0.542	0.175
	21.0	34.0	4.32	0.690	0.127
	27.9	46.1	4.20	0.915	0.091
	30.6	52.0	4.0	1.0	0.077

TABLE 4.1

Distributor plates	D_o, cm.	S, cm.	N	ϕ
A	0.10	1.8	57	29×10^{-4}
B	0.159	1.8	57	74×10^{-4}
C	0.159	1.8	22	29×10^{-4}
-	0.238	1.8	57	166×10^{-4}

TABLE 4.2

Experimental Results

Distributor A Solid: (224 μ) ungraded silver sand

Maximum spoutable bed height = 5.24 cm. U_{mf} = 5.7 cm./sec.

$U - U_{mf}$	H_{mf} = 5.8 cm.		H_{mf} = 10.5 cm.		H_{mf} = 16.5 cm.	
cm./sec.	D_B, cm. obs.	D_B, cm. calc.	D_B, cm. obs.	D_B, cm. calc.	D_B, cm. obs.	D_B, cm. calc.
0.00	0.80		1.39		1.83	
0.30	0.81	0.805	1.33	1.215		
0.60	0.87	0.926	1.40	1.357	1.99	1.906
1.00	0.94	1.050			2.20	2.091
1.30			1.53	1.607	2.18	2.217
1.40	1.13	1.154				
1.60					2.33	2.335
1.70	1.00	1.224				
1.80						
2.00	1.13	1.289	1.73	1.815		
2.30						
2.40					2.47	2.630
2.70	1.26	1.43	1.96	2.00		
2.80						
3.00					2.905	2.838
3.40			2.00	2.18		
3.80					2.80	3.105
3.90	1.48	1.645				
4.00			2.20	2.325		
5.10	1.80	1.841	2.53	2.580	3.47	3.52
5.50						
6.00	2.07	1.980	2.81	2.778	3.67	3.80

TABLE 4.2 continued

$U - U_{mf}$ cm./sec.	H_{mf} = 22.4 cm.		H_{mf} = 25.0 cm.	
	D_B, cm. obs.	D_B, cm. calc.	D_B, cm. obs.	D_B, cm. calc.
0.00	2.39			
0.30	2.46	2.256	2.72	2.479
0.60	2.45	2.445	3.00	2.683
1.00	2.63	2.665	3.03	2.918
1.30	2.73	2.810	3.20	3.081
1.80	2.92	3.05	3.5	3.338
2.30	3.18	3.28		
2.40			3.73	3.63
2.80	3.39	3.50		
3.00			3.90	3.912
4.00	3.86	4.00	4.40	4.367
5.10	4.46	4.445	5.08	4.853
5.50	4.52	4.610	5.39	5.027
6.20	4.97	4.879		

TABLE 4.3

Experimental Results

Distributor A Solid: (237 μ) graded glass beads.

Maximum spoutable bed height = 5.35 cm. U_{mf} = 7.0 cm./sec.

$U - U_{mf}$	H_{mf} = 6.0 cm.		H_{mf} = 10.5 cm.		H_{mf} = 16.1 cm.	
cm./sec.	D_B, cm. obs.	D_B, cm. calc.	D_B, cm. obs.	D_B, cm. calc.	D_B, cm. obs.	D_B, cm. calc.
0.5	1.10	0.991	1.38	1.459	1.70	2.042
1.0			1.41	1.649	1.80	2.271
1.1	1.2	1.177				
1.5			1.52	1.808		
1.7	1.18	1.323				
2.0			1.72	1.95	2.4	2.649
2.3	1.30	1.45				
3.0	1.56	1.584	2.10	2.208	2.8	2.984
3.5					3.1	3.144
3.6	1.64	1.691				
4.0						
4.1	1.82	1.776	2.62	2.468		
4.2						
4.4					3.70	3.422
4.5						
4.7			2.84	2.604		
5.2	2.12	1.952				
5.4			3.23	2.757	4.18	3.72
6.1			3.42	2.906	4.57	3.923
6.2	2.40	2.104				
7.0	2.76	2.22	3.90	3.094	5.16	4.181

TABLE 4.3 continued

$U - U_{mf}$ cm./sec.	H_{mf} = 22.5 cm.		H_{mf} = 27.2 cm.	
	D_B, cm. obs.	D_B, cm. calc.	D_B, cm. obs.	D_B, cm. cals.
0.5	2.36	2.707	2.90	3.185
1.0	2.52	2.98	2.98	3.491
2.0	3.10	3.447	3.82	4.021
3.0	3.80	3.872		
3.1			4.52	4.557
4.0	4.58	4.275		
4.2			5.06	5.069
4.5	4.72	4.472		
5.4	5.26	4.820	6.00	5.611
6.1	5.55	5.086	6.39	5.921
7.0	6.50	5.423	7.10	6.316

TABLE 4.3 continued

Distributor B Solid: (237 μ) graded glass beads

U - Umf cm./sec.	H_{mf} = 6.0 cm.		H_{mf} = 10.5 cm.		H_{mf} = 16.1 cm.		H_{mf} = 22.5 cm.	
	D_B, cm. obs.	D_B, cm. calc.	D_B, cm. obs.	D_B, cm. calc.	D_B, cm. obs.	D_B, cm. calc.	D_B, cm. obs.	D_B, cm. calc.
0.5	1.32	0.991	2.12	1.459	2.39	2.042		
1.0	1.46	1.150	2.10	1.649	2.60	2.271	3.59	2.98
1.5	1.52	1.277	2.40	1.808				
2.0	1.63	1.388	2.43	1.950	2.90	2.699	4.00	3.447
3.0	1.94	1.584	2.77	2.208	3.4	2.984	4.56	3.872
3.5			2.90	2.329	3.5	3.144	4.80	4.076
4.0	2.20	1.759	3.20	2.445				
4.5	2.31	1.841	3.20	2.559	4.00	3.452	5.39	4.472
5.0	2.44	1.921	3.40	2.670	4.26	3.601		
5.4	2.52	1.983	3.53	2.757	4.40	3.720	5.79	4.82
6.0			3.90	2.885				
7.0	2.85	2.22	4.18	3.094	5.2	4.18	6.62	5.423

TABLE 4.3 continued

Distributor C Solid: (237μ) graded glass beads.

H_{mf} = 10.5 cm.

$(U - U_{mf}$ cm./sec.	0.5	1.0	1.5	2.0	2.7	3.0	4.0	4.7	5.4	6.1
(D_B) obs. cm.	1.71	1.70	1.70	1.82	2.00	2.23	2.62	2.9	3.16	3.52

TABLE 4.4

Data reported in the literature

(I) Date reported by Cookes et al.(102)

Condition	U cm./sec.	U/U_{mf} -	H_{mf} cm.	(D_B)obs. cm.	(D_B)calc. cm.
Solid: coal	36	7.2	20	15	16.2
U_{mf} = 5 cm./sec.	36	7.2	40	24	27.4
ρ_s = 1.4 gm./cm^3.	24	4.8	20	12.5	11.5
	24	4.8	40	21	19.3
Distributor: multi-	18	3.6	20	9.8	9.1
orifice with 0.1	18	3.6	40	16	14.8
orifices per cm^2.	18	3.6	60	22	20.4
	18	3.6	80	27	26.0

D = 30 cm. x 1.2 cm.

(two-dimensional bed)

TABLE 4.4 continued

(II) Data reported by Mcgrath and Streatfield(109)

Condition	U cm./sec.	U/U_{mf} -	H_{mf} cm.	$(D_B)_{obs.}$ cm.	$(D_B)_{calc.}$ cm.
Solid: alkalized alumina	65	1.18	1.3	1.65	1.25
	70	1.272	1.3	1.68	1.35
U_{mf} = 55 cm./sec.	65	1.18	2.6	2.50	1.70
	70	1.272	2.6	2.60	1.85
ρ_s = 1.4 gm./cm^3	65	1.18	5.2	2.90	2.64
	70	1.272	5.2	3.33	2.85
D_p = 1540 μ	65	1.18	7.8	3.34	3.60
Distributor: multi-orifice	70	1.272	7.8	4.10	3.85
plate with 2.5 orifices	75	1.362	7.8	5.00	4.00
per cm^2.	65	1.18	10.5	4.17	4.57
	70	1.272	10.5	5.30	4.90
D = 30.5 cm. x 15.2 cm.	65	1.18	13.3	5.00	5.60
(three-dimensional bed)	70	1.272	13.3	7.35	6.00

TABLE 5.1

Details of multi-orifice distributors

Cross-sectional area of column = 45.45 $cm.^2$

Distributors	Orifice spacing S cm.	Orifice diameter D_o cm.	Number of Orifices N	Plate characteristics ϕ
1	6.6	0.05	5	2.21×10^{-4}
2	3.3	0.05	11	4.86×10^{-4}
3	9.6	0.10	3	5.3×10^{-4}
4	7.2	0.10	5	8.84×10^{-4}
5	4.8	0.10	8	14.14×10^{-4}
6	2.4	0.10	15	26.5×10^{-4}

TABLE 5.2

Solid Particles *

	Diakon	Sand S_1	Sand S_2	Sand S_3	Catalyst C_1
Mean particle diameter, μ	281	177	277	138	106
particle density, $gm./cm^3$.	1.167	2.64	2.64	2.63	0.915
U_{mf}, cm./sec.	3.25	4.0!!	7.6	1.95	0.455

* See Table (2.3) (Chapter 2) for details.

!! In Table (2.3) is given as 2.6 cm./sec. In a two-dimensional column this is found to be around 4.0 cm./sec.

TABLE 5.3

Experimental Results

Solid: Diakon (281 μ) U_{mf} = 3.25 cm./sec.

$\frac{U_{mf}}{U}$	Z/S 1 S = 6.6 cm.	Z/S 2 S = 3.3 cm.	$\frac{U_{mf}}{U}$	Z/S 4 S = 7.2 cm.	Z/S 5 S = 4.8 cm.
0.788	3.12	2.97	0.694	2.65	2.80
0.720	2.77	2.73	0.572	-	2.34
0.620	2.27	2.35	0.500	1.92	1.88
0.540	2.16	2.05	0.434	1.70	1.62
0.481	1.88	1.79	0.383	1.48	1.42
0.434	1.58	1.59	0.342	1.34	1.27
			0.315	1.25	1.15
			0.289	1.12	0.94

TABLE 5.4

Experimental Results

Solid: Silver sand S_2 (277 μ) U_{mf} = 7.6 cm./sec.

	Z/S		
$\frac{U_{mf}}{U}$	6 S = 2.4 cm.	5 S = 4.8 cm.	4 S = 7.2 cm.
0.914	3.99	3.75	
0.855	3.70	3.42	3.53
0.763	3.12	3.10	3.06
0.703	2.90	2.91	2.90
0.648	2.67	-	2.54
0.592	2.42	2.36	2.50
0.558	2.22	2.27	2.38

continued...

TABLE 5.4 continued

$\frac{U_{mf}}{U}$	Z/S		
	6	5	4
	S = 2.4 cm.	S = 4.8 cm.	S = 7.2 cm
0.522	2.04	2.03	2.15
0.467	1.79	1.86	1.92
0.420	1.61	1.63	
0.351	1.38	1.42	
0.300	1.16		
0.263	1.02		

TABLE 5.5

Experimental Results

Solid: Rounded sand S_3 (138 μ) U_{mf} = 1.95 cm./sec.

$\frac{U_{mf}}{U}$	Z/S			
	6	5	4	3
	S = 2.4 cm.	S = 4.8 cm.	S = 7.2 cm.	S = 9.6 cm.
0.756	3.04	2.92	2.95	3.13
0.66	2.60	2.71	2.56	2.70
0.53	2.12	2.04	1.93	1.98
0.441	1.80	1.71	1.60	1.68
0.377	1.58	1.46	1.40	1.44
0.33	1.46	1.32	1.25	1.22
0.293	1.34	1.13	1.13	1.19
0.264	1.17	1.12	1.00	
0.24	1.10	1.04	0.94	
0.21	0.92	0.96	0.77	

TABLE 5.6

Experimental Results

Solid: Diakon (281 μ) U_{mf} = 3.25 cm./sec. Distributor 5

n	$\frac{n}{N}$	U/U_{mf}		
		Bed height H_{mf} = 21.5	Bed height H_{mf} = 46.5	Bed height H_{mf} = 66.6
1	0.125	-	1.05	1.058
2	0.250	1.125	1.138	1.12
3	0.375	1.20	1.21	1.21
4	0.500	1.27	1.25	1.26
5	0.625	1.31	1.30	1.30
6	0.750	1.36	1.36	1.35
7	0.875	1.448	1.46	1.44
8	1.000	1.610	1.54	1.52

TABLE 5.7

Experimental Results

Solid: graded silver sand S_1 (177 μ) U_{mf} = 4.0 cm./sec. Distributor 5

n	$\frac{n}{N}$	U/U_{mf}		
		Bed height H_{mf} = 21.7	Bed height H_{mf} = 36.4	Bed height H_{mf} = 56.2
1	0.125	1.08	1.062	1.065
2	0.250	1.17	1.158	1.150
3	0.375	1.22	1.235	1.250
4	0.500	1.282	1.300	1.300
5	0.625	1.366	1.385	1.370
6	0.750	1.410	1.420	1.450
7	0.875	1.467	1.48	1.530
8	1.000	1.870	1.86	1.840

TABLE 5.8

Experimental Results

Solid: Cracking catalyst C_2 (106 μ) U_{mf} = 0.455 cm.sec^{-1}. Distributor 5

Repeatability of Results

n	$\frac{n}{N}$	U/U_{mf}		
		Bed height H_{mf} = 22.0	Bed height H_{mf} = 45.0	Bed height H_{mf} = 70.3
1	0.125	1.375	1.82	1.64
		1.86	1.31	1.50
2	0.25	1.70	1.36	1.50
		1.80	1.66	1.54
3	0.375	2.12	1.94	2.05
		-	2.25	2.36
4	0.500	2.42	2.32	2.13
		2.25	2.45	2.20
5	0.625	2.78	3.04	3.10
		3.06	3.72	2.85
6	0.750	3.42	3.25	3.55
		3.68	3.65	3.33
7	0.875	4.09	3.76	4.0
		3.66	-	3.9
8	1.000	4.45	4.3	4.25
			4.12	4.50

Gravity Flow Data

TABLE 6.1

Repeatability of the results

Solids are specified in Table (2.3) (Chapter 2)

Solids	Orifice diam. D_o, cm.	Observed sec.	gms.	W gm./min.	Average W gm./min.	Deviation %
		35	154.5	264		
Glass beads G_3 (237 μ)	0.4762	35	154.4	263	264.0 ∓1	∓ 0.4
		40	176.6	265		
		60	266.5	266.5		
Glass beads G_4 (270 μ)	0.4762	40	177.0	265.8	266.0 ∓0.5	∓ 0.2
		45	198.0	265.8		
		30	236.9	473.8		
Silver & Sand S_2 (277 μ)	0.635	40	314.7	473.0	473.3 ∓0.5	∓ 0.1
		40.9	322.5	473.2		
		30	99.6	199.2		
Diakon (281 μ)	0.635	30	98.0	196.0	198 ∓ 2	∓ 1.0
		30	00.4	198.8		

TABLE 6.2

Effect of bed height

Solid	Orifice diam. D_o, cm.	Flow rate W gm./min. H = 10 cm.	H = 20 cm.	H = 30 cm.
	1.270	-	3869	3854
Glass beads	1.1112	2709	2716	2711
G_3	0.873	1540	1433	1441
(237 μ)	0.635	575.4	576.3	575
	0.4762	264.0	266.0	263.7
	0.3175	82.1	82.1	82.0
	0.238	39.9	39.7	39.8

TABLE 6.3

Experimental Results

Orifice diam. D_o, cm.	Flow Rate W. gm./min.						
	Glass G_4 270μ	Sand S_2 277 μ	Sand S_1 177 μ	Diakon 281μ	Catalyst C_2 106 μ	Catalyst C_1 74 μ	Coal 128 μ
Q.238	42.5	35.8	34.3	14.3	17.2	15.8	11.6
0.3175	93.7	77.4	74.3	32.7	29.8	28.5	25.7
0.4765	266.0	215	202	91.2	77.2	67.7	68.0
0.635	596.7	473.3	424.5	198	133	124	135.8
0.873	1396	1136	975.3	468	253.2	239	289
1.1112	2703	2164	1844.5	870	464.5	422	575.2
1.270	3830	3055.5	2655.5	1029	602.3	536	768.3

TABLE 6.4

Cracking catalyst C_2

D_p = 106 μ ρ_B = 0.581 gm./cm^3.

D_o, cm.	N	A_e, cm^2.	$\rho_B \cdot A_e \cdot \sqrt{9}$	W, gm./min.
0.238	1	0.0391	0.712	17.2
	2	0.0782	1.424	34.5
	4	0.1564	2.848	70.0
	9	0.3519	6.408	153.2
0.3175	1	0.072	1.32	29.81
	2	0.144	2.64	60.0
	4	0.488	5.28	129.3
	9	0.648	11.88	271.5
0.4762	1	0.167	3.04	77.25
	2	0.334	6.08	155.0
	4	0.668	12.16	320.0
0.635	1	0.302	5.50	133.0
	2	0.604	11.1	271.2
	4	1.208	22.2	533.7
0.8731	1	0.577	10.5	275.0
	2	1.154	21.0	540.0
	4	2.308	42.0	1100.0
1.112	1	0.945	17.2	464.47
	2	1.89	34.4	940.0
1.27	1	1.24	22.6	602.1
	2	2.48	45.2	1210.0

TABLE 6.5

Coal

D_p = 128 μ ρ_B = 0.490 gm./cm^3.

D_o, cm.	N	A_e, cm^2.	$\rho_B \cdot A_e \sqrt{g D_e}$	W, gm./min.
0.238	1	0.038	0.272	11.65
	4	0.076	1.088	49.12
	7	0.266	1.904	83.03
	9	0.342	2.448	106.33
	14	0.532	3.808	170.25
0.318	1	0.0705	0.594	25.71
	2	0.141	1.188	53.0
	4	0.282	2.396	103.32
	7	0.4935	4.158	180.55
	9	0.635	5.346	230.12
0.4762	1	0.1645	1.72	68.00
	2	0.329	3.44	141.21
	4	0.658	6.88	280.63
	6	0.987	10.32	421.28
0.635	1	0.298	3.6	135.8
	2	0.596	7.2	290.0
0.87312	1	0.575	8.15	289.0
	2	1.15	16.3	610.0

TABLE 6.6

Diakon

D_p = 281 μ ρ_B = 0.688 gm./cm.^{3}

D_o, cm.	N	A_e, cm.^{2}	$\rho_B . A_e \sqrt{g D_e}$	W, gm.min.$^{-1}$
0.2381	1	0.0308	0.296	14.3
	2	0.0616	0.592	29.5
	4	0.1232	1.184	59.0
	7	0.2156	2.072	105.0
	9	0.2772	2.664	125.7
	14	0.4312	4.144	208.25
0.4762	1	0.1495	2.122	91.2
	2	0.2990	4.244	180.5
	4	0.598	8.488	364.2
	7	1.0465	14.854	638.8
	9	1.3455	19.098	822.1
0.635	1	0.278	4.62	198.0
	2	0.556	9.24	408.2
	3	0.834	13.86	594.2
	5	1.390	23.1	987.2
	7	1.946	32.34	1353.8
0.8731	1	0.5445	10.7	468.2
	2	1.089	22.4	940.0
	3	1.5335	32.1	1402.0
	5	2.7225	53.5	2342.6
	7	3.8115	74.9	3279.3

TABLE 6.7

Glass beads G_4

D_p = 270 μ ρ_B = 1.79 gm./cm^3.

D_o, cm.	N	A_e, cm^2.	$\rho_B . A_e \sqrt{g D_e}$	W gm./min.
0.238	1	0.0312	0.78	42.49
	2	0.0624	1.56	84.05
	4	0.1248	3.12	169.55
	7	0.2184	5.46	244.12
	14	0.4368	10.92	590.10
0.3175	1	0.0613	1.815	93.55
	2	0.1226	3.63	200.2
	3	0.1839	5.445	282.0
	5	0.3065	9.075	465.75
	7	0.4291	12.705	654.50
	9	0.5517	16.335	838.0
0.4762	1	0.150	5.551	265.2
	2	0.300	11.10	532.0
	3	0.45	16.653	796.5
	5	0.75	27.76	1312.0
	7	1.05	38.86	1862.0
0.635	1	0.2794	12.1	595.73
	2	0.5588	24.2	1193.5
	3	0.8382	36.3	1787.4
	5	1.397	60.5	2980.0
0.87312	1	0.552	28.2	1396.0

TABLE 6.8

Silver sand S_2

D_p = 277 μ ρ_B = 1.58 gm./cm^3.

D_o, cm.	N	A_e, cm^2.	$\rho_B . A_e \sqrt{g . D_e}$	W. gm./min.
0.238	1	0.031	0.681	35.8
	2	0.062	1.362	70.05
	4	0.124	2.724	142.2
	7	0.2168	4.767	245.0
	14	0.4337	9.534	490.0
0.4762	1	0.15	4.92	215.9
	2	0.30	9.84	430.0
	3	0.45	14.76	650.0
	4	0.60	19.68	860.0
	7	1.05	34.44	1533.0
	9	1.35	44.28	1882.0
0.635	1	0.278	10.6	475.3
	2	0.5564	21.2	946.8
	3	0.8346	31.8	1425.1
	5	1.391	53.0	2380.0
	7	1.947	74.2	3228.0
0.87312	1	0.545	24.6	1138.0
	2	1.090	49.2	2272.5
	3	1.635	73.8	3414.8
	5	2.725	123.0	5685.0

TABLE 6.9

Distributor Plates

(1) Multi-orifice flat plates (7.9 cm. diam. column)

(NOTE: by stopping up orifices with Plasticine, the number of open orifices on a given plate was varied as desired.)

N	D_o, cm.	S, cm.	ℓ , cm.	ϕ , %
37	0.159	1.18	0.318	1.55
37	0.238	1.18	0.318	3.38
37	0.200	1.18	0.318	2.38
37	0.238	1.18	0.635	3.38
37	0.238	1.18	1.27	3.38
30	0.238	1.27	0.318	2.74
19	0.238	1.59	0.318	1.74
19	0.400	1.59	0.318	4.9
19	0.318	1.59	0.318	3.09
19	0.318	1.59	0.635	3.09
19	0.318	1.59	1.270	3.09
14	0.238	1.81	0.318	1.27
9	0.476	2.38	0.318	3.28
9	0.476	2.38	0.635	3.28
9	0.476	2.38	1.27	3.28
5	0.635	3.13	0.082*	3.27
5	0.635	3.13	0.318	3.27
5	0.635	3.13	0.635	3.27
5	0.635	3.13	1.27	3.27

* = 32 Thou.

(2) Multi-nozzle plates (see Table (6.33).

(3) Single-orifice plates (see Tables (6.10) - (6.13).

(4) Single-nozzle plates (see Tables (6.15) - (6.16)

Flowback Data - Single-Orifice Distributors

Table (6.10) - 106 μ catalyst C_2 (2-D bed)

$A = 44.45\ cm.^2$

D_o cm.	Q_o $cm^3./sec.$	U_o cm./sec.	H_{mf} = 32.2 cm.		H_{mf} = 52.2 cm.		H_{mf} = 70.3 cm.	
			ω gm./min.	ω_o gm./min.$cm.^2$	ω gm./min.	ω_o gm./min.$cm.^2$	ω gm./min.	ω_o gm./min.$cm.^2$
0.476	5	28.3	15.76	88.55	16.5	92.5		
$\phi = 4 \times 10^{-3}$	6.7	37.65	12.89	72.4	12.5	70.0	9.67	59.3
	8.35	47.15	10.13	57.92	9.75	54.8	8.00	45.0
	11.7	66.0	6.00	33.7	6.36	35.7		
	13.4	75.5	5.1	28.5	4.8	27.1	4.42	24.9
	16.7	99.3	3.46	19.5	3.17	17.8	3.8	21.3
	20.0	113.0	2.18	12.24	2.0	11.3	2.1	11.8
	23.4	132.0	1.62	9.1	1.24	7.0	1.1	6.2
	29.2	165.0	0.916	5.14	0.54	3.00	0.68	3.8
	33.4	189.0	0.53	3.00	0.30	1.7	0.35	1.98
	41.8	236.0	0.19	1.00	0.184	1.00	0.14	0.80
	45.0	255	0.00	0.00	0.00	0.00	0.00	0.00
	0.0	0.0	22.5	126.0	23.0	129.2	23.1	130

TABLE (6.10) continued

D_o CM.	Q_o cm./sec.	U_o cm./sec.	H_{mf} = 32.2 cm.		H_{mf} = 52.2 cm.		H_{mf} = 70.3 cm.	
			ω gm./min.	ω_o gm./min.cm^2	ω gm./min.	ω_o gm./min.cm^2	ω gm./min.	ω_o gm./min.cm^2
0.635	10.0	31.6	28.0	88.3	27.55	87		
$\phi = 7.15 \times 10^{-3}$	13.4	41.9	17.2	59.0	17.3	54.5		
	16.7	52.4	13.3	42.0	14.1	44.5	15.1	47.6
	21.0	65.5	9.3	29.4	9.3	29.4	9.7	30.5
	25.0	78.5	6.55	20.7	6.4	19.8	6.2	19.5
	29.2	91.6	4.45	14.1	3.76	11.8	4.2	13.2
	33.4	105.0	3.1	10.2	3.0	9.45		
	37.6	117.8	2.36	7.5	2.1	6.69	1.82	5.7
	41.6	131.0	1.64	5.2	1.45	4.6		
	45.9	144.0	1.13	3.6	1.07	3.4	1.0	3.15
	50.0	157.0	0.57	1.8	0.65	2.04	0.60	1.89
	0.0	0.0	-	-	-	-	49.6	165.2

TABLE (6.10) continued

D_o CM.	Q_o cm./sec.	U_o cm./sec.	H_{mf} = 32.2 cm.		H_{mf} = 52.2 cm.		H_{mf} = 70.3 cm.	
			ω gm./min	ω_o gm./min.cm.^{2}	ω gm./min.	ω_o gm./min.cm.^{2}	ω gm./min.	ω_o gm./min.cm.^{2}
0.794	33.4	67.3	22.3	45	19.2	38.8		
$\phi = 11.1 \times 10^{-3}$	37.6	75.8	17.0	34	16.4	33.2		
	41.8	84.2	13.8	27.8	12.87	26.0		
	46.0	92.6	10.6	21.4				
	50.0	101.0	8.24	16.7	7.45	15.0		
	58.5	117.8	5.58	11.2	5.30	10.7		
	67.0	134.7	3.8	7.7	3.25	6.6		
	75.0	152.0	3.0	6.06	2.2	4.3		
	83.5	168.0	2.15	4.34	1.34	2.7		
	100.0	202.0	1.25	2.52	0.47	0.95		
	0.0	0.0	-	-	79.0	159.5		

TABLE (6.10) continued

D_o CM.	Q_o cm./sec.	U_o cm./sec.	H_{mf} = 32.2 cm.		H_{mf} = 52.2 cm.		H_{mf} = 70.3 cm.	
			ω gm./min	ω_o gm./min.cm.^{2}	ω gm./min.	ω_o gm./min.cm.^{2}	ω gm./min.	ω_o gm./min.cm.^{2}
0.952	68.0	95		16.4	26.0			
$\phi = 16 \times 10^{-3}$	76.5	107.5			13.5	19.1		
	85.0	119.4			10.5	15.9		
	94.0	131.6			7.1	10.0		
	102	143.5			4.61	6.5		
	111	155.3			2.91	4.1		
	0.00	0.00			120.0	169.0		

TABLE (6.11) Ungraded catalyst (20-150μ)(cylindrical bed) $V_\omega = 4.9 \times 10^3 cm^3$. $A = 153.3\ cm^2$.

D_o cm.	Q_o cm^3/sec.	U_o cm./sec.	H_{mf} = 25.8 cm.		H_{mf} = 51.0 cm.		H_{mf} = 74.79 cm.		H_{mf} = 103.0 cm.	
			ω gm./min.	ω_o gm./min.cm^2	ω gm./min	ω_o gm./min.cm^2	ω gm./min.	ω_o gm./min.cm^2	ω gm./min.	ω_o gm./min.cm^2
0.952	50	70.5	54.0	76.0	52.0	73.5	52.7	74.1	52.0	73.5
	66.7	94.0	35.4	50.0	42.5	60.0	37.6	53.0	38.3	54.0
	100.0	140.5	17.0	24.0	17.6	25.0	17.9	25.3	20.6	29.0
	134.0	187.4	9.6	13.5	8.1	11.5	7.1	10.0	9.0	12.7
	167.0	234.0	6.00	8.46	3.4	4.8	2.85	4.0	4.5	6.4
$\phi = 4.6 \times 10^{-3}$	200.0	281.0	3.70	5.23	2.8	4.0	1.42	2.00	3.15	4.45
	234.0	328.0	3.00	4.24	1.43	2.0	1.00	1.41		
	268.0	375.0	1.67	2.36						
	334.0	468.0	0.50	0.70					0.41	0.58

TABLE (6.11) continued

D_o cm.	Q_o $cm.^3/sec.$	U_o cm./sec.	H_{mf} = 25.8 cm.		H_{mf} = 51.0 cm.		H_{mf} = 74.79 cm.		H_{mf} = 103.0 cm.	
			ω gm./min.	ω_o $gm./min.cm.^2$	ω gm./min	ω_o $gm./min.cm.^2$	ω gm./min.	ω_o $gm./min.cm.^2$	ω gm./min.	ω_o $gm./min.cm.^2$
0.635	13.4	42.0	46.5	146.0	40.0	126				
	16.7	52.5	38.0	120.0	41.1	130	31.2	75.6		
	25.0	78.8	24.4	77.0	31.0	98	25.1	79.0	36.7	116.0
	33.4	105.0	16.2	51.0			18.6	58.6	24.4	77.0
	41.6	131.0	11.4	33.6	11.3	35.6	11.3	35.7		
	50.0	158.0	7.9	25.0	7.0	22.0	6.7	21.1	7.5	23.6
	67.0	211.0	4.2	13.2	3.0	9.45	3.1	9.8	2.75	8.7
	83.5	263.0	2.44	7.8	1.55	4.9	1.8	5.67	1.4	4.4
	100.0	316			0.9	2.84	1.53	4.8	1.34	4.2
	117.0	368.0	0.85	2.68	1.6	5.05	1.47	4.6	1.00	3.3
	150	473.0				NO FLOWBACK				

$\phi = 2.05 \times 10^{-3}$

TABLE (6.11) continued

D_o cm.	Q_o cm^3/ sec.	U_o cm./ sec.	H_{mf} = 25.8 cm.		H_{mf} = 51.0 cm.		H_{mf} = 74.79 cm.		H_{mf} = 103.0 cm.	
			ω gm./min.	ω_o gm./min.cm^2	ω gm./min	ω_o gm./min.cm^2	ω gm./min.	ω_o gm./min.cm^2	ω gm./min.	ω_o gm./min.cm^2
0.476	20.9	117.0	15.4	86.5	16.0	90.0				
	25.0	140.0	12.0	67.5	11.5	64.6				
	29.2	164.0	8.9	50.0	9.55	53.6				
$\phi = 1.16 \times 10^{-3}$	33.4	187.0	5.5	30.8	6.30	35.4				
	37.6	211.0	4.4	24.6	6.00	33.7				
	45.9	257.0	2.5	14.0	2.6	14.6				
	54.4	304	1.35	7.55	1.4	7.86				
	62.6	351	0.74	4.08	0.8	4.50				
	75.0	422	0.10	0.56	0.10	0.56				

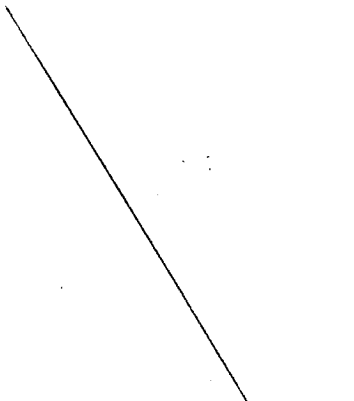

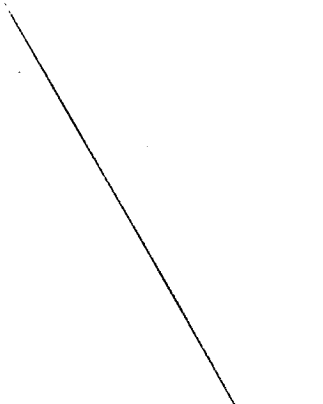

TABLE 6.12

138 rounded sand S_3 (2-D bed)

			H_{mf} = 70.2 cm.		H_{mf} = 35.8 cm.	
D_o cm.	Q_o $cm^3/sec.$	U_o cm./sec.	W gm./min.	W_o $gm./min.cm.^2$	W gm./min.	W_o $gm./min.cm.^2$
0.476	16.7	93.6	21.6	121	22.0	124
$\phi = 4 \times 10^{-3}$	25.00	140.5	10.2	57.8	10.5	59
	29.2	164.0	7.8	44.0	8.0	45
	33.4	187.3	5.98	33.6	5.2	29.2
	41.8	234	3.71	20.8	3.7	20.8
	46.2	257.5	3.06	17.2	3.2	18.0
	54.2	304.3	1.84	10.33	1.5	8.45
	0.0	0.0	49.5	278.0		
0.635	20.9	65.5	44.1	138.8		
$\phi = 7.15 \times 10^{-3}$	29.2	91.6	34.4	108.0		
	33.4	104.7	31.4	99.1		
	41.6	131.0	21.9	69.0		
	50.0	157.5	16.5	52.2		
	67.0	211.0	10.4	32.8		
	83.5	264.0	5.75	18.1		
	100.0	316.0	2.92	9.2		
0.794	33.4	67.4	95.3	192.0		
$\phi = 11.1 \times 10^{-3}$	37.6	75.8	80.2	162.0		
	41.8	84.2	67.8	138.0		
	50.0	101.0	52.0	105.0		
	67.0	134.7	33.2	67.0		
	83.5	168.0	25.8	51.7		
	100.0	202.0	17.2	34.6		
	117.0	236.0	12.85	26.0		
	150.0	303.0	6.55	13.2		

TABLE 6.13 - 128μ Coal (2-D bed) H_{mf} = 50 cm.

D_o = 0.476 cm.				D_o = 0.635 cm.				D_o = 0.794 cm.			
Q_o $cm^3/s.$	U_o cm/s.	ω g/min.	ω_o $g/min.cm^2$	Q_o $cm^3/s.$	U_o cm/s.	ω g/min.	ω_o $g/min.cm^2$	Q_o cm^3/s	U_o cm/s	ω g/min.	ω_o $g/min.cm^2$
3.34	19.3	13.4	75.0	6.7	21.0	27.9	88.0	16.8	34.0	27.6	55.7
5.0	28.8	10.3	57.0	10.0	31.6	19.1	60.4	25.0	51.0	16.3	31.6
6.7	38.5	8.5	47.8	13.4	42.0	13.2	41.7	33.4	67.4	8.86	17.9
8.35	48.2	6.35	35.5	16.7	52.4	8.3	26.1	37.6	75.8	5.95	12.0
10.0	57.7	3.40	19.0	21.0	65.5	5.8	18.2	41.8	84.2	4.06	8.18
11.7	67.4	2.96	16.6	25.0	78.5	3.6	11.3	46.0	92.6	2.92	5.9
13.4	77.0	1.89	10.3	29.2	91.6	1.95	6.1	50.0	101.0	1.88	3.8
16.7	96.0	0.85	4.8	33.4	105.0	1.13	3.6	158.5	117.8	0.93	1.86
				37.6	117.8	0.76	2.38				
0.0	0.0	17.7	100.0	0.0	0.0	34.1	107	0.0	0.0	59.0	119.3

TABLE (6.14) Effect of wind box volume

D_o = 0.952 cm. H_{mf} = 75 cm. (20-150μ) catalyst

(cylindrical bed) A = 153.3 cm^2.

Q_o	U_o	V_ω=19.2 x $10^3 cm^3$.	V_ω=41.5 x $10^3 cm^3$.	V_ω=63.8 x $10^3 cm^3$.	V_ω=86.1 x $10^3 cm^3$.
cm^3./sec.	cm./sec.	ω,gm./min.	ω,gm./min.	ω,gm./min.	ω,gm./min.
50	70.5	37.8	31.2	24.0	17.5
66.7	94.0	27.0	21.1	17.2	12.0
100.0	140.5	12.0	12.8	10.0	7.2
134.0	187.4	4.8	5.9	4.9	4.3
167.0	234.0	3.7	3.2	3.0	1.7
200.0	281.0	2.0	1.2	0.8	0.8
234.0	328.0	0.5	0.8	0.0	0.0

SINGLE-NOZZLE DISTRIBUTORS

TABLE (6.15) - 106 μ catalyst C_2 (2D - bed)

D_o = 0.794 cm. H_{mf} = 50.2 cm.

Q_o	U_o	ℓ = 7.6 cm.	ℓ = 5.6 cm.	ℓ = 3.4 cm.	ℓ = 1.36 cm.	ℓ = 10 cm.
cm^3./sec.	cm./sec.	ω,gm./min.	ω,gm./min.	ω,gm./min.	ω,gm./min.	ω ,gm./min.
29.2	59.0	16.0	19.95	25.1	30.6	12.52
33.4	67.4	13.0	15.44	18.8	23.4	10.00
37.6	76.0	10.1	12.4	15.36	17.3	7.78
41.8	84.4	6.78	8.9	11.30	13.0	5.90
46.0	92.6	4.53	6.4	7.92	10.2	3.50
50.0	101.0	4.0	4.0	6.20	7.53	2.30
54.4	109.5	1.83	-	4.00	6.00	1.48
58.5	118.0	1.10	1.85	3.20	4.20	0.55
67.0	135.0	0.40	1.20	2.10	2.55	0.00
75.0	152.0	0.17	0.50	0.90	1.90	-
83.5	168.5	0.00	0.30	0.50	0.90	-

TABLE 6.16

Ungraded catalyst (20 - 150 μ) (2-D bed)

D_o = 0.635 cm. H_{mf} = 75 cm. A = 153.3 $cm.^3$

Q_o $cm.^3$/sec.	U_o cm./sec.	ℓ = 3.0 cm. ω, gm./min.	ℓ = 6.35 cm. ω, gm./min.	ℓ = 8.9 cm. ω, gm./min.
46.0	146	17.3	13.3	9.55
50.0	158	14.2	10.4	6.90
58.5	185	10.55	6.4	3.50
67.0	211	7.25	2.54	1.30
75.0	237	4.97	1.50	0.78
83.5	263	2.50	-	0.36
92.0	291	1.50	0.4	0.20
100.0	316	0.90	0.2	0.00
108.4	343	0.60	0.00	0.00

Flowback of Solids Through Multi-Orifice Distributors

(7.9 cm. diam. column)

(Data represents the average of at least three measurements. The Plots show the repeatability of the results).

TABLE (6.17)

D_o = 0.238 cm. N = 37 ϕ = 3.4% S/D_o = 5

(106 μ catalyst C_2)

H_{mf} = 25.1 cm.		H_{mf} = 35.2 cm.		H_{mf} = 45.3 cm.	
U, cm./sec.	ω, gm./min.	U, cm./sec.	ω, gm./min.	U, cm./sec.	ω, gm./min
1.412	0.53	2.12	0.566	2.056	0.627
2.120	2.80	2.83	2.4	2.74	3.55
2.82	4.76	3.545	3.843	3.44	8.31
3.53	5.22	4.241	8.973	4.11	16.2
4.27	8.425	4.94	15.04	4.77	15.8
4.97	8.96	5.65	17.2	5.47	17.78
5.675	12.615	6.35	15.27	6.155	15.43
6.41	15.9	7.045	11.8	6.838	13.25
7.12	13.0	7.755	11.66	7.5	11.48
7.81	11.7	8.75	9.25	8.455	9.31
8.81	9.75	9.72	7.216	9.4	6.668
9.82	7.25	10.58	5.27	10.252	5.14
10.68	5.46	12.325	3.12	12.0	3.52
11.56	4.31	14.11	2.02	13.7	1.84
12.48	3.27	17.62	0.76	17.1	0.74
14.4	2.285	19.78	0.41	20.53	0.32
17.82	0.875	21.1	0.281	21.8	0.08
19.96	0.362	21.6	No flowback		
21.26	0.175				

TABLE (6.18)

D_o = 0.238 cm. N = 30 ϕ = 2.74% S/D_o = 5.35 106μ catalyst C2

H_{mf} = 15.0		H_{mf} = 25.2 cm.		H_{mf} = 35.0 cm.	
U,cm./sec.	ω,gm./min.	U,cm./sec.	ω,gm./min.	U,cm./sec.	ω,gm./min.
1.112	0.000	1.21	0.31	1.39	0.09
1.39	0.114	1.74	0.351	2.066	0.60
2.074	0.35	2.09	0.217	2.74	2.01
2.76	0.452	2.8	0.644	3.42	5.39
3.443	1.054	3.44	1.36	4.16	7.34
4.15	2.16	4.2	2.55	4.82	7.54
4.18	3.22	4.9	4.89	5.53	9.26
5.47	5.1	5.57	6.37	6.24	8.0
6.1	6.36	6.3	8.15	6.91	7.12
6.745	4.14	6.98	7.3	7.6	5.94
7.4	3.88	8.65	4.885	8.55	4.33
8.7	4.1	10.35	2.91	10.35	2.62
10.42	2.3	12.1	1.67	12.1	1.55
13.92	0.825	13.81	0.902	13.81	0.803
15.65	0.422	15.52	0.503	15.52	0.55
17.42	0.21	17.28	0.273	17.28	0.26
17.9	0.09	17.9	No flowback	18.0	No flowback
18.6	No flowback				

TABLE (6.19)

D_o = 0.238 cm. N = 19 ϕ = 1.74% S/D_o = 6.7 106 μ Catalyst C_2

H_{mf} = 25.3 cm.		H_{mf} = 35.3 cm.		H_{mf} = 45.5 cm.	
U,cm./sec.	ω ,gm./min.	U,cm./sec.	ω ,gm./min.	U,cm./sec.	ω ,gm./min.
2.085	0.365	2.055	0.132	2.041	0.16
2.79	1.0	2.71	0.44	2.72	1.4
3.5	2.09	3.45	1.97	3.4	2.46
4.18	3.0	4.13	3.16	4.11	3.4
4.93	3.32	4.88	3.49	4.8	3.27
5.56	2.28	5.57	2.41	5.46	2.7
6.255	1.70	6.256	2.0	6.2	2.1
7.0	1.29	6.9	1.42	6.86	1.52
7.7	0.935	7.61	1.03	7.6	1.16
8.67	0.69	8.75	0.58	8.51	0.75
10.46	0.172	10.59	0.18	10.3	0.15
11.28	No flowback	11.16	0.10	11.21	No flowback

TABLE (6.20)

D_o = 0.318 N = 19 ϕ = 3.09% S/D_o = 5 106 μ cat.C_2

H_{mf} = 20.0 cm.		H_{mf} = 30.7 cm.		H_{mf} = 50.5 cm.	
U, cm./sec.	ω, gm./min.	U, cm./sec.	ω, gm./min.	U, cm./sec.	ω, gm./min.
1.55	1.29	1.21	1.59	1.546	1.66
1.9	2.16	1.56	2.25	1.89	2.65
2.77	4.05	1.90	0.85	2.742	4.031
3.46	10.17	2.76	5.67	3.42	11.6
4.16	13.22	3.46	12.626	4.12	16.22
4.85	17.78	4.15	19.45	4.79	18.266
5.54	15.21	5.545	16.92	5.47	16.67
6.25	14.5	6.26	14.47	6.155	14.45
6.94	12.14	6.94	12.91	6.85	12.923
7.64	10.28	7.61	10.61	7.54	9.83
8.6	8.23	8.6	8.55	8.5	7.58
9.54	5.52	9.52	5.612	9.4	5.617
10.39	4.3	10.36	4.5	10.28	4.37
12.11	2.78	12.1	2.7	11.98	2.578
13.85	1.7	13.86	1.58	13.7	1.542
17.3	0.545	17.3	0.57	17.1	0.587
19.0	0.33	19.0	0.32	19.15	0.27
20.5	No flowback	20.53	No flowback	20.55	No flowback

TABLE (6.21)

D_o = 0.476 cm. N = 9 ϕ = 3.285% S/D_o = 5 106 μ cat.C_2

H_{mf} = 20.3 cm.		H_{mf} = 30.6 cm.		H_{mf} = 50.5 cm	
U, cm./sec.	ω, gm./min.	U, cm./sec.	ω, gm./min.	U, cm./sec.	ω, gm./min.
1.9	15.75	1.92	22.1	1.9	25.1
2.77	36.1	2.77	53.5	2.77	63.7
3.46	51.3	3.46	60.0	3.46	69.0
4.15	49.0	4.15	55.75	4.14	56.2
4.842	44.6	4.85	46.0	4.85	45.5
5.54	38.3	5.54	37.1	5.54	38.7
6.227	30.24	6.23	31.2	6.3	30.0
6.92	25.69	6.92	25.4	6.92	25.63
7.627	19.116	7.626	20.3	7.63	19.7
8.584	15.98	8.584	16.0	8.58	15.7
9.511	11.87	9.5	12.6	9.52	11.73
10.39	9.83	10.4	10.6	10.39	9.6
12.1	7.1	12.1	7.03	12.1	6.7
13.82	4.54	13.83	4.65	13.83	4.4
17.28	1.84	17.3	1.72	17.3	1.66
20.18	0.55	20.18	0.5	20.2	0.57
23.7	No flowback	23.75	No flowback	23.62	No flowback

TABLE(6.22) (106 μ catalyst)

D_o = 0.635 cm. N = 9 ϕ = 3.27% S/D_o = 5

H_{mf} = 30.5 cm.		H_{mf} = 50.6 cm.		H_{mf} = 70.2 cm.	
U, cm./sec.	ω, gm./min.	U, cm./sec.	ω, gm./min.	U, cm./sec.	ω gm./min.
1.562	8.75	1.54	9.45	3.42	92.7
1.91	47.5	1.88	46.6	4.1	77.5
3.48	91.2	3.42	90.8	4.8	76.3
4.17	72.12	4.1	78.4	5.47	60.8
4.87	64.2	4.8	69.5	6.16	49.5
5.56	58.32	5.47	61.2	6.85	42.55
6.26	50.1	6.16	55.5	7.53	35.4
6.95	42.17	6.85	41.6	8.5	25.2
7.65	31.32	7.53	32.3	9.42	18.9
8.63	25.0	8.5	24.9	10.26	15.0
9.55	16.55	9.42	15.26	12.0	10.1
10.41	14.7	10.26	13.9	13.7	8.1
12.15	10.65	12.0	10.5	17.1	4.94
13.9	7.1	13.7	7.19	20.5	1.72
17.36	3.55	17.1	3.6	23.56	No flowback
20.84	1.41	20.5	1.38		
23.42	No flowback	23.38	No flowback		

TABLE (6.23) (128 μ coal)

D_o = 0.318 cm. N = 19 ϕ = 3.09% S/D_o = 5

H_{mf} = 24.7 cm.		H_{mf} = 35.0 cm.		H_{mf} = 45.2	
U, cm./sec.	ω, gm./min.	U. cm./sec.	ω, gm./min.	U, cm./sec.	ω, gm./min.
2.0	0.61	2.0	0.2	2.5	7.5
2.5	0.25	2.5	2.5	2.5	4.5
5.0	4.0	4.0	0.5	5.0	5.0
5.0	15.0	5.0	9.98	6.52	18.0
6.48	17.5	6.5	16.0	7.5	17.53
7.5	15.64	7.5	16.6	8.5	14.6
8.5	14.3	8.5	13.5	10.0	10.0
10.0	9.7	10.0	10.4	12.0	5.8
12.0	6.3	12.0	5.4	14.5	1.1
14.5	3.2	14.5	3.3	20.0	0.2
17.0	0.6	17.0	0.8	22.1	No flowback
20.0	0.3	20.0	0.4		
22.0	No flowback	22.5	No flowback		

TABLE (6.24) (128 μcoal)

$V_\omega = 2 \times 10^3 cm^3$. $D_o = 0.476$ cm. N = 9 $\phi = 3.288\%$

U	H_{mf} = 45.5cm	H_{mf} = 65.8 cm
cm./sec	ω, gm./min.	ω, gm./min
1.1	0.12	-
2.45	10.0	30.0
2.45	0.2	40.1
3.4	45.0	44.0
4.4	47.0	49.5
6.46	40.0	33.0
8.5	21.0	20.0
10.0	14.4	14.0
12.15	9.3	9.7
14.4	4.0	4.8
17.2	2.0	2.1
20.0	1.0	1.1
24.0	No flowback	No flowback

TABLE (6.25) (138μ rounded sand)

$D_o = 0.238$ cm. N = 19 $\phi = 1.74\%$

U	H_{mf} = 15.7cm.	H_{mf} = 25.3cm.	H_{mf} = 40.2cm.
cm./sec.	ω, gm./min.	ω, gm./min.	ω, gm./min.
2.53	1.0	0.1	0.3
3.5	1.0	0.2	0.61
4.1	0.8	1.1	1.6
5.0	2.45	3.2	2.78
6.3	5.43	3.4	4.59
7.0	6.0	4.8	5.0
8.0	7.26	6.8	5.97
9.0	8.0	7.2	6.95
10.5	8.2	9.1	9.4
12.0	9.8	9.0	9.98
12.8	10.64	10.2	10.3
13.9	9.6	8.3	8.3
15.0	6.96	6.2	6.4
17.55	4.0	3.6	3.4
20.0	2.2	1.98	1.92
22.0	1.1	1.2	1.2
24.5	0.5	0.5	0.46
27.8	No flowback	No flowback	No flowback

TABLE (6.27) 106μ catalyst

D_o = 0.238 cm. N = 37 ϕ = 3.4%

U cm./sec.	ℓ = 0.635 cm. ω, gm./min.	ℓ = 1.27 cm. ω, gm./min.
1.51	0.55	0.64
1.88	0.59	0.62
2.67	4.35	2.1
3.35	5.9	9.65
4.0	12.0	9.3
4.68	14.9	13.0
5.35	13.0	10.1
6.03	11.4	8.0
6.7	10.2	7.54
7.35	9.0	5.78
8.3	7.4	4.2
9.2	5.0	2.58
10.0	3.78	1.74
11.7	2.1	0.84
13.6	1.5	0.38
15.7	-	No flowback
16.7	0.52	
18.4	0.2	
19.2	No flowback	

TABLE (6.28) 106 μ catalyst

D_o = 0.318 cm. N = 19 ϕ = 3.09%

U cm./sec.	ℓ = 3.8 cm. ω, gm./min.	ℓ = 2.54 cm. ω, gm./min.	ℓ = 1.27 cm. ω, gm./min
1.55	-	1.39	2.32
1.90	-	1.16	1.51
2.76	10.65	3.76	4.65
3.44	12.43	9.7	10.7
4.12	8.11	13.94	12.15
4.48	5.46	-	-
4.8	1.74	13.21	11.87
5.52	0.52	9.76	9.9
6.2	0.134	6.8	8.45
6.94	-	3.97	5.44
7.2	No flowback	-	-
7.64		2.1	4.12
8.6		1.19	3.1
9.54		0.32	1.65
10.15		No flowback	
10.41			1.042
12.15			0.3
14.0			No flowback

TABLE (6.29) 106 μ catalyst

D_o = 0.476 cm. N = 9 ϕ = 3.285%

U cm./sec.	ℓ = 2.54 cm. ω, gm./min.	ℓ = 1.27 cm. ω, gm./min.	ℓ = 0.635 cm. ω, gm./min.
2.74	61.0	62.0	50.5
3.42	58.7	58.0	57.1
4.12	47.1	54.2	56.0
4.79	39.5	47.3	50.0
5.5	31.3	41.5	38.3
6.16	24.4	32.0	33.4
6.85	17.77	26.0	26.0
7.53	13.7	20.3	21.5
8.5	6.9	14.6	16.3
9.4	3.3	8.1	10.4
10.25	2.0	6.0	8.2
11.9	1.67	3.15	5.2
12.0	0.75	-	-
12.8	0.46	-	-
13.9	0.2	1.67	3.1
14.5	No	-	-
15.4	flowback	0.84	---
16.3		0.58	-
17.45		No	-
19.65		flowback	No flowback

TABLE (6.30) 106 μ catalyst

D_o = 0.476 cm. N = 9 ϕ = 3.285%

U cm./sec.	V_ω=19.2x10^{3}cm.^{3} ω, gm./min.	V_ω=41.5x10^{3}cm.^{3} ω, gm./min.	V_ω=62.2x10^{3}cm.^{3} ω, gm./min.	V_ω=86.1x10^{3}cm.^{3} ω, gm./min
1.97	14.0	30.0	14	10.0
1.97	1.0	-	32	36.4
2.85	44.0	43.0	50.0	32.0
3.47	60.0	54.0	46.4	40.4
4.2	52.0	46.0	39.9	34.4
4.9	38.5	34.8	32.0	30.1
5.65	29.7	28.2	26.0	24.9
6.24	26.0	24.2	23.1	22.3
6.9	21.9	20.4	19.8	19.7
7.66	18.2	17.8	18.0	18.0
8.6	12.0	10.8	11.8	11.0
10.45	9.0	8.5	8.2	6.2
12.1	7.6	6.2	5.8	3.9
13.9	4.0	4.0	4.1	0.9
17.5	1.0	1.1	0.6	-
19.55	-	-	No	No
19.8	No	-	flowback	flowback
20.0	flowback	-		
20.5		No		
		flowback		

The Limiting Gas Velocities

* Tables (6.31) - (6.31d) are presented as examples but the complete results are given in Table (6.32).

TABLE (6.31) - $Re_{\ell im}$ as a function of S/D_o

106 μ catalyst fluidized with air - 7.9 cm. diam. column.

D_o = 0.238 cm. ℓ = 0.318 cm.

S, cm.	S/D_o	$Re_{\ell im}$
1.18	5.0	1008
1.27	5.35	1075
1.59	6.7	1029
1.81	7.62	1332
2.30	9.7	1128
3.10	13.0	1040
3.40	14.3	1080
3.40	14.3	1080

TABLE (6.31a) - $Re_{\ell im}$ as a function of ϕ

106 μ catalyst fluidized with air - 7.9 cm. diam. column.

D_o = 0.238 cm. ℓ = 0.318 cm.

N	ϕ, %	U, cm./sec.	$U\ell_o$, cm./sec.	$Re_{\ell im}$
37	3.4	21.6	636	1008
29	2.65	16.2	612	970
23	2.10	12.58	600	952
19	1.74	10.78	6.9	981
13	1.19	7.445	625	990
7	0.64	2.935	615	975

TABLE (6.31b) - $Re_{\ell im}$ as a function of ϕ

128 μ coal fluidized with CO_2 - 7.9 cm. diam. column

D_o = 0.238 cm. ℓ = 0.318 cm.

N	ϕ , %	U , cm./sec.	$U\ell_o$. cm./sec.	$Re_{\ell im}$
23	2.1	11.47	546	1595
19	1.74	9.54	548	1600
13	1.19	6.50	545	1590
11	1.01	5.58	553	1610

TABLE (6.31c) - $Re_{\ell im}$ as a function of ϕ

106 μ catalyst fluidized with helium - 7.9 cm.diam.column

D_o = 0.2 cm. ℓ = 0.318 cm.

N	ϕ ,%	U ,cm./sec.	U_o,cm./sec.	$Re_{\ell im}$
13	0.836	21.0	2505	432
11	0.716	18.85	2659	456
9	0.576	14.32	2500	430
7	0.45	11.50	2559	440

TABLE (6.31d) - $Re_{\ell im}$ as a function of D_o/D_p

106 μ catalyst fluidized with air - 7.9 cm. diam. column

ℓ = 0.318 cm.

D_o,cm.	D_o/D_p	$Re_{\ell im}$
0.159	15	729
0.20	18.9	988
0.238	22.4	1100
0.318	30	1410
0.40	37.75	1955
0.476	45	2290
0.635	60	3040

TABLE (6.32) Criteria for the prevention of flowback of solids

System	D_p, μ	D_o, cm.	ℓ, cm.	D_o/D_p	ℓ/D_o	Ar	$Re_{\ell im}$	R *
air - cat.	106	0.238	0.318	22.4	1.334	25.14	1097	55.0
air - sand	138	0.238	0.318	17.2	1.334	137.5	2500	90.0
CO_2 - cat.	106	0.238	0.318	22.4	1.334	55.1	1500	77.0
CO_2 - sand	138	0.238	0.318	17.2	1.334	305.0	2800	127.5
He - cat.	106	0.238	0.318	22.4	1.334	2.74	530	21.2
air - coal	128	0.238	0.318	18.6	1.334	37.3	1110	55.6
CO_2 - coal	128	0.238	0.318	18.6	1.334	82.9	1599	79.0
air - cat.	106	0.318	0.318	30.0	1.0	25.14	1410	76.5
CO_2 - cat.	106	0.318	0.318	30.0	1.0	55.1	2232	108.0
CO_2 - sand	138	0.318	0.318	23.0	1.0	305.0	3424	182.0
He - cat.	106	0.318	0.318	30.0	1.0	2.74	742	29.6
He - cat.	106	0.20	0.318	18.85	1.6	2.74	440	17.5
air - cat.	106	0.20	0.318	18.85	1.6	25.14	988	44.6
air - cat.	106	0.40	0.318	37.75	0.8	25.14	1955	93.2
air - cat	106	0.476	0.318	45.0	0.67	25.14	2290	122.0
air - cat	106	0.159	0,318	15.0	2.0	25.14	729	35.0
CO_2 - cat.	106	0.20	0.318	18.85	1.6	55.1	1155	64.0
CO_2 - cat.	52	0.238	0.318	45.8	1.334	6.8	1776	57.7
air - cat.	52	0.238	0.318	45.8	1.334	1.62	1192	41.0
air - cat.	74	0.238	0.318	32.2	1.334	8.3	1329	53.5
air - glass	120	0.238	0.318	19,85	1.334	109.3	1600	91.4
CO_2 - glass	120	0.238	0.318	19.85	1.334	243.0	3460	130.0
air - coal	200	0.476	0.318	23.8	0.67	154.3	2420	150.0
air - coal	200	0.318	0.318	15.9	1.0	154.3	1600	95.0
air - coal	200	0.40	0.318	20.0	0.8	154.3	2300	125.0
$CC\ell_2F_2$ - cat.	106	0.476	0.318	45.0	0.67	207.0	5371	304.0

TABLE (6.32) continued

System	D_p, μ	D_o, cm.	ℓ, cm.	D_o/D_p	ℓ/D_o	Ar	$Re_{\ell im}$	R *
$CC\ell_2F_2$ - cat.	106	0.4	0.318	37.75	0.80	207.0	4290	247.0
$CC\ell_2F_2$ - cat.	106	0.318	0.318	30.0	1.0	207.0	3615	191.0
$CC\ell_2F_2$ - cat.	106	0.238	0.318	22.4	1.334	207.0	2620	136.0
air - cat.	106	0.635	0.318	60.0	0.5	25.14	2040	167.0
air - cat.	106	0.635	0.635	60.0	1.0	25.14	2700	138.0
air - cat.	106	0.635	1.27	60.0	2.0	25.14	2470	116.0
air - cat.	106	0.476	0.635	45.0	1.334	25.14	1897	100.0
air - cat.	106	0.476	1.270	45.0	2.67	25.14	1693	84.5
air - cat.	106	0.476	2.54	45.0	5.334	25.14	1341	70.0
air - cat.	106	0.476	3.8	45.0	8.0	25.14	1093	63.0
air - cat.	106	0.318	1.27	30.0	4.0	25.14	992	46.0
air - cat.	106	0.318	2.54	30.0	8.0	25.14	696	43.6
air - cat.	106	0.318	3.8	30.0	12.0	25.14	494	38.8
air - cat.	106	0.238	0.635	22.4	2.67	25.14	900	47.6
air - cat.	106	0.238	1.27	22.4	5.334	25.14	737	38.2
air - cat.	106	0.238	1.9	22.4	8.0	25.14	572	34.3
air - cat.	74	0.476	2.54	64.4	5.334	8.3	1406	60.0
air - cat.	52	0.476	2.54	91.55	5.334	3.1	1655	53.0
air - cat.	74	0.318	1.27	43.0	4.0	8.3	986	45.5
air - cat.	74	0.318	2.54	43.0	8.0	8.3	681	37.6
air - cat.	74	0.318	3.8	43.0	12.0	8.3	552	33.4
CO_2 - cat.	106	0.318	2.54	30.0	8.0	55.1	957	61.6
CO_2 - cat.	74	0.318	2.54	43.0	8.0	17.4	872	53.0
air - sand	138	0.238	0.635	17.25	2.67	137.5	2240	76.0
air - sand	138	0.238	1.27	17.25	5.334	137.5	1870	63.0
air - sand	138	0.238	1.9	17.25	8.0	137.5	1397	56.5
air - sand	138	0.318	1.27	23.0	4.0	137.5	2420	88.0
air - sand	138	0.318	2.54	23.0	8.0	137.5	1806	73.0
air - sand	138	0.318	3.8	23.0	12.0	137.5	1350	65.0
air - sand	138	0.476	1.27	34.5	2.67	137.5	4385	140.0

TABLE (6.32) continued

System	D_p, μ	D_o, cm.	ℓ, cm.	D_o/D_p	ℓ/D_o	Ar	$Re_{\ell im}$	R *
air - sand	138	0.476	2.54	34.5	5.334	137.5	3780	116.0
air - sand	138	0.476	3.8	34.5	8.0	137.5	2860	104.0
$CC\ell_2F_2$ - cat.	106	0.635	0.318	60.0	0.5	207.0	8448	442.0
$CC\ell_2F_2$ - cat.	106	0.635	0.635	60.0	1.0	207.0	8000	348.0
$CC\ell_2F_2$ - cat.	106	0.635	1.270	60.0	2.0	207.0	6820	290.0

* $R = \left(\frac{\ell}{D_o}\right)^{-0.27} \cdot \left(\frac{D_o}{D_p}\right)^{0.87} \cdot Ar^{0.43}$

TABLE (6.33)

Uncontrollable downflow of solids through long cylindrical nozzles (critical nozzle velocities)

Nozzle ℓ, cm.	U_o^2 (predicted)		U_o^2 (experimental)		
	eqn(6.48)	eqn(6.49)	N: 7 * D_o: 0.635 cm. ϕ: 1.45%	N: 9 D_o: 0.476 cm. ϕ: 3.3%	N: 19 D_o: 0.318 cm. ϕ: 3.09%
4	-	-	-	-	40
5	290	179	-	121	82
8	464	286	204	296	264
10	580	358	381	397	360
12	695	430	440	478	457
15	870	537	545	570	520
18	1045	645	660	-	-
20	1160	716	-	-	-

* 14.0 cm. diam. column.

NOTATION

A	cross sectional area of bed
A_o	total orifice area on the distributor
A_e	effective orifice area on the distributor
a_o	surface area of an orifice
C_D	drag on a single sphere
D	bed diameter
D_o	orifice diameter
D_B	bubble diameter
D_{Bo}	bubble diameter at the distributor surface
D_p	mean particle diameter
e	voidage fraction
e_{mf}	voidage fraction at incipient fluidization
e_j	voidage in the effective volume of a fluid jet
g	acceleration due to gravity
H	expanded bed height
H_{mf}	incipient bed height
H_m	maximum spoutable bed height
h	bed height above distributor
k_o	orifice constant
ℓ	plate thickness or nozzle length
ℓ_c	critical nozzle length
M_s	mass of defluidized solids resting on distributor
n	number of operative orifices or nozzles
N	total number of orifices or nozzles
p	fluid pressure
ΔP_D	pressure drop through the distributor
ΔP_B	pressure drop through the bed
ΔP_{Bt}	theoretical bed pressure drop
Q_o	volumetric flow rate per orifice
S	orifice spacing
U	superficial velocity
U_B	bubble velocity
U_{mf}	gas velocity at incipient fluidization
U_o	Orifice velocity
$U\ell$	limiting gas velocity
$U\ell_o$	limiting gas velocity through the orifices
V_j	effective volume of jet

V_ω	Wind box volume
W_B	weight of bed
W	free flowback rate (gravity flow)
ω	flowback rate (fluidized bed conditions)
ω_o	flowback flux (fluidized bed conditions)
Z	height of defluidized zones on distributor
Z_j	height above which jet interaction occurs
Z_R	height of defluidized zones at angle of repose
θ_R	angle of repose of solid particles
μ_f, μ_g	fluid viscosity, gas viscosity
ρ_f, ρ_g	fluid density, gas density
ρ_B	bulk density of solid particles
ρ_s	particle density
ϕ	plate characteristics (or fractional free area)
λ_s, λ_r	shape factor, roundness factor

The rest of the symbols are clearly defined within the text.

REFERENCES

1. Harrison, D., Chem.Proc.Engng., 1966, 47, 118.

2. Gregory, S.A., Proc.Int. Symp. on Fluidization, Eindhoven,1967, 751.

5. Morley, R.J., B.I.O.S. Report No.333, Item No.30.

9. Sittig, M., Petroleum Refiner Process Hand Book, (Houston Gulf Publishing Co.), 1952, 91.

10. Braca, R.M. and Fried, A.A., in (Othmer,D.F., Fluidization, Reinhold, 1956, 117).

11. Stemerding, S., de Groot, J.H. and Kuypers, N., Jt.Symp.1963, Society of Chemical Ind., 1964, 35.

12. Turner, R., ibid, 47.

14. Daniels, L.S., Petrol Refiner, 1946, 25, 435.

15. Zenz, F. and Othmer, D.F., 'Fluidization and Fluid-particle systems', Reinhold, 1960.

16. Cooper, E.D., Black, D.E. and Ambeson, C.B., Chem.Engng.Prog.,1965, 61, 89.

18. Federov, I.M., Teoriya i Raschot Protyessa Sushki Vo VzVeshemon Sostoyonu, Gosenegezdat, Moscow, 1955.*

20. Avery, D.A. and Tracey, D.H., Tripartite Chemical Engng.Conference, Montreal, Inst. Chem.Engrs., 1968, 28.

21. Picter, J.W.D. and Robinson, L.W.J., Proc.Inst.Chem.Engrs, VTG/VDI (joint meeting), Brighton, 1968, 166.

22. Wormald, D and Bunwell, E.M., Brit.Chem.Engng., 1971, 378.

23. Gvozdev, V.D. et al., International Chem.Engng., 1963, 3, 562.

24. Agarwall, J.C., Davis, W.L.J. and King, D.T., Chem.Engng.Prog.,1962 58, 11, 85.

25. Gregory, S.A., Brit. Chem.Engng., 1960, 5, 340.

26. Hiby, J.W., Chem.Ing.Tech., 1964, 36, 228.

27. Whitehead, A.B. and Dent, D.C., Proc.Int.Symp. on Fluidization, Eindhoven, 1967, 739.

28. Whitehead, A.B., Gartside, G. and Dent, D.C., The Chemical Engng. J., 1970, 1, 175.

29. Zuiderweg, F.J., Proc. Int.Symp. on Fluidization, Eindhoven, 1967, 739.

30. Wright, S.J., Proc. Inst. Chem. Engrs., VTG/VCI (joint meeting), Brighton, 1968, 161.

31. Vaněcek, V. and Drbohlav, R., 'Fluidized Bed Drying', Leonard Hill - London, 1966, 95.

32. Kelsey, J.R., Tripartite Chemical Engng. Conference, Montreal, Inst.Chem.Engrs., 1968, Discussion on page 86.

33. Squires, A.M., Chem.Engng.Prog., 1962, 58, 4, 66.

34. Deshpande, A.D. et al., Indian J. Technal., 1967, 5, 1.

35. Horsler, A.G. and Thompson, B.H., Tripartite Chemical Engng.Conference, Montreal, Inst.Chem.Engrs., 1968, 58.

36. Losh, C.E., Legler, B.M. and Hales, M.P., ibid, 75.

47. Counselman, T.B., Mining Congress J., 1951, 37, 30.

50. Kunii, D. and Levenspiel, O., 'Fluidization Engineering', John Wiley, 1969.

51. Wike, E. and Hedden, K., Chem.Ing.Tech., 1952, 41, 1247. *

52. Zemshov, I.F., Slepanov, A.S. and Densiov, V.F., Khim Mashinoster, 1960, 6, 21. *

53. Gregory, S.A., J.App.Chemistry, 1952, 2, Supp.No.1, S1.

56. Petrie, J.C. and Black, D.C., Chem.Engng., Prog.Symp.Ser., 1966, 62, 67, 64.

57. Gregory, S.A., Private Communication, Senior Lecturer, Chem.Eng.Dept., The University of Aston in Birmingham.

58. Geldart, D. and Kelsey, J.R., Tripartite Chemical Engng. Conference, Montreal, Inst. Chem.Engrs., 1968, 114.

59. Agarwal, O.P. and Storraw, J.A., Chemistry and Industry, 1951, 278.

60. Morse, R.D. and Ballou, C.O., Chem.Engng.Prog., 1951, 47, 4, 199.

61. Grosh, E.W., A.I.Ch.E.J., 1955, 1, 3, 358.

62. Dotson, J.M., ibid, 1959, 5, 2, 169.

63. Rowe, P.N. and Stapleton, W.M., Trans. Inst. Chem. Engrs.,1961,38,181.

64. Fakhimi, S. and Harrison, D., 'Chemeca 70', The Inst. of Chem. Engrs., Session 1, p 29.

65. Hovmand, S., Freedman, W. and Davidson, J.F., Trans.Inst.Chem.Engrs., 1971, 49, 3, 149.

66. Grekel, H., Hujsak, K.L. and Mungen, R., Chem.Engng.Prog.,1964, 60, 1, 56.

67. Volk, W., Jhonson, C.A. and Stotler, H.H., Chem.Eng.Prog., 1962, 58, 3, 44.

68. Gomezplata, A. and Schuster, W.W., A.I.Ch.E.J., 1960, 6, 454.

69. Grek, F.Z., Khim.Prom., 1966, 42, 6, 67.

70. Zenz, F.A., Tripartite Chemical Engng. Conference, Montreal, Inst.Chem.Engrs., 1968, 136.

71. Yufa, M.S., Khim, i Neft Mash, 1965, 7, 24.

72. Whitehead, A.B., in (Davidson J.F. and Harrison, D., Fluidization, Academic Press, 1971).

73. Zabrodsky, S.S., 'Hydrodynamics and Heat Transfer in Fluidized Beds', Cembridge Mass. M.I.T. Press, 1966.

74. Fakhimi, S., Ph.D. Thesis, Cambridge University, 1969.

75. Toei, R. and Akao, T., Tripartite Chemical Engng.Conference,Montreal, Inst. Chem.Engrg., 1968, 34.

76. Serviant, G.A., Bergougnou, M.A., Baker, C.G.J. and Bulani, W., Con.J. of Chemical Engng., 1970, 48, 469.

77. Kassim, W.M.S., M.Sc. in Process Analysis and Development, The University of Aston in Birmingham, 1969.

78. Van Winkle, M., 'Distillation', McGraw Hill, New York, 1967.

79. Jameson, G.J. and Kupferberg, A., Chem.Eng.Sci., 1967, 22, 1053.

80. Kupferberg, A. and Jameson, C.J., Trans.Inst.Chem.Engrs.,1969,47,T241.

81. Leva, M. 'Fluidization', McGraw Hill, New York 1959.

82. Davidson, J.F. and Harrison, D., 'Fluidized Particles', Cambridge,1963.

83. Rowe, P.N., Trans.Inst.Chem.Engrs., 1961, 39, 175.

84. Godard, K. and Richardson, J.F., Tripartite Chemical Engng. Conference, Montreal, Inst. Chem.Engrs., 1968, 126.

85. Davies, L. and Richardson, J.F., Trans.Inst.Chem.Engrs.,1966, 44, T293.

86. McCann, D.J. and Prince, R.G.H., Chem.Eng.Sci., 1969, 24, 801.

87. Sutherland, J.P., Chem.Eng.Sci., 1964, 19, 839.

88. Trivedi, R. and Rice, W.J., Chem.Engng. Prog.Symp. Ser.,1966, 57.

89. Shannon, P.T., Ph.D. Thesis, Illinois Institute of Technology, 1959.

90. Student's Project, Chem.Eng.Dept., The University of Aston in Birmingham, 1970.

91. Fraiman et al., Khimiya I Tekhnologia Topliva, 1 Nassel, 1962,7,44.

92. Ukhlov, V.V. and Volkov, V.F., Khim. Prom., 1971, 7, 541.

93. Glass, D.H., Proc.Inst.Chem.Engrs., VTG/VDI (joint meeting), Discussion, Brighton, 1968, 177.

94. Abramovich, G.N. 'The Theory of Turbulent Jets', Cambridge Mass. M.I.T. Press, 1963.

95. Yasui, G. and Johanson,L.N., A.I.Ch.E.J., 1958, 4, 445.

96. Toei, R. et al., Chem.Engng., Tokyo, 1965, 29, 851.

97. Romero, J.B. and Smith, D.W., A.I.Ch.E.J., 1965, 29, 851.

98. Kobayashi, H., Arai, F. and Shiba, T., Chem.Engng., Tokyo, 1965, 29, 858.

99. Baumgarten, P.K. and Pigford, R.L., A.I.Ch.E.J., 1960, 6, 115.

100. Lanneau, K.P., Trans.Inst.Chem.Engrs., 1960, 38, 125.

101. Kato, K. and Wen, Y., Chem.Eng.Sci., 1969, 24, 1351.

102. Cookes, et al., Tripartite Chemical Engng. Conference, Montreal, Inst.Che.Engrs., 1968, 21.

103. Geldart, D., Powder Technology, 1968, 1, 355.

104. Bakker, P.J., Chem.Eng.Sci., 1960, 12, 260.

105. Botterill, J.S.M., George, J.S. and Besford, H., Chem.Eng.Prog. Symp. Ser., 1966, 62, 62, 7.

106. Zenz, F.A., Hydrocarb. Process. Petrol Refin., 1967, 46, 171.

107. Lefroy, G.A. and Davidson, J.F., Trans.Inst.Chem.Engrs., 1969,47,T120.

108. Broughton, J., Research Fellow, Mech.Eng.Dept., The University of Aston in Birmingham.

109. McGrath. L. and Streatfield, R.E., Trans.Inst.Chem.Engrs., 1971,49,70.

110. Bulov, A.D. and Tyuraev, I.Y., Protsessy Khim. Tekhnol. Gidrodinam, Teplo-i Massopevedacha, Akad. Nauk SSSR, Otd. Obshch. i Tekh Khim., s.b. Statei, 1965, 22-25.

111. Pilpel, N.J., Brit.Chem.Engng., 1966, 11, 699.

112. Beverloo, W.A., Leniger, H.A. and Van De Velde, J., Chem.Eng.Sci., 1961, 15, 260.

113. Newton, R.H., Diunham, G.S. and Simpson, T.P., Trans.Amer.Inst. Chem.Engrs., 1945, 41, 215.

114. Jones, T.M. and Pilpel, N.J., Pharm. Pharmc., 1965, 16, 44.

115. Brown, R.L. and Richards, J.C., 'Principles of Powder Mechanics', Pergamon Press, 1970.

116. Miles, J.E.P., Schofield, C. and Valentin, F.H.H., paper presented at the symposium on "The Behaviour of Granular Materials" at the Tripartite Chemical Engng. Conference, Montreal, Inst.Chem.Engrs., 1968.

117. Holland, J., Miles, J.E.P., Schofield, C. and Shook, C.A., Trans.Inst.Chem.Engrs., 1969, 47, T154.

118. Jottrand, R., Brit.Chem.Engng., 1958, 143.

119. Hughes et al., Chem.Eng.Prog., 1955, 51, 557.

120. Kutateladze, S.S. and Sorokin, Y.L., in (Kutateladze, S.S. 'Problems of Heat and Hydraulics of Two-phase Media', Pergamon Press). 1969, 385.

121. Bene, T., Int. Chem. Engng., 1964, 4, 625.

122. Innes, W.B., Analytical Chemistry, 1956, 28, 332.

123. Wadell, Hakon, Jour. Geol., 1935, 43, 250.

124. Douglas, J.F., 'An Introduction to Dimensional Analysis for Engineers', Pitman, 1969.

125. Manual - Calibration Data for 'Metric' Series Rotameters, Rotameter Manufacturing Company Limited.

PATENTS

3. Robinson, C.E., USP 212, 508(1879).
4. Card, W.L. and Dane, J.C., USP 300, 042(1884).
6. Frazer, T. and Yancey, H.F., USP 1, 534, 840(1925).
7. Odell, W.W., USP 1, 984, 380(1934).
8. Lewis, W.K. and Gilliland, E.R., USP 2, 357, 901(1944).
13. Becker, G., USP 2, 373, 008(1945).
17. Pyzel, R., USP 3, 361, 539(1968).
19. White, F.S., USP 2, 528, 098(1950).
37. Blanding, F.H., USP 2, 431, 455(1947).
38. Arnold, M.H.M. and Young, R.J., BP 606, 765(1948).
39. Franklin, R.G. and I.C.I., BP 610, 439(1948).
40. Pears, T.J. and I.C.I., BP 683, 703(1952).
41. Dill, G.D., USP 2, 288, 613(1942).
42. Hartley, J.C., USP 2, 371, 619(1945).

43. Brassert, H.A., USP 2, 404, 944(1946).

44. Brassert, H.A. and Ramseyer, C.F., USP 2, 389, 133(1945).

45. Johonson, C.A., USP 2, 367, 281(1945).

46. Snuggs, J.F., USP 2, 367, 694(1945).
Hemminger, C.E., USP 2, 444, 990(1948).
Watson, K.M., USP 2, 463, 729(1949).
Ford, L.J., USP 2, 582, 688(1952).
Huff, L.C., USP 2, 607, 622(1952).

48. Dolton, B.S., BP 729, 571(1955).

49. Dolton, B.S., USP 2, 841, 476(1958).

54. Gregory, S.A. and Trees, J., BP 811, 366(1959).

55. Reeve, L., BP 866, 044(1961).

* These works were referred to by other authors but have not been read.